Energy yield analysis and evaluation of solar irradiance models for a utility scale solar PV plant in South Africa

by

Tafara Mahachi

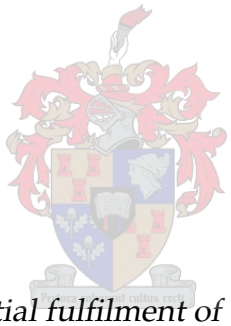

Thesis presented in partial fulfilment of the requirements for the degree of Master of Engineering (Electrical and Electronics) in the Faculty of Engineering at Stellenbosch University

Supervisor: Dr. A. J. Rix

December 2016

DECLARATION

By submitting this thesis electronically, I declare that the entirety of the work contained therein is my own, original work, that I am the sole author thereof (save to the extent explicitly otherwise stated), that reproduction and publication thereof by Stellenbosch University will not infringe any third party rights and that I have not previously in its entirety or in part submitted it for obtaining any qualification.

Date: December 2016 .....

ABSTRACT

Energy yield analysis and evaluation of solar irradiance models for a utility scale solar PV plant in South Africa

T. Mahachi

Department of Electrical and Electronic Engineering,
University of Stellenbosch,
Private Bag X1, Matieland 7602, South Africa.

Thesis: MEng (E & E)

December 2016

It is critical for electrical utility providers to be certain of the field performance of their systems in order to realize returns on project investments. Due to the actual output of installed solar PV modules being far more involved than in standard test conditions, some real world systems outperform simulations. The output of a solar PV system depends on various factors like local weather, system design characteristics, etc. Various energy forecasting simulation software exist and PVsyst is one of the most reliable when given the right input data. It is vital that software simulated energy yield values closely correlate with the actual field performance.

In this study, the cause of the seasonal differences in measured and simulated energy yield for a solar PV power plant in South Africa is investigated. It was observed that a fixed tilt 75 MW_P operational system significantly outperformed the software simulations in winter months during its first year of operation. Normally it is expected that simulations perform better than real world systems. In order to achieve our goals, an initial yield assessment was done in PVsyst and simulation results were evaluated against measured data. Differences in actual and estimated weather conditions were avoided by using irradiance and ambient temperature values recorded at the solar PV plant site. Due to the overestimation of losses in the PVsyst model, the simulated results did not correlate with the measured values of energy yield. In the simulations, the real world system was underestimated by a yearly average value of 6.4% and 5% using the Hay and Perez model respectively.

Understanding the performance drivers and losses within a solar PV system is crucial for ensuring reliable and high performance solar PV systems. Due to the overestimation of losses in the default PVsyst loss model, system loss values were then derived from the data recorded on the solar PV plant site. Findings from the calculated losses were then used to improve the PVsyst model for the solar PV plant. After using 30 minute average input data and the

improved PVsyst loss model, the real operational system was slightly underestimated by the improved simulation model by a yearly average value of 0.78%. Seasonal differences between measured and simulated energy yield were still observed. These differences were larger in winter than in summer and they were also in correlation with the variances in the measured and PVsyst estimated Plane-Of-Array irradiance.

Due to the seasonal differences between the improved PVsyst model and the measured energy yield values in winter months, irradiance models that estimate the Plane-Of-Array irradiance from Global Horizontal Irradiance measurements were evaluated for South African climatic conditions. The most common irradiance decomposition models namely Orgill and Hollands, Erbs, Louche, Reindl_1, Reindl_2, DISC and Dirint were evaluated as well as combinations of the Isotropic, Sandia, Klucher, Hay, Reindl and Perez transposition models with the best performing decomposition models. Based on the root mean square values, the best performing decomposition models were the Dirint, Louche and Disc whereas the Perez, Reindl and Hay transposition models performed the best for South African sites. On a monthly basis, simulations done using measured Plane-Of-Array irradiance were within 2% of the field recorded values. It was then concluded that the choice of irradiance data, transposition and loss models has a significant effect on the short and long term energy predictions.

UITTREKSEL

Ontleding van energie opbrengs en evaluasie van'n sonstralingsmodel vir 'n fotovoltaïese aanleg in Suid-Afrika

(" Energy yield analysis and evaluation of solar irradiance models for a utility scale solar PV plant in South Africa")

T. Mahachi

Departement van Elektriese en Elektroniese Ingenieurswese ,
Universiteit van Stellenbosch,
Privaatsak X1, Matieland 7602, Suid Afrika.

Tesis: MIng (E & E)

Desember 2016

Dit is belangrik dat maatskappye uitvind hoe goed hulle sisteme in die praktyk presteer sodat hulle verseker kan wees van 'n goeie opbrengs op hulle belegging in die projek. Omdat die werklike uitsette van son fotovoltaïese (FV) modules baie meer kompleks is as in standaard toetstoestande, vertoon sommige sisteme onder werklike toestande (in die praktyk) beter as in die simulasies. Die uitsette van 'n son FV sisteem hang af van verskillende faktore soos die plaaslike weer, die ontwerpkenmerke van die sisteem, ens. Daar bestaan verskillende soorte simulasie sagteware wat voorspellings kan maak, waarvan PVsyst een van die mees betroubaarste is as die regte data ingevoer word. Dit is veral belangrik dat die sagteware-gesimuleerde energie opbrengs waardes met die werklike prestasies in die veld moet ooreenstem.

Tydens hierdie studie is daar ondersoek ingestel na die oorsake van seisoenale verskille in die gemete en gesimuleerde energie opbrengs van 'n son FV aanleg in Suid-Afrika. Daar is gevind dat 'n 75 MW_P operasionele sisteem die sagteware simulasies gedurende die wintermaande gedurende die eerste jaar nadat dit in werking gestel het, ver oortref. Gewoonlik word daar verwag dat simulasie beter sal vaar as sisteme in die praktyk. Om ons doelwitte te bereik is daar 'n aanvanklike opbrengs assessering in PVsyst gedoen en die bevindinge is teen gemete data evalueer. Verskille in werklike en geskatte weerstoestande is vermy deur om stralings waardes en omringende temperature wat op die terrein self gemeet is, te gebruik. Aangesien die verliese in die Psyst model verkeerd geskat is, het die gesimuleerde resultate nie met die gemete energie opbrengs ooreengestem nie. In die simulasie is die werklike sisteme met 'n gemiddeld van 6.4% en 5 % onderskat gebruik van die hooi en Peres model onderskeidelik.

Dit is baie belangrik om die prestasie drywers en verliese binne 'n son FV sisteem te verstaan om sodoende die betroubaarheid en hoë opbrengs van die sisteem te verseker. Weens die oorskatting van verliese in die verstek PVsyst verlies model, is verlieswaardes verkry uit data wat by die aanleg self opgeteken is. Die berekende verlies syfers is toe gebruik om die PVsyst model van die aanleg te verbeter. Nadat gebruik gemaak is van 30-minuut gemiddelde inset data en die verbeterde PVsyst verlies model, is die werklike operasionele sisteem met 'n jaarlikse waarde van 0.78% deur die verbeterde simulasie model, effens onderskat. Seisoenale verskille tussen die gemete en simuleerde energie opbrengs is egter nog-steeds opgemerk. Hierdie veskille is in die winter groter as in die somer en het ooreengestem met die verskille in die gemete en deur die PVsyst geskatte Plane-Of-Array straling.

Weens die seisoenale verskille tussen die verbeterde PVsyst model en die gemete energie opbrengs in die wintermaande, is stralingsmodelle wat die "Plane-Of-Array-straling van Global Horizontal Irradiance skat vir Suid-Afrikaanse toestande ge-evalueer. Die volgende modelle is ge-evalueer: Orgill en Hollands, Erbs, Louche, $Reindl_1$, $Reindl_2$, DISC en Dirint, asook kombinasies van Isotropic, Sandia, Klucher, Hay, Reindl en Perez transposisie modelle. Gebaseer op die wortel van die gemiddelde kwadraat waardes, is die modelle wat die beste presteer die Dirint, Louche en DISC modelle en die transposisie modelle wat in Suid-Afrika die beste presteer is Perez, Reindl en Hay. Op 'n maandelikse basis is simulasies wat met Plane-Of-Array straling gedoen is, binne 2% van die waardes wat in die praktyk opgeteken is. Daar is tot die slotsom gekom dat die keuse van stralingsdata, transposisie en verlies modelle 'n belangrike effek het op lang- sowel as kortstermyn energie voorspellings.

ACKNOWLEDGEMENTS

I would like to express my sincere gratitude to the following people and organisations:

- Dr Arnold Rix, my supervisor,
- Scatec Solar for financial assistance and providing data required in the project,
- My family and good friend, Marecia for the support and encouragement,
- Jesus, the lord for the gift of life.

LIST OF PUBLICATIONS

National conference

- T. Mahachi, A. Rix, "PVsyst model improvement using field data from a 75 MWP solar PV power plant in South Africa," in Proc. 24th SAUPEC, 2B-1,Vereeniging, South Africa, 26-28 January, 2016.

- T. Mahachi, A. Rix, "Comparison of various long term averaged meteorological data sources for a site in South Africa.," submitted to 25th SAUPEC, Stellenbosch, South Africa, January, 2017.

International conference

- T. Mahachi, A. Rix, "Evaluation of Irradiance Decomposition and Transposition Models for a region in South Africa," in Proc. 42nd IEEE IECON, Florence, Italy, 24-27 October, 2016.

Journal article

- Hary Bien Aimé Randriamasinoro, Arnold Johan Rix and Tafara Mahachi, "A Novel Method to Retrieve the Photovoltaic One Diode Model Parameters," to be submitted, October, 2016.

DEDICATIONS

To my mom and dad

CONTENTS

LIST OF FIGURES

LIST OF TABLES

NOMENCLATURE

Abbreviations

AC	Alternating Current
AM	Air Mass
Ambtemp	Ambient temperature
AOI	Angle Of Incidence
ASCII	American Standard Code for Information Interchange
BW	Bid Window
BYD	Build Your Dream
CdTe	Cadmium Telluride
CF	Capacity Factor
CIS	Copper Indium Silinum
CM	Circuit Mismatch
CSP	Concentrated Solar Power
CSV	Comma Separated Values
DC	Direct Current
DHI	Diffuse Horizontal Irradiance
DISC	Direct Insolation Simulation Code
DNI	Direct Normal Irradiance
EQT	Equation Of Time
$E-W$	East-West
FF	Fill Factor
GCR	Ground Cover Ratio
GHI	Global Horizontal Irradiance
GPI	Global Plane Irradiance
GW_P	Gigawatt peak
IAM	Incidence Angle Modifier
ISO	International Organisation of Standardisation
LID	Light Induced Degradation

LST	Local Solar Time
MAD	Mean Absolute Difference
$MAPD$	Mean Absolute Percentage Difference
$MAPE$	Mean Absolute Percentage Error
MBE	Mean Bias Error
MPP	Maximum Power Point
MW_P	Megawatt peak
MWh	Megawatt hour
$NASA$	National Aeronautics and Space Administration
NOD	Number Of Days
$NREL$	National Renewable Energy Laboratory
$N-S$	North-South
POA	Plane Of Array
PR	Performance Ratio
PV	Photovoltaic
$PVGIS$	Photovoltaic Geographical Information System
$REFIT$	Renewable Energy Feed in Tariff
$REIPPPP$	Renewable Energy Independent Power Producer Procurement Program
$RMSE$	Root Mean Square Error
SAM	System Advisor Model
$SAURAN$	South African Universities Radiometric Network
$SODA$	Solar radiation data
STC	Standard Test Conditions ($1000W/m^2$)
TXT	Text file
USA	United States of America
$WindVel$	Wind Velocity

Constants

α	Temperature coefficient for BYD polycrystalline modules (-0.47)	[%/°C]
κ	5.535×10^{-6} for angles in degrees and 1.041 for angles in radians	[-]
G_{sc}	Solar constant (1367)	[W/m^2]

ρ_g	Ground albedo (0.2)	[-]
G_{STC}	Irradiance at standard test conditions (1000)	[W/m^2]
k	Boltzmann's constant $(1.38064852 \times 10^{-23})$	[m^2 kg s^{-2} K^{-1}]
q	Elementary charge $(1.60217662 \times 10^{-19})$	[Coulombs]

Greek Symbols

α_{min}	Minimum Solar elevation angle	[°]
α_s	Solar elevation angle	[°]
δ	Declination angle	[°]
η	Specific bins of clearness	[-]
$\eta_{PV_{max}}$	PV module maximum efficiency	[%]
γ_{Az}	Solar azimuth correction angle	[°]
γ_s	Solar azimuth angle	[°]
G	Global Horizontal Irradiance	[W/m^2]
ω	Hour angle	[hours]
ϕ	Latitude	[°]
θ_{AOI}	Angle of incidence of the sun	[°]
θ_{Az}	Surface azimuth angle	[°]
θ_t	Surface tilt angle	[°]
θ_Z	Solar zenith angle	[°]

Roman Symbols and Variables

A	PV module area	[m^2]
a, b, c	Functions of clearness index	[-]
A_i	Anisotropy index	[-]
alt	Altitude	[m]
b_0	ASHRAE parameter provided by solar PV module manufacturer	[-]
d	Minimum module role spacing	[m]
d'	Module role spacing	[m]
E_{array}	Real array energy	[kWh]
$E_{DC,Ohmic}$	Yearly energy DC Ohmic losses	[kWh]

E_{ideal}	Ideal energy output of a solar PV system	[kWh]
$E_{inverter_{input}}$	Energy at the inverter input terminals	[kWh]
E_{system}	Actual measured grid energy	[kWh]
F	Modulation function, equal to zero when the skies are completely overcast	[-]
F_1	Empirically fitted complex function that represent circumsolar	[-]
F_2	Empirically fitted complex function that represent horizon brightening	[-]
$G_{b,t}$	Direct beam irradiance component in the plane of array	[W/m^2]
$G_{d,t}$	Sky diffuse irradiance component in the plane of array	[W/m^2]
$G_{g,t}$	Ground reflected irradiance in the plane of the array	[W/m^2]
$G_{i,calc}$	Estimated irradiance values	[W/m^2]
$G_{i,meas}$	Measured irradiance values	[W/m^2]
G_b	Direct Beam Irradiance	[W/m^2]
G_d	Diffuse Horizontal Irradiance	[W/m^2]
G_n	Direct Normal Irradiance	[W/m^2]
G_o	Extraterrestrial Irradiance	[W/m^2]
G_t	Plane of Array Irradiance	[W/m^2]
h	Elevation of the module	[m]
I_0	Diode reverse saturation current	[A]
I_{cell}	Solar cell current	[A]
I_d	Diode current	[A]
I_{MP}	Current at maximum power point	[A]
I_p	Transformer primary input current	[A]
I_s	Transformer secondary output current	[A]
I_{SC}	Short circuit current	[A]
I_D	Diffusion current	[A]
I_S	Drift current	[A]
k_{nc}	Polynomial in air mass	[-]
$k_{t'}$	Variation of the clearness index	[-]
k_d	Diffuse fraction	[-]
k_n	Direct beam transmittance	[-]
k_t	Clearness index	[-]

l	Width of the module	[m]
lon_{act}	Actual latitude	[°]
lon_{ref}	Reference latitude	[°]
m	Diode ideality factor	[-]
n	Normal	[-]
N_p	Number of turns in the primary winding of a transformer	[-]
N_s	Number of turns in the secondary winding of a transformer	[-]
P_{25}	Temperature corrected output power of a PV array	[kW]
$P_{AC+transf_{loss}}$	Percentage AC Ohmic and transformer power loss	[%]
P_{actual}	Actual power of the solar PV system	[kW]
$P_{DC,Ohmic}$	Percentage DC Ohmic power losses	[%]
P_{grid}	ower injected into the grid	[kW]
$P_{inverter_{input}}$	Power at the inverter input terminals	[kW]
$P_{inverter_{loss}}$	Percentage inverter power loss	[%]
$P_{inverter_{output}}$	Power at the inverter output terminals	[kW]
P_{loss}	PV power loss due to temperature	[kW]
$P_{max,array}$	Maximum power output of the total PV array	[kW]
$P_{max,module}$	Maximum power output of the individual solar PV modules	[kW]
P_{MPP}	Maximum power point	[-]
$P_{substation_{input}}$	Substation transformer input power	[kW]
$P_{substation_{loss}}$	Percentage substation transformer power loss	[%]
$P_{system_{STC}}$	Rated output power of a solar PV system	[kW]
R	Row width	[m]
R	Actual sun-earth distance according to day of year	[m]
R_{av}	Mean sun-earth distance	[m]
R_p	Parallel resistance	[Ohm]
R_s	Series resistance	[Ohm]
T	Absolute temperature	[K]
T_{dp}	Dew point temperature	[°C]
$T_{mod_{avg}}$	Annually average module temperature during production	[°C]
T_{mod}	Module temperature during production	[°C]

V_{cell}	Solar cell output voltage	[V]
V_d	Voltage across the diode	[V]
V_{MP}	Voltage at maximum power point	[V]
V_{OC}	Open circuit voltage	[V]
V_p	Transformer primary alternating voltage	[V]
V_{rev}	Reverse bias voltage of a solar cell	[V]
V_s	Transformer secondary output voltage	[V]

Subscripts

calc	Calculated
i	i-th data point
meas	Measured
N	Number of items
nom	Nominal
serie	Series

Vectors and Tensors

E	Electric field

CHAPTER 1

INTRODUCTION

1.1 History and background

Edmund Becquerel, a 19 year old French physicist, presented the photovoltaic (PV) effect for the first time in 1839. He achieved this by illuminating a metal electrode in a weak electrolyte solution, causing a voltage to appear [1]. The photovoltaic effect in solids was studied for the first time by Adams and Day almost 40 years later and they managed to build selenium-based cells with efficiencies of 1% to 2% [1]. In 1904 Albert Einstein published the theoretical explanation of the photovoltaic effect. The first generation of single crystal silicon-based cells were introduced in the 1940s by a Polish scientist, Czochralski, and there were several attempts to commercialise PV in the 1950s but the cost was prohibitive [1]. In 1958 PV emerged as a practical source of energy when it was used in space for the Vanguard 1 satellite [1]. A relatively cheaper cell designed from a poorer grade of silicon was introduced in the 1970s by Elliot Berman. In the 1980s large utility scale PV systems appeared and PV began to be used in many terrestrial applications that were off-grid, like highway lights, small home systems, calculators, signs, etc. In 1984 ARCO Solar introduced the first amorphous silicon module and in 1986 they introduced the first commercial thin film PV module. In the 1990s the cost of PV dropped whilst the efficiencies of cells increased to 20%, which catalysed the growth of PV and by 2002 the worldwide PV production was increasing by 20% per year, making it a fast growing energy technology [2]. According to research done by Fraunhofer, for the last 35 years, each time the cumulative production doubled, the price went down by 19.1%, as shown in Figure 1.1 [3]. Consequently, the price of PV is now comparable to that of fossil fuels. Vast Mega-Watt projects exist now and some of them will be described in the section to follow.

1.2 Solar PV

Fossil fuels (oil, coal or gas) are the main sources of energy worldwide and their use causes greenhouse gas emissions into the atmosphere, thereby contributing to global warming. Other sources of energy like nuclear energy may release carbon in smaller amounts but their radioactive waste poses danger to the environment since it remains active over thousands of years. Due to the increase in energy demand, fossil fuels reserves are decreasing. This calls for the use

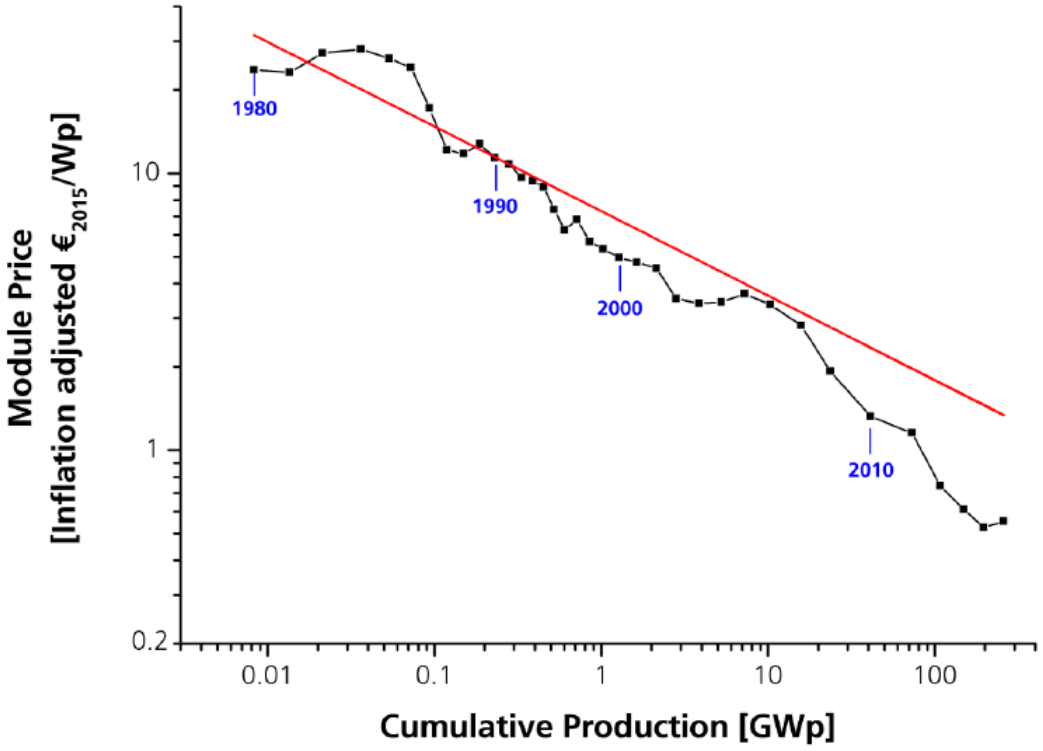

Figure 1.1: Historical change of PV module pricing from 1980 to 2015 [3].

of viable alternative renewable and sustainable sources of energy such as wind, solar, tides, geothermal heat energy etc. Of these, solar energy is most readily available globally.

Solar energy is harnessed from sunlight and it has little or no harmful effects on the environment. Solar PV also avoids the emissions of carbon dioxide into the atmosphere and low maintenance is required. As a result, solar energy has received much attention in recent times and increasing numbers of large scale solar PV plants are being constructed [4]. Due to the abundance of sunlight, especially in Africa, solar energy is thought to be a promising renewable energy source for the future [5].

The solar PV industry also creates employment opportunities especially during the installing stage. However, this technology requires a high initial investment in order to be implemented, though little additional investment is required after installing the solar PV system.

1.2.1 Solar PV worldwide

The global cumulative PV installation up until 2015 is as shown in Figure 1.2. At the end of 2015, the total cumulative installations amounted to 242 GW_P and the percentages by region of the total global installations (including off-grid systems) is 21% for China, 16% for Germany,

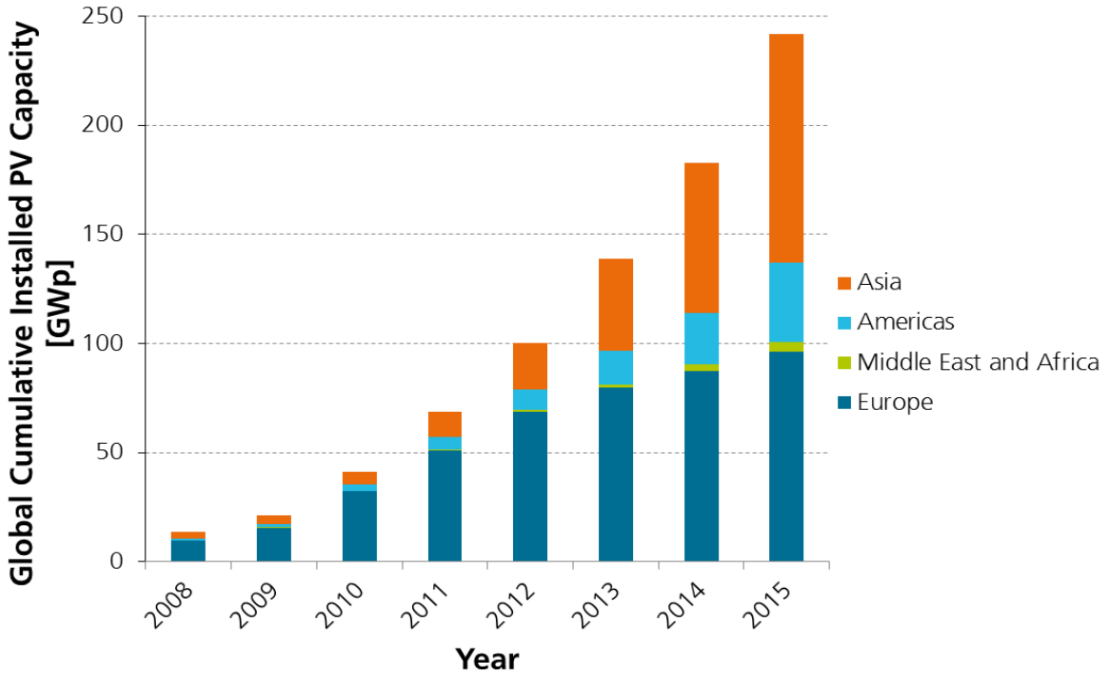

Figure 1.2: Global cumulative PV installation until 2015 [3].

8% for Italy, 16% for Rest of Europe, 14% for Japan, 13% for North America and 12% for rest of world. The global capacity of solar PV is expected to reach the GW-range by the mid-twenty first century, due to the expansion of the MW-range solar PV systems [2]. As of September 2016, the world's largest solar PV power station is the 850 MW_P Longyangxia Dam Solar Park which was installed in two phases, with the first phase (320 MW_P) completed in 2013 and the second phase (530 MW_P) completed in 2015.

1.2.2 Solar PV in SA

Due to the demand for electricity slowly eclipsing the supply and the need to reduce the greenhouse gas emissions, solar PV is amongst the most viable alternative sources of renewable and sustainable energy under scrutiny. South Africa's energy needs could be met by fully exploring the pollution free and virtually limitless solar resource abundant throughout the country. As shown in Figure 1.3, South Africa receive high levels of solar radiation, with most areas averaging more than 2000 kWh/m^2 annually though it relies mostly on coal as the source of electrical energy. However, extensive efforts are being made to reduce the country's strong reliance on fossil fuels and the government set a target to purchase 10% of its electricity from renewable sources by the year 2020 [7]. In South Africa, megawatt solar PV systems are very new and there is great scope for their development in the future. Solar PV is one of the renewable en-

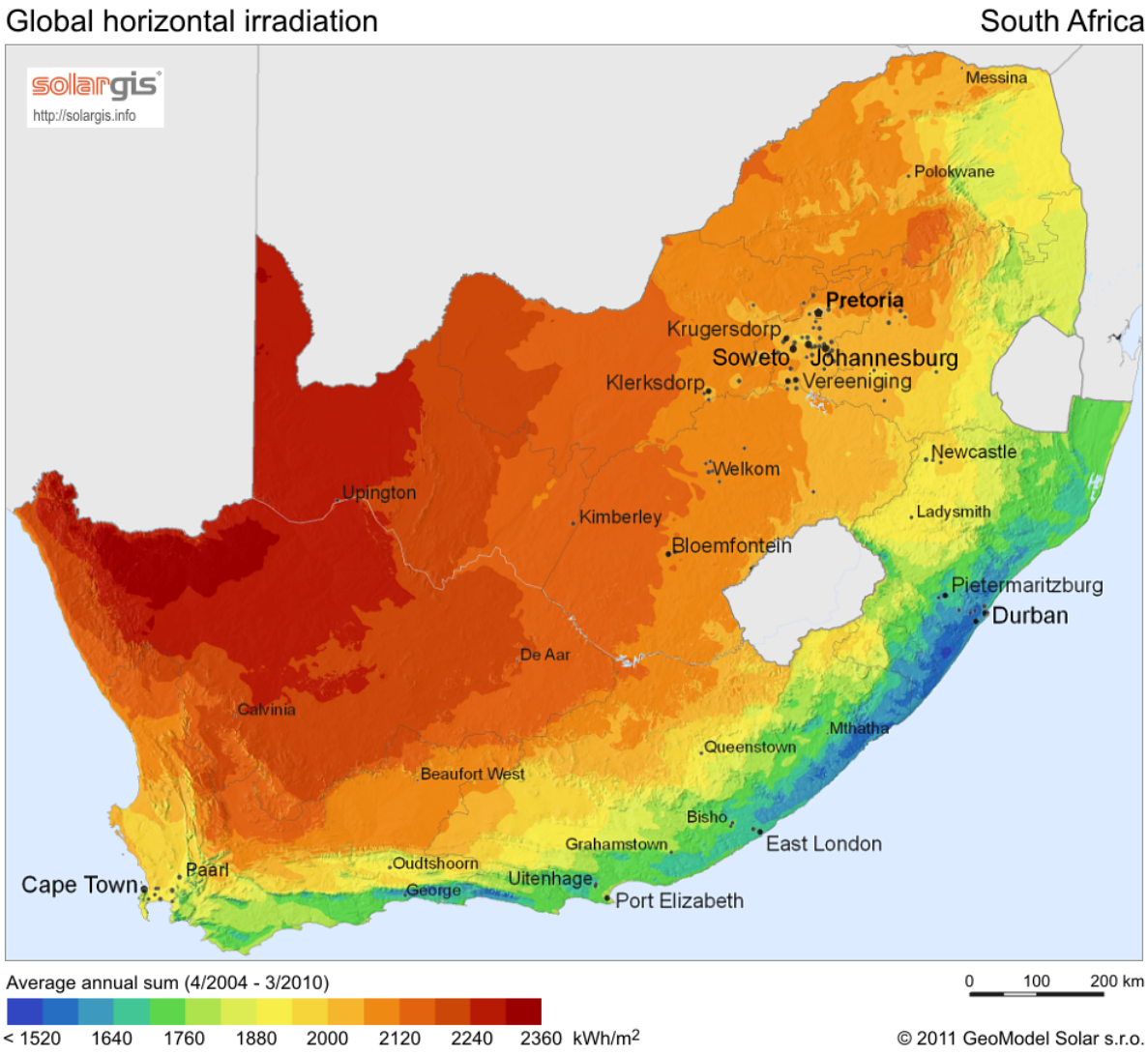

Figure 1.3: Global horizontal data for South Africa [6].

ergy technologies that has attracted investment from independent power producers courtesy of the competitive bidding process called the Renewable Energy Independent Power Producer Procurement Program (REIPPPP) introduced by the government of South Africa on 3 August 2011 [7]. Table 1.1 shows the pricing implemented in five successful bid windows (1, 2, 3, 3.5 and 4) in the first four years of the REIPPPP in South Africa. From the table it can be seen that the REIPPPP is delivering energy at increasingly cost competitive rates as shown by the decreasing renewable price path from bid windows (BW) 1 to 4. The price for solar PV dropped by 75% to ZAR0.82 $/kWh$ between bid window 1 and bid window 4, which is comparable to that of new coal generation [8]. By March 2016, 2.2 GW of the procured capacity was delivering 2.1 GW and this represents 31% towards the 2020 target of 7 GW and also 12% of the 2030 target of 17.8 GW.

Of all the solar PV projects awarded in the first bidding round in South Africa, of interest

is the 75 MW_P Kalkbult solar PV power plant. Completed 3 months ahead of schedule in a record time (January 2013 - September 2013), the fixed tilt, 75 MW_P power plant was the first grid-connected and operational REIPPPP project in South Africa. The data measured at the 75 MW_P solar PV power plant will be used in this study.

In the development stage of a solar PV system, simulation tools are used to forecast its energy yield. In order to realise returns on project investments, it is critical for solar PV plant owners to be certain of the performance in the field. As a result, it is therefore vital for the initial energy yield forecast values of a solar PV system to correlate with the actual performance. However, due to various factors that affect the energy output of a solar PV plant, the simulation results does not always correlate with real world energy output of solar PV systems. Therefore, better simulation models can be developed by investigating on the cause of the differences between simulated and measured energy output of a solar PV plant.

1.3 Project description

1.3.1 Problem statement

The first grid connected solar PV system in South Africa exhibited differences in the initial energy yield assessment and the actual plant performance in its first year of operation, i.e. 2014. Measured energy yield data for the 75 MW_P solar PV plant in South Africa does not correlate with software software simulated values, especially in winter months. Therefore it is necessary to investigate and evaluate the cause of the variances between the measured and software simulated energy yield for the 75 MW_P solar PV plant and then improve the energy simulation model. A detailed analysis and comparison of measured and software-simulated energy production, irradiance decomposition and transposition models is also done.

Table 1.1: Decreasing renewables price path (March 2016) [8].

	BW1 ZAR/kWh	**BW2** ZAR/kWh	**BW3** ZAR/kWh	**BW3.5** ZAR/kWh	**BW4** ZAR/kWh
Solar PV	3.29	1.96	1.05	-	0.82
Solar CSP	3.20	3.00	1.74	1.62	-
Onshore wind	1.36	1.07	0.78	-	0.68
Small hydro	-	1.23	-	-	1.12
Landfill gas	-	-	1.00	-	-
Biomass	-	-	1.49	-	1.45

1.3.2 Goals and Objectives

The focus of study in this thesis is on determining the cause of the differences between the initial energy yield prediction and the measured energy yield for Kalkbult solar PV plant as indicated by the owner, Scatec Solar. After that, recommendations that will improve the energy yield prediction model and therefore minimise the differences in the simulated and measured energy yield for the solar PV power plant will be made. The improved model will enable accurate forecasting of the available generation capacity of the solar PV plant as required by the utility provider.

Energy yield simulation software uses different irradiance models that convert Global Horizontal Irradiance (GHI) into Plane-Of-Array (POA) irradiance and there is no standard combination of irradiance decomposition and transposition models. While there are various irradiance models in use, it is necessary to find those that perform best under South African conditions.

To achieve the overall aim, the objectives in this research are as follow:

- Critically study and understand the simulation software used to predict the energy yield i.e. look for factors that cause uncertainty in energy yield prediction.
- Validate the input meteorological data used in the simulation software as well as the energy yield data monitored at the solar PV plant site.
- Perform a sensitivity analysis to determine the influence of the irradiance equipment uncertainty on the energy yield.
- Perform an initial energy yield assessment using PVsyst simulation software using default loss assumptions and site-recorded input meteo-data (Global Horizontal Irradiance and ambient temperature) according to the PVsyst report in Appendix A.
- Critically evaluate the energy yield simulated results against measured grid energy data.
- Compare, contrast and investigate the variances between the measured and PVsyst simulated energy yield (complete a root cause diagnosis).
- Make recommendations that will improve the energy yield prediction model.
- Perform another energy yield assessment using the improved PVsyst model.
- Simulate irradiance decomposition models that convert GHI to the horizontal beam and diffuse components by modelling in Matlab.

- Evaluate the irradiance decomposition models using statistical methods to find the best performing model under South African weather conditions.
- Simulate irradiance transposition models in combination with the best performing decomposition model by modelling in Matlab.
- Evaluate the combinations of the irradiance transposition models and the best performing decomposition models using statistical methods.
- Draw final conclusions and make recommendations for future work.

1.3.3 Significance of the Research

While this study is limited to a specific time period and location, it indicates the significance of performing proper assessments regarding the implementation of tilted radiation models in predicting energy yield using simulation software. Due to the lack of a standard combination of decomposition and transposition models, empirical validations of the available solar radiation models give modellers and developers confidence that their respective algorithms simulate reality. The findings show the influence of diffuse radiation on the performance of the irradiance transposition models, and the analysis contributes to the enhancement of performance models' accuracy when forecasting the expected energy yield of a solar PV system. Results from this research enable accurate estimation of the available generation capacity of solar PV plants using simulation software like PVsyst. Being certain of performance in the field is critical for system owners to realize returns on project investments.

1.3.4 Thesis Outline

Different methodologies are applied for different objectives in each chapter and also results and findings are discussed in each chapter. The layout of the rest of this thesis is as follows:

Chapter 2: In this chapter, the theory behind solar PV systems is presented. Firstly a discussion of the solar resource is done, followed by an introduction to photovoltaic systems. The convention used to describe the solar position is presented, as well as the physics behind solar PV systems, from a PV cell to the PV array. Various PV technologies and substructure systems or mounting types are presented and finally a description of the PVsyst simulation software package is given.

Chapter 3: In this chapter an overview of the meteorological data used in this study is given and then various Global Horizontal Irradiance (GHI) data sources are evaluated

against the measured GHI data. Then a sensitivity analysis is done to see the influence of the measuring equipment uncertainty on the energy yield.

Chapter 4: In this chapter a year-long energy yield analysis and performance evaluation of the first grid-connected 75 MW_P fixed-axis Kalkbult solar photovoltaic (PV) system in South Africa for the operational year 2014 is presented. Measurements obtained from the currently operating Kalkbult solar PV system are evaluated and compared to PVsyst simulated results.

Chapter 5: The differences between the measured and PVsyst simulated energy yield were concluded to be mostly due to the PVsyst default loss model overestimating the actual losses of Kalkbult solar PV system. So in this chapter, the improvement of the PVsyst loss model using the year long data recorded on the solar PV site in 2014 is described.

Chapter 6: In this chapter the irradiance models that estimate Plane-Of-Array irradiance from Global Horizontal Irradiance measurements are evaluated for South African climatic conditions. This is due to the irradiance models in PVsyst software underestimating the Plane-Of-Array irradiance for the site.

Chapter 7: In this chapter conclusions are drawn from the findings in this research study and recommendations for future research are made.

CHAPTER 2

THEORETICAL BACKGROUND

In this chapter the theory behind solar PV systems is presented. Firstly there is a discussion of the solar resource, followed by an introduction to photovoltaic systems. The convention used to describe the solar position is presented, as well as the physics behind solar PV systems, from a PV cell to the PV array. In addition, various PV technologies and substructure systems or mounting types are presented. Finally a description of the PVsyst software package and how it works is given.

2.1 The solar resource

2.1.1 Solar geometry

The sun's position relative to the observer on the earth's surface is an important input required when modelling PV system performance. The position of the sun is described using the convention shown in Figure 2.1 [1]. In the figure, θ_Z is the zenith angle of the sun, θ_{Az} is the surface azimuth angle, γ_s is the solar azimuth angle, α_s is the solar elevation angle equal to $90° - \theta_Z$, θ_T is the surface tilt angle and θ_{AOI} is the angle of incidence of the sun.

In order to have a clear understanding of the angles in Figure 2.1, the starting point is to define the following parameters [1]:

- The **solar azimuth angle (γ_s)** is the angle of the sun's position relative to the north-south axis.
- The **solar elevation angle (α_s)** is defined as the height of the sun i.e the angle between the local horizon directly under the sun and the centre of the sun's disc. It is expressed using the declination angle (δ) and the local latitude (ϕ) of the site as follows:

$$\alpha_s = 90° - \phi + \delta. \tag{2.1.1}$$

- **Declination angle (δ)** is defined as the angle between the sun and the equator [1]. Its value varies between -23.45° to 23.45° in relation to the day of the year assigned [9]. The declination angle is expressed as follows:

$$\delta = 23.45 sin\left(\frac{360}{365}(284 + NOD)\right), \tag{2.1.2}$$

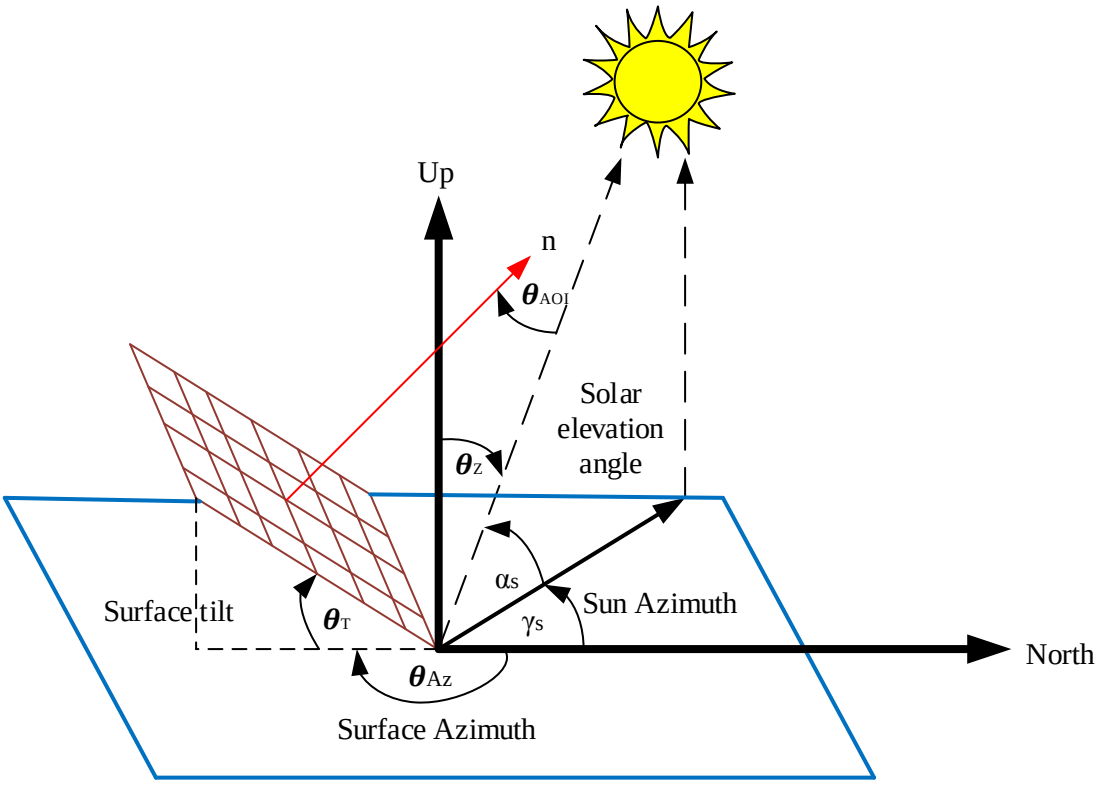

Figure 2.1: Solar position.

where NOD or number of days is the day of year starting from the 1st of January.

- **Local solar time (LST)** is defined as the exact time at the longitude where the observer is positioned and it is expressed as follows:

$$LST = time_h + EQT + \frac{lon_{act} - lon_{ref}}{15}, \tag{2.1.3}$$

where lon_{act} is the actual longitude, lon_{ref} is the reference longitude, and EQT is the **equation of time** which is defined as the difference between the true and mean solar times and it is expressed as follows [9]:

$$EQT = \left[0.123cos\left(\frac{360}{365}(88 + NOD)\right) - 0.167sin\left(\frac{720}{365}(10 + NOD)\right)\right] \tag{2.1.4}$$

and

$$time_h = hour + \frac{minutes}{60} + \frac{seconds}{3600}. \tag{2.1.5}$$

- **Hour angle (ω)** is a measure of the time of any day with respect to the time when the sun is at its highest point in the sky (solar noon) [9]. The hour angle is defined using the **local solar time (LST)** as follows:

$$\omega = (12 - LST) \cdot 15. \tag{2.1.6}$$

- The **zenith angle (θ_Z)** is the angular position of the sun relative to an axis/line perpendicular to the surface of the earth and it is given by:

$$\theta_Z = cos^{-1}\big(cos(\phi)cos(\delta)cos(\omega) + sin(\delta)sin(\phi)\big), \tag{2.1.7}$$

where δ is the declination angle and ϕ is the latitude at a certain location [9].

- **Angle of incidence (θ_{AOI})** is the angle between the sun's beam and the perpendicular projection of the surface (n). The angle of incidence is determined as follows:

$$\theta_{AOI} = cos^{-1}[cos(\theta_Z)cos(\theta_T) + sin(\theta_Z)sin(\theta_T)cos(\gamma_s - \theta_{Az})], \tag{2.1.8}$$

where θ_Z is the zenith angle of the sun, θ_T is the surface tilt angle, γ_s is the azimuth angle of the sun and θ_{Az} is the surface azimuth angle.

- **Absolute air mass (AM_a)** is the relative measure of the atmosphere's optical length, which is simply approximated as follows:

$$AM = \frac{1}{cos(\theta_Z)} = sec(\theta_Z). \tag{2.1.9}$$

The air mass approximation is fairly accurate for zenith angles less than 80°, so when the sun is close to the horizon more accurate and complex models are warranted [10]. The actual air mass (AM_{actual}) at a certain altitude (alt) is obtained as follows [9]:

$$AM_{actual} = \frac{e^{-0.0001184 \cdot alt}}{cos(\theta_Z) + 0.5057(96.08 - \theta_Z)^{-1.634}}. \tag{2.1.10}$$

At sea level, the air mass is equal to 1 when ($\theta_Z = 0$) i.e. when the sun is directly overhead. Air mass increases as the path of direct sunlight through the atmosphere becomes longer, i.e. when the zenith angle becomes larger. On the other hand, the thickness of the atmosphere lessens as the land elevation increases and therefore the air mass is reduced.

2.1.2 Irradiation

The solar radiation incident on the PV cell or module is the beginning point for electrical energy generation. Irradiance is defined as the instantaneous solar power measurement over some area and it is measured in W/m^2 [10]. Whereas insolation is a measurement of the amount of solar energy cumulated on a surface area within a period of time.

2.1.2.1 Extraterrestrial radiation

Solar radiation is composed of many wavelengths (λ) that carry different amounts of energy. About 98% of the solar radiation is carried by waves with lengths of $0.3 \leq \lambda \leq 3\ \mu m$. Figure 2.2

shows the spectral extraterrestrial radiation for the ultraviolet, visible and infrared waves in the ($\lambda < 0.38\ \mu m$), ($0.38\ \mu m < \lambda < 0.78\ \mu m$) and ($\lambda > 0.78\ \mu m$) regions, respectively. The ultraviolet region contains about 6.5% of the total energy, whereas the visible region contains anther 47.9% and the infrared contains the remaining 45.6% of the total energy.

Figure 2.3 shows the extraterrestrial irradiation (G_o) or the intensity of the sun incident on a surface tangent to the top of the Earth's atmosphere. The extraterrestrial irradiation is expressed on a plane that is normal to the sun in W/m^2 and its value changes throughout the year according to the sun-earth distance that varies predictably during the year due to the elliptical orbit of the earth [10]. The extraterrestrial irradiation can be empirically represented by the equations that follow:

$$G_o = G_{sc} \cdot \left(\frac{R_{av}}{R}\right)^2, \tag{2.1.11}$$

$$\left(\frac{R_{av}}{R}\right)^2 = 1.00011 + 0.034221cos(b) + 0.00128sin(b) + 0.000719cos(2b) + 0.000077sin(2b), \tag{2.1.12}$$

where G_{sc} is the solar constant, equal to 1367 W/m^2, R is the actual sun-earth distance according to the day of the year, R_{av} is the mean sun-earth distance, $b = 2\pi\frac{DOY}{365}$ radians and DOY is the day of the year, given as an integer.

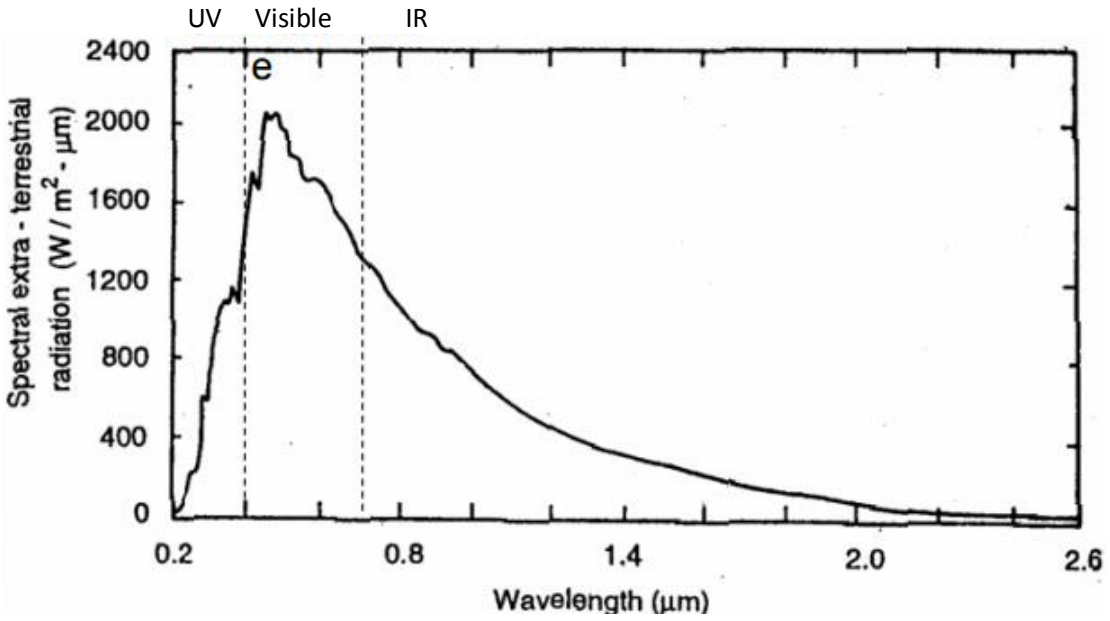

Figure 2.2: Spectral extraterrestrial radiation [1].

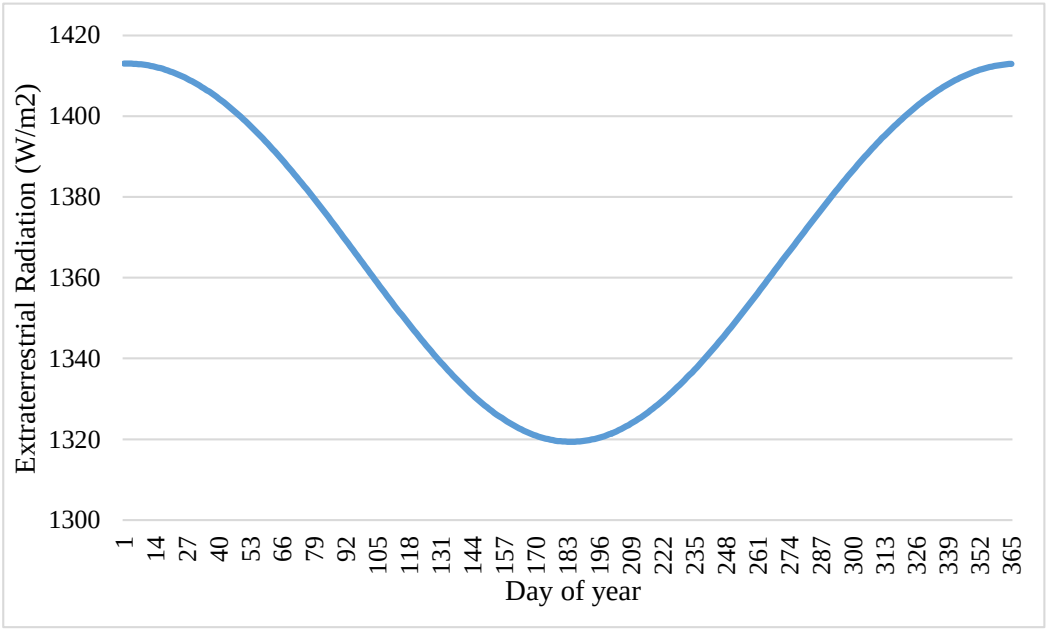

Figure 2.3: Annual variation in extraterrestrial radiation.

2.1.2.2 Global Horizontal Irradiance (GHI)

Global Horizontal Irradiance (GHI) is the amount of terrestrial irradiance that reaches a surface horizontal to the surface of the earth. It can be measured with a variety of instruments like pyranometers and PV reference cells which will be discussed in Chapter 3. If the Global Horizontal Irradiance (G) cannot be directly measured, it can be computed from the diffuse horizontal irradiance (G_d) and direct normal irradiance (G_n) using the equation that follows:

$$G = G_d + G_n cos(\theta_Z), \tag{2.1.13}$$

where θ_Z is the sun zenith angle.

Diffuse Horizontal Irradiance (DHI) is the terrestrial irradiance scattered by the atmosphere and received by a horizontal surface as shown in Figure 2.4. It is typically measured with a pyranometer, by blocking the beam component of the radiation and if not measured, it can be calculated according to Equation 2.1.13. Direct Normal Irradiance (DNI) comes from the beam of the sun as shown in Figure 2.4 and can be directly measured using a pyrheliometer [10]. DNI can be calculated according to Equation 2.1.13 but if diffuse and global radiation measurements are not available, models are used to estimate it and these models will be discussed in Chapter 6.

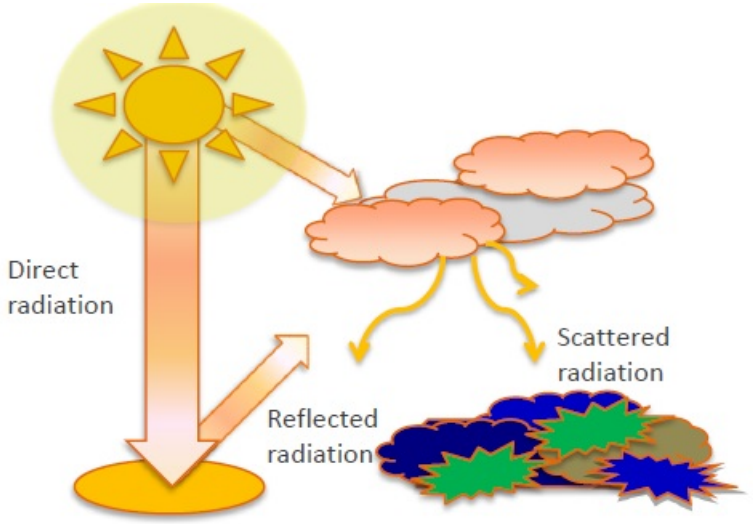

Figure 2.4: Direct, reflected and diffuse radiation.

2.1.2.3 Plane-Of-Array (POA) irradiance

In general, solar applications are tilted to a certain optimum angle so as to maximise the output energy yield. Therefore it is necessary to determine the inclined surface incident irradiation from the horizontal measurement. The Plane-Of-Array irradiance (G_t) is determined as follows [10]:

$$G_t = G_{b,t} + G_{g,t} + G_{d,t}, \tag{2.1.14}$$

where $G_{b,t}$ is the direct beam irradiance component in the plane of array, $G_{g,t}$ is the ground reflected irradiance in the plane of the array and $G_{d,t}$ is the sky diffuse irradiance component in the plane of array. Models that estimate POA irradiance components from GHI will be discussed in Chapter 6. The direct POA beam component is calculated from the DNI values as follows:

$$G_{b,t} = G_n cos(\theta_{AOI}), \tag{2.1.15}$$

where G_n is the direct normal irradiance and θ_{AOI} is the solar angle of incidence on the array surface. The ground reflected diffuse irradiance component is determined as follows:

$$G_{g,t} = G \cdot \rho_g \cdot \frac{1 - cos(\theta_T)}{2}, \tag{2.1.16}$$

where ρ_g is the ground albedo and θ_T is the surface tilt angle.

2.2 Photovoltaic applications

Photovoltaic is a procedure for producing electrical power by making use of semiconductors that exhibit the photovoltaic effect to convert solar radiation into direct current (DC) electricity.

It is of great importance to understand the characteristics of solar cells, modules and arrays in order to begin any research on PV systems. These characteristics are useful in the design, development, energy production and integration of solar PV systems.

2.2.1 Solar cell physics

A solar cell makes use of the photovoltaic effect to convert solar energy directly into electricity. There are various types of solar cells made from different semi-conductor materials. However, the solar cells use the same operating principle. The most common solar cell is made from a semiconductor silicon and it is configured as a p-n junction as shown in Figure 2.5. Semi-conductor materials absorb photons from the sun and this results in the generation of charge carriers that are subsequently separated by a metallurgical junction [1]. Diffusion of electrons from a region of high electron concentration (n-region) to a region of low electron concentration (p-region) occurs in the p-n junction when p- and n-regions are directly adjacent to each other. Similarly, there is the diffusion of holes from the p-region to the n-region as shown in Figure 2.5. A diffusion current I_D is formed from the p-region to the n-region [11]. When the holes diffuse across the p-n junction they recombine with electrons on the n-region. A charge separation is created when negatively charged acceptor ions are uncovered by the flow of holes from the p-region and the positively charged donor ions are also uncovered by the flow of electrons from the n-region. This sets up an electric field (E) that is oriented from the positive charge to the negative charge direction as shown in Figure 2.6 and the electric field inhibits further diffusion of electrons and holes across the p-n junction. A diode is generated across the p-n junction by the established electric field and this promotes charge flow (drift current - I_S). The drift current (I_S) shown in Figure 2.6 goes against and balances out the diffusion current I_D. The space

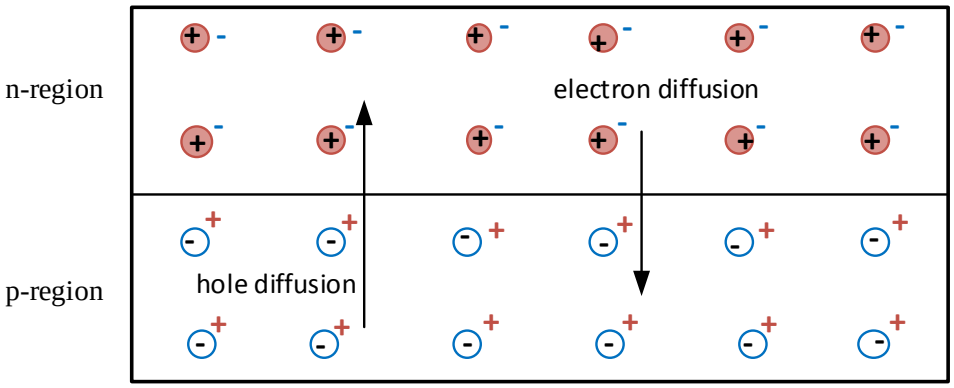

Figure 2.5: Diffusion current I_D from the p-region to the n-region.

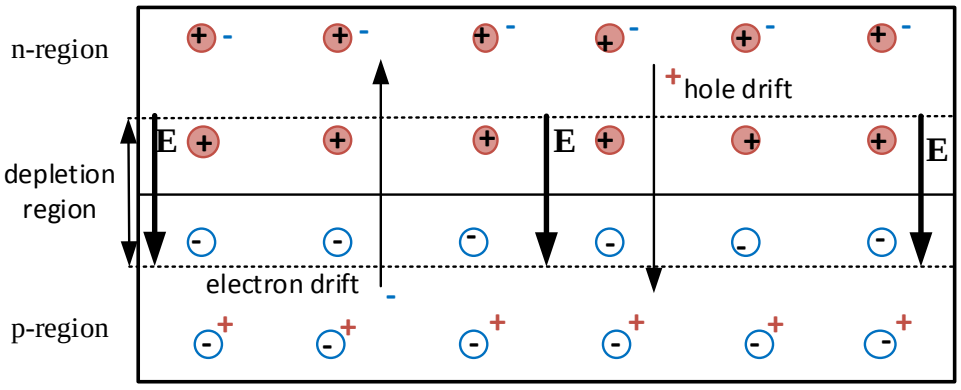

Figure 2.6: Drift current I_S from the n-region to the p-region and the depletion zone.

where holes and electrons have diffused across the p-n junction and where there are essentially no mobile electrons or holes is called the depletion or space charge zone.

As the sun shines, it emits radiant energy in small units called photons. When a light photon that possesses more energy than the band-gap energy hits a solar cell, it is absorbed and an electron is excited from the valence bond of the semiconductor used to make the solar cell [1]. The band-gap in a solid is the energy range where no electron states exist. As the electron gains energy from the photon, it breaks free from its usual position related with its atom and leaves behind a localized hole [11]. As the charge carriers reach the depletion zone, the electric field pushes the electrons into the n-region and sweeps the holes into the p-region, creating a photo-generated drift current. As a result, the holes accumulate in the p-region and electrons occupy the n-region as shown in Figure 2.7, which then creates a potential difference that can be used to drive the photo-generated current to a load [11]. Concurrently the potential difference that results from the photovoltaic effect causes a reduction in the size of the depletion region of the p-n junction, and this results in increased diffusion current through the space charge zone [11]. Hence, when the solar cell is isolated from an external circuit , when the switch shown in Figure 2.7 is in the open position, the photo-generated voltage causes the diffusion current and the drift current to eventually reach equilibrium inside the solar cell.

2.2.2 Equivalent solar cell model

When the switch shown in Figure 2.7 is closed and a solar cell is integrated to an external circuit, the photogenerated current flows from the p-region, through the wire to the load and carries on until it reaches the n-region. The power from a solar cell that is transmitted to the load under a certain sunlight illumination relies on the external potential difference applied to

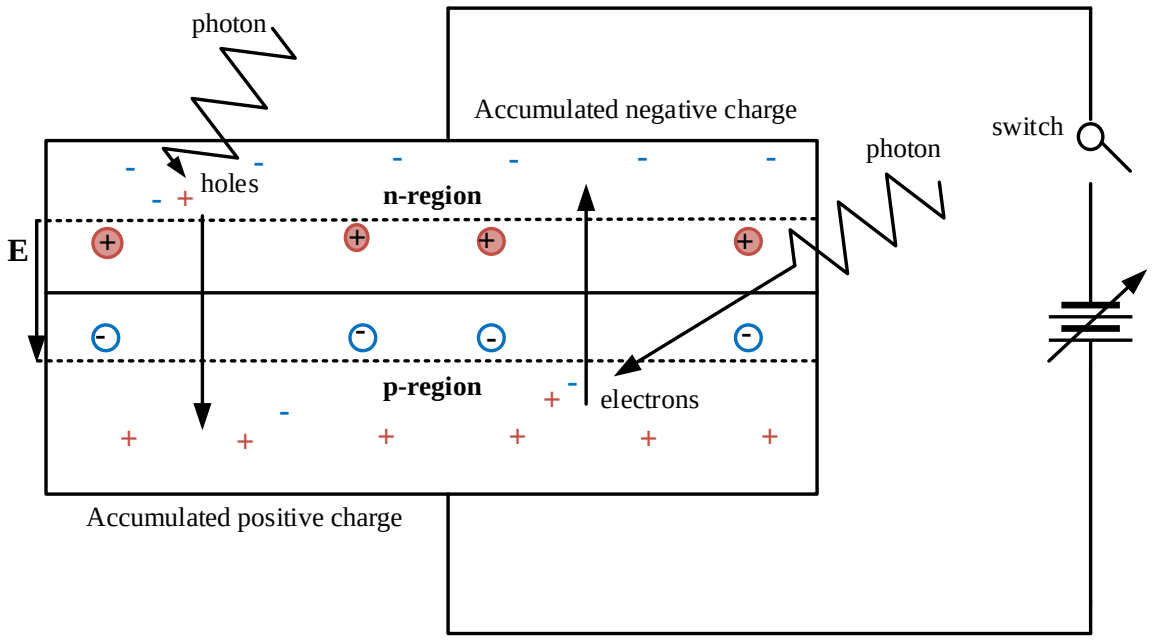

Figure 2.7: Illustration of the drift current, photo-generated voltage and current.

the solar cell, and in grid-connected systems this voltage is normally applied through a power electronic converter. The ideal model of a solar cell consists of a current source representing the photogenerated current (I_{SC}), in parallel with a diode, representing the p-n junction of a solar cell. Other effects, not accounted for by the ideal diode model exist in real solar cells. These are the losses of the semiconductor itself and the leakage current that is proportional to the solar cell's terminal voltage. The former effect is represented by a series resistance R_S and the latter effect is characterised by a parallel resistance R_P, as shown in Figure 2.8. The mathematical model of a solar cell is expressed as follows [1]:

$$I_{cell} = I_{SC} - I_d = I_{SC} - I_0\left[e^{\left(\frac{qV_d}{mkT}\right)} - 1\right] - \frac{V_d}{R_P} \tag{2.2.1}$$

and

$$V_{cell} = V_d - I_{cell}R_S, \tag{2.2.2}$$

where, I_{cell} is the cell output current which is proportional to the illumination intensity of sunlight, I_d is the diode current, I_0 is the diode reverse saturation current which depends on temperature, m is the diode ideality factor with $m = 1$ representing an ideal diode, q is the elementary charge, k is the Boltzmann's constant, T is the absolute temperature and V_{cell} is the output voltage of the cell.

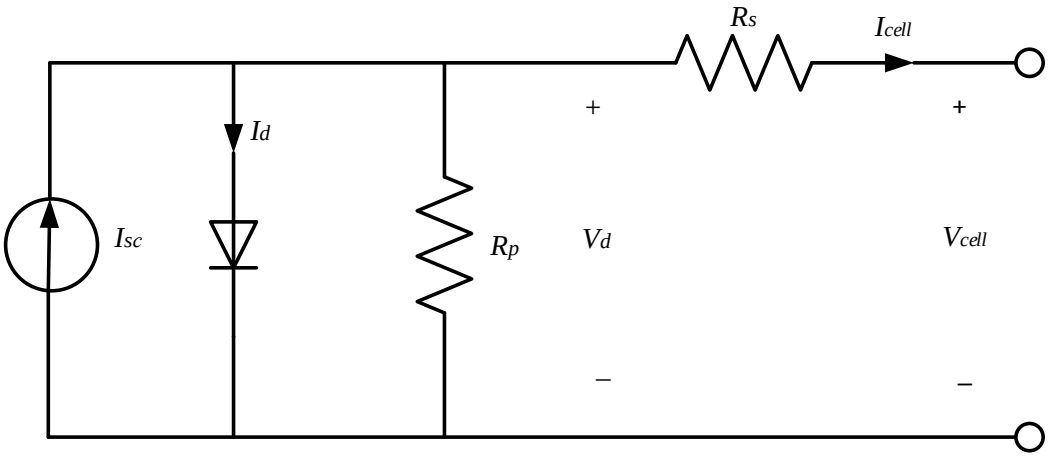

Figure 2.8: Solar cell equivalent model.

2.2.3 From cells to modules to arrays

A solar cell produces about 0.5 V, so it is rare to have an application for which an individual cell is of any sensible use [1]. However, solar photovoltaic cells can be connected in series to create modules or PV panels in order to produce more power. For example, a few years ago 36 cells were connected in series and the modules were designated as 12 V modules. The module voltage V_{module}, from cells wired in series is obtained by multiplying Equation 2.2.2 by the total number of cells (n) in the module as follows [1]:

$$V_{module} = n \cdot (V_d - IR_S). \tag{2.2.3}$$

Thus a module serves as the basic building block for solar PV applications. Multiple solar PV modules can be wired in parallel to raise the current and in series to raise the voltage. Such module combinations yield high power and are known as arrays. The I-V curves of the modules are simply summed up along the voltage axis for a string of modules in series. For modules in parallel, the sum of the individual module currents amounts to the total current and the voltage is the same across each module [1]. Multiple strings (modules in series) can also be combined into a large array. Figure 2.9 shows the differences between cells, modules and arrays.

2.2.4 PV I-V curve

Solar irradiance, shading and ambient temperature all have impact on the PV I-V curves and their effects on the I-V curve are discussed in this section.

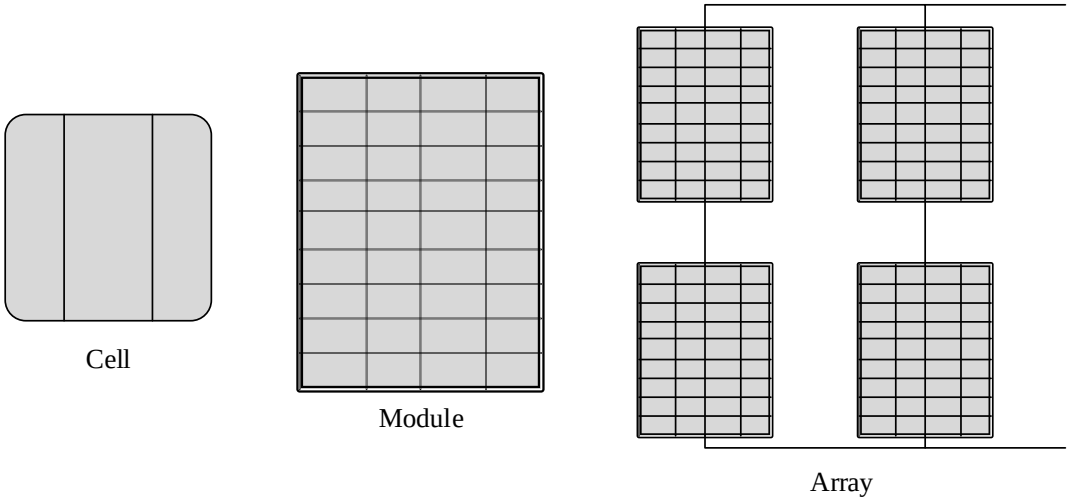

Figure 2.9: Photovoltaic cells, modules and arrays.

2.2.4.1 Maximum power point (P_{MPP})

The important characteristics of a solar cell are the output power P_{cell} and current I_{cell} versus the output voltage V_{cell} characteristics. The I-V charcteristics describe the behaviour of a solar cell or PV module under irradiance level and ambient temperature conditions in steady state cases. Figure 2.10 shows the I-V and P-V characteristics of a solar PV module. The significant parameters are: short circuit current I_{SC}, open circuit voltage V_{OC} and the maximum power point MPP. The MPP given by ($P_{MPP} = I_{MP} \cdot V_{MP}$) represents a maximum point corresponding to the maximum producible power and it defines an area covered by the largest rectangle for any point on the I-V curve.

2.2.4.2 Impacts of Irradiance on the I-V curve of a module

Photovoltaic output power relies significantly on the incident irradiance. This is due to the fact that the irradiance is linearly proportional to the short circuit current I_{SC} of a PV module, while the open circuit voltage V_{OC} of a PV module varies only slightly in an exponential manner with the intensity of solar radiation [9]. In Figure 2.11 the relation between the incident irradiance and the PV current and voltage of a BYD 240 P6-30 PV module is shown.

2.2.4.3 Impacts of temperature on the I-V curve of a module

Module temperature largely depends on the ambient temperature. When the module temperature increases more than the Standard Test Conditions (STC) temperature, the short circuit current of a module increases slightly. STC is defined as the solar radiation G of 1000 W/m^2, a

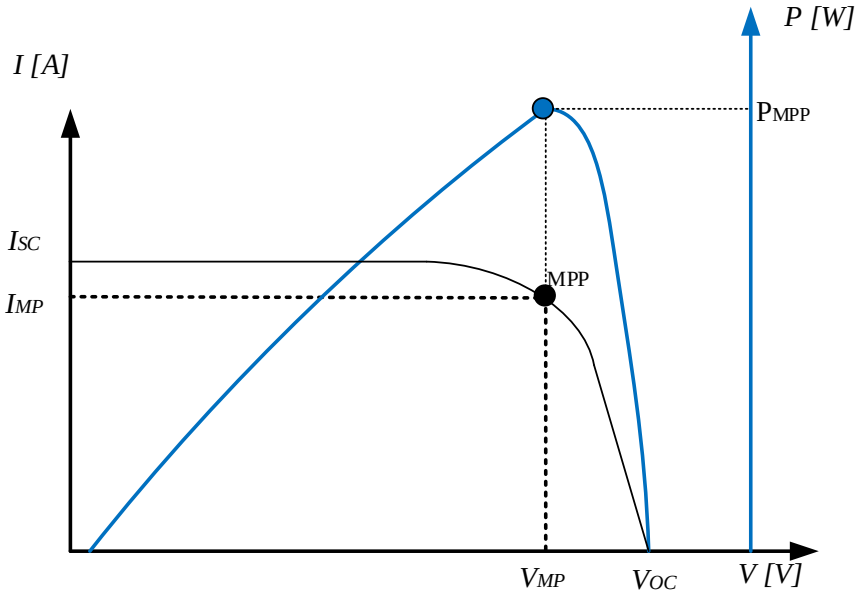

Figure 2.10: I-V and P-V characteristic curves of a solar PV module.

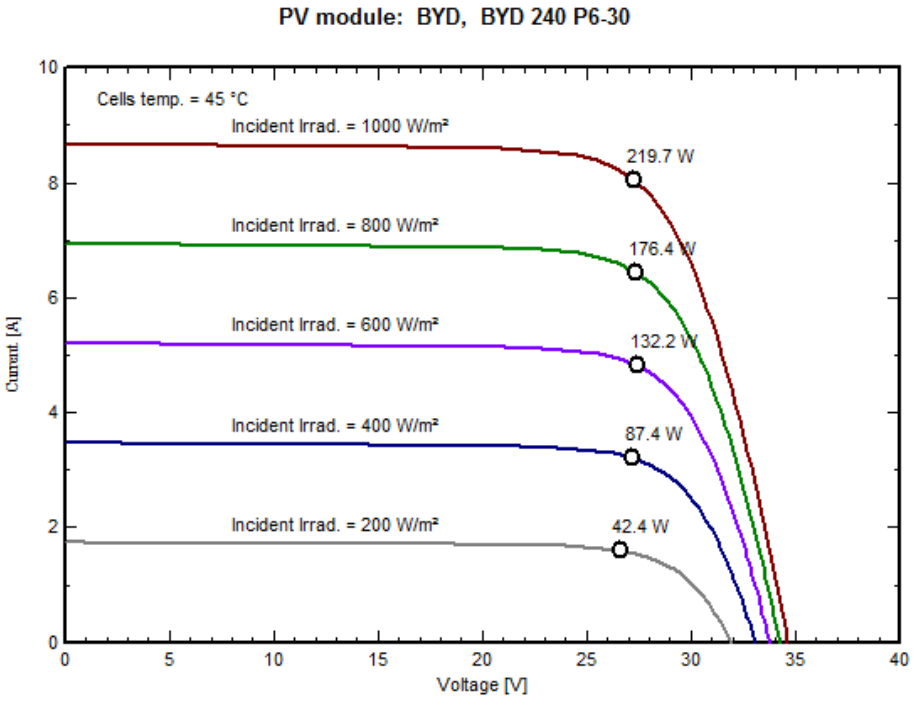

Figure 2.11: Impacts of the incident irradiance on the PV module's current and voltage.

module temperature of 25 °C and an air mass (AM) of 1.5. However, the open circuit voltage is strongly affected when the module temperature exceeds 25 °C. In other words, the decreas-

ing voltage is proportionally higher than the increasing current, thus the PV output power is reduced. Figure 2.12 describes the relation between the current and voltage of a BYD 240 P6-30 PV module and the temperature.

2.2.4.4 Shading impacts on the I-V curve of a module

Shading is amongst the most significant causes of losses in a solar PV system. Losses due to shading depends on the module type (placement of bypass diode, fill factor), the severity of shade and also the string configuration [12]. If there is one shaded module in a string, then the whole string underperforms since current is continuous in the PV string. A shaded cell/module has reduced I_{SC} as shown in Figure 2.13 and for current to continue flowing, the shaded cell has to operate in reverse bias near V_{rev} [12]. There are many different types of shading and the main ones are: horizon shading caused by structures faraway, nearby shading caused by obstructions like telephone poles or trees and self shading from adjacent solar PV rows. Some of the shading types are easier to model and quantify than others. To minimise losses due to shading, the best solution is to avoid partial shading wherever possible. However, there are a couple of technical solutions to the problem of shading, like having one inverter per module or making use of the inverter to find a new maximum power point. Special blocking and bypass

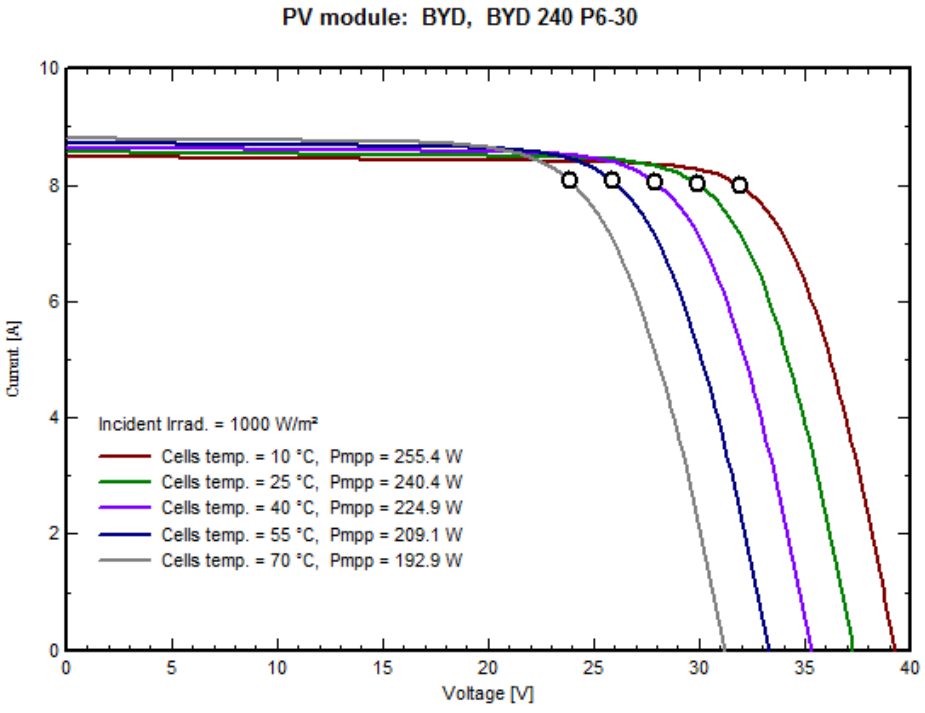

Figure 2.12: Impacts of temperature on the PV module's current and voltage.

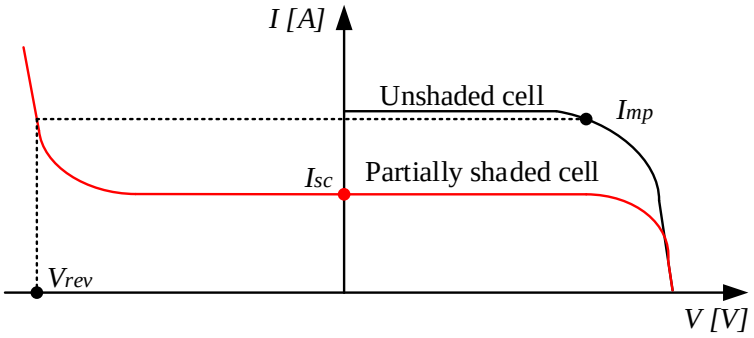

Figure 2.13: Full I-V curve of a partially shaded cell.

diodes that allow current flow around shaded cells are also used as shade mitigation measures [1]. The bypass diode operation is shown in Figure 2.14 and shading analysis will be covered in detail in the chapters to follow.

2.2.5 Fill factor (FF) and module efficiency (η_{PV})

The fill factor represents the ratio of the maximum obtainable power (i.e. area of the largest rectangle which fits in the I-V curve as shown in Figure 2.10) to the product of the short circuit current I_{SC} and the open circuit voltage V_{OC} of a PV module. Its importance is linked with the output power, the higher the fill factor the higher the output of a PV cell/module [9]. The values of the fill factor usually determine the quality of a particular solar cell and the ideal FF value is 1. However, solar cells with FF values greater than 0.7 are regarded to be of high

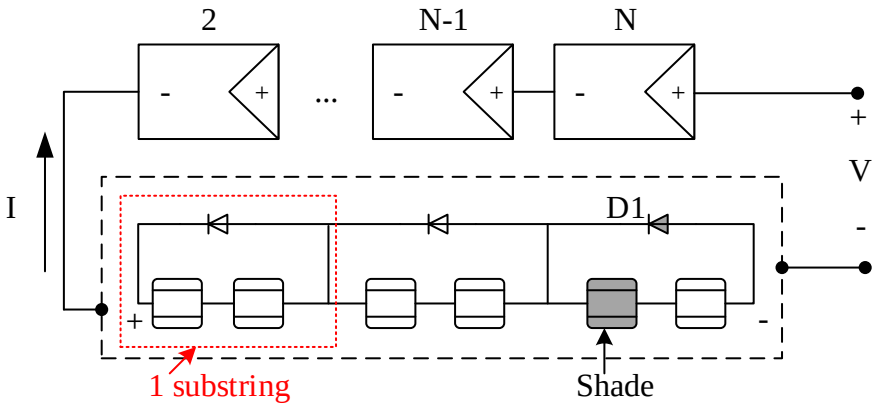

Figure 2.14: Bypass diode operation in PV modules.

quality. The FF is expressed as follows [1]:

$$FF = \frac{I_{MP} \cdot V_{MP}}{I_{SC} \cdot V_{OC}}. \tag{2.2.4}$$

PV cell/module efficiency determines the amount of usable electrical power and is related to the module technology and manufacturer. The efficiency is the ability of the module to convert sunlight to electricity and mathematically determines the module's output power per unit area. A PV module's maximum efficiency is expressed as follows [9]:

$$\eta_{PV_{max}} = \frac{I_{MP} \cdot V_{MP}}{G \cdot A} \cdot 100\%, \tag{2.2.5}$$

where A is the PV module area and G is the global radiation which is considered to be 1000 W/m^2 at STC.

2.3 Photovoltaic systems

2.4 PV systems' applications

PV systems are grouped into two main categories, namely stand alone (off-grid) and grid-connected (on-grid) systems. A diesel generator or wind energy can be integrated with stand alone systems to form a hybrid system. The main difference between the two main PV system categories is the energy storage. In off-grid systems the electrical energy produced is stored in batteries whereas the public grid utility is where the excess energy produced from grid connected systems is deposited. Nowadays, grid connected systems are installed more often and incentives are offered by some countries to encourage people to invest in PV systems and reduce green house gas emissions. European countries like Greece and Germany introduced the "feed in tariff" while USA introduced the "net metering" mechanism [9]. PV systems can provide electricity for water pumping, home appliances, villages and various other applications. Figure 2.15 gives an overview of the different PV system applications.

2.4.1 Simplified description of a photovoltaic system

A general representation of a grid-connected solar PV system is shown in Figure 2.16. The most essential components in a grid-connected solar PV system are solar PV modules, inverters and transformers (not necessarily needed but are mainly used at utility scale). These components are described in detail in the sections to follow.

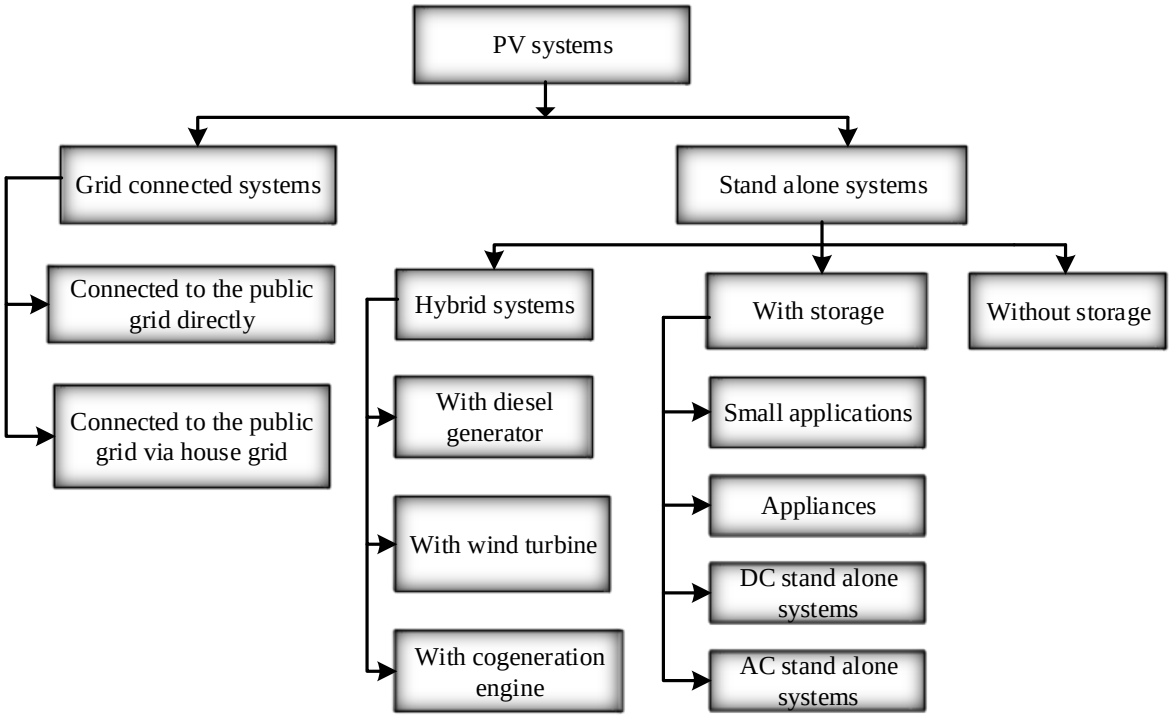

Figure 2.15: PV systems applications.

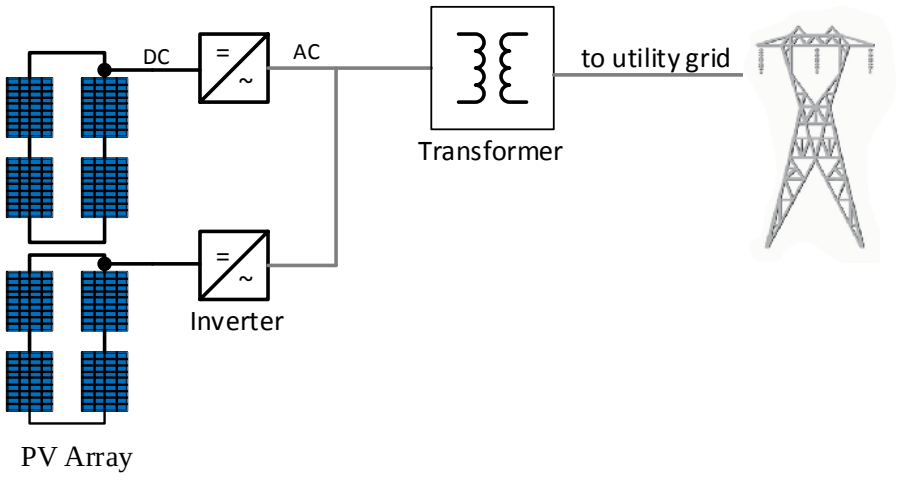

Figure 2.16: Simplified block diagram of a grid connected solar PV system.

2.4.2 Photovoltaic cell/module technology

Photovoltaic modules generate electrical energy from incident sunlight making use of the photovoltaic effect. Single junction PV cell/module technology is separated into two main types, namely: silicon crystalline and thin film technologies. Multi-junction technology is under research to cover the entire incident radiation wavelength and also improve the module efficien-

cies [9]. The choice of a certain technology type depends on different compromises, such as price, efficiency and associated bulk. Figure 2.17 shows the various PV module technologies, i.e. thin film, monocrystalline and polycrystalline modules. In 2015, between 50 and 65 GW_p of PV module production was done, and the annual PV production by technology is as shown in Figure 2.18. The global annual PV production in 2015 was 4.2 GW_P for thin film, 43.9 GW_P for polycrystalline and 15.1 GW_P for monocrystalline [3]. A summary of these PV module technologies follows [13]:

2.4.2.1 Crystalline technology

The most common PV modules available on the market are made of crystalline silicon PV cells. In general, silicon cells are longer lasting and more efficient PV cells than non silicon based cells. In the past decade, the average commercial wafer-based silicon modules' efficiency increased from about 12% to 17% and NREL has a graph with up to date efficiencies [3]. However, at higher operating temperatures their efficiency decreases. Crystalline technology is divided into monocrystalline and polycrystalline as shown in Figure 2.17.

- **Monocrystalline** is the most efficient and oldest PV cells technology and the cells are made from silicon wafers. The cells present very low impurity quantities and the cells are designed in many shapes that include semi-round, round or square bars with thicknesses of 0.2 to 0.3 *mm* [13]. Monocrystalline modules have efficiencies between 15% to 18%, and their colour is dark blue to black and also grey. Monocrystalline silicon modules are the best performing single junction modules up to date and they boast of about 23% efficiency [3]. The record lab cell efficiency for monocrystalline modules is 25.5% [3].

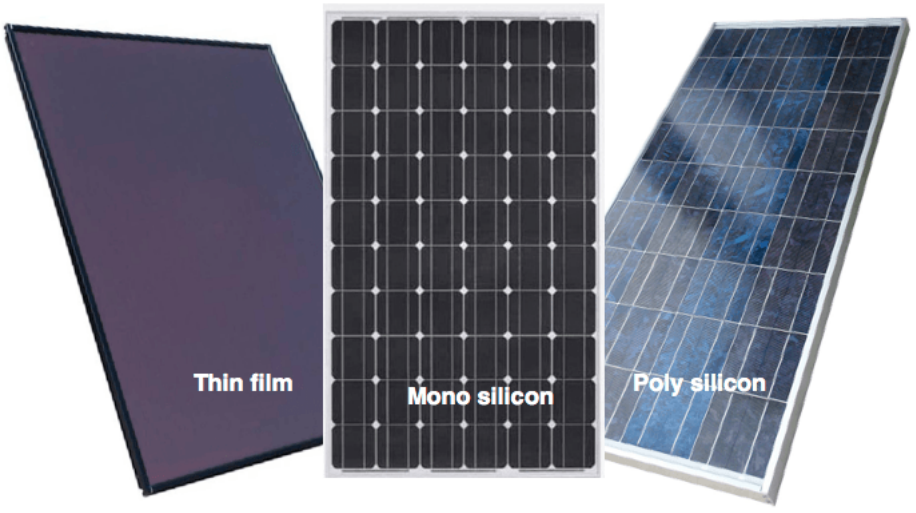

Figure 2.17: Thin film, Monocrystalline and Polycrystalline modules [14].

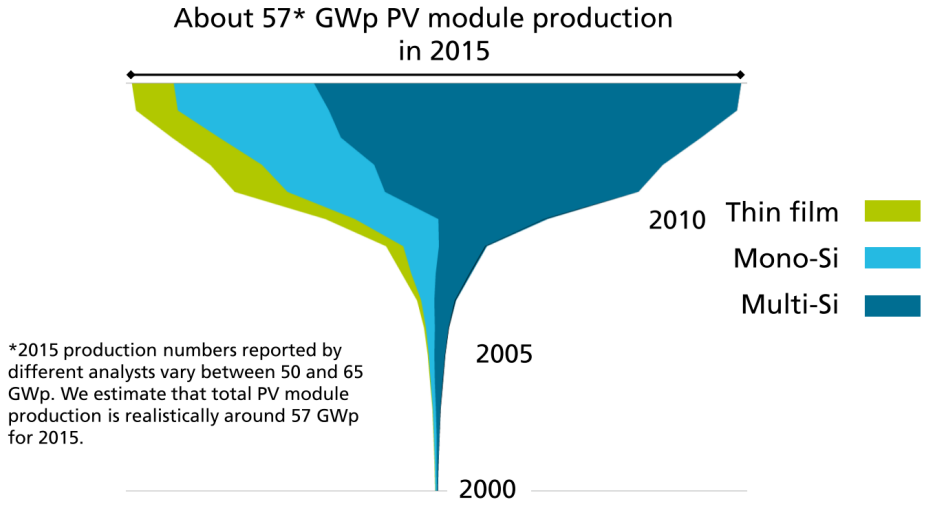

Figure 2.18: Annual PV Production by Technology [3].

However reports have been made of multi-junction solar cells achieving efficiencies of up to 46% and concentrator technology with modules reaching efficiencies of 38.9%.

- **Polycrystalline** modules are made in square forms with thicknesses of 0.24 to 0.3 mm, their efficiencies range from 13% to 16% and are found in blue, silver, brown, green, gold and grey [13]. The record lab cell efficiency for polycrystalline modules is 20.8% [13]. In general, polycrystalline modules are cheaper than monocrystalline modules per unit area though the module structure is similar. Larger square cells are used to increase the efficiency and also lower the cost of polycrystalline modules. However the purity of the polycrystalline cells is lower than that of the monocrystalline cells.

2.4.2.2 Thin film technology

Thin film technology involves the depositing of materials in very thin and consecutive layers of molecules or atoms. The production of thin film modules requires less materials and energy, thus making them less expensive than those produced by the crystalline technology. The lower price comes at the expense of low module efficiency, but nowadays the stability and efficiencies of the thin film models are improving [15]. Cadmium Telluride (CdTe), copper Indium Silinum (CIS) and Amorphous silicon are used as semiconductor materials. Due to the high light absorption of these semiconductor materials, a layer thickness of less than 0.001 mm is theoretically sufficient for incidence irradiance conversion [9]. A few years ago, researchers reported thin film module efficiencies of 5% to 7% for amorphous silicon, 7% to 8.5% for CdTe and 9% to 11% for CIS PV modules [9]. However, findings in a recent study done in Germany

have shown that the highest lab efficiency is 20.5% for CIS and 21% for CdTe thin film solar cells [3]. Unlike crystalline cells, the substrate in thin film cells can be cut to any size, therefore the technology is not limited to standard wafer sizes though the rectangular formats are the most common [9]. Thin film technology is less sensitive to higher operating temperatures, therefore it gives higher energy yield than crystalline technology at certain conditions. Its long narrow strip design makes it less sensitive to shading, unlike in crystalline modules where one shaded cell affects the whole module. Thin film technology also utilises diffuse and low light intensity, better than the crystalline technology [9].

2.4.3 Inverters

An inverter is an essential interface component needed to make a good grid connection. It converts the input direct current (DC) power produced by the PV arrays into output alternating current (AC) power compatible with the grid power quality, voltage and frequency (50 Hz in the case of South Africa) requirements. The inverter permits the transfer of current from the PV arrays to the grid side. In addition, the inverter also provides other functionalities like anti-islanding, where it automatically isolates the power supply from the utility grid i.e. when the grid is not energised. In a conventional grid-connected system, the inverter input terminals (DC side) are connected to the PV arrays while its output terminals (AC side) are connected to the transformers that in turn inject power into the grid, as shown in Figure 2.16. In recent studies, inverter efficiencies for state-of-the art brand products were reported to be 98% and higher [3]. Inverter efficiency depends on the system load and is defined as the ratio between the power delivered by the inverter (power output) and the power supplied to the inverter (power input). Efficiency is higher for loading rates close to the inverter rated power than for low loading rates, therefore the efficiency is not constant [16].

2.4.4 Transformers

A transformer is an essential when the generated electricity is to be injected into the utility grid as depicted in Figure 2.19. It steps up the voltage of the generated alternating current from the inverters, to the distribution network voltage (132 kV in the case of the Kalkbult solar PV plant connection to the power grid in South Africa). Transformers are also used to step down the utility grid voltage to voltages usable in homes (230V in the case of South Africa). In reality the output power of a transformer decreases due to various losses. Since the product of current and voltage is proportional to the electric power, low current levels can be maintained via high voltages for any given power levels, resulting in low (I^2R) losses. In principle the

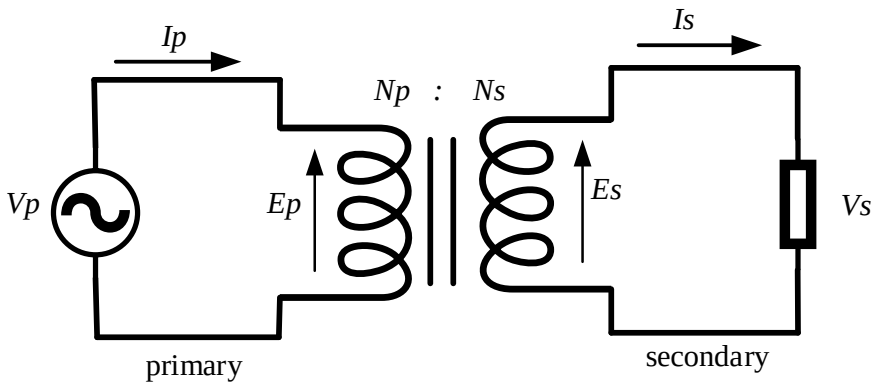

Figure 2.19: Principle of electromagnetic induction in a transformer.

transformer's operation is based on electromagnetic induction. A transformer consists of two or more coils of conductive material wound around a common core of ferromagnetic material [16]. For a two winding transformer, common magnetic flux in the core and magnetic field generated by the varying current in the primary winding connects the primary and secondary coils. An electromotive force (EMF) or voltage is induced in the secondary winding as a result of the varying magnetic field, as shown in Figure 2.19. The number of turns in the primary or secondary coils determines the performance under the voltage [16]. Efficiencies of transformers are usually around 98% and if we consider the ideal case (efficiency = 100%), the following equations can be formulated:

$$\frac{V_p}{V_s} = \frac{I_s}{I_p} = \frac{N_p}{N_s}, \tag{2.4.1}$$

where V_p is the primary alternating voltage, V_s is the secondary output voltage, I_p is the primary input current, I_s is the secondary output current, N_p is the number of turns of the primary winding, and N_s is the number of turns of the secondary winding. The power at the primary side is equal to the power at the secondary side under these circumstances.

2.4.5 Photovoltaic mounting systems

Solar PV modules can be mounted as a fixed type, or as a single or dual axis tracker type. The various mounting types are discussed in the sections to follow:

2.4.5.1 Fixed tilt system

In the fixed type, the PV module is permanently attached to a non-moving surface such as the roof or a ground mounted structure. This type doesn't take into account the sun's direction

at any particular angle though the PV modules are tilted at an optimum angle (rule of thumb: equal to the local latitude angle) as shown in Figure 2.20, to maximise the annual energy production [1]. A slightly higher angle will give more energy yield in winter and vice versa for increased summer energy yield. In the southern hemisphere the PV modules face towards the equator (i.e. North) whereas in the Northern hemisphere the PV modules face south.

2.4.5.2 Single axis tracking system

A single axis tracker consists of a solar PV module rotating around a horizontal or tilted shaft under the action of a DC motor or hydraulic system controlled according to the position of the sun. One way of doing single axis tracking is to estimate the sun's position by means of two light intensity sensors placed on either side of the solar PV module. Either one of the two sensors will be illuminated and the other shadowed depending on the sun rays' intensity. However, the position of the sun can be accurately calculated and then precise tracking of the sun is achieved. There are four ways to do single axis tracking, namely horizontal N-S axis (E-W tracking), horizontal E-W axis (N-S tracking), rotation about a fixed vertical axis and rotation about a polar axis as shown in Figure 2.21 [1]. Single axis tracker's power efficiency is around 25% more than that of the fixed mount, according to simulations done in PVsyst for the Kalkbult site in South Africa. Increased yield for single axis trackers is more pronounced closer to the equator than towards higher latitudes. The disadvantage of single axis trackers is that they only track the movement of the sun in one axis i.e. east to west, whilst the actual motion of the sun is also in the north-south direction, depending on the season.

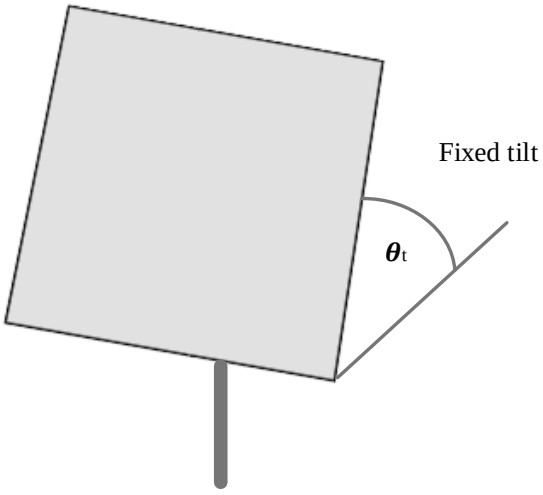

Figure 2.20: Fixed tilt mounting.

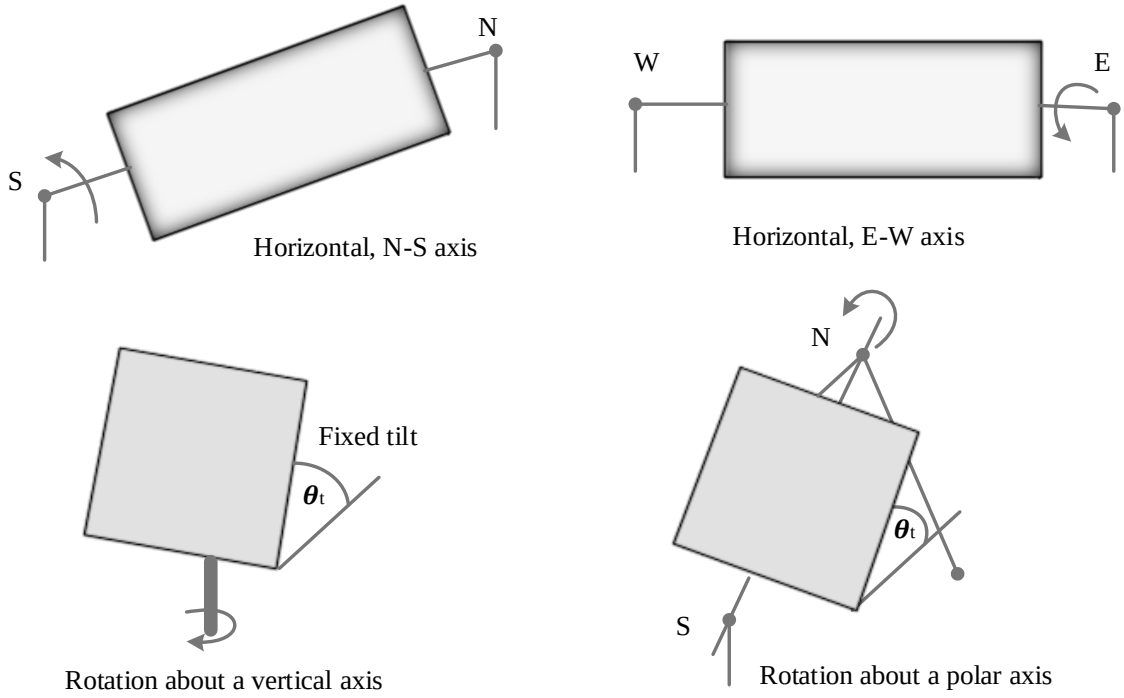

Figure 2.21: Four ways to do single axis tracking.

2.4.5.3 Dual axis tracking system

A dual axis tracking system overcomes the disadvantages of the single axis tracking system. In addition to the east-west tracking, the dual axis tracker also follows the angular height of the sun, thus it measures the horizontal as well as the vertical axis as shown in Figure 2.22 [17]. Thus the movement of the sun is tracked in both the azimuth and altitude angles, as a result, the solar PV modules are always pointing directly to the sun [1]. According to literature, dual axis trackers works well even during cloudy days unlike the single axis trackers that have almost the same efficiency as that of the fixed mount during cloudy days [17]. When simulated in PVsyst, dual axis trackers yield power efficiencies that are 36% more than that of the fixed mount, according to simulations done in PVsyst for the Kalkbult site in South Africa. However they come at a price of lower reliability (more maintenance), higher complexity and are more expensive compared to fixed tilt and single axis tracking systems.

2.5 Modelling in PVsyst

When it comes to predicting the energy yield of a solar PV plant, a number of simulation tools can be utilised. Among them, PVsyst is one of the well known and is recognized for producing reliable energy yield profiles given the right input data [18]. PVsyst software was developed by

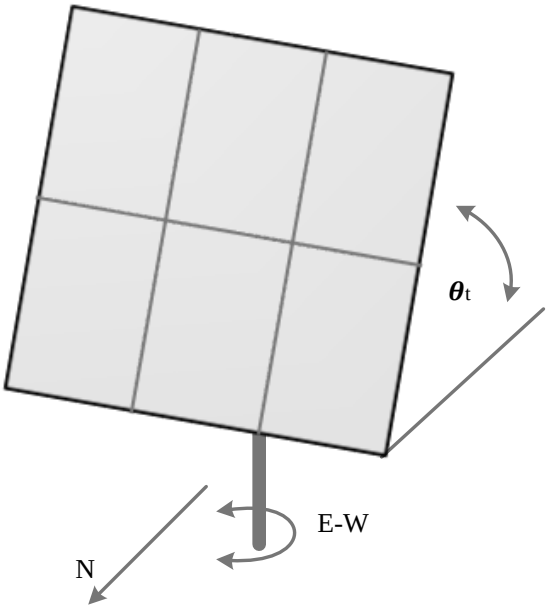

Figure 2.22: Dual axis tracking.

Andre Mermoud in 1992 at the University of Geneva in Switzerland. It is a simulation and planning software for the study, design, sizing and data analysis of solar PV systems [19]. PVsyst calculates the expected energy yield and performance ratio (PR) for an arbitrary location. The more accurate energy yield is as a result of the effects of several parameters customised in PVsyst. The software includes general solar energy tools, extensive PV systems components and meteo databases. A database of solar PV modules and inverters is included and the user can also import data from the PHOTON database [20]. In cases where the device is not in the database, one can define it by using the manufacturer database. PVsyst deals with stand alone, DC-grid, grid connected and pumping PV systems. Apart from yield prediction, the software is a powerful tool for the potential design improvements of solar PV systems. PVsyst is available freely for a 30 day trial after which it will be running in demo mode and in this mode a simulation cannot be run.

PVsyst has various detailed models for solar energy output, however the software also assumes a couple of default parameters and these have to be customised in order to fully simulate the real capabilities of a solar PV system. There are various energy yield simulation software packages and in this study the industry standard PVsyst V6.39 was used [18, 21]. Figure 2.23 describes the simulation process followed in order to calculate the expected energy generated by a solar PV system in PVsyst software. PVsyst offers different levels of PV system study i.e. the preliminary and project design levels, where the former level is the pre-sizing step of

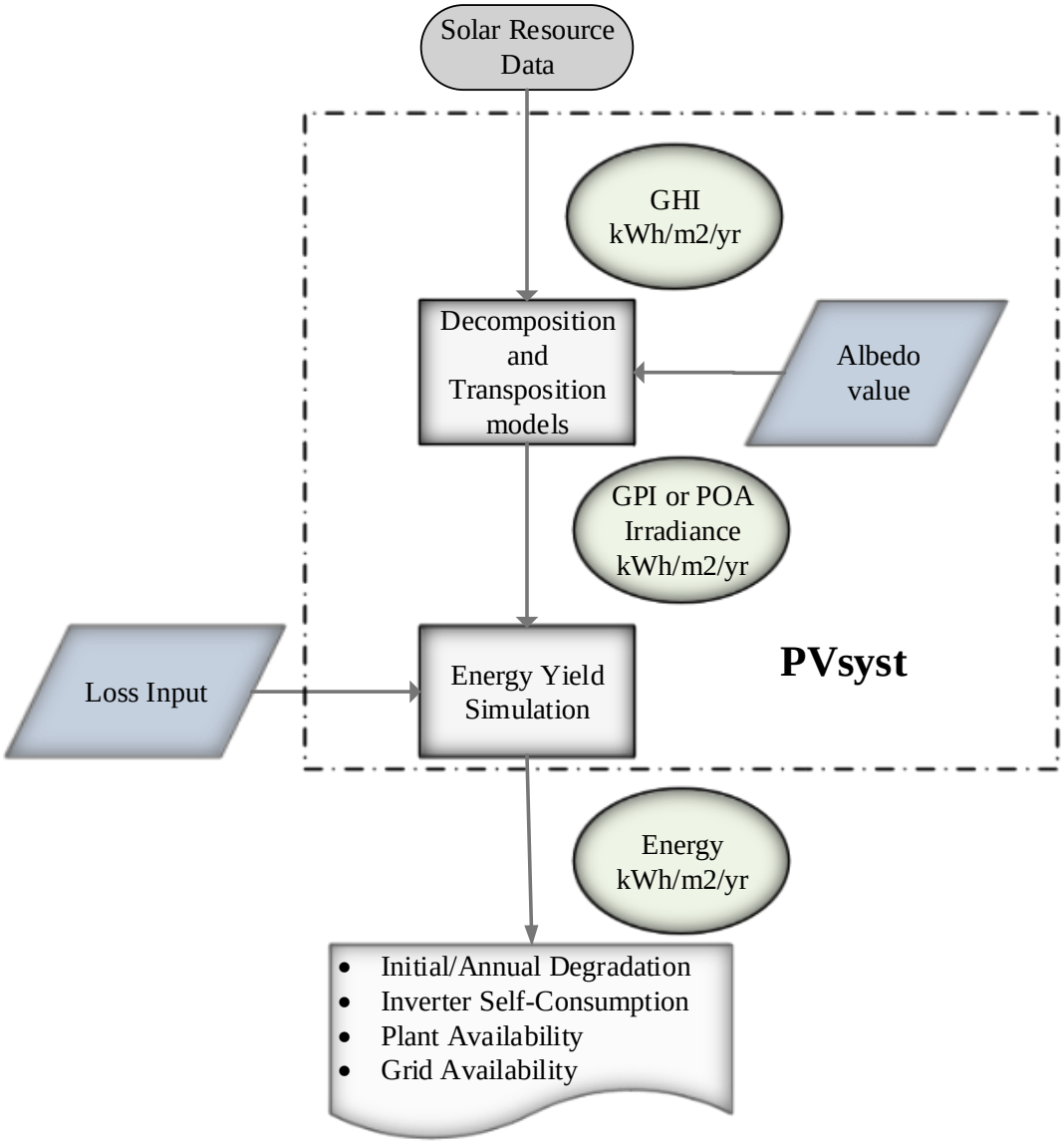

Figure 2.23: The PVsyst simulation process.

a project whereas the latter is where a thorough system design is done using detailed hourly simulations. In order to run a simulation in PVsyst, the user has to define the plane orientation, choose the specific components and the user is assisted in the design of the PV array and inverter sizing.

PVsyst presents the results in the form of a full report [19]. The PVsyst report from which the initial simulation parameters were obtained was done using version 5 of PVsyst whilst in this study version 6 is used. The main differences between the two versions are given in Appendix B. In PVsyst, results can be displayed in hourly, monthly or yearly values and even exported as comma separated values (CSV) file. The results show the energy yield, performance

ratio and specific yield of the simulated solar PV facility. Further, a "Loss Diagram" is displayed and this is useful for identifying the weaknesses of the system design. PVsyst also provides tools for performing a detailed economic evaluation, using real component prices. Included are also some specific tools like graphs and tables of solar geometry parameters or meteo data, a clear sky irradiance model, behaviour of PV array under module mismatch and partial shadings, optimising tools for voltage or orientation, etc [19]. PVsyst makes use of meteo-data from Meteonorm and National Aeronautics and Space Administration (NASA). PVsyst also allows for the importing of meteo-data. Appendix C describes how meteorological data is imported into PVsyst using the "ASCII format" or the "PVsyst standard format". By using site-recorded irradiance and ambient temperatures, the prediction is considered a 'weather normalised' prediction since the discrepancies between actual and estimated weather conditions are avoided [18].

CHAPTER 3

DATASET INTEGRITY AND RELIABILITY

In this chapter an overview of the data used in this study is given and then various Global Horizontal Irradiance (GHI) data sources are evaluated against the measured GHI data using statistical methods. After that a sensitivity analysis is done to see the influence of the measurement equipment's accuracy on the energy yield.

3.1 Introduction

The availability of ground measured solar radiation data is on the rise but the stations are far too few resulting in a too low spatial density. In order to fill the gaps, satellite-derived and interpolated solar radiation products are used as alternatives. Satellite-derived, interpolated and terrestrial model-predicted meteo-values are applied as input in simulation tools to forecast the energy yield of a solar PV plant, when there is no ground measurements situated in the vicinity of the considered site [22]. In the development stage, the irradiation is important to solar PV systems since there is a quasi-linear relationship between the PV output and the solar energy input. Simulation tools give access to various popular sources of meteorological data and this shows that the available meteo-data sources are far from being exact.

Data monitoring in utility scale PV is an essential part of maximising the energy output of solar PV systems, it serves for the comparison of the initial energy yield assessment with the current plant performance and also captures historic production data. The uncertainty in the solar resource can make the difference between loss and profit and that stresses the importance of having a reliable alternative source of data when there are no ground measurements available. Due to the uncertainty and quality issues regarding the various methods implemented by each solar radiation database, there is a need to evaluate the databases against real time measurements so as to have the best alternative source of solar radiation for the region under investigation. The analysis done in this section on existing solar resource databases shows that they possess enough information for the simulation stage of a power plant.

In this chapter, meteo-data measured at Kalkbult solar PV plant is compared to long term averaged and time series meteo-data for specific years. The comparisons are done with the aim

of looking for reliable and most suitable alternative solar radiation sources. The analysis will show how the long term averaged meteo-data represent reality, though inter-year variability of the irradiance is expected.

3.2 Solar PV plant site description

The 75 MW_P, Kalkbult solar PV plant is situated in the Northern Cape region of South Africa at Latitude 30.2° South and Longitude 24.1° East as shown in Figure 3.1. The solar PV plant is around 1200 metres above sea level, located in a semi-arid region with generally high solar radiation. The Kalkbult solar PV plant was the first grid-connected solar PV project to be operational in South Africa as part of the REIPPPP. The Kalkbult site is known to have abundant sunlight with an average of 11.5 daily sunny hours and an average annual solar radiation of 5.8 kWh/m^2 daily. The site has a minimum solar duration of 9.97 hours in June and a maximum solar duration of 13.11 hours in December, as shown in Figure 3.2. As a result, Kalkbult experiences longer solar duration hours during the summer season and shorter solar duration hours during the winter period.

Figure 3.1: Kalbult solar PV plant site.

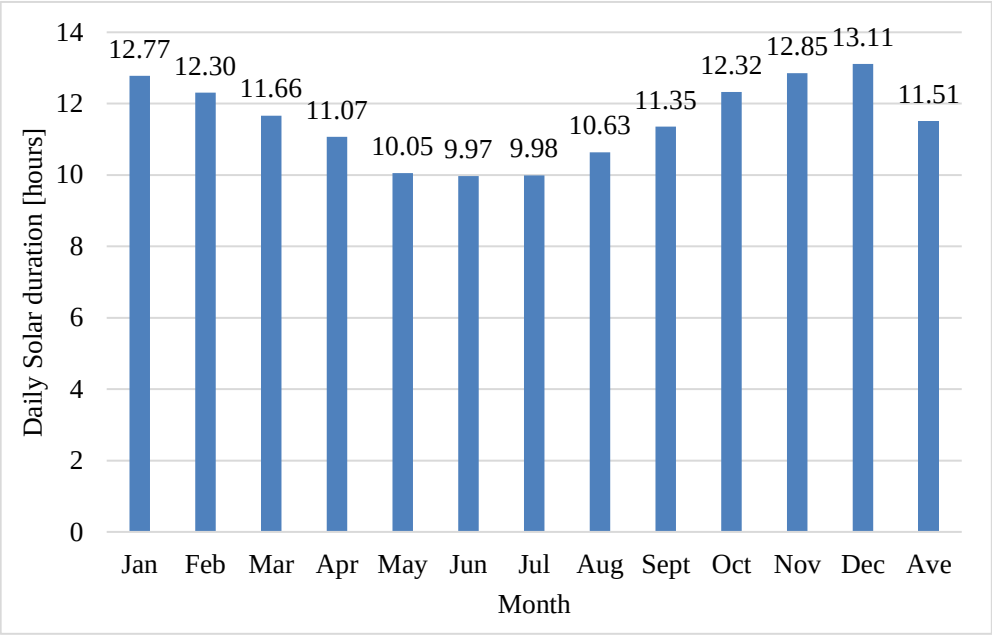

Figure 3.2: Solar duration for Kalbult site.

3.3 Datasets

3.3.1 Overview

To successfully analyse the performance of a solar PV system, high quality weather data is required. The data has to be measured with a high time resolution and the derived values have to be obtained by using standard methods [23]. The essential parameters needed for the analysis of meteorological data sources in this study are GHI and ambient temperature. Other meteorological parameters such as Global Plane Irradiance (GPI), rain intensity, wind, humidity and module temperature will be used for further analysis of the plant performance. Higher performance EKO MS-802 pyranometers calibrated to International Organization for Standardization (ISO) standards and reference cells were used to take the solar radiation measurements at Kalkbult. Preference was given to data recorded using pyranometers over that from reference cells, since pyranometers give more accurate measurements than reference cells. This is due to reference cells having shortcomings in spectrum, temperature and degradation even when properly calibrated. The parameters recorded at the Kalkbult solar PV plant site, with a 30 minute resolution, are as follows:

1. Global Horizontal Irradiance (GHI).

2. Plane-Of-Array (POA) irradiance or Global Plane Irradiance (GPI).

3. Ambient temperature.

4. Module surface temperature.

5. Wind velocity.

6. Rain intensity.

7. Relative humidity.

8. Absolute air pressure.

For the evaluation of irradiance models that estimate tilted plane irradiance from GHI, the following measured data is required: Global Horizontal Irradiance (GHI), Diffuse Horizontal Irradiance (DHI), Direct Normal Irradiance (DNI) and Plane-Of-Array (POA) irradiance.

3.3.2 Measurement instrumentation accuracy

Distinguishing the performance of the solar PV system from the solar resource variability requires both a measurement of the incoming irradiation as well as the energy generated by the system. The uncertainty of the data source should be noted and reported as this is good practice for all measurements.

Billing type energy meters should be used for electricity yield measurements or instead true-rms power meters should be used [24]. The precision of inverter integrated measurements is usually questionable but the obtained values can prove to be useful for detecting relative alterations in a solar PV system over time.

Generally two possibilities exist when choosing irradiation sensor technology: solar reference cell sensors and pyranometers, shown in Figure 3.3a and Figure 3.3b respectively [25]. According to literature, pyranometers measure on average 2 to 4% more irradiance than crystalline silicon sensors [24]. Irradiance sensors require to be checked, cleaned and recalibrated at least once a year in order to correct any bias in the measurement [24]. Pyranometers are based on a thermocouple device and they measure irradiance between 280 and 2800nm, thus almost spectrally unselective. The uncertainty of pyranometers is influenced by the following parameters [26]:

1. Pyranometer tilt angle.

2. Ambient temperature.

3. Pyranometer dome temperature.

(a) Reference cells (b) Pyranometer

Figure 3.3: Reference cells and Pyranometer installed at Kalkbult solar PV plant.

4. Spectral distribution of the solar resource and irradiance level.

5. Change rate of the irradiance during measurement.

According to the literature, the daily uncertainties expected for secondary standard pyranometers, first class pyranometers and second class pyranometers are below 2%, below 5% and below 10% respectively [27]. Experienced people in laboratories that calibrate according to ISO 9846, ISO 9847 or the equivalent have reported calibration uncertainties in the range of 1 to 2 % [27]. The overall uncertainty of the instantaneous irradiance measurement based on secondary standard pyranometers is around 2-3 % according to literature [28]. At Kalkbult, EKO MS-802 secondary standard pyranometers, with a measuring uncertainty of 2% are used to take the GHI and GPI measurements.

3.3.3 Data quality control

All the data used in this study was scrutinised for possible data quality issues. To ensure a high quality data set, the 30 minute interval measured meteorological data was verified as follows:

- The data was examined for missing values.
- Consistency checks: Checking for out of range data (spikes that could contain measurements over five times greater than the normally observed values).
- Removal of negative irradiance values as shown in Figure 3.4.
- Limit checks: Removal of non-zero solar radiation after sunset and before sunrise.
- Checking whether standard time was used throughout the year or converted to local or daylight savings during some parts of the year.
- Checking whether the timestamp indicates the beginning, middle or end of the period.

Less than 1% of the total number of 30-minute data were deleted from weather station 1 and 2 datasets (i.e. 96 data points out of the total 17520 for each weather station) and the remaining data from the four weather stations (1-4) were averaged for each 30 minute interval measured parameter. Missing values were observed in the measured data, from the 9th to the 12th of December.

3.4 Data source validation procedures

In order to compare the goodness of fit between the measured data and the other sources of meteorological data, the following statistical parameters were used: Root Mean Square Error

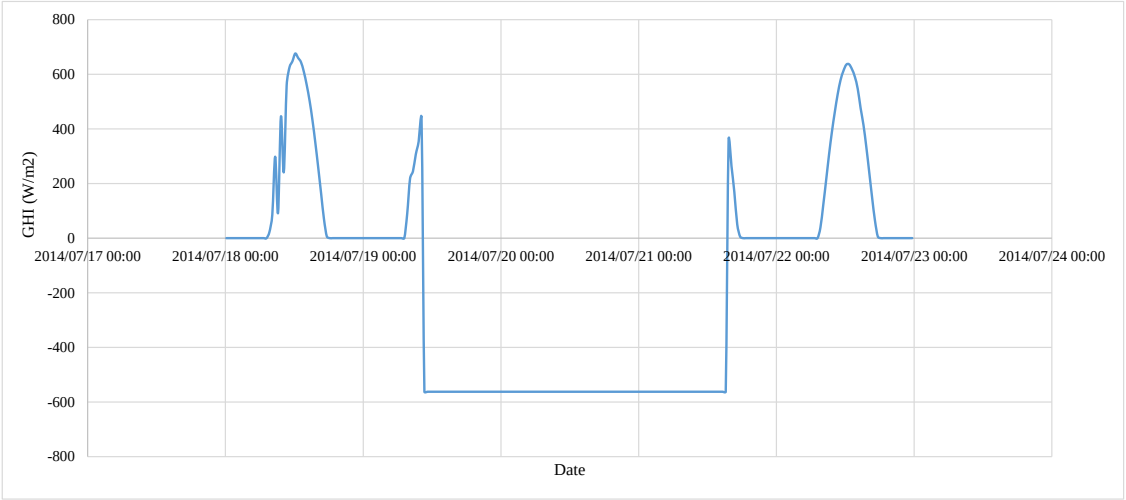

Figure 3.4: Example of negative GHI data.

(RMSE), mean absolute deviation (MAD) and the mean absolute percentage deviation (MAPD [29].

The RMSE gives the deviation between the measured value and the other meteorological data source value. The RMSE should be as close to zero as possible and it is calculated as follows:

$$RMSE = \sqrt{\frac{1}{N}\sum_{n=1}^{N}(H_n - F_n)^2}, \tag{3.4.1}$$

where H_n is the measured value, F_n is the estimated meteorological data source value and n is the number of periods i.e. months in this case.

The MAD parameter is used to measure the statistical dispersion and is calculated as follows:

$$MAD = \frac{1}{N}\sum_{n=1}^{N} \mid H_n - F_n \mid . \tag{3.4.2}$$

The mean absolute percentage difference (MAPD) also known as the mean absolute percentage error (MAPE) is used to assess the accuracy of the other meteorological data sources compared to the measured data, it is calculated as follows:

$$MAPE = \frac{1}{N}\sum_{n=1}^{N}\left|\frac{H_n - F_n}{H_n}\right| \cdot 100\%. \tag{3.4.3}$$

The MBE provides long term performance information of the deviation between the measured H_n and estimated F_n meteorological data values. It is calculated as a percentage as follows:

$$MBE(\%) = \frac{1}{N}\sum_{n=1}^{N}\frac{H_n - F_n}{H_n} \cdot 100\%. \tag{3.4.4}$$

3.5 Comparison of meteorological data sources

There are various sources of meteorological data, including measured, interpolated, terrestrial model predicted and that predicted from satellite-derived models. However, the various meteorological databases differ in the input data, methodology, covered area, spatial revolution and time intervals. In this study, seven different solar radiation data sources are validated using ground measurements from Kalkbult, averaged from the four weather stations on site. This was done with the aim of looking for reliable and most suitable alternative solar radiation sources. The various solar radiation data sources were limited to the ones commonly used in simulation tools and those from local companies.

Global Horizontal Irradiation (GHI) data measured at Kalkbult solar PV power plant in South Africa was compared to the solar resource values from available databases: SODA HelioClim-3 [30], Meteonorm7.1 [31], PVGIS-Helioclim [32], Climate-SAF PVGIS [32], Meteonorm6.1 [31], NASA-SSE [33] in order to verify that each of the data sets is applicable to the Kalkbult site. NASA-SSE and SODA HelioClim-3 data are sourced from satellite records whereas Meteonorm and PVGIS data are collected by interpolating results from records of the nearby meteorological stations and the use satellite data where measured weather records are not available [21]. Table 3.1 shows the spatial resolution and time periods over which the meteorological data was gathered for each source. PVGIS Helioclim and Climate-SAF PVGIS provides long term annual and monthly averages determined from different temporal periods as given in Table 3.1, whereas, SoDa offers time series meteo-data for the year required. Meteonorm and NASA also offers time series data averaged over a certain time period (years). Related work was done for regions in Europe and Asia [34, 35].

A brief review of the various available meteorological data sources is presented next.

3.5.1 Meteonorm

Meteonorm is considered to be a more robust meteorological data source and the uncertainty associated with the GHI is considered to be less than that of the other meteo-data sources in Europe [19, 21]. Meteonorm incorporates solar applications calculation procedures and a catalogue of meteorological data of any desired location in the world [22]. Meteonorm solar radiation data is derived from 1325 meteo stations all over the world and five geostationary satellites and 30 years of experience [31]. Twelve of the stations are in South Africa. Solar radiation data from Meteonorm6.1 is averaged from 1981 to 2000 and that for Meteonorm7.1 is averaged from 1991 to 2010. Meteonorm7.1 is the default meteo-data source in the current

Table 3.1: Summary of meteorological data sources in monthly values.

Data source	Time period	Spatial resolution	Availability
Kalkbult measured	2014 onwards	-	-
Meteonorm6.1	1981 - 2000	Interpolation	pay
Meteonorm7.1	1991 - 2010	Interpolation	pay
Climate-SAF PVGIS	1998 - 2010	$1 \times 1\ km$	free
PVGIS-Helioclim	1981 - 1990	$1 \times 1\ km$	free
SODA HelioClim-3	2004 onwards	$3 \times 3\ km$	pay
NASA-SSE	1983 - 2005	$1° \times 1°$	free

PVsyst version 6.39 and before that the Meteonorm6.1 was the default source of meteorological data in PVsyst simulation tool, up to version 6.35 [19].

3.5.2 NASA-SSE

The National Aeronautics and Space Administration (NASA-SSE) satellite and model-based solar radiation is averaged monthly from 22 years of satellite data, i.e. 1983 to 2005 [33]. The solar radiation data is derived from satellite images of more than 15 geostationary weather satellites and it can be accessed in hourly values [33]. NASA-SSE is a reliable global solar radiation data provider for the areas with sparse or non-existent surface measurements. The data is freely accessed with a spatial resolution of $110 \times 110\ km$.

3.5.3 PVGIS

Photovoltaic Geographical Information System (PVGIS) provides a map-based inventory of solar energy resource. PVGIS also provides a capability assessment of the electricity generation from photovoltaic systems in Africa, Europe and South-West Asia [32]. PVGIS has two differently averaged datasets that are freely accessed in monthly values, PVGIS-Helioclim averaged from 1981 to 1990 and Climate-SAF PVGIS averaged from 1998 to 2011. The PVGIS-Helioclim data set and the Climate-SAF PVGIS are based on radiation values interpolated from two different measurement techniques (terrestrial measurements and satellite images) [19].

3.5.4 SODA HelioClim-3

HelioClim-3 is a long-term and near-real time surface solar irradiance database. It contains 15 minutes interval accessible surface solar irradiance, from images taken by the Meteostat series satellites since 2004, with a spatial resolution of $3 \times 3\ km$ [30]. This satellite-based method used to estimate the surface solar radiation, is called HelioSat-2 [36]. When necessary, the 15 minute solar radiation data is summarised to hourly, daily, monthly and yearly values. The solar radiation data covers Africa, Europe and Atlantic Ocean. HelioClim-3 can be accessed via the SoDa service (www.sodais.org). To access the data, one has to pay, except for the whole year 2005, which is available for tests.

3.6 Data validation, comparison and analysis

3.6.1 Meteorological data source validation using 2014 data

3.6.1.1 Yearly GHI comparison

The GHI comparison between the measured data and each of the alternative data sources is shown in Table 3.2. The annual measured GHI value of 2117 kW/m^2 measured at Kalkbult solar PV power plant is within 2.95% of MeteoNorm6.1, 4.10% of MeteoNorm7.1, 0.33% of Climate- SAF PVGIS, 3.74% of PVGIS-Helioclim, 1.33% of SODA HelioClim-3 and 0.84% of NASA-SSE database. Differences in the estimates using the several solar radiation databases are within a reasonable range and also agree with literature studies [35]. According to the annual values, Climate-SAF PVGIS appears to be the most accurate alternative meteorological data source, followed by SODA HelioClim-3. A super refinement will follow, using monthly values for each data source.

3.6.1.2 Monthly GHI comparison

The GHI data obtained from the different sources under investigation better approximates the field data when the statistical metrics (RMSE, MAD, MAPE and MBE) are close to zero [43]. All the solar radiation data sources under investigation agree among themselves within 5of the reference measured irradiation. SODA HelioClim-3 appears to be delivering the most accurate GHI estimate over the course of a year, followed by SolarGIS, Climate-SAF PVGIS, PVGIS-Helioclim, NASA-SSE database, MeteoNorm6.1 and then MeteoNorm7.1, in that order. The trend is in accordance with the respective monthly MAPE, MAD, RMSE and MBE values. As can be seen in Table 3.3, the monthly error analysis indicates that SODA HelioClim-3 best es-

Table 3.2: Comparison of annual Global Horizontal Irradiation data from different sources.

Data source	**Origin**	**Annual GHI** kWh	**Difference** %
Measured	ground	2117	0.00%
SODA HelioClim-3	satellite	2145.16	1.33%
Meteonorm7.1	ground + satellite	2203.8	4.10%
Meteonorm6.1	ground + satellite	2179.5	2.95%
Climate-SAF PVGIS	ground + satellite	2110	-0.33%
PVGIS-Helioclim	ground + satellite	2196.1	3.74%
NASA-SSE	satellite + model	2099.3	-0.84%

timates the GHI for the site under investigation compared to the other meteorological data source considered in this study. This is owing to the SODA HelioClim-3 monthly error metrics (MAPE of 1.90%, MAD of 2.97, RMSE of 4.01 and MBE of -1.63%) results being closer to zero than those of the other meteorological data sources, as shown in Table 3.3. On the other hand, Meteonorm7.1 has the highest mean absolute percentage error (MAPE) of 5.36%, thus it shows the highest irradiation overestimation compared to the other meteo-data sources, though SODA HelioClim-3 yield results that are more closer to the reference irradiation for this dataset. Good regional estimates are obtained from databases with coarser spatial resolution (e.g. NASA-SSE), however deviations may be shown for studies at local level since the databases ignore local terrain and climate features [35]. Figure 3.5 shows the close relation between the measured and the estimated GHI for the Kalkbult site from the meteo-data sources. From Figure 3.5 it can be noted that the SODA HelioClim-3 GHI curve best follows the measured GHI curve, thus it gives a better representation of the reference dataset.

3.6.1.3 Ambient temperature comparison

The PV module temperature is a substantial parameter affecting the performance of a solar PV system. In this study we evaluate the ambient temperatures since they are used as input in the simulation tools, instead of the module temperatures. The measured ambient temperature data is compared to the estimates from various meteo-data sources in Table 3.4.

The annual average ambient temperature value measured at the Kalkbult solar PV power plant is within 9% of NASA-SSE and 1.13% of both Meteonorm6.1 and Meteonorm7.1. These differences are within a reasonable range and all the data sources are thus considered appropriate to be used for the yield simulation with Meteonorm being the first preference.

Table 3.3: Solar irradiation (GHI) monthly error analysis using 2014 data.

Data source	RMSE	MAD	MAPE	MBE
Meteonorm6.1	9.97	8.03	4.89%	-3.54%
Meteonorm7.1	12.2	9.13	5.36%	-4.39%
Climate-SAF PVGIS	8.77	7.37	4.12%	-0.25%
PVGIS-Helioclim	10.5	7.62	4.27%	-3.79%
HelioClim-3	4.01	2.97	1.90%	-1.63%
NASA-SSE	9.26	7.79	4.30%	0.39%

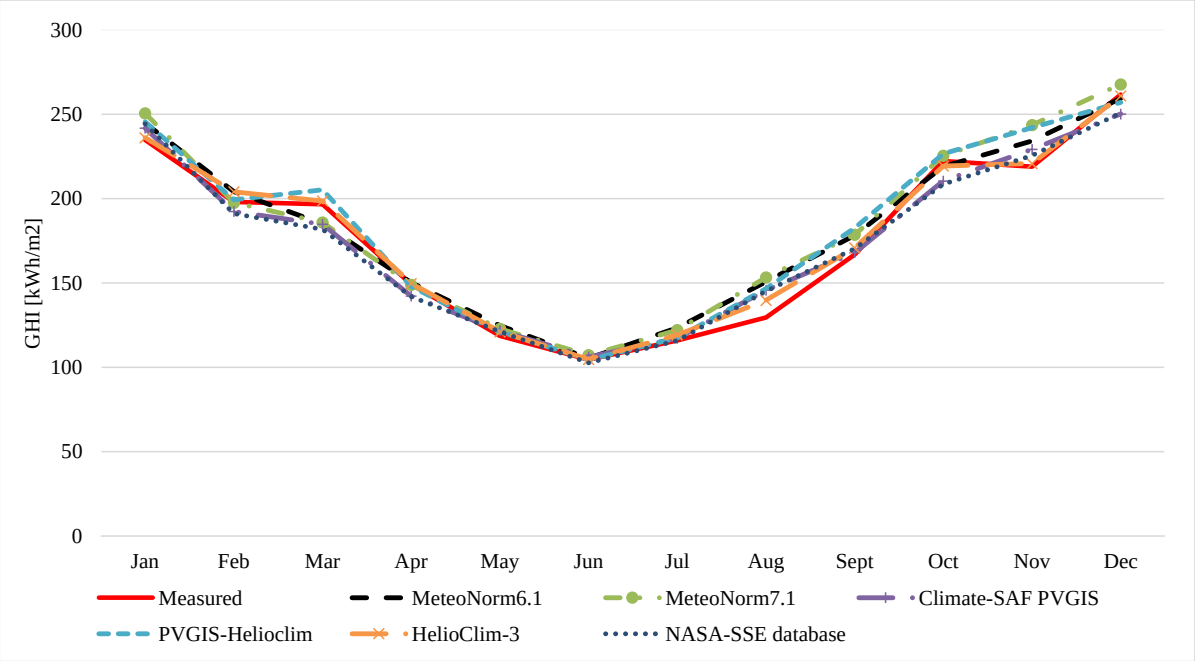

Figure 3.5: Comparison of the measured and different long term averaged GHI data sources for 2014.

Table 3.4: Comparison of monthly average ambient temperature data from different sources.

Month	**Measured** °C	**Meteonorm6.1** °C	**Meteonorm7.1** °C	**NASA-SSE** °C
January	26.5	24	24.1	22.8
February	24.4	24.2	23.9	21.9
March	21	21.6	21.3	19.9
April	16.6	17	16.9	16.4
May	13.1	13.1	13.1	12.1
June	7.8	10	9.8	7.9
July	8.2	9.4	9.5	7.8
August	11.6	11.8	12	10.7
September	15.9	15.2	15.2	14.5
October	20.5	19.4	19.4	17.7
November	20.7	20.8	21.1	20
December	26.1	23.4	23.7	21.9
Annual	17.7	17.5	17.5	16.1

3.6.2 Inter-annual variability

The monthly GHI averages of the various long term data is compared to the measured GHI data for Kalbult site. The other six data sources have different time coverage, temporal and spatial resolution. According to literature, it is not advised to mechanically compare the meteo-databases since they differ in applied methods, time coverage, primary measurements, etc. [38]. Due to weather variations each year, the yearly measured values tend to differ from the long term average data. Figure 3.6 shows the difference between the measured GHI data for Kalkbult in 2014 and the average GHI from the six long term data sources considered in this study. The measured data is within the inter-annual variability limits for the individual months of $\pm 3.1\%$ to $\pm 6.5\%$, reported in literature for some other regions within South Africa [38].

3.6.3 Sensitivity analysis of GHI and Ambient temperature measurements

The uncertainty of the equipment used to measure the irradiance and temperature values used in this study is $\pm 2\%$. Therefore, we investigated the percentage change caused on the PVsyst simulated energy yield when measured GHI and ambient temperature combinations are over-estimated or underestimated by margins of 2% . The results showed the effect of the uncertainty in measured data on the simulated energy yield, caused by the tolerances in the measurement equipment.

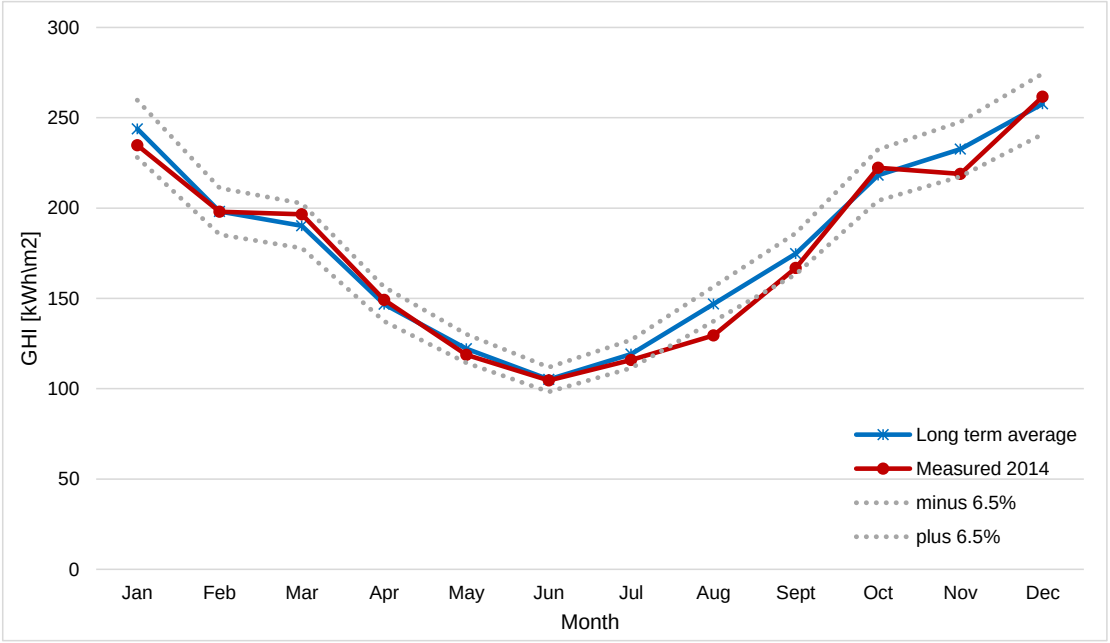

Figure 3.6: Comparison between measured and average long term GHI data sources.

Table 3.5 shows the resulting percentage change of the PVsyst simulated energy yield when ambient temperature (Amb temp) and GHI combinations are underestimated/overestimated by margins of 2%. From the analysis it was observed that the uncertainty in GHI measurements has more effect on the energy yield than the uncertainty in ambient temperature measurements. Thus the accuracy of ambient temperature is of less importance in solar PV systems in comparison to the irradiation. Overestimating the GHI measurements by 2% whilst keeping the ambient temperature constant results in a 1.8% increase in the energy yield, whereas overestimating the ambient temperatures by the same margin whilst keeping the GHI constant results in only a slight decrease of 0.2% in the energy yield. The best case would be overestimating the GHI by 2% and at the same time underestimating the ambient temperature by 2% which would lead to an increase in the energy yield of 2%. A 2% decrease in the energy yield is experienced when the GHI is underestimated by 2% and the ambient temperature is overestimated by the same margin of 2%.

3.7 Conclusion

Comparisons were made of various meteorological data sources, for Kalkbult site. The various meteorological data sources give different values of solar radiation for the same site. The results of the analysis indicated that all the meteorological data sources under investigation agree within 5% of the reference, measured solar radiation. The observed differences between the measured meteo values and the other meteo-data sources are within a reasonable range and the

Table 3.5: Sensitivity analysis of GHI and ambient temperature measurements.

Parameter	**Change** %	**Energy yield** *MWh*	**Error** %	**PR** %
Amb temp and GHI	0%, 0%	146319	0%	82.1
GHI	+2%	148946	+1.795%	81.9
GHI	-2%	143593	-1.863%	82.3
Amb temp	+2%	146007	-0.2132%	81.9
Amb temp	-2%	146628	+0.2112%	82.3
Amb temp and GHI	+2%, +2%	148640	+1.586%	81.7
Amb temp and GHI	-2%, -2%	143905	-1.650%	82.4
Amb temp and GHI	+2%, -2%	143279	-2.078%	82.1
Amb temp and GHI	-2%, +2%	149249	+2.003%	82.0

measured data is within the inter-annual variability limits for the individual months of $\pm 3.1\%$ to $\pm 6.5\%$. However, HelioClim-3 data yield a better representation of reality for Kalkbult, compared to the other meteo-data sources as observed from the statistical results. Determining the best alternative meteo-data source when there are no ground measurements is difficult since not all of the databases provide solar radiation data and ambient temperatures for every site on the globe. From the study it was observed that some of the meteo-data sources do not provide temperature measurements.

Differences in the various data sources are linked to the way the solar radiation data is produced, some use discrete grids that vary in size, other perform interpolations. The meteo-data sources also vary due to climate variability since the values are either measurements for given years or averaged periods and those vary from one source to another. The differences in the meteo-data sources are also due to the fact that, the satellite images used in estimating the weather data are constantly evolving and improving, so the techniques and methods vary from one source to another. The resolution of some of the satellite images is good enough to see larger hills or mountains but not trees and houses, thus the horizon information might not be detailed enough to account for the local terrain and climate features. Consequently, it is best for each solar PV plant to have its own meteorological and solar radiation station on site.

CHAPTER 4

SOLAR PV SYSTEM ENERGY YIELD AND PERFORMANCE ANALYSIS

In this chapter a year-long energy yield analysis and performance evaluation of the first grid-connected 75 MW_P fixed-axis solar photovoltaic (PV) system in South Africa, Kalkbult, for the operational year 2014 is presented. The objective is to evaluate field data and to compare the initial energy yield assessment with the current plant performance. Primarily, measurements obtained from the currently operating solar PV system are evaluated and compared to PVsyst simulated results. In this study, the parameters evaluated are meteorological data, global grid energy output, specific yield, performance ratio (PR) and capacity factor (CF). In addition, monthly, seasonal, and annual variations are presented in detail.

4.1 Introduction

For solar PV plant owners to realise returns on project investments, it is critical that they are certain of the performance in the field. In order to do this, they utilise data monitoring. Data monitoring in utility scale solar PV plants serves for the comparison of the initial energy yield assessment with the current plant performance. As a result, it is therefore vital for the initial energy yield forecast values to be closely correlated to the actual performance. Various simulation software can be utilised when it comes to the initial energy yield assessment of a solar PV plant. PVsyst is one of best known simulation software packages and produces reliable yield profiles. It requires entry of sub-(hourly), daily or monthly Global Horizontal Irradiation, ambient temperature and wind speed is treated as optional.

In this study, the aim is to analyse the operational data from a utility scale solar PV power plant in order to ascertain the performance characteristics of the facility. In order to achieve this, a comparison of the initial energy yield assessment with the plant performance for the first operational year, 2014, is done. In addition, a performance analysis of the 75 MW_P fixed-axis solar PV system with respect to the meteorological conditions of Kalkbult is provided.

Energy yield comparisons between the field measurements and PVsyst calculations, variance analysis, and further energy prediction of the best-case solar PV system performance using PVsyst simulation software will be covered in this study. The PVsyst simulations are according to the PVsyst file in Appendix A provided by the utility provider. About 69.2% of systems designed in 2013 using polycrystalline module technology were reported to have PR values of 80% [23].

4.2 Methodology

An analysis of the energy yield of a 75 MW_P solar PV system was carried out by comparing the field measured data with the initial energy yield assessment done in PVsyst. PVsyst6.39 was used for the simulation and meteorological data measured on the solar PV plant site was used as input. Quality checks were performed on the meteorological data and the energy meter readings. The monthly, seasonal and yearly energy production was analysed from the alternating current (AC) energy meter recordings at the solar PV system. In this study, energy reductions due to inverter faults or failures were not taken into account, only the global energy yield output of the solar PV system was considered. The energy production of the solar PV system was compared to the energy production simulated by PVsyst6.39. In addition, the measured performance ratio (PR) and capacity factors (CF) were compared to the simulated results.

4.3 System description

Scatec Solar, the owner of the 75 MW_P solar PV plant was a preferred bidder during the REIPPP in December 2011. The plant was completed three months ahead of schedule in record time (January 2013 to September 2013) [39]. Kalkbult solar PV power plant makes use of a fixed tilt sub-structure system and the modules are tilted at an angle of 30°. The solar PV system consists of 84 SMA inverters and 312 504 BYD polycrystalline modules spanning an area of 105 *ha*. Table 4.1 contains data with regard to the solar PV system. The modules used have a conversion efficiency of 14.75% and this implies that each solar PV module only converts 147.5 W/m^2 of the Standard Test Conditions (STC) power density (1000 W/m^2) into useful direct current (DC) electrical energy [5]. The module data-sheet is provided in Appendix D and the inverter data-sheet is given in Appendix E.

Table 4.1: Data of the Kalkbult solar PV system.

Description	**Module Specification**
Module manufacturer	BYD
Solar module model	BYD240P6-30
Nominal power (P_{nom})	240 W_P
Short circuit current (I_{SC})	8.9 A
Open circuit voltage (V_{OC})	37.54 V
Module efficiency	14.75%
	Inverter Specification
Inverter manufacturer	SMA
Inverter model	Sunny Central 800CP
Nominal power (Pnom)	80 kW AC
Voltage at Pnom	29.55 V
Current at Pnom	8.12 A
	System specification
Substructure	Fixed axis
Rating	75 MW_P

4.4 Results and discussion

4.4.1 Irradiance

Figure 4.1 and Figure 4.2 depict the average monthly GHI and GPI for Kalkbult solar PV plant site, respectively. The measured annual Global Horizontal Irradiance and Plane-Of-Array irradiance for Kalbult are 2117 kWh/m^2 and 2384 kWh/m^2 respectively. The definition of seasons used in this study are according to fixed dates at even intervals of months as shown in Table 4.2. The highest amount of solar radiation is received in summer (December to February), whereas in winter (June to August) there is the least amount. Therefore according to the measured irradiance figures, the solar PV plant's energy yield is expected to be larger in summer than in any of the other season. Consequently, a lower energy yield is expected in winter than in any other season.

4.4.2 Ambient and module temperatures

Figure 4.3 shows the measured monthly average ambient and module temperatures for Kalkbult. It can be seen that summer months are generally hotter than winter months, with the low-

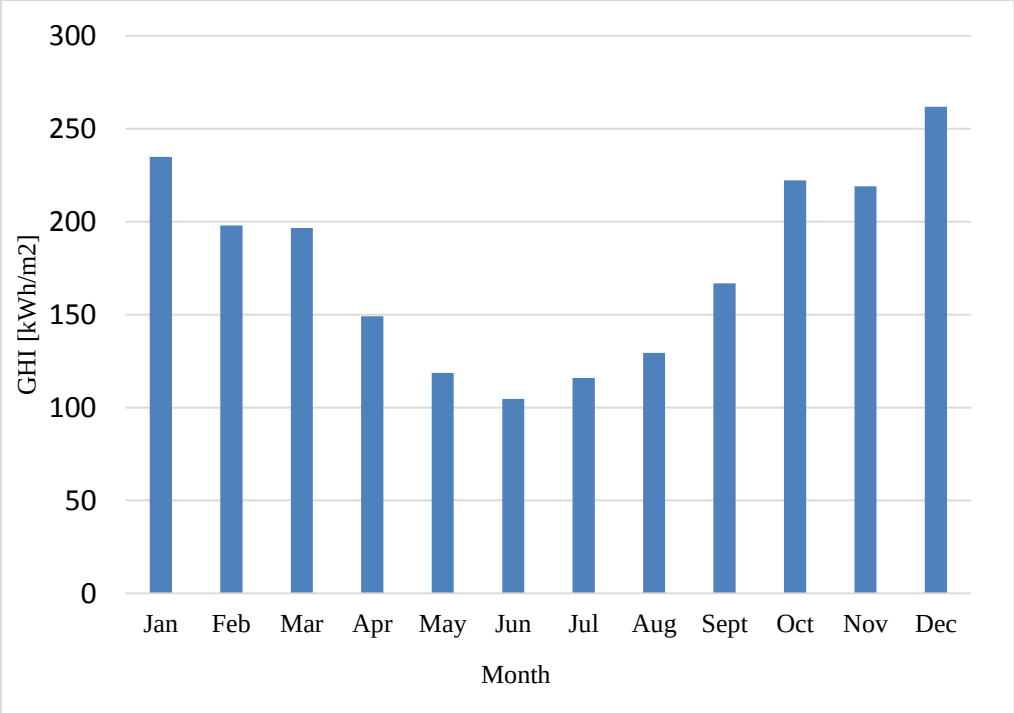

Figure 4.1: Average monthly GHI for Kalbult solar PV plant.

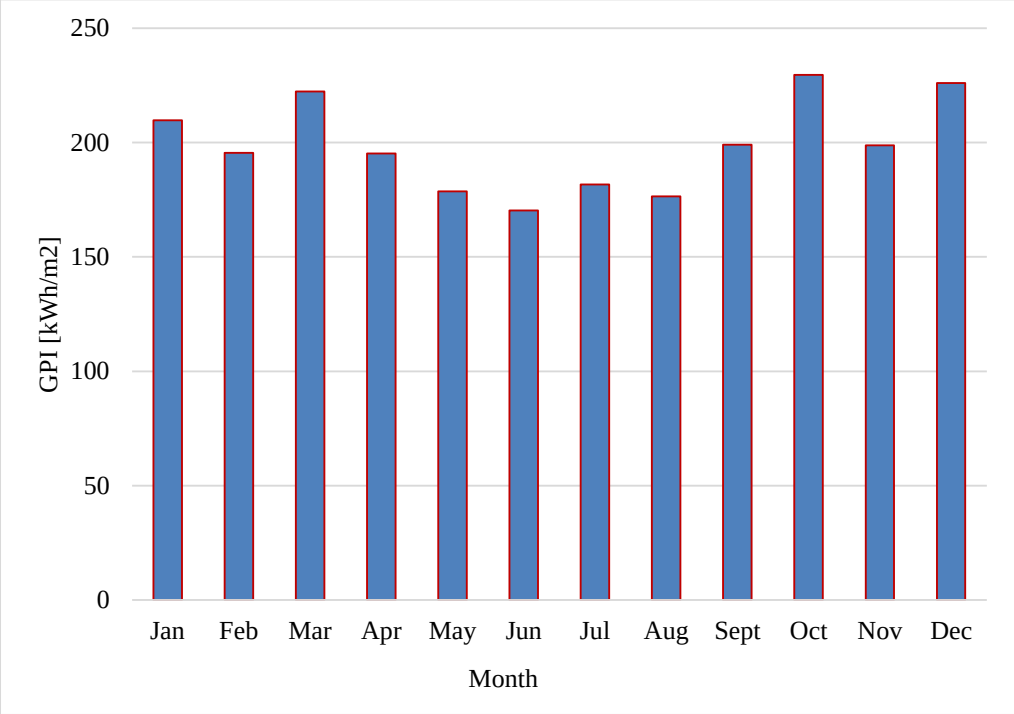

Figure 4.2: Average monthly GPI for Kalbult solar PV plant.

Table 4.2: Seasons.

Season	Interval in months
Summer	December - February
Autumn	March - May
Winter	June - August
Spring	September - November

est ambient and module temperatures being recorded in winter. As shown in Figure 4.3, module temperatures are generally higher than ambient temperatures by a factor of approximately 10 °C monthly. Kalkbult's measured annual average ambient temperature during production time is 23 °C for the period of this study whereas the respective measured annual module temperature value is 33 °C. In typical high solar radiation regions, the module temperatures often reach 65 °C or higher in peak operating conditions.

4.4.3 Energy production

The electrical energy output of a solar PV system depends on various factors like the incident irradiance on the collectors, cell temperature, solar incidence angle, load resistance, and various

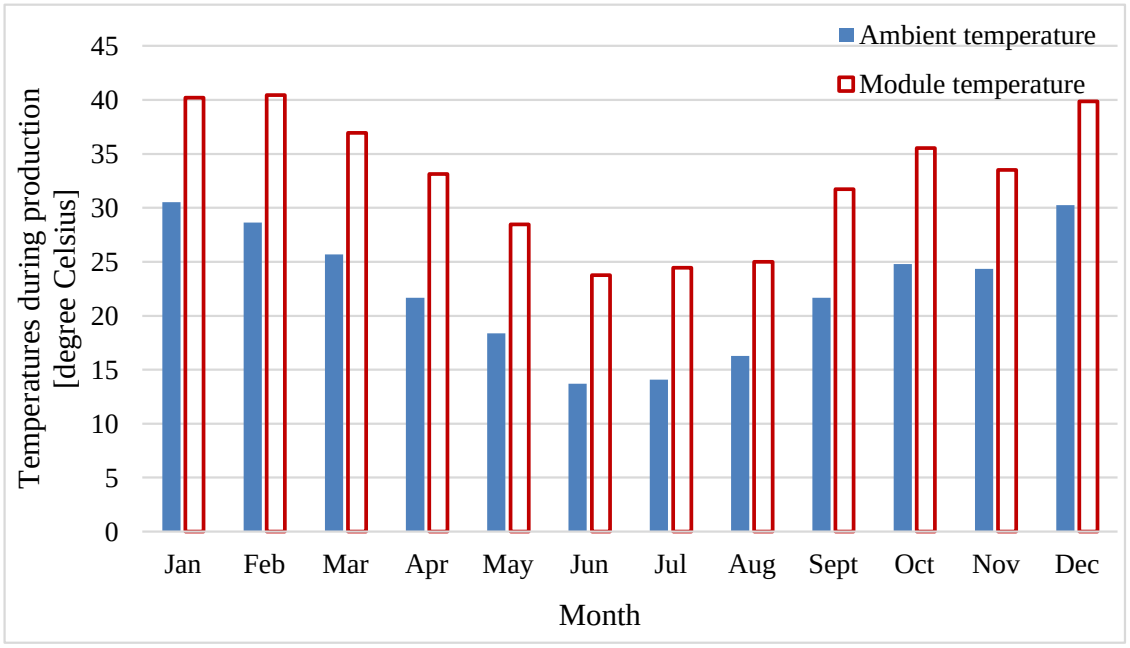

Figure 4.3: Average monthly ambient and module temperatures during production.

losses within the solar PV system [40]. Theoretically, energy production is calculated as follows:

$$Energy\ production(kWh) = Actual\ Power(kW) \cdot time(h). \tag{4.4.1}$$

Figure 4.4 shows the monthly energy production for Kalkbult solar PV plant and it follows the same trend as that of the measured GPI given in Figure 4.2. The system performance of a solar PV system is determined by the electrical energy that it produces and the 75 MW_P Kalkbult solar PV system's total annual energy production is 149 868 MWh which is enough to provide energy for 35 000 households, thus each household consumes on average 11.7 kWh/day. The produced energy would have been more if solar PV modules with a lower temperature coefficient than that of polycrystalline silicon (-0.47 %/°C) were used, provided that the alternative PV module's efficiency is also as high as that of polycrystalline modules [41]. The temperature coefficient of a solar PV module expresses the rate of change of its output power as a function of the module operating temperature. As the module temperature increases, solar PV modules suffer a drop in open circuit voltage i.e. solar PV semiconductor technologies experience an increasing performance loss and that results in less energy production [42].

4.4.3.1 Seasonal energy production

The seasonal energy distribution of the total annual energy production is 25.5% in summer, 25.1% in autum, 26.3% in spring and 23.1% in winter, as shown in Figure 4.5. Kalkbult solar PV

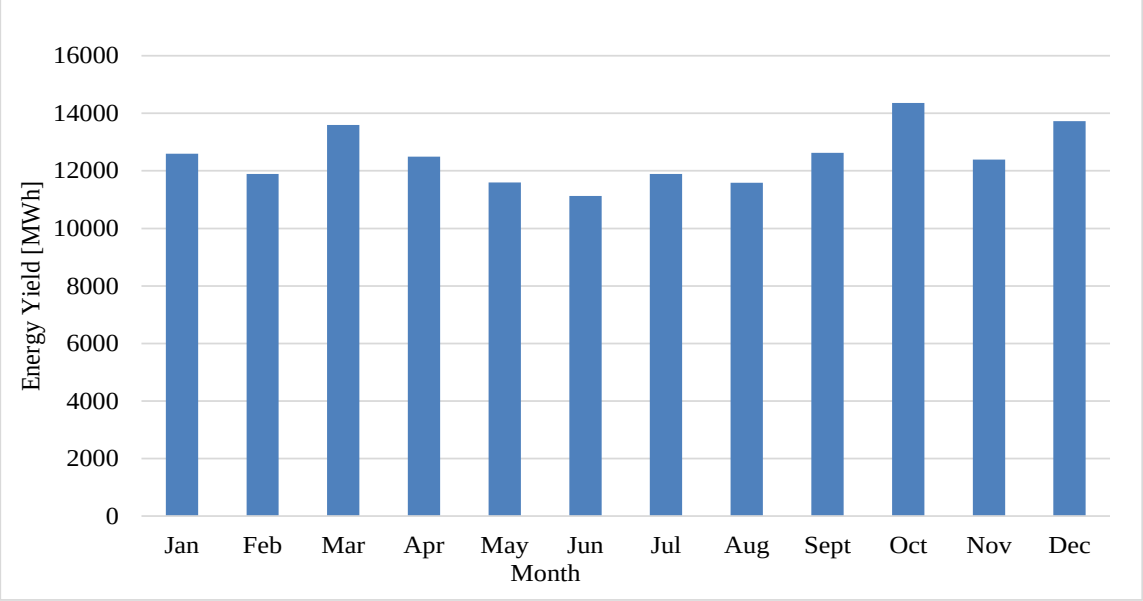

Figure 4.4: Monthly energy production for Kalkbult solar PV power plant.

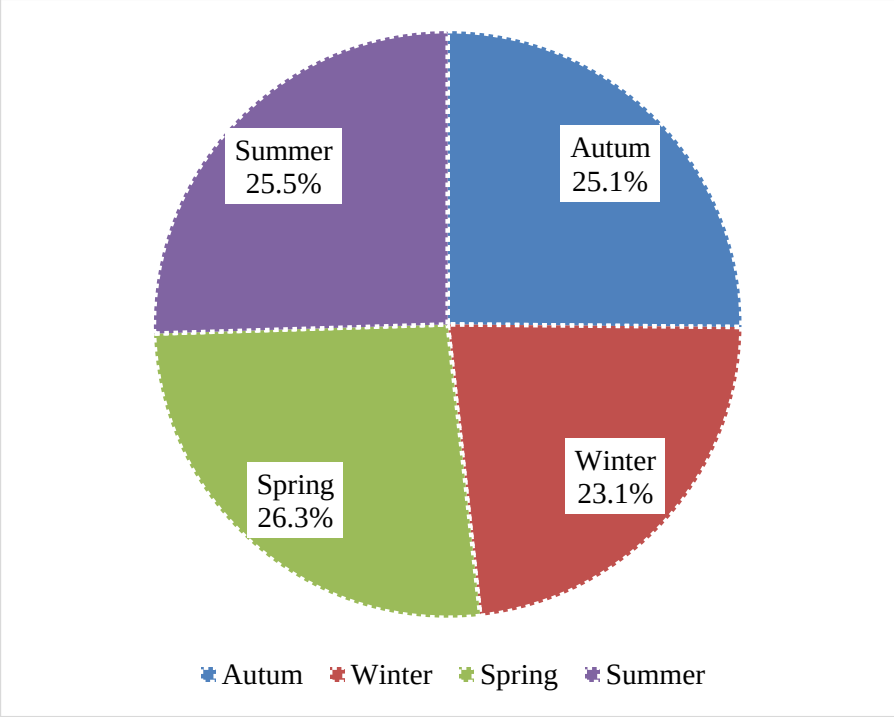

Figure 4.5: Seasonal energy production of Kalkbult solar PV power plant.

plant's highest seasonal energy production was measured in spring with a value of 39 369 *MWh* whereas the average seasonal energy production is 37 467 *MWh*. The lowest seasonal energy production of 34 601 *MWh* was measured in winter and this was due to the low solar radiation experienced in winter as shown in Figure 4.6.

The highest energy production was measured in spring which has slightly lower seasonal Global Plane Irradiance (GPI) than summer. It was expected that the energy yield measured in summer and spring would be more or less the same due to the similarities of the measured GPI in the two seasons i.e. 26.5% and 26.3% respectively. But the higher module temperatures of 40.15 °C in summer compared to the 33.66 °C in spring outweighed the positive effect of the high solar radiation on the plane of the array [43]. Figure 4.7 shows that the modules operated at 6.5 °C warmer in the summer season than in spring. Due to the high temperature coefficient of the polycrystalline silicon modules (- 0.47 %/°C), a drop in the performance of solar PV modules is experienced at high temperatures [44]. As a result of this, the solar PV modules operating at lower temperatures produced more energy than those operating at higher temperatures, explaining why more energy was measured in spring than in summer.

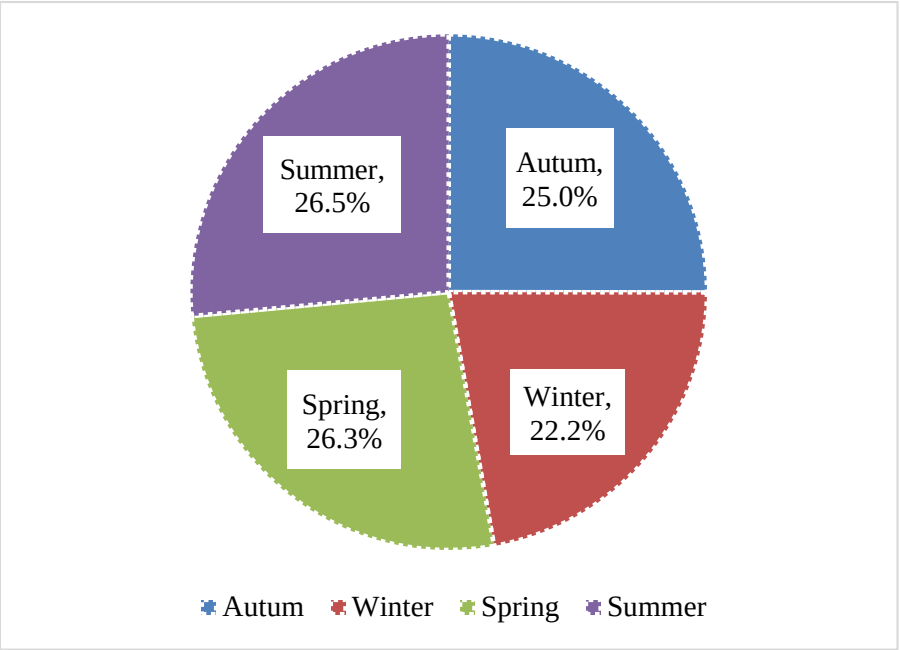

Figure 4.6: Seasonal GPI as a percentage of the total annual GPI for Kalkbult.

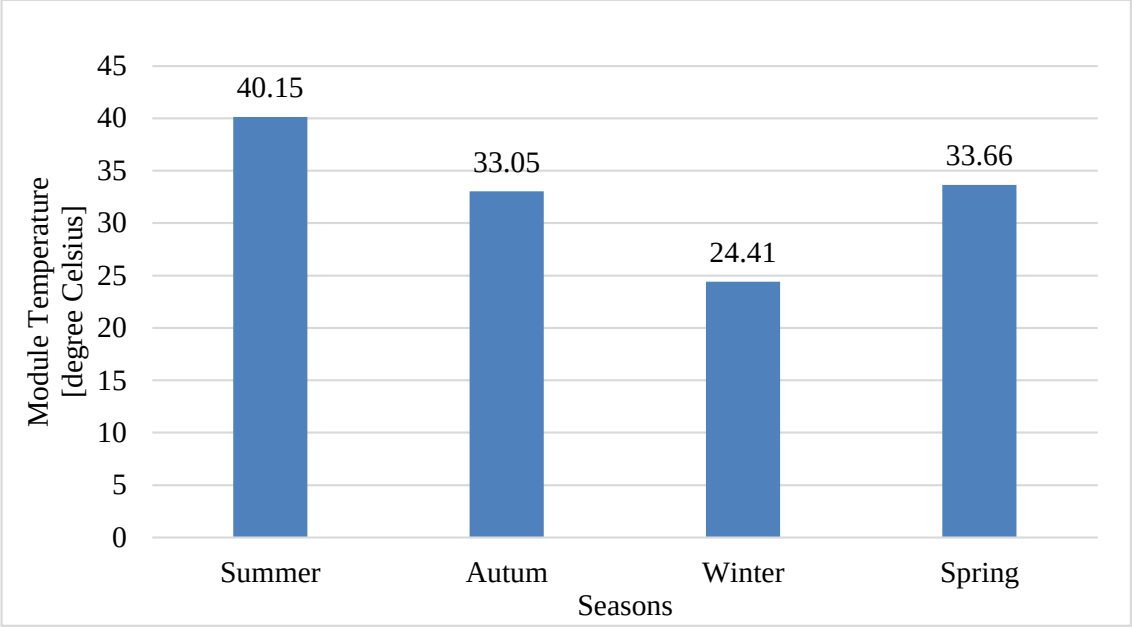

Figure 4.7: Seasonal average module temperature for Kalkbult solar PV system during production.

4.4.3.2 Comparison between the measured and expected energy yield for 2014

Figure 4.8 is a comparison of the monthly measured grid energy and the expected energy normalised to the average monthly energy production. The expected energy was simulated in

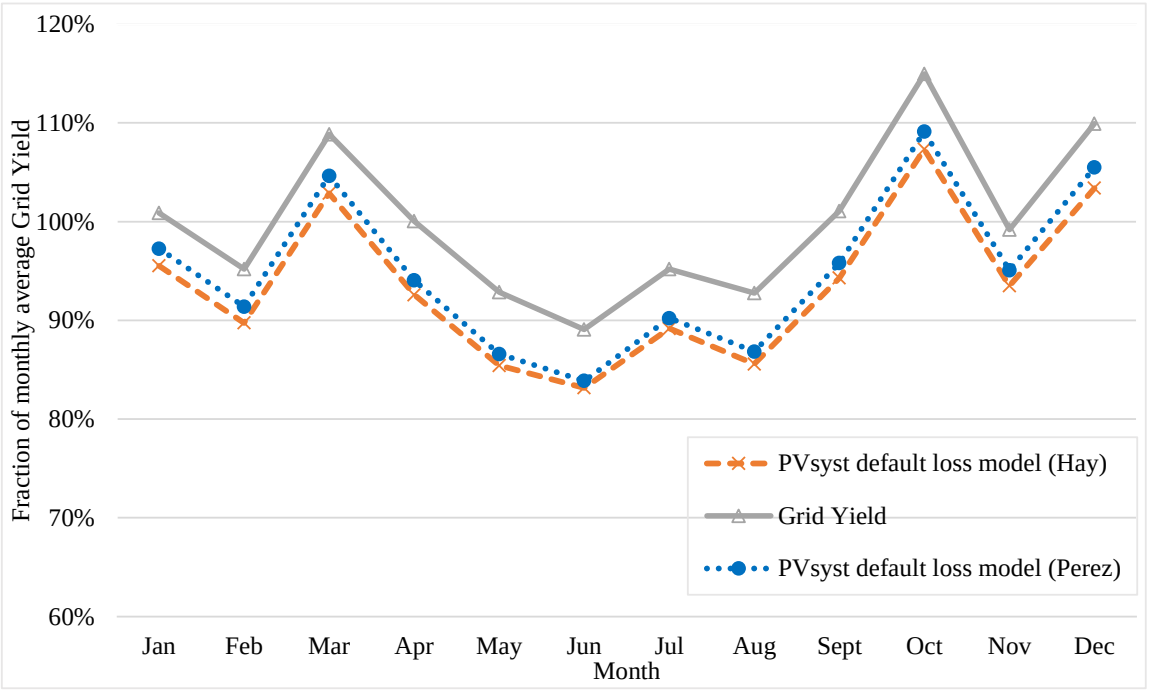

Figure 4.8: Monthly energy production comparison for 2014 (measured vs expected).

PVsyst using the initial simulation parameters and site measured meteorological data. The differences in the measured and PVsyst simulated energy yield are due to the the fact that the losses in PVsyst are overestimated compared to the actual operating losses. Therefore, the actual losses in the Kalkbult solar PV system will be calculated as described in Chapter 5 so as to improve the PVsyst loss factor model.

Kalkbult solar PV power plant's annual electrical energy production is compared to the PVsyst simulation results in Table 4.3. From Table 4.3 it can be seen that the energy production simulated in PVsyst6.39 and making use of the site measured meteorological data as input, deviates from the measured grid energy by 6.4% and by 5.0% from the Hay and Perez models, respectively. It should also be noted that only the global energy output of the solar PV plant was used in this study, energy reductions due to faulty inverters were not taken into account. Using initial simulation parameters, PVsyst modelled an annual energy production of 140279.5 *MWh* using the Hay model and 142 417.1 *MWh* using the Perez model, thus underestimating the electrical energy generation of the installed system. This is due to the over estimation of losses in PVsyst. In the next chapter there will be a description of how the PVsyst model for the Kalbult solar PV system was improved.

Table 4.3: Measured vs simulated annual energy yield for the Kalkbult solar PV plant.

	Annual energy production *MWh*	**Variance from grid energy** %
Grid-energy	149 868	0.0
Expected energy (Hay)	140 279.5	6.4
Expected energy (Perez)	142 417.1	5.0

4.4.4 Specific yield

Specific yield is defined as the ratio of the solar PV system's AC energy delivered to the grid in kWh over the actual STC rating of the solar PV system in kW_P [45]. From the definition, the factors that affect the annual energy production and also variations that affect the specific yield can be deduced. Theoretically specific yield is calculated as follows:

$$Specific\ yield = \frac{Actual\ AC\ energy\ output(kWh)}{DC\ rated\ power\ on\ PV\ module(kW_P)}. \tag{4.4.2}$$

Figure 4.9 shows the monthly specific yield for Kalkbult solar PV power plant. Generally the measured monthly specific yield values show the same trend as that of the monthly measured GPI and energy production. The period of highest measured specific yield for Kalkbult is in October and that corresponds to the higher solar radiation measured in that month. Therefore, specific yield strongly relies on the solar radiation which is the major contributing factor to

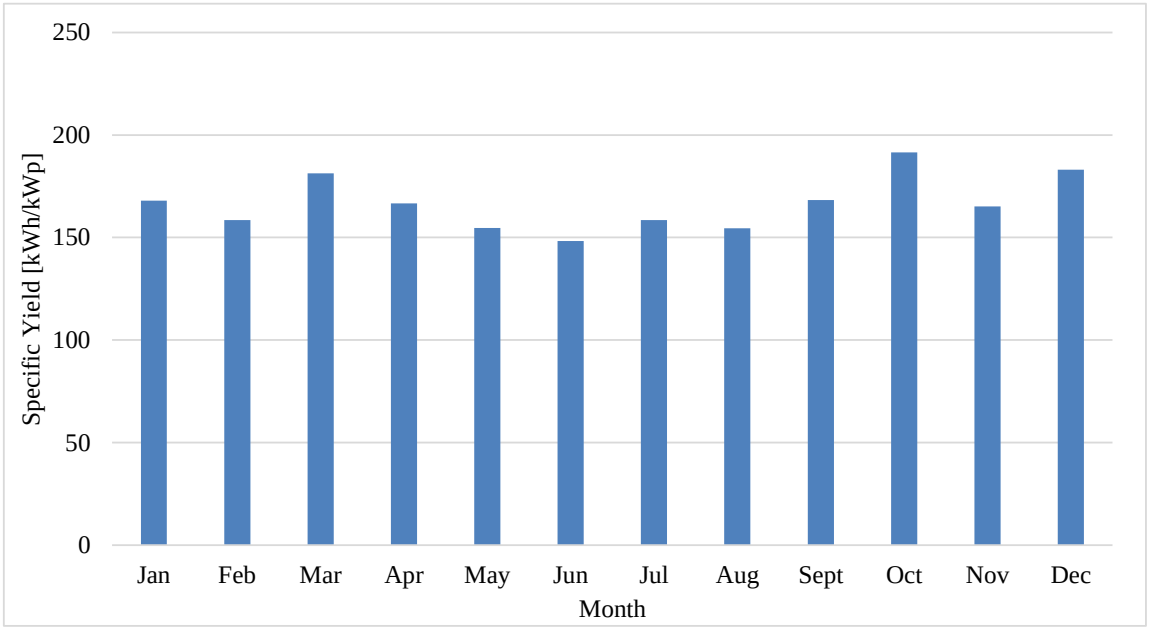

Figure 4.9: Monthly specific yield for Kalkbult solar PV system.

specific yield. An annual AC specific yield of 1998.24 kWh/kW_P was measured for Kalbult, whereas the PVsyst software simulated a value of 1870.4 kWh/kW_P.

4.4.5 Performance ratio

4.4.5.1 General PR formula

The performance ratio (PR) is used to indicate the installation quality of a system though it doesn't necessarily quantify the amount of energy generated. Literature suggests that a low PR system located at a good irradiation site is highly likely to produce more energy than a high PR system located at a lower irradiation site [46]. The findings of another study proved that the higher the PR, the higher the conversion rate of solar energy into electrical energy [47]. New solar PV system's PR values that range from 60% to 90% were reported in literature [48–52]. The PR of a solar PV system is determined as follows:

$$PR = \frac{E_{system}}{E_{ideal}}, \tag{4.4.3}$$

where, E_{system} is the actual measured grid energy in kWh and E_{ideal} is ideal energy output of the solar PV system that would have been obtained in kWh if the system suffered no losses. E_{ideal} is determined as follows:

$$E_{ideal} = P_{system_{STC}} \cdot \frac{G_t}{G_{STC}}, \tag{4.4.4}$$

where G_t is the measured Plane-Of-Array (POA) irradiance or GPI in kWh/m^2, G_{STC} = the irradiance at standard test conditions i.e. 1 kWh/m^2, and $Psystem_{STC}$ is the rated DC output power of the solar PV system in kW under standard test conditions [45]. The orientation of the PV modules and that of the device that measures the solar irradiation must be the same, so that they get exposed to the same temperatures and same solar insolation [44].

This study presents a seasonal PR of 87.3% in winter, 84.3% in autumn, 83.7% in spring and 80.7% in summer, as shown in Table 4.4. The actual annual average PR for the Kalbult solar PV plant is 83.8% whereas the annual average PR from PVsyst simulation software is 79.3%. In literature, actual PR values in Europe were reported to be 1.8-8.0 percent above PVsyst projections and PR values in the ranges of 83-84.9% were calculated from the field measurements [18].

Because of the amount of solar radiation received during each season, the highest PR would be expected to be in summer and the lowest in winter. However, the solar PV system performs best in winter whereas in summer a large drop in performance is experienced. The trend shows that the performance ratio doesn't necessarily quantify the energy generated by a solar PV

Table 4.4: Seasonal performance ratio for Kalkbult solar PV plant.

Season	**Performance ratio** %
Summer	80.7
Autumn	84.3
Winter	87.3
Spring	83.7

system. The lower PR values in summer are as the result of the negative influence of higher temperatures recorded during the season. If the pyranometers are not cleaned, the PR goes up and this is due to the fact that the measured irradiance is less than the incident irradiance on the PV collectors, thus from Equation 4.4.3, the ideal energy would be less, leading to increased calculated PR values.

4.4.5.2 Temperature corrected PR

The National Renewable Energy Laboratory's (NREL) report suggests that large seasonal variations in PR, which can range from $\pm 2\%$ to $\pm 10\%$ can be caused by the strong dependence of PR on temperature [53]. Research done in the Netherlands revealed that PR could on average reach 82.1% in winter and drop to 73.2% in summer [23]. Therefore the PR of a system can be temperature corrected to a common temperature of 25 °C to solve the problem of seasonal variation in PR [48, 54]. However, the resulting PR correction is usually higher since modules more frequently operate at temperatures above 25 °C. Therefore, temperature correcting the PR to 25 °C changes the actual yearly PR value of a solar PV system. As a result of this, a site-dependent year average module temperature to which the PR can be corrected is defined. In this case it is 33.2 °C, the yearly average module temperature for the Kalkbult solar PV plant site in 2014.

Researchers in India came up with a temperature corrected PR formula which makes use of the average cell temperature for the whole year [53]. This formula requires an initial project file that depicts the range of the module temperature and the intensity of solar radiation for one complete year. Researchers [55] and [54] use the same temperature correction method as used in this study. The resulting ideal energy that can be substituted into Equation (4.4.3) to get the temperature corrected PR is calculated as follows:

$$E_{ideal} = P_{system_{STC}} \cdot \frac{G_t}{G_{STC}} \cdot \left(1 - \frac{\alpha \cdot (T_{mod_{avg}} - T_{mod})}{100}\right), \tag{4.4.5}$$

where: $T_{mod_{avg}}$ = the average module temperature computed from one year of field recorded data (°C), α = peak power temperature coefficient which corresponds to the installed system (%/°C, negative), and T_{mod} = measured module temperature during production, (°C).

The resulting temperature corrected seasonal PR values are 83.6% in summer, 84.4% in autumn, 84% in winter and 84% in spring, as shown in Table 4.5. The resulting temperature corrected average PR value for the Kalkbult solar PV plant is 84%.

4.4.5.3 Normal PR versus temperature corrected PR

The difference between the normal PR formula and the temperature corrected PR formula is that the latter contains an additional term which translates the rated power to the annual average operating module temperature. As shown in Figure 4.10 the problem of seasonal variations was eliminated without changing the yearly average PR value of the 75 MW_P, Kalkbult solar PV system.

In general, a decline in temperatures and also monitoring of solar PV systems so as to detect and rectify defects early, causes an increase in the PR [56]. Literature studies [57–59] show that the performance of solar PV systems is affected by higher ambient temperatures in a negative manner, since the system's efficiency is lowered because of increased losses due to temperature rise. This explains why the PR for Kalkbult is higher in winter months and lower in summer months, as shown by the monthly PR values in Figure 4.11. As a result, choosing solar PV modules with a lower temperature coefficient would improve the performance of the system especially in high ambient temperature locations [13]. Thin film modules have a lower temperature coefficient which is around -0.25 %/°C, so they are ideal for high ambient temperature conditions [60]. Shading also plays an important role in the PR of a system, therefore well designed and well ventilated utility scale solar PV systems have higher performance ratio [56].

Table 4.5: Seasonal temperature corrected performance ratio for Kalkbult solar PV plant.

Season	**Performance ratio** %
Summer	83.6
Autumn	84.4
Winter	84.0
Spring	84.0

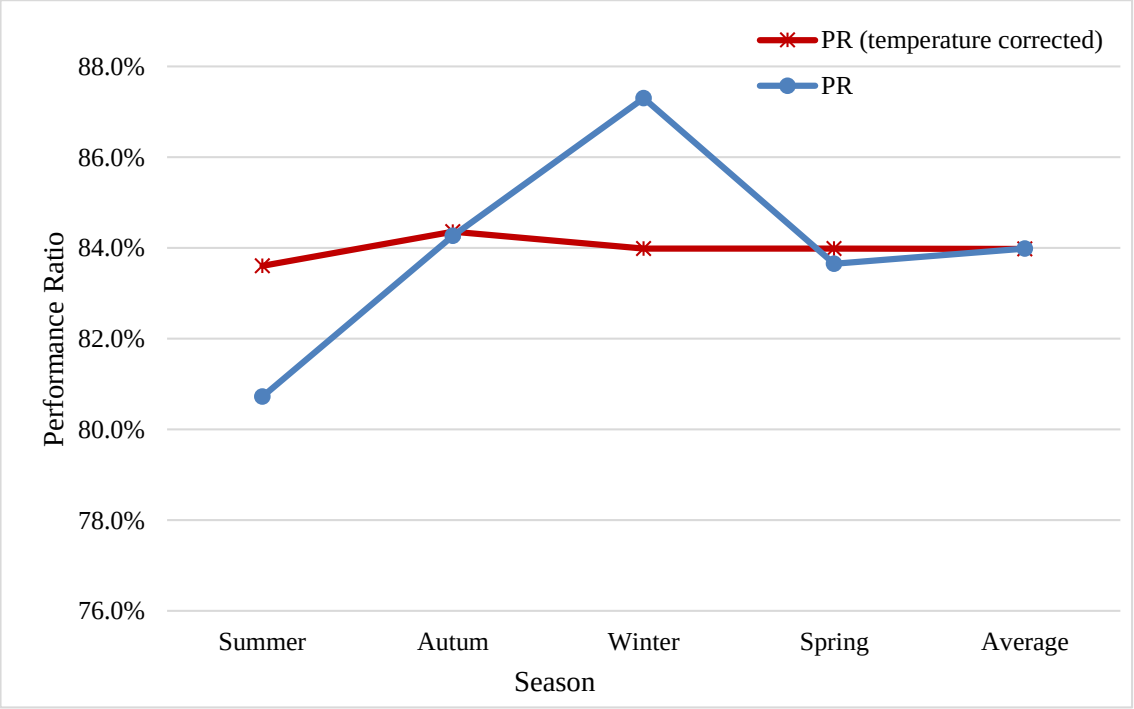

Figure 4.10: Seasonal corrected and uncorrected performance ratio of Kalkbult solar PV power system.

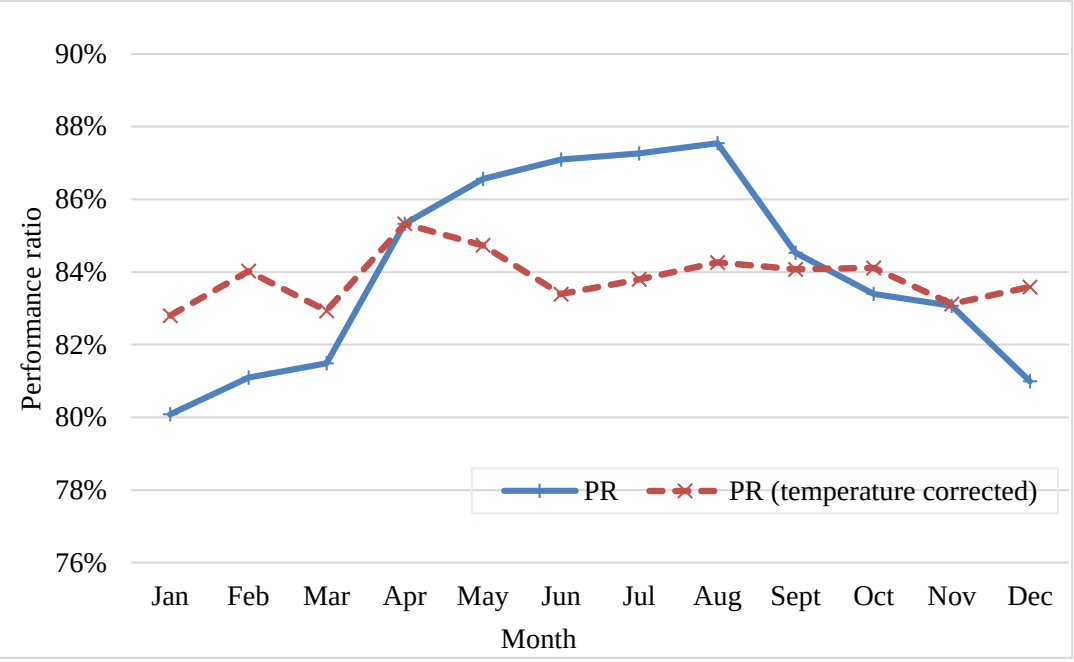

Figure 4.11: Monthly PR and temperature corrected PR of Kalkbult solar PV system.

4.4.6 Plant performance degradation

In general, it is assumed that the performance degradation of solar PV systems is caused by only the solar PV modules. However when evaluating the performance it is recommended to look at the balance between the system and the weather data [53]. NREL reported that a new system's standard PR is expected to be a minimum 77% and that the system's performance decreases by about 1% annually [5]. Using the PR for Kalkbult solar PV system, the system's PR would be expected to be around 69.4% after the next 20 years, as shown in Figure 4.12.

4.4.7 Capacity factor

The capacity factor (CF) of a solar PV system is the ratio between the measured output of a power generation plant over a period of time and its potential output if it had operated at the nameplate full capacity during the entire time [61]. Theoretically, CF is calculated as follows [5]:

$$CF = \frac{Energy\ output\ (MWh)}{365 \cdot 24(h) \cdot installed\ capacity\ of\ the\ PV\ system(MW_P)}. \tag{4.4.6}$$

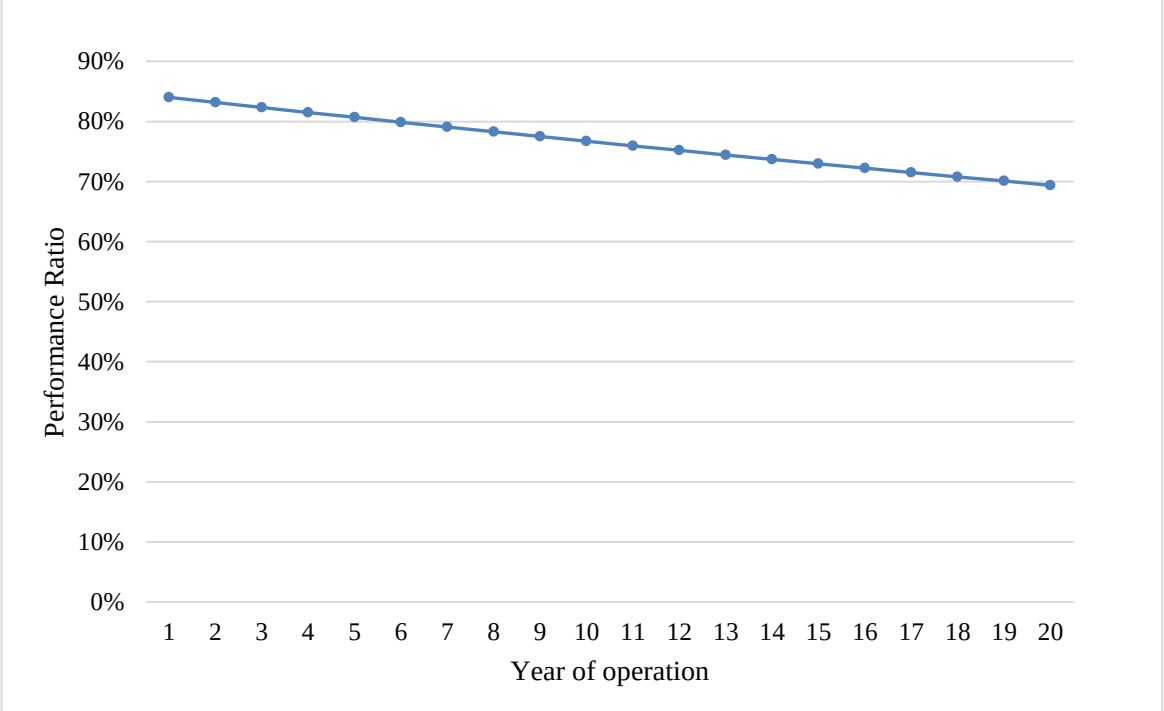

Figure 4.12: The expected performance ratio for the next 20 years of the Kalkbult solar PV system.

Environmental variations i.e. temperature, irradiance and the degradation of the solar PV modules are not taken into consideration in this parameter [53]. Moreover it assumes that the solar PV plant produces power for 24 hours a day, which isn't the case in reality. Equation (4) was used to calculate the measured capacity factor. The fixed-tilt solar PV system considered in this study has a CF of 22.8% whereas PVsyst modelled a CF of 21.35%. According to the literature, fixed-tilt solar PV systems are expected to have CF values between 20.8% and 26% in high solar radiation regions [62].

4.4.8 Performance summary for Kalkbult solar PV plant in 2014 and 2015

The performance summary of the Kalkbult solar PV system in its first year of operation (2014) and in 2015 is shown in Table 4.6. From the table it can be seen that different solar radiation was received in the first two years of the solar PV plant's operation. More GHI was received in 2014 than in 2015, as shown by the yearly GHI values of 2117 kWh/m^2 and 2057 kWh/m^2 recorded in 2014 and 2015, respectively. Consequently, the Plane-Of-Array irradiance of 2384 kWh/m^2 measured in 2014 is higher than that of 2283 kWh/m^2 recorded in 2015. As a result, the grid energy measured in 2015 was 6.55% lower than that recorded in 2014. Performance ratios of 83.8% and 81.8% were calculated for operational years 2014 and 2015, respectively. Specific yield values of 1998 kWh/kW_P and 1867 kWh/kW_P and capacity factor values of 22.8% and 21.3% were calculated for operational years 2014 and 2015, respectively.

4.5 Conclusion

The main aim of the study was achieved. The $75MW_P$ grid connected fixed tilt Kalkbult solar PV system generally produced more energy than what had been expected and the variance is 6.4% using the Hay model and 5% using the Perez model, with a PV simulator test tolerance

Table 4.6: The Kalbult solar PV plant's performance summary for 2014 and 2015.

Parameter	2014	2015
GHI	2117 kWh/m^2	2057 kWh/m^2
GPI	2384 kWh/m^2	2283 kWh/m^2
Grid energy	149868 MWh	140048 MWh
Specific yield	1998 kWh/kW_P	1867 kWh/kW_P
Performance ratio	83.8%	81.8%
Capacity factor	22.8%	21.3%

of $\pm 3\%$ [41]. The actual output of an installed solar module is affected by far more than STC conditions as it depends upon local weather, system design characteristics and many other factors. The overestimation of losses in PVsyst is the main cause of the observed difference in the PVsyst simulated and measured grid energy.

The yearly energy production of the installed 75 MW_P solar PV system amounts to 149 868 MWh in the first year of operation, whereas the energy yield obtained from the initial simulation done in PVsyst6.39 underestimated the installed system's energy production by 6.4%. The percentage distribution with respect to measured seasonal energy production is 25.5% in summer, 26.27% in spring, 25.14% in autumn and 23.09% in winter. This resulted in an overall system performance ratio of 84.0% whereas the initial energy yield simulation in PVsyst6.39 modelled a PR of 79.3% making use of measured GHI data as input. In addition to this, the specific yield and capacity factor of the installed system are 1998.24 kWh/kW_P and 22.81% respectively.

The PVsyst simulated specific yield value is 6.4% lower than the value calculated from the measured data. Variances between the measured and simulated results were caused by various factors and these are discussed in detail in the chapters to follow. Kalkbult solar PV system's winter PR was observed to be 87.30% and this is due to the lower ambient temperatures measured in winter which caused the solar PV modules to produce more energy. On the other hand, more solar radiation was received in summer than in any other seasons but the PR was 80.72% i.e. lower than that of the other seasons. That was due to the high ambient temperatures measured in summer which caused a drop in the system's efficiency and performance. The choice of irradiance datasets may affect the output of a system by about 3%, so using high-accuracy irradiance sensors are the key to reducing the uncertainty between the measured and expected energy [63]. It is also quite evident that the solar PV system's performance is not only dependent on irradiance but on different factors like ambient and cell temperatures, soiling, wind velocity, design flaws, plant failure, etc.

In conclusion, using solar PV modules with a low negative temperature coefficient, like thin film, would also improve the performance of the systems in high temperature conditions. Differences between the measured energy yield and the PVsyst expected energy were mostly due to the overestimation of system losses in PVsyst software. Therefore there is a need to create an accurate PVsyst loss model for Kalkbult solar PV system and this will be discussed in the next chapter.

CHAPTER 5

IMPROVED LOSS FACTOR MODEL

In the previous chapter, the differences observed between the measured grid energy and PVsyst energy yield simulated using measured GHI and default loss values were discussed. The differences were concluded to be mostly due to the PVsyst default loss model overestimating the actual losses of the Kalkbult solar PV system. So in this chapter, the improvement of the PVsyst loss model will be discussed using the year long data recorded on the solar PV site in 2014.

5.1 Introduction

In moderate climates the statistical average performance ratio (PR) of new photovoltaic (PV) installations has improved over the last 20 years. The typical PR was about 70% before 2000, while nowadays it is in the range of 80% to 90% [3]. This continuous improvement in the performance ratio is as a result of continuous operational monitoring and the analysis of the recorded data on a solar PV plant site. To ensure reliable and high quality solar PV systems, it is important that reliable evaluation methods of PV system losses and performance should be established and verified by quantitative analysis [64]. An essential part of enhancing the performance of an installed solar PV system is to understand the power losses which occur in the system and to develop methods to minimise these losses [65]. Various large solar PV systems use analytical monitoring to avoid economic losses due to operational problems [24, 66]. The power loss of solar PV systems is worth considering since there is rapid growth in the production of electricity from solar PV systems [67]. Therefore this analysis is needed for a better understanding of loss mechanisms in utility scale solar PV systems and for the design of low-loss solar PV systems.

In this chapter, there is a description of how the losses of a grid connected 75 MW_P solar PV power plant in South Africa are investigated. The solar PV plant makes use of a fixed 30° tilt substructure system that supports 312 504 BYD polycrystalline modules. Figure 5.1 shows a full description of the system, the respective losses to be quantified and their location within the plant. Power losses are firstly analysed, then practical methods are used to present and review the losses using quantitative values calculated from the 30-minute averaged field data, whilst

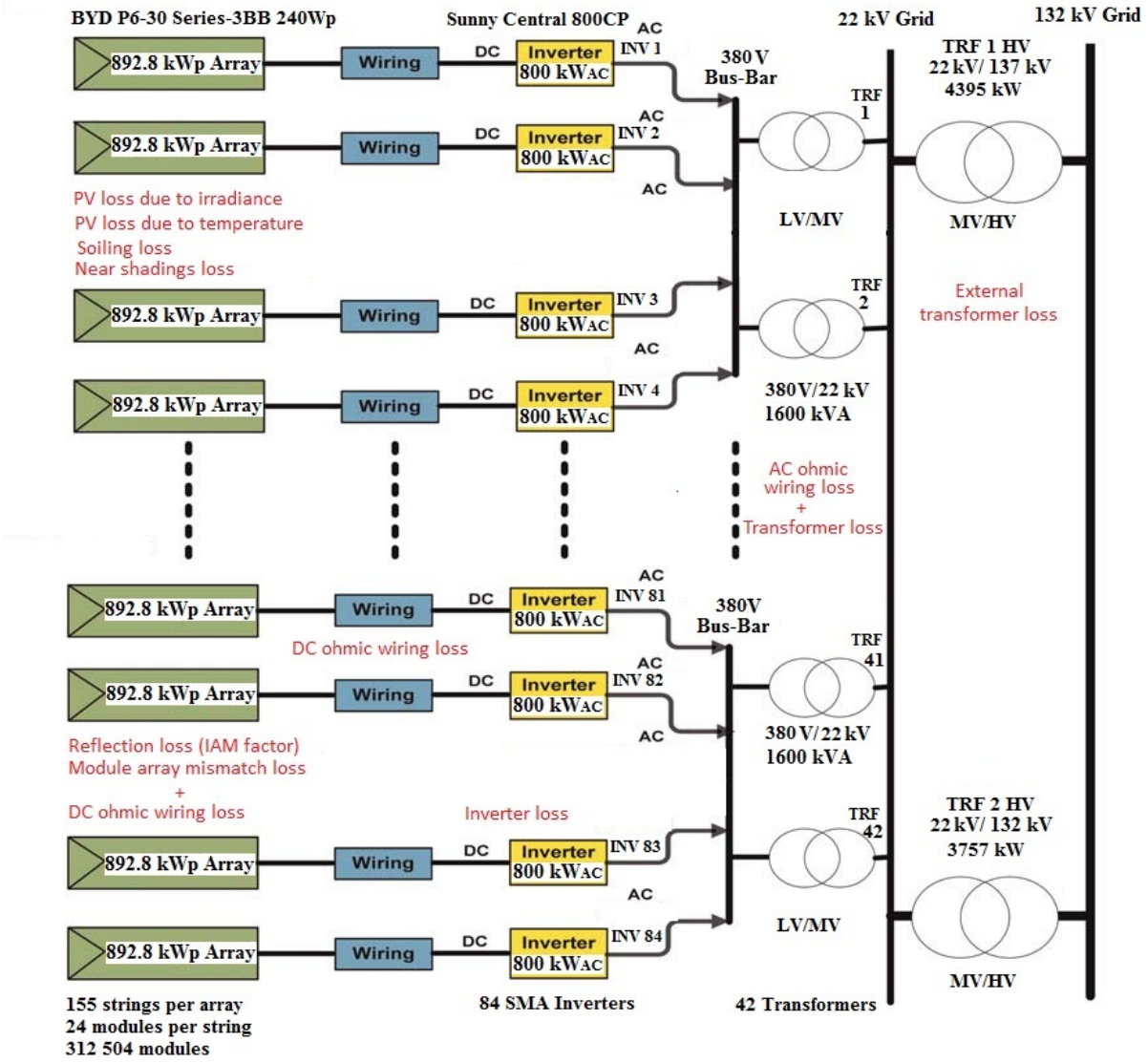

Figure 5.1: Losses in a solar PV system.

preserving high accuracy by doing the calculations both in Matlab and Excel. The calculated losses are then used to improve the default PVsyst model for the 75 MW_P solar PV power plant. The PVsyst default loss model uses reasonable parameter values in order to execute an initial simulation, whereas the improved model makes use of modified parameter values according to the measured system performance. The improved model enables accurate forecasting of the available generation capacity, as required by the utility provider.

5.2 Factors affecting the output of a solar PV system and loss calculation

Economic risks associated with solar resource availability, system design and technology maturity must be quantified and minimised in order to secure competitive financing for a solar

PV system. In this section, the factors that affect the solar PV system output are presented and quantified. Figure 5.2 is a summary of the factors that determine the real world energy output of a solar PV system.

5.2.1 Near shadings loss

Near shading losses are due to the mutual shadings of modules in adjacent rows, and horizon shading from structures that are far away, as well as nearby obstructions like buildings or trees, which lead to the under performance of solar PV systems. The near shading losses due to trees or buildings can sometimes be avoided by relocating the objects in the vicinity of the solar PV system. It is usually impossible to completely avoid the influence of inter-row shading on the energy yield because of space limitations, but with a careful planning procedure the inter-row shading effects can be minimised [68]. There is a direct correlation between power loss due to partial shading and the distance between the rows of the solar PV modules, therefore in order to minimise the row shading losses it is essential to calculate the appropriate inter-row spacing [69]. Figure 5.3 shows the sun path chart for the Kalkbult site located at a Latitude of 30.2 °S and a Longitude of 24.1 °E. In order to minimise shading effects of a north facing, 30° tilt fixed axis system, the distance between rows is selected to avoid shading from 8:30 AM to 4:15 PM on the shortest day of the year (winter solstice) i.e. 22 June. The minimum solar elevation angle (α_{min}) for the selected time interval is 13° as illustrated in Figure 5.3.

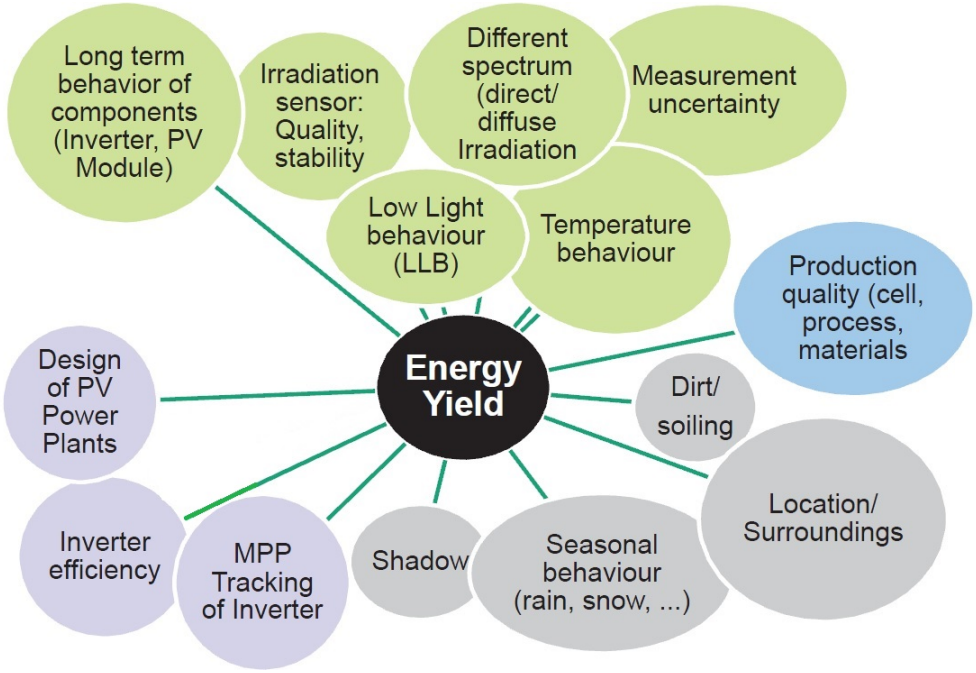

Figure 5.2: Factors affecting the output of a solar PV system [10].

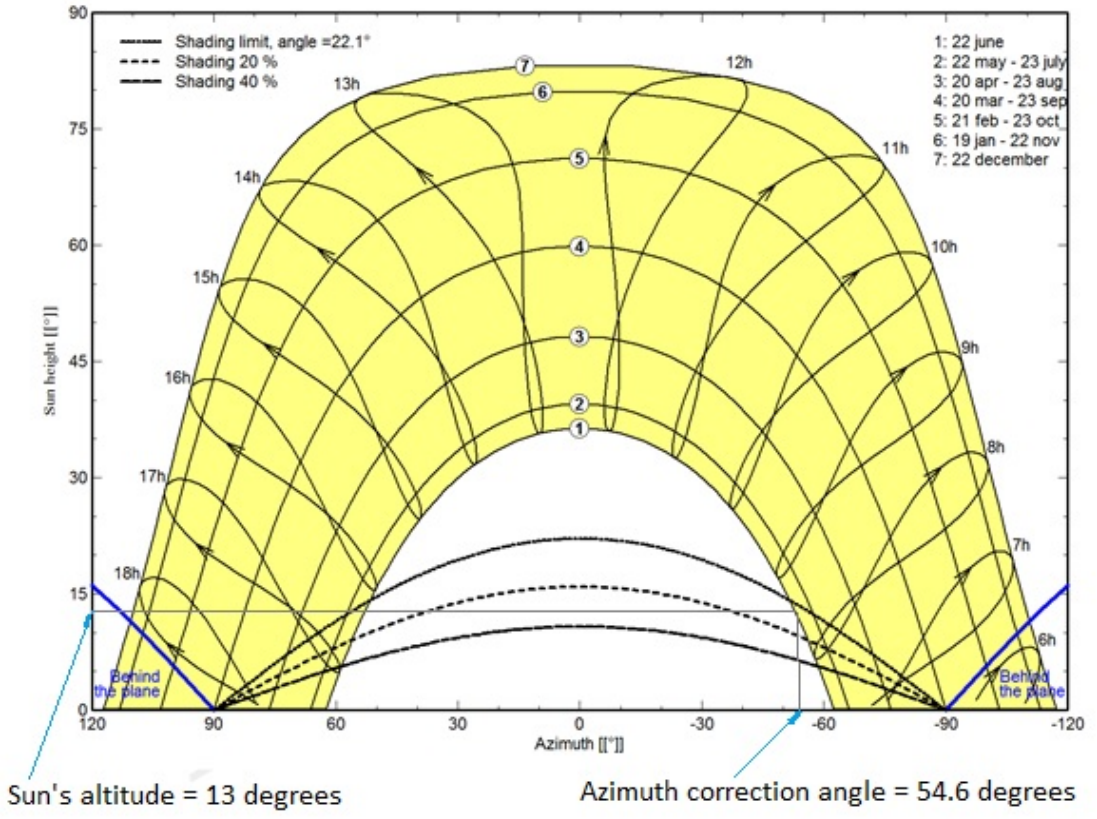

Figure 5.3: Sun path diagram for Kalkbult site showing the sun's height and azimuth angles as simulated in PVsyst [19].

The module inter-row spacing (d') is calculated as follows:

$$d' = \frac{h}{tan(\alpha_{min})} = \frac{l \cdot sin(\theta_T)}{tan(\alpha_{min})} = 7.15, \tag{5.2.1}$$

where α_{min} is the solar elevation angle in degrees, l is the module width, θ_T is the module tilt angle equal to 30° and h is the elevation of the module.

The minimum module row spacing (d) is then:

$$d = d' \cdot cos(\gamma_{Az}) = 4.14\ m, \tag{5.2.2}$$

where γ_{Az} is the azimuth correction angle.

The row width (R) is then calculated as follows:

$$R = d + [l \cdot cos(\theta_T)] = 7\ m. \tag{5.2.3}$$

The inter-row spacing is chosen such that the shading derate factor is 0.975 and for fixed systems this amounts to a ground cover ratio (GCR) of 0.47. The resulting distance between rows is as shown in Figure 5.4. The shading losses were calculated in PVsyst using the inter row spacing distance on site and the trajectory of the sun, simulated in hourly step values. This

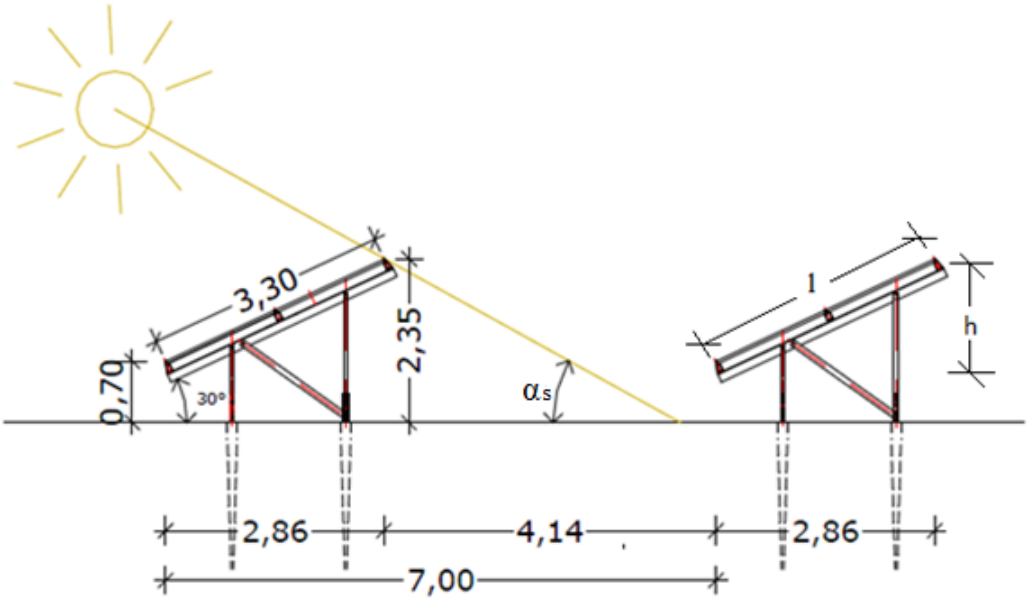

Figure 5.4: Inter-row spacing for modules at Kalkbult solar PV plant.

geometric calculation determined the portions of the arrays in shade during each time step, and a resultant near shading loss of 2.5% was obtained. Literature suggests that the relative shading loss shows that for series-connected solar array, the losses are higher than for the parallel connected array, this is due to the fact that shading a single module in a string lowers its current, causing the whole string to under-perform since current is continuous in a string [70].

5.2.2 Reflection/Incidence angle loss

Fixed-tilt solar PV modules receive varying amounts of solar radiation throughout the day and this is primarily due to the constant change of the angle of incidence (AOI) [71]. The angle of incidence at which the sun enters the atmosphere and strikes the surface of the solar PV module determines the reflection losses of a PV system. There will be a certain degree of reflectance at angles of incidence which are not normal to the solar panels. The incidence effect relates to the reduction of the irradiance on the PV cell's surface with respect to normal incidence irradiance [19]. Reflection losses are based on an Incidence Angle Modifier (IAM) which is estimated as follows [21]:

$$IAM = 1 - b_0\left(\frac{1}{cos(\theta_{AOI})} - 1\right), \tag{5.2.4}$$

where: θ_{AOI} is the solar incidence angle on the plane and b_0= is a module parameter provided by the manufacturer. The IAM depends only on one parameter b_0, and the manufacturer recommended a b_0 value of 0.05 for BYDP6-30 polycrystalline modules. The resulting reflection loss was calculated as 2.5%.

5.2.3 Soiling loss

The accumulation of dirt and its effect on system performance is difficult to predict as it depends on the site rainfall conditions, the environment of the system and the frequency at which the modules are cleaned [21]. While average energy losses due to soiling are typically in the range 1-6% [72], for some locations soiling can account for up to 70% of all the losses [24]. Researchers, operators and developers of solar power plants are constantly seeking better methods to quantify soiling-related losses and several methods do exist [73, 74]. For this analysis, soiling losses have been estimated based on the 30 minute interval measured precipitation for the site as shown in Figure 5.5. Soiling losses were quantified according to the loss scale shown in Table 5.1 [21]. As noted in Figure 5.5, the amount of rain that falls is higher in summer (December to February), than in winter months, (June to August). As a result, soiling losses are more likely to be experienced in winter than in any other season. The resulting monthly values for the soiling loss are shown in Table 5.2. The site's average yearly soiling losses were calculated as 1.75%. Independent soiling measurements permit more accurate determination of soiling losses compared to estimates based on precipitation or plant metrics alone. Therefore, at utility scale facilities, an ongoing measurement of soiling loss is an important component of performance monitoring that will also inform the cleaning schedule of the modules in order to

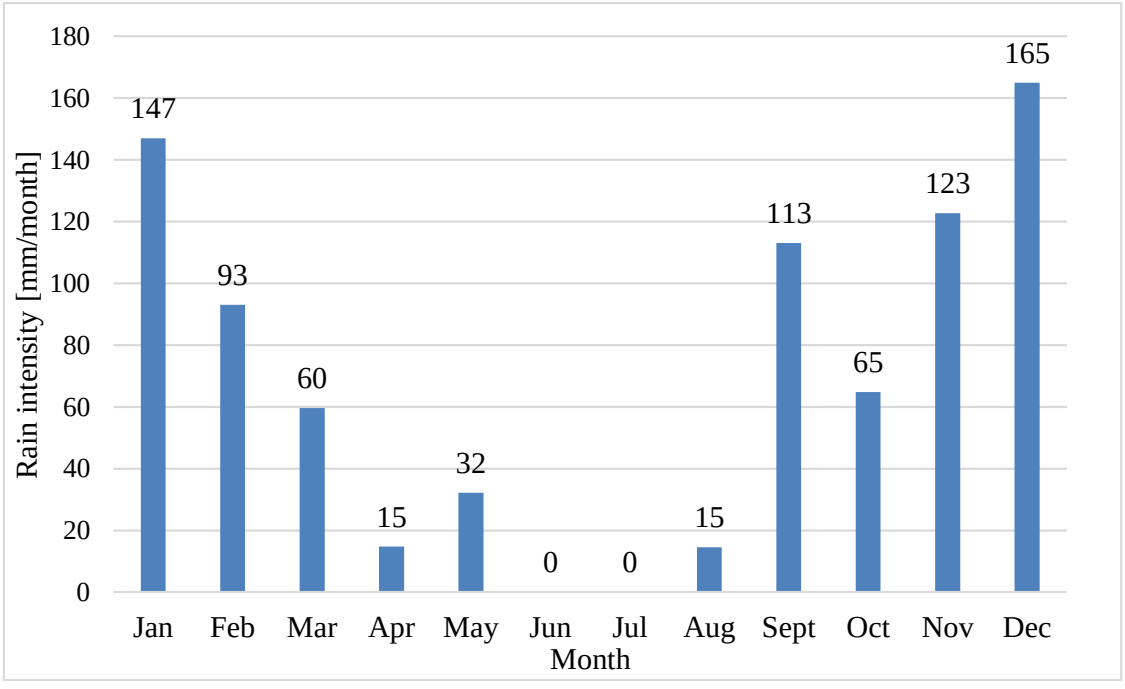

Figure 5.5: Rainfall pattern for Kalkbult site in 2014.

Table 5.1: Soiling loss scale.

Monthly Precipitation mm	**Soiling loss** %
0-20	3%
20-40	2%
>50	1%

Table 5.2: Soiling loss values predicted from received precipitation.

Month	**Rainfall** mm	**Soiling loss** %
January	146.97	1%
February	93.01	1%
March	59.59	1%
April	14.77	3%
May	32.16	2%
June	0.06	3%
July	0.12	3%
August	14.56	3%
September	113.08	1%
October	64.85	1%
November	122.76	1%
December	164.99	1%
Annual	68.91	1.75%

reduce the soiling losses [19, 72]. Further investigation into soling is therefore recommended for future studies.

5.2.4 PV loss due to irradiance level

The conversion efficiency of a PV module increases at high light intensities and decreases at low light intensities [75]. In practice there is a gain/loss in the module output with respect to the standard irradiance conditions that the modules are rated at, (1000 W/m^2) [21]. The module efficiency according to measured incident irradiance on the collector plane was determined from the plot of the module efficiency as a function of the Plane-Of-Array irradiance at a module temperature of 33.22 °C, as shown in Figure 5.6. For the 75 MW_P fixed-tilt system under

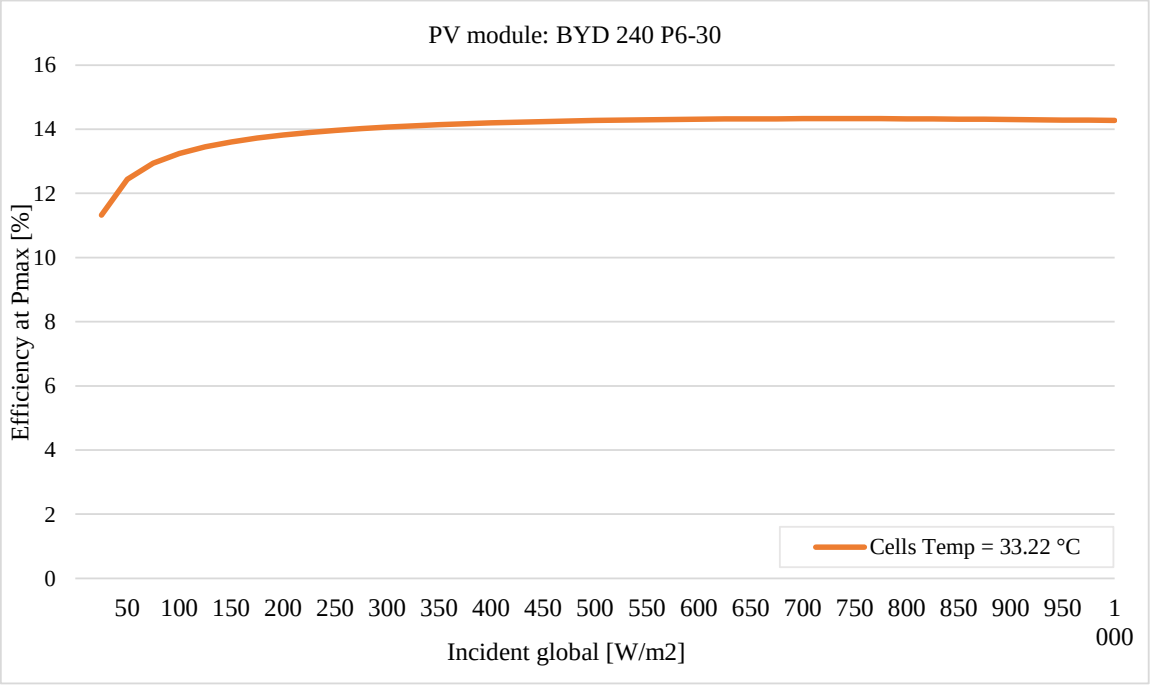

Figure 5.6: Efficiency vs Irradiance curve at a module temperature of 33.22 °C.

investigation, the PV loss due to irradiance level was extracted from the above-mentioned plot and it is 0.45 % with respect to standard test conditions (STC), as shown in Table 5.3.

5.2.5 PV loss due to temperature

The thermal characteristics of solar PV modules have a significant impact on the performance of PV systems. Increasing temperatures lower the open circuit voltage of PV modules significantly whilst slightly increasing the current, thereby causing a decrease in cell performance [76]. Literature suggests that direct measurement of module temperatures can improve accuracy when continuously forecasting expected system performance and losses [77].

Figure 5.7 shows the measured annual distribution of the back of module temperature and

Table 5.3: Relative efficiency loss with respect to STC.

Temperature °C	**POA** W/m^2	**Module Efficiency** %	**Relative efficiency loss** %
25	1000	14.75	-
33.22	567	14.30	0.45
STC = 1000 W/m^2, 25 °C and AM = 1.5			

the ambient temperature for the solar PV plant under investigation. It can be seen that the distribution of ambient temperature is centred on approximately 25 °C and it ranges from -10 to 40 °C, whereas the back of module temperature is centred on approximately 35 °C and ranges from -5 to 65 °C. This shows that in the case of the solar PV plant, the modules operate at temperatures above 25 °C on average and this in turn results in losses due to module temperature rise with respect to standard test conditions (STC) [78]. The PV loss due to temperature is based on the power temperature coefficient of the module, and the BYD P6-30 polycrystalline module has a peak power temperature coefficient of - 0.47 %/ °C at STC.

The PV loss due to temperature (P_{loss}) is then determined according to the following expression [78]:

$$P_{loss} = P_{actual} - P_{25}, \tag{5.2.5}$$

where: P_{actual} = the actual power of the solar PV system and P_{25} = is the temperature corrected yield of the PV array by compensating measured PV array yield to PV array yield at STC, and can be calculated as follows [65, 78, 79]:

$$P_{25} = P_{actual}(1 - \alpha(T_{mod} - 25\ ^{\circ}\mathrm{C})), \tag{5.2.6}$$

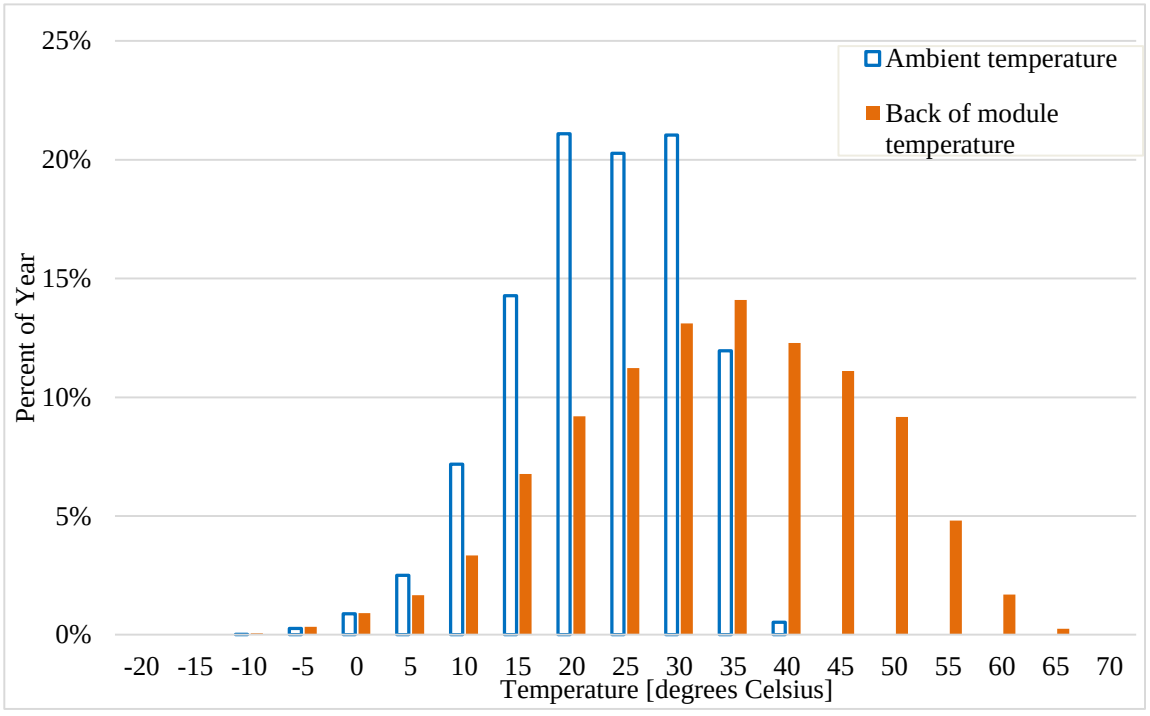

Figure 5.7: Average monthly ambient and module temperatures during production.

where α is the peak power temperature coefficient and T_{mod} is the measured module temperature.

According to the data recorded at the solar PV power plant, the overall PV loss due to temperature amounted to 6.3% during production. In high solar radiation regions, the module temperatures often reach 65 °C or higher in peak operating conditions and at 65 °C the conventional solar module's power output is reduced by up to 20% [42]. In the case of the Solar PV power plant under investigation the majority of solar energy production occurred when the ambient temperature was lower than the back of module temperature. Figure 5.8 depicts the distribution of energy production at low, (≤25 °C) and high, (>25 °C) module temperatures for the 75 MW_P solar PV power plant. The majority of solar energy production occurs when the ambient temperature is lower than the back of module temperature, as shown in Figure 5.7 and Figure 5.8. The energy generated at module temperatures of 25 °C or higher, accumulated to 87% of the total generation and the average energy weighted module temperature is approximately 40 °C, as can be observed in Figure 5.8.

5.2.6 Module array mismatch and Ohmic wiring losses

Due to the lack of specific I-V measurements of the solar PV modules in the field and real array energy, mismatch losses and Ohmic wiring losses were combined and calculated so as

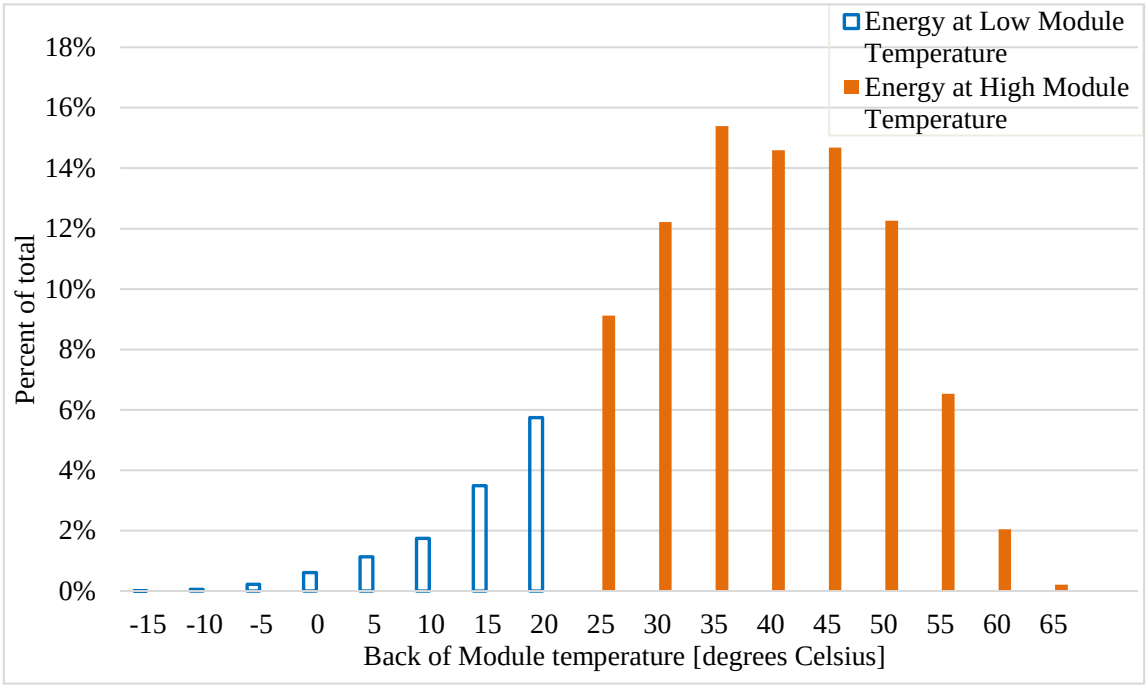

Figure 5.8: Average monthly ambient and module temperatures during production.

to make the calculated energy at the inverter input terminals equal to the measured inverter input energy.

5.2.6.1 Mismatch loss

Due to variations in the current-voltage characteristics, the PV modules connected in parallel or series to a PV array do not necessarily operate at their maximum power point [29]. The sum of the maximum output of the individual modules ($P_{max,module}$) is always greater than the maximum power output of the total PV array ($P_{max,array}$) at the same operating irradiance level [24]. The resulting difference is commonly called circuit mismatch (CM) [80]. Reducing mismatch losses improves the global PV array efficiency, and mismatch losses can be calculated as follows:

$$CM = \frac{\sum_{n=1}^{N} P_{max,module} - P_{max,array}}{\sum_{n=1}^{N} P_{max,module}}, \tag{5.2.7}$$

where n is the number of modules in an array.

5.2.6.2 DC Ohmic wiring loss

In utility scale PV systems, the cause of DC Ohmic wiring losses is the resistance of the cabling that interconnects PV modules. The total DC Ohmic wiring loss between the modules and the inverters is related to the type, thickness and length of the cables [21]. In addition to the cable loss, the transition resistances in fuses, terminals and connectors also contribute as DC Ohmic losses. DC Ohmic power loss ($P_{DC,Ohmic}$) can be accurately calculated by multiplying the square of the 30-minute averaged DC array current (I) with the resistance of the cables (R) as follows:

$$P_{DC,Ohmic} = I^2 R. \tag{5.2.8}$$

The sum of all DC-Ohmic power losses ($P_{DC,Ohmic}$) during the year multiplied by time gives the yearly energy DC-Ohmic losses ($E_{DC,Ohmic}$). The yearly energy losses are expressed as follows:

$$E_{DC,Ohmic} = \sum I^2 R t. \tag{5.2.9}$$

Since the voltage sense leads are connected to the inverter input terminals, the real array energy (E_{array}) is mostly not measured, but it is basically given by summing up the energy at the inverter input ($E_{Inverter_{input}}$) and the DC-Ohmic wiring losses as follows:

$$E_{array} = E_{Inverter_{input}} + E_{DC,Ohmic}. \tag{5.2.10}$$

In the case of the solar PV system, the combined mismatch and DC-Ohmic wiring losses were calculated from measurements as 1.77 %.

5.2.7 Inverter loss

In the case of grid-connected solar PV systems, the inverter changes DC power from the solar PV array to AC power for exporting to the utility grid. The AC energy from the inverter depends on the input at the inverter terminal i.e. the output power from the arrays and the inverter losses [81]. Inverter losses are due to Ohmic and switching losses in semiconductors, as well as standby power. The inverter efficiency is expressed as the ratio of the power at the inverter output terminals ($P_{inverter_{output}}$) to the power at the input terminals ($P_{inverter_{input}}$). The inverter losses ($P_{inverter_{loss}}$) of 2.60% were determined as follows:

$$P_{inverter_{loss}} = 100\left(1 - \frac{P_{inverter_{output}}}{P_{inverter_{input}}}\right). \tag{5.2.11}$$

Kalkbult solar PV plant's inverters operated at efficiencies between 94% and 99% in 2014, as shown in Figure 5.9. More data on the efficiency of each of the 84 inverters is provided in Appendix F. The best performing inverter efficiency is 98.60% which is equal to the rated efficiency in the datasheet [82] whereas the worst performing inverter was operating at 94.04%. The inverter with the best performance (Inverter 38) was used to show the efficiencies of the inverter at different output power levels for the whole year, and the results are shown in Figure 5.10. From Figure 5.10, it is observed that the inverter conversion efficiency increases and remains constant at high output power levels ($>$ 150 kW) and it decreases at low output power levels ($\leq$150 kW). The relationship between the inverter power loss and its output power is linear.

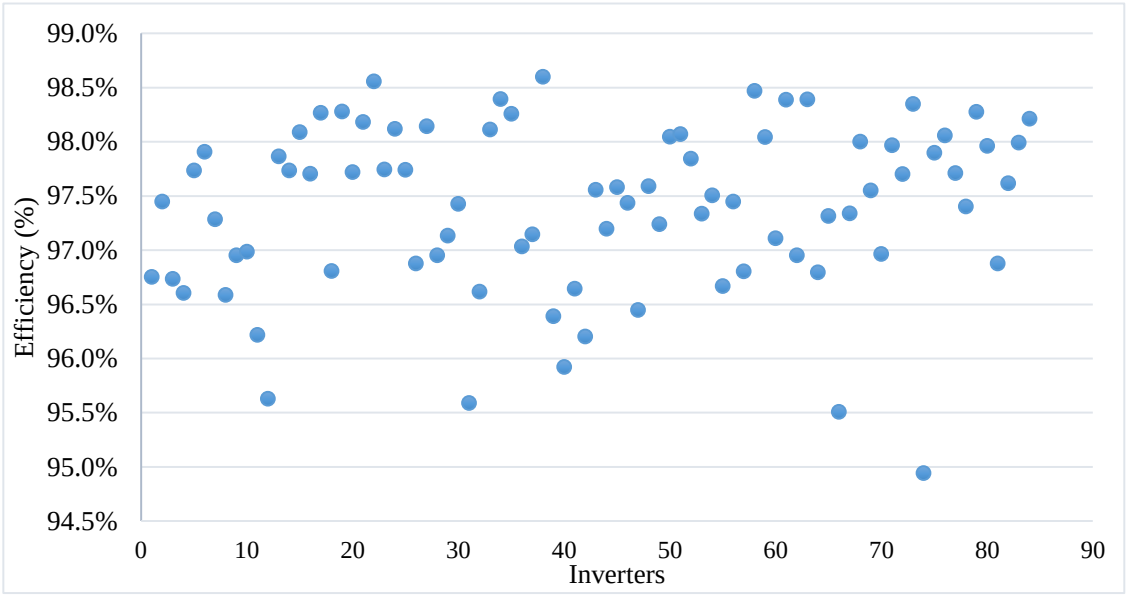

Figure 5.9: Inverter efficiency.

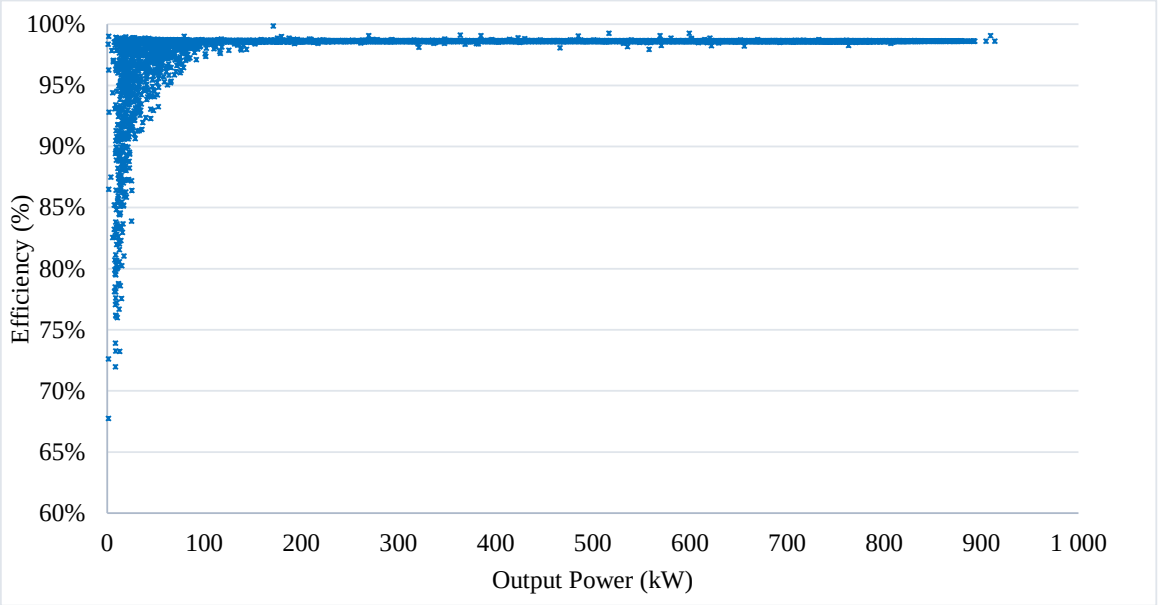

Figure 5.10: Inverter efficiency at different output power levels.

5.2.8 AC Ohmic and external transformer losses

AC Ohmic losses occur between the inverters and the utility connection point [21]. In this section, the AC Ohmic losses were combined with the transformer losses due to insufficient measured field data for the two to be calculated separately. Losses in the transformers are due to hysteresis and eddy-currents in the core, as well as Ohmic losses in the primary and secondary windings [19]. The system under investigation consists of 42 transformers, each connected to 2 inverters. The resulting AC Ohmic and transformer losses ($P_{AC+transf_{loss}}$) of 1.99% were calculated from the ratio of the power at the substation transformer input terminals ($P_{substation_{input}}$) to the power at the inverter output terminals ($P_{inverter_{output}}$) as follows:

$$P_{AC+transf_{loss}} = 100\left(1 - \frac{P_{substation_{input}}}{P_{inverter_{output}}}\right). \tag{5.2.12}$$

5.2.9 Substation transformer loss

Electricity is transmitted along power lines at high voltages to reduce the Ohmic losses. In order to achieve this, another transformer installed at the substation is used to step up the voltage. The substation transformer loss ($P_{substation_{loss}}$) of 0.344% was calculated from the ratio of the power supplied to the grid (P_{grid}) to the power at the input terminals of the substation transformer ($P_{substation_{input}}$) as follows:

$$P_{substation_{loss}} = 100\left(1 - \frac{P_{grid}}{P_{substation_{input}}}\right) \tag{5.2.13}$$

Further losses will occur during transmission and also as the electricity will be stepped down to levels usable by the consumer, but these losses are beyond the scope of this study.

5.3 PVsyst model correction

The starting point for evaluating the losses of a PV system is to calculate the energy which would be produced if the system always worked at standard test conditions (STC). In this section the 75 MW_P solar PV plant's system losses are listed, along with the PVsyst simulated losses for both the default loss and improved loss models. In PVsyst some losses are explicitly specified by the user and some losses are due to models. Losses specified by the user are as follows [83]:

- Soiling loss.
- Mismatch loss.
- Module quality loss.
- Availability loss.
- Reflection loss.
- Light induced degradation (LID) loss.
- Array wiring losses.

Losses due to models are as follows [83]:

- Spectral loss.
- PV loss due to irradiance level.
- PV loss due to temperature.
- Inverter losses.
- External transformer loss.

Module quality loss expresses the real behaviour of modules with respect to the manufacturer's specifications and was kept at 0% for all the models, i.e. the average manufacturer specified inferior tolerance [83] and LID losses were not quantified in this study because this loss mechanism is not proposed as default by the PVsyst software [19].

5.3.1 Loss analysis (Measured vs PVsyst model losses)

Table 5.4 shows the loss analysis results. The GHI to global irradiance incident in the collector plane (i.e. Global Plane Irradiance - GPI) conversion ratio is 12.3% for simulations done in PVsyst, whereas the conversion ratio from the field data was calculated as 12.61%. Soiling losses estimated according to the measured precipitation are close to half the respective PVsyst default loss model value. It can be seen that the improved PVsyst model's values for inverter loss, AC Ohmic and external transformer losses are close to the respective calculated losses. The calculated mismatch and DC Ohmic losses are half the respective PVsyst default loss value, and inverter losses calculated from measured values are within 0.3% of the respective improved PVsyst model value. The improved PVsyst model value for the PV loss due to temperature is close to the calculated value whereas the respective default loss model value is 2.1% greater than the calculated value. The results show that the PVsyst software package tends to underestimate the electrical energy generated by the installation due to the overestimation of losses for this solar PV power plant. The PVsyst simulation accuracy is in the order of

Table 5.4: Loss analysis results.

Parameter	**PVsyst default model**	**Determined from measured data**	**Improved PVsyst model**
GHI [kWh/m^2]	2 117	2 117	2 117
Global incident in coll. plane	12.3 %	12.61 %	12.3%
Near shadings irradiance loss	-3.0 %	-2.50%	-3.0%
Reflection loss	-2.6 %	-2.50 %	-2.6%
Soiling loss	-3.0 %	-1.75%	-1.8%
Effective coll. plane irradiance [kWh/m^2]	2 179	2 227	2 206
PV loss due to irradiance level	-0.3 %	-0.45%	-0.3%
PV loss due to temperature	-8.4 %	-6.3%	-6.4%
Mismatch + DC Ohmic loss	-3.2 %	-1.77%	-1.3%
Inverter loss during operation	-1.8 %	-2.60 %	-2.3%
Transformer and AC Ohmic loss	-1.36 %	-1.99%	-2.07%
Substation transformer loss	-	-0.344 %	-
Deviation from the Grid yield	6.3 %	0%	2.07%

2 to 3% (MBE - Mean Bias Error) due to uncertainty with regard to the model used to transpose GHI to the incident irradiation in the collector plane [19].

5.3.2 Energy yield comparison using 2014 measured data

Figure 5.11 shows the energy yield from the energy meters at the solar PV plant normalised to the monthly average grid yield, in comparison to the simulated energy yield from the improved PVsyst model and the PVsyst default loss model using the Hay irradiance model. Thirty minute averaged GHI data was used as input in PVsyst simulation tool and the data was imported using the "PVsyst standard format" tool described in Appendix C. The PVsyst file showing the results from the simulation is given in Appendix G. It can be observed from Figure 5.11 that the improved PVsyst model more closely follows the measured grid yield trend line compared to the PVsyst default loss model. The improved model's trend line follows that of the measured data from January to March and then from October to December. The differences of approximately 4% observed from April to September show that the arrays are outperforming the improved model simulation. The differences can be traced back to the radiation transposition models used within PVsyst that calculate relatively less Plane-Of-Array (POA) irradiance in winter months, as shown in Figure 5.12. Solar radiation models will be investi-

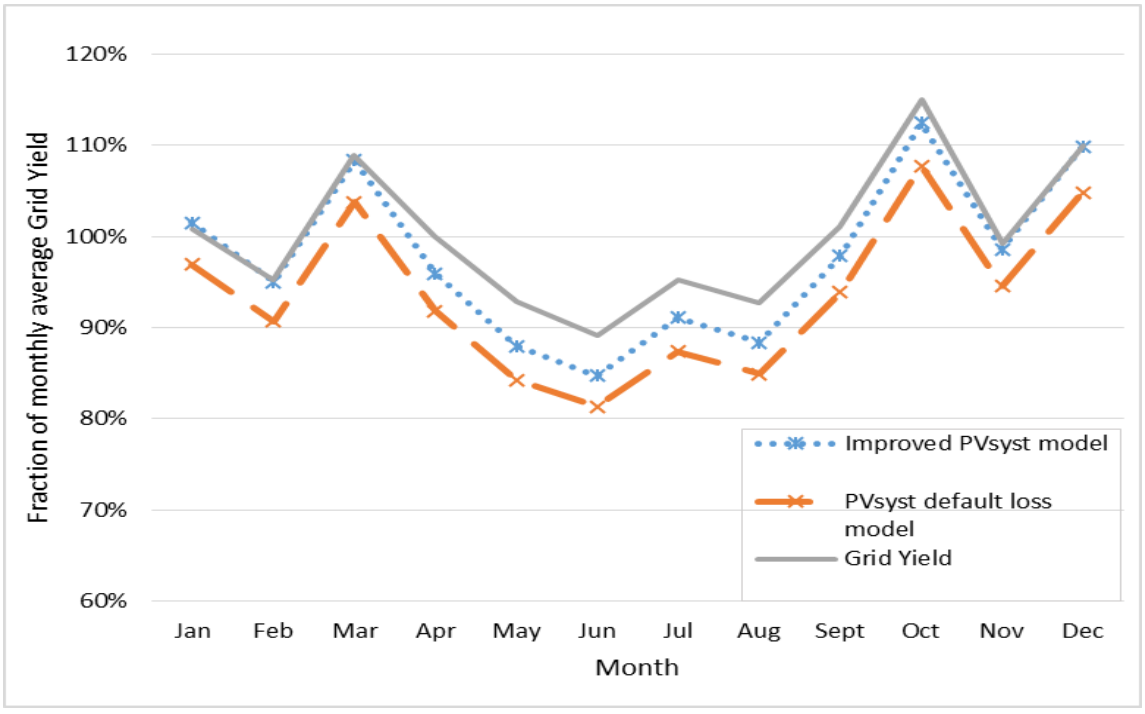

Figure 5.11: Comparison between simulated yield and grid yield using the Hay model and GHI input data.

gated further in the next chapter. In the literature, a real-world system that also outperformed PVsyst software by an average over performance of 5.4% was reported [18]. A better performance model with all the losses derived from accurately measured data and losses given as monthly values would produce simulation results even closer to the field data.

The differences in expected and measured energy yield are also due to the respective variances in the models used to calculate losses. Some loss values are expressed as constant yearly values in PVsyst, whereas in reality the loss values vary with time. The PVsyst simulated energy yield using the default loss model is 6.4% lower than the actual measured grid yield, as shown in Figure 5.11, therefore the PVsyst default loss model overestimated the solar PV system's losses. The energy yield from the improved model in combination with the Hay irradiance model is 4% better than the yield obtained when using the default loss model and this resulted in an energy yield which is 2.3% lower than the energy meter readings.

Figure 5.13 shows the measured grid energy yield normalised to the average monthly energy yield, in comparison to the PVsyst simulated energy yield from the default and improved loss models using 30 minute GHI data as input and the Perez irradiance model. The PVsyst file showing the results from the simulation is given in Appendix H. By comparing Figure 5.13 to Figure 5.11, it can be observed that the energy yield values obtained from the Perez model follow the measured data better compared to the values obtained from the Hay model. Differences in the measured and PVsyst simulated energy yield reduced to highest monthly values

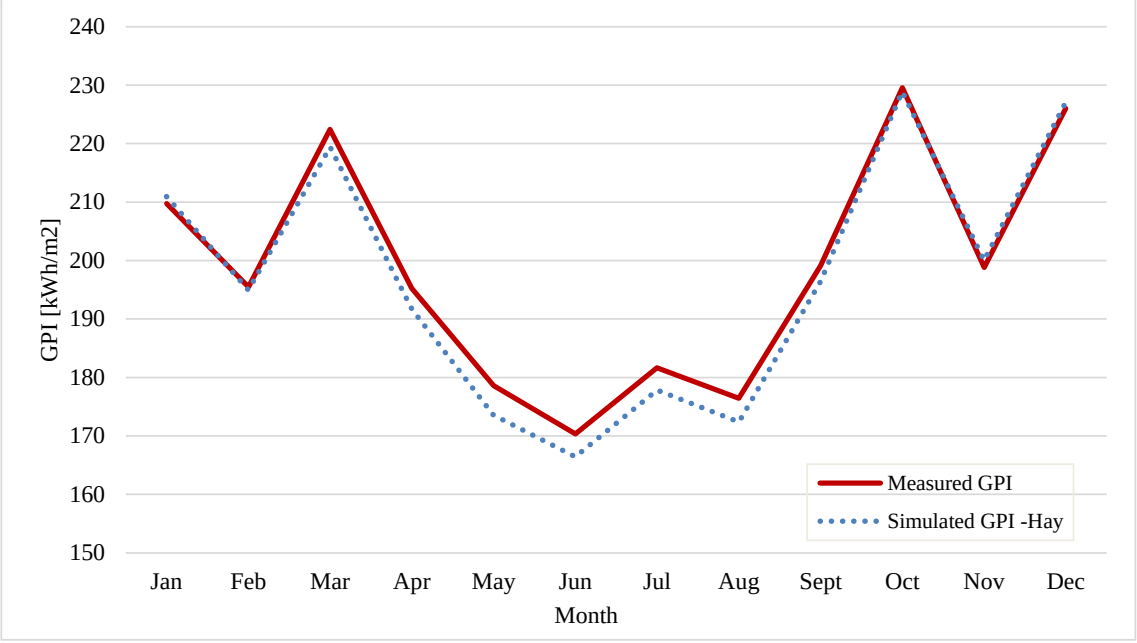

Figure 5.12: Comparison between predicted and measured Plane-Of-Array irradiance.

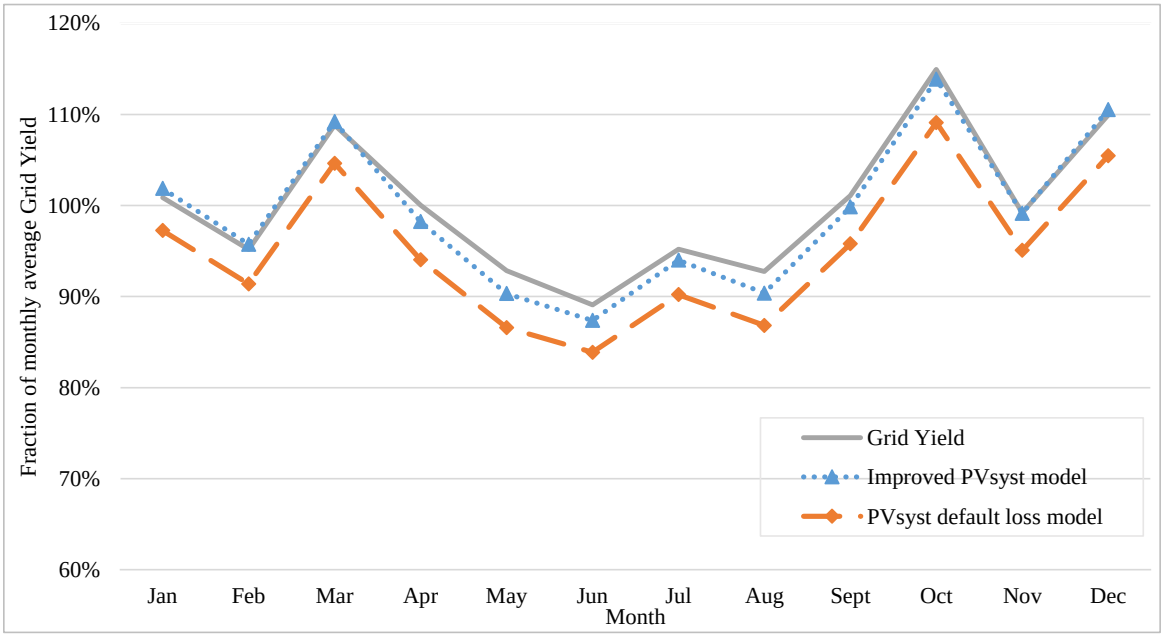

Figure 5.13: Comparison between simulated yield and grid yield using 30 min averaged GHI input data.

of 3% and a yearly average value of 0.78% when using the Perez irradiance model. It was also observed that the "Import ASCII meteo file" format of importing data into PVsyst is more accurate than the "PVsyst standard format". This is due to the ASCII format allowing the input of sub-hourly meteo data whereas the PVsyst standard format allows for the input of hourly values only.

Figure 5.14 shows the percentage differences between the measured and simulated energy yield using input GHI and POA irradiance data. The PVsyst file showing the results from the simulation is given in Appendix I. From the figure it can be observed that using Plane-Of-Array irradiance as input in PVsyst simulation tool results in energy yield calculations that are within 2% of the field recorded values. It can also be observed that the monthly energy yield values from the Perez and Hay models are within 3% and 4% of the measured monthly values, respectively. Therefore measured Plane-Of-Array irradiance reduces the errors in predicting the available generation of a solar PV system using simulation tools. Validation of the improved PVsyst model using data for operational year 2015 is in Appendix J. It was observed that the monthly energy yield simulated from the 30-minute averaged values for 2015 is closer to the measured energy yield compared to that for 2014 obtained from hourly values. It was also observed that the solar radiation patterns for 2014 and 2015 are different. The percentage differences between the measured and simulated energy yield for 2015 are within 2% for

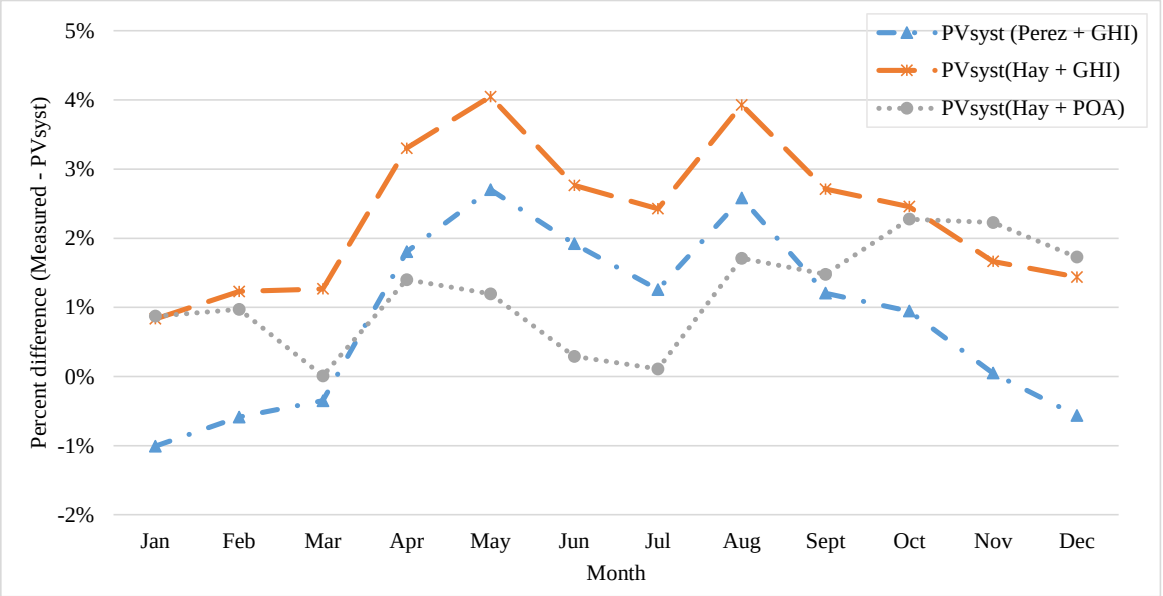

Figure 5.14: Percentage differences between measured and simulated energy yield using input GHI and POA irradiance data.

the majority of the months, less than the uncertainty of the PVsyst simulation tool, except for October, November and May. These differences in energy yield are in accordance with the respective differences in the measured and simulated Global Plane Irradiance, caused by the irradiance models not transposing GHI into GPI correctly.

The main uncertainties regarding the PV production using PVsyst software are: the meteorological data (source and annual variability) as well as the PV model (Hay or Perez model), soiling, and the validity of the manufacturer's specifications [83].

5.4 Case study: Single and double axis trackers

Table 5.5 shows the PVsyst simulated yearly energy yield values for the 75 MW_P Kalkbult solar PV power plant if it were a single or double axis tracker. The energy yield values are simulated in PVsyst software whilst keeping the module area, PV array and inverters the same. A gain in energy of 15% resulted when the solar PV system was simulated as a single axis tracker at a tilt angle of 0°, using the Perez model and the resulting PVsyst file is given in Appendix K, whereas a gain of 13.7% resulted when the Hay model was used at the same tilt angle and the resulting PVsyst file is given in Appendix L. When the solar PV plant was simulated as a single axis tracker at an optimum tilt angle of 30°, this resulted in a 25.2% gain in energy yield when using the Perez model and 23.3% gain when using the Hay model in PVsyst. The

Table 5.5: Energy yield analysis.

N-S axis tracker	Tilt angle	Perez model	Hay model
		MWh	MWh
Single axis tracking	0°	172358	170345
Single axis tracking	30°	187602	184793
Double axis tracking	-	204819	202059

respective PVsyst reports using the Perez and Hay models at thirty degrees tilt angle are given in Appendix M and Appendix N, respectively. Simulating the 75 MW_P solar PV power plant as a double axis tracker yielded a 36.7% gain in energy using the Perez model and 34.8% gain using the Hay model. The PVsyst files when the 75 MW_P is simulated as a dual axis tracker using the Perez and Hay models are given in Appendix O and Appendix P, respectively.

5.5 Conclusion

An essential part of enhancing the performance of installed solar PV systems is understanding the energy losses which occur in the system and developing methods to minimise these losses where possible. From the analysis it can be concluded that it is important to evaluate the losses in each part of the solar PV system and to make specific improvements in order to decrease the major losses. This will help to improve the design of future solar PV systems.

The PVsyst V6.39 (Perez) default loss model overestimated the solar PV plant's actual losses by 6.4%. The calculation of the losses in the operational system resulted in an improved PVsyst model and when simulated in hourly values, gave a 4% higher yield using the Hay irradiance model. Different irradiance models in PVsyst resulted in variances between the measured and simulated energy yield of 0.78% and 2.3% for the Perez and Hay models respectively. The improved model is essential for accurately forecasting PV system generation capacity, as required by the utility providers. According to the analysis, the operational system significantly outperformed the software simulations. On a monthly basis, PVsyst exhibits a seasonal variation in the energy yield error magnitude, appearing to be biased higher in winter than in summer. The differences in the improved model and the grid yield observed in the winter season were mostly due to the radiation transposition models calculating relatively less Plane-Of-Array irradiance in winter months, and the models will be investigated further. In conclusion, the analysis contributes to the enhancement of the performance model's accuracy when continuously forecasting expected system performance and losses.

CHAPTER 6

IRRADIANCE MODELS

Accurately estimating the solar irradiance on tilted surfaces is a prerequisite for the reliable prediction of the energy yield of solar PV systems. In this chapter, irradiance models that estimate Global Plane Irradiance (GPI) from Global Horizontal Irradiance (GHI) measurements are evaluated for South African climatic conditions. Seven irradiance decomposition models namely Orgill and Hollands, Erbs, Louche, Reindl_1 , Reindl_2 , Disc and Dirint are evaluated as well as combinations of the Isotropic, Sandia, Klucher, Hay, Reindl and Perez transposition models with the best performing decomposition models.

6.1 Introduction

Solar radiation decomposition and transposition models are required for accurate yield forecasting of solar PV plants. Therefore empirical validations of the available solar radiation models are required to make modellers and developers confident that their respective algorithms simulate reality [84]. A comparison between the PVsyst simulated and measured energy yield of a solar PV plant located in South Africa was done in literature [85] with the results showing that the PVsyst simulated energy yield does not correlate a 100% with the measured energy yield, especially in winter months. An annual plane-of-array (POA) energy estimation using the PVsyst simulation tool can vary by over 1.45% by simply interchanging the transposition models within PVsyst i.e. Hay/Davies and Perez models as shown in Figure 6.1 [86]. Due to the lack of a standard combination of decomposition and transposition models for converting Global Horizontal Irradiance (GHI) to Global Plane Irradiance (GPI), various combinations are in use and this leads to different estimates of GPI, even when the same GHI is used as input [4]. GHI measurements are often available, whereas the solar PV modules are tilted to maximise the yearly energy yield and for this yield calculation the GPI is required. Few locations in South Africa have reliable, measured GHI and GPI data sets and that makes GPI estimation important.

Estimating GPI from GHI involves two steps, the decomposition of GHI into direct and diffuse horizontal components using irradiance transposition models and then the transposition of the two horizontal components into the Plane-Of-Array direct beam, ground reflected and diffuse components using irradiance transposition models [86]. In the literature there are

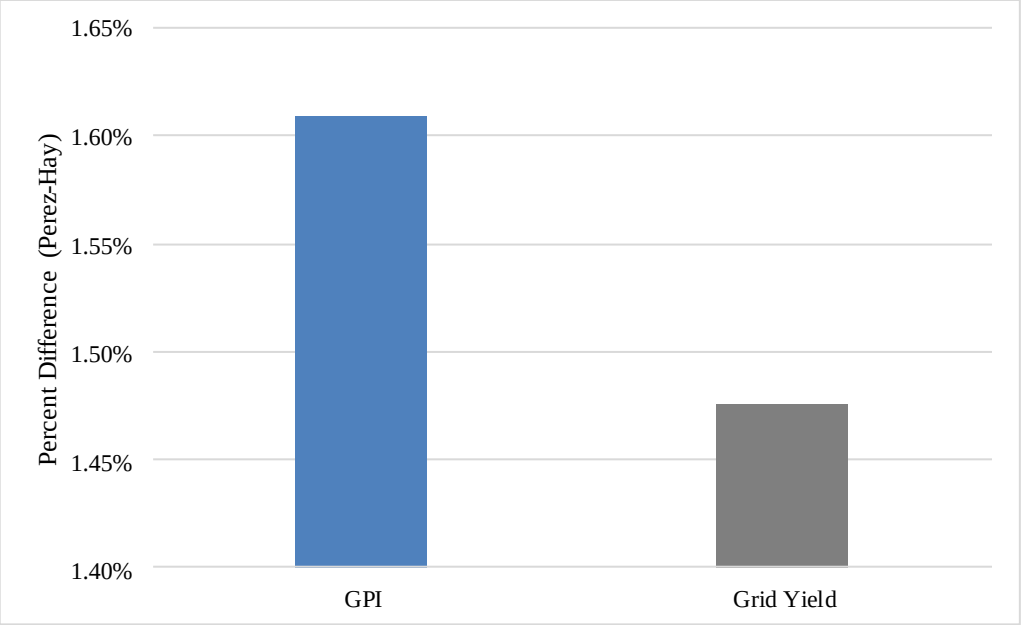

Figure 6.1: Annual differences in POA irradiance and AC energy between the Perez and Hay/-Davies transposition models as implemented in PVsyst.

numerous studies which assess and compare solar radiation models for non-South African regions, with recent studies being done in the USA [86] and countries in Northern Africa i.e. Egypt and Algeria [84, 87, 88].

The main objective of this study is to compare six transposition models, namely: Isotropic, Sandia, Klucher, Hay/Davies, Reindl and Perez for a region in South Africa. Firstly, the Dirint, Disc, Erbs, Louche, Orgill and Hollands, Reindl_1 and Reindl_2 irradiance decomposition models are separately evaluated using measured Global Horizontal Irradiance (GHI), Direct Normal Irradiance (DNI) and Diffuse Horizontal Irradiance (DHI) from weather stations at Bloemfontein and Sutherland i.e. areas close to the solar PV plant. This is due to the unavailability of measured DNI and DHI at Kalkbult. The Bloemfontein and Sutherland weather stations' data are available through the South African Universities Radiometric Network (SAURAN) [89] and the global and diffuse irradiance measurements are taken using Kipp and Zonen CMP 11 standard pyranometers whilst Direct Normal Irradiance measurements are taken using the SOLYS trackers and CHP1 pyrheliometers [27]. Sutherland is at latitude -32.4° and longitude 20.7° whilst Bluemfontein is at latitude -29.1° and longitude 26.2°. The measured GHI and GPI data from an operational 75 MW_P solar PV plant in South Africa is used to evaluate the transposition models in combination with the decomposition models that best estimate the DHI and DNI for Bloemfontein and Sutherland. The irradiance decomposition and transposition models selected here

are those that are commonly used in PV design or simulation tools such as PVsyst (Erbs, Dirint, Hay and Perez), SAM (Isotropic, Reindl, Perez), PV*SOL (Reindl and Hay/Davies), PVWatts (Perez) and RETScreen (Erbs and Isotropic) [90]. Further analysis is done to investigate the additional bias introduced by using satellite-derived GHI when there are no ground measurements for GHI.

6.2 Methodology

Figure 6.2 is a summary of how the combination of a decomposition and transposition model or a transposition model is used to estimate the GPI from the available ground measurements [86]. From the figure it can be seen that the conversion of GHI into GPI involves two steps when there is no measured DHI i.e. the decomposition of GHI into its direct and diffuse horizontal components followed by the transposition of the decomposed components into GPI or Plane-Of-Array (POA) irradiance.

The relative abilities of the different decomposition and transposition models to estimate the solar radiation on a tilted surface were tested using statistical methods. In this study, the irradiance models were modelled in Matlab and the following statistical estimators were used to evaluate them: root mean square error (RMSE) and mean bias error (MBE). These estimators should be close to zero to indicate high modelling accuracy [84].

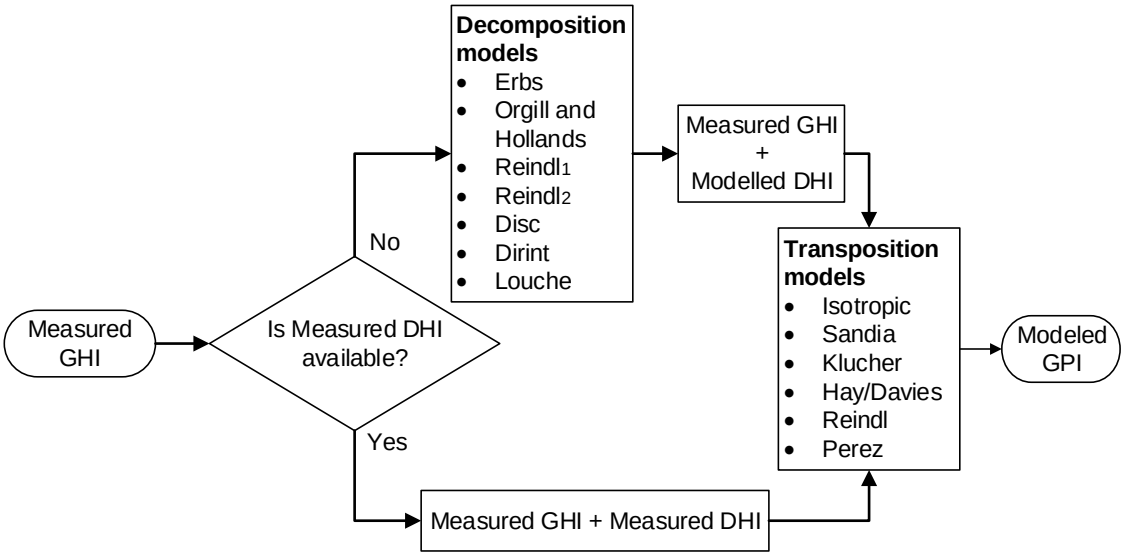

Figure 6.2: Flowchart showing how to model GPI from measured GHI.

6.2.1 Root Mean Square Error (RMSE)

The RMSE compares the actual deviation between the measured ($G_{i,meas}$) and estimated ($G_{i,calc}$) irradiance values, thereby yielding information on the short term performance of the model [84]. The RMSE gives the model scatter and is always positive. The smaller the RMSE, the better the model with a RMSE value of zero representing the ideal case. The RMSE values are obtained as follows:

$$RMSE = \sqrt{\frac{1}{N}\sum_{i=1}^{N}(G_{i,meas} - G_{i,calc})^2}. \tag{6.2.1}$$

The subscript N represents the total number of solar radiation data points and i refers to the $i-th$ data point of the solar radiation data. The subscripts "$meas$" and "$calc$" refer to the measured and calculated values respectively.

6.2.2 Mean Bias Error (MBE)

The MBE provides long term performance information of the deviation between the measured ($G_{i,meas}$) and estimated ($G_{i,calc}$) irradiance values. The MBE is the average difference between the measured and modelled values. A low MBE value is desired, to indicate high modelling accuracy and a negative value shows an average overestimation in the modelled values. A disadvantage of the MBE is that overestimation from one observation may be cancelled by an underestimation from a separate observation, which is why it is seldom used for short term evaluations [84]. MBE is determined as follows:

$$MBE(\%) = \frac{1}{N}\sum_{i=1}^{N}\frac{G_{i,meas} - G_{i,calc}}{G_{i,meas}} \cdot 100\%, \tag{6.2.2}$$

where, subscripts N, i, $meas$, and $calc$ are as defined in Equation 6.2.1. The mean percentage error (MPE) gives the percentage errors by which the forecasts from the model deviate from the actual values of the quantity being forecast. Researchers suggest that daily percentage errors between -10% and +10% and monthly bias errors within 3% are acceptable [91]. A brief discussion on the models that are considered in the analysis follows.

6.3 Irradiance Decomposition models

The decomposition models considered in this study are listed in Table 6.1. These models use coefficients estimated from fixed sets of measured data [86]. A number of these decomposition models make use of the clearness index (k_t) to calculate the diffuse fraction (k_d). The clearness

Table 6.1: Decomposition models.

Model	Year - Test sites	Input variables
Orgill and Hollands [92]	1977 - Canada	k_t
Erbs [93]	1982 - USA	k_t
Louche [94]	1991 - France	k_t
Reindl$_1$ [95]	1990 - USA and Europe	k_t
Reindl$_2$ [95]	1990 - USA and Europe	k_t,α_s
Disc [96]	1987 - USA	k_t,α_s
Dirint [97]	1992 - USA and Europe	Δk_t,α_s,T_{dp}

index is determined as follows:

$$k_t = \frac{G}{G_o}, \tag{6.3.1}$$

where, G_o is the extra-terrestrial irradiance. The diffuse fraction is multiplied by the Global Horizontal Irradiance (G) to get the direct horizontal irradiance (G_d) and it is expressed as follows:

$$k_d = \frac{G_d}{G}. \tag{6.3.2}$$

Alternatively some models calculate the direct fractions to find the DNI. Some models, like the Dirint model, also take the solar elevation angle (α_s), the dew point temperature (T_{dp}) and the variability of clearness index (Δk_t) into account when computing DHI and DNI. The scattered terrestrial irradiance received by a horizontal surface is the Diffuse Horizontal Irradiance (DHI). The sum of the DNI projected onto the horizontal surface and DHI gives the GHI, i.e. the total radiation on a horizontal surface as expressed by Equation (2.1.13). In some solar PV systems the GHI is measured, and decomposition models are used to estimate the DHI and DNI. The decomposition models will be presented and evaluated in the sections to come, (For detailed descriptions of the transposition models, we refer the reader to the references in Table 6.1).

6.3.1 Orgill and Hollands

Orgill and Hollands developed the first relationship between the hourly diffuse fraction (k_d) and clearness index (k_t), based on 4 years of data acquired from one location in Toronto [92].

The correlation is divided into three zones as follows [92]:

$$k_d = 1 - 0.249k_t : (k_t < 0.35), \tag{6.3.3}$$

$$k_d = 1.577 - 1.84kt : (0.35 \leq kt \leq 0.75), \tag{6.3.4}$$

$$k_d = 0.177 : (k_t > 0.75). \tag{6.3.5}$$

The range ($k_t < 0.35$) represents values from extremely overcast days with up to 90% of the total solar radiation being diffuse, whereas the range ($k_t > 0.75$) has values that represent relatively clear periods with some cloud cover but the sun itself not shaded by a cloud [92]. The (k_d) value for the range ($k_t < 0.35$) was recommended to be a constant 0.177 due to the unpredictable nature of cloud reflection and limited frequency of data in the range, i.e. only 5.6% of the measured data over the four year period. The range ($0.35 \leq k_t \leq 0.75$) constituted of most of the measured data over the four year period i.e. 62% [92].

6.3.2 Erbs

Erbs adapted the (k_t - k_d) correlation in 1982, and extended it to latitudes from 31° to 42° North [93]. The model was validated using hourly pyrheliometer and pyranometer data from four stations in the United States of America (USA), based on pyrheliometric measurements. The Erbs model is divided into three zones as follows [93]:

$$k_d = 1 - 0.09k_t \times k_t : (k_t < 0.22), \tag{6.3.6}$$

$$k_d = 0.9511 - 0.1604k_t + 4.388k_t^2 - 16.638k_t^3 + 12.336k_t^4 : (0.22 < k_t \leq 0.8), \tag{6.3.7}$$

$$k_d = 0.165 : (k_t > 0.8). \tag{6.3.8}$$

Following the procedure of Orgill and Hollands [92], a constant value of 0.165 was chosen for values of (k_t) greater than 0.8 because the data in that range is not understood well enough to justify fitting a curve to them [93].

6.3.3 Louche

In 1991, Louche established correlations on Global Horizontal Irradiance and Direct Normal Irradiance for a mediterranean site [94]. Louche's model estimates the transmittance of beam (k_b), using the clearness index (k_t). The model is based on global (G) and direct beam irradiance (G_b) data recorded between October 1983 and June 1985 at a metereological station in Ajaccio (Corsica, France). The model is defined as follows:

$$k_b = -10.627k_t^5 + 15.307k_t^4 - 5.205k_t^3 + 0.994k_t^2 - 0.059k_t + 0.002. \tag{6.3.9}$$

The direct beam irradiance (G_b) is then determined using the direct transmittance as follows:

$$G_b = k_b \cdot G_o, \tag{6.3.10}$$

where, G_o is the extraterrestrial irradiance.

6.3.4 Reindl$_1$ and Reindl$_2$

The climatic-geometric variables' influence on the hourly diffuse fraction (k_d) was studied in 1991 by Reindl et al. [95]. From measurements of global and diffuse irradiance on a horizontal surface taken from five locations in USA and Europe, Reindl et al. estimated the diffuse fraction (k_d) using two models, namely Reindl$_1$ and Reindl$_2$. The first model's (Reindl$_1$) expression for the diffuse fraction was established using the clearness index k_t as follows [95]:

$$k_d = 1.02 - 0.248k_t : (k_t \leq 0.3), \tag{6.3.11}$$

$$k_d = 1.45 - 1.67kt : (0.3 < kt < 0.78), \tag{6.3.12}$$

$$k_d = 0.147 : (k_t \geq 0.78). \tag{6.3.13}$$

The second correlation known as the Reindl$_2$ model, uses the solar elevation (α_s) and the clearness index (k_t) as input to estimate the diffuse fraction (k_d) [95]. The model is expressed as follows [95]:

$$k_d = 1.02 - 0.254k_t + 0.0123sin(\alpha_s) : (k_t \leq 0.3), \tag{6.3.14}$$

$$k_d = 1.4 - 1.749kt + 0.177sin(\alpha_s) : (0.3 < kt < 0.78), \tag{6.3.15}$$

$$k_d = 0.486k_t - 0.182sin(\alpha_s) : (k_t \geq 0.78). \tag{6.3.16}$$

6.3.5 DISC

The Direct Insolation Simulation Code (DISC) model is a quasi-model developed in 1987 by Maxwell [96]. The model converts hourly Global Horizontal Irradiance (GHI) to Direct Normal Irradiance (DNI) and it is a combination of a physical model with experimental fits for other conditions. Maxwell's model was developed using one year's meteorological data for Atlanta, Georgia in the USA and it was validated using three sites in the USA with different climates: Albuquerque, New Mexico; Brownsville, Texas; and Bismarck, North Dakota [98]. The modeled DNI is computed as follows [98]:

$$G_n = G_o \cdot k_n, \tag{6.3.17}$$

where G_o is the hourly extraterrestrial irradiance, and k_n is the direct beam transmittance calculated as follows:

$$k_n = k_{nc} - \Delta k_n \tag{6.3.18}$$

and

$$\Delta k_n = a + be^{c \cdot AM}. \tag{6.3.19}$$

Clear sky limit (k_{nc}) is a polynomial in air mass (AM) and it is expressed as follows:

$$k_{nc} = 0.866 - 0.122AM + 0.0121AM^2 - 0.000653AM^3 + 0.000014AM^4. \tag{6.3.20}$$

The DISC model is partitioned into two parts, ($k_t \leq 0.60$) and ($k_t > 0.60$), and a,b,c are functions of the clearness index (k_t), expressed as follows:

for $k_t \leq 0.60$,

$$a = 0.512 - 1.56k_t + 2.286k_t^2 - 2.222k_t^3, \tag{6.3.21}$$

$$b = 0.370 + 0.962k_t^3, \tag{6.3.22}$$

$$c = -0.280 + 0.932k_t - 2.048k_t^2, \tag{6.3.23}$$

for $k_t > 0.60$,

$$a = -5.743 + 21.77k_t - 27.49k_t^2 + 11.56k_t^3, \tag{6.3.24}$$

$$b = 41.4 - 118.5k_t + 66.05k_t^2 + 31.90k_t^3, \tag{6.3.25}$$

$$c = -47.01 + 184.2k_t - 222.0k_t^2 + 73.81k_t^3. \tag{6.3.26}$$

While the model has been evaluated for three different continental sites with latitude from 28° to 45° North, it was mentioned that it is not entirely clear whether the DISC model will perform well at sites that are outside this latitude range [96]. This is due to the range of air mass, or zenith angle for the model design and validation being for continental sites within the 28° to 45° North latitudes [98].

6.3.6 Dirint

The Dirint model is based on the DISC model, a quasi-physical model developed by Maxwell in 1987 [96]. The Dirint model was developed in 1992 by Perez et al. with the aim of enhancing the performance of the DISC model. Consequently, the Dirint model uses a clearness index variation parameter k_t' that does not depend on the the zenith angle and it is expressed as follows [97] :

$$k_t' = k_t / (1.031 \cdot e^{[-1.4/0.9+9.4/AM)]} + 0.1). \tag{6.3.27}$$

The Dirint model also introduces a stability index parameter ($\Delta k'_t$), that varies with time and is expressed as follows:

$$\Delta k'_t = 0.5 \cdot (|k'_{t(i)} - k'_{t(i+1)}| + |k'_{t(i)} - k'_{t(i-1)}|), \tag{6.3.28}$$

where $i-1$, i and $i+1$ refer to the previous, current and next hourly record, respectively [98]. Utilizing the k'_t, $\Delta k'_t$ and zenith angle parameters, the Dirint model was characterised as a three dimensional model [97]. The 4-D model has an additional input variable i.e. the dew point temperature T_{dp}. The Dirint model's formulation of the hourly direct irradiance (G_n) was then expressed as follows:

$$G_n = G_o \cdot k'_b \cdot e^{[-1.4/0.9+9.4/AM)]}/0.87291, \tag{6.3.29}$$

where $k'_b = 0$ if $k'_t < 0.2$, otherwise $k'_b = ak'_t + b$, where a and b are coefficients in a lookup table given in [97] and G_o is the extraterrestrial irradiance.

According to the article in which the model was first published, the Dirint model performed only slightly better than the DISC model whilst using the following input variables: GHI, solar constant, altitude of location, zenith angle, as well as the lookup matrices for the correction coefficients and dew point temperature T_{dp} [97].

6.4 Irradiance Transposition models

The transposition models evaluated in this work and their required input parameters are listed in Table 6.2. For detailed descriptions of the transposition models, the reader is referred to the references in Table 6.2. Estimation of global inclined/tilt irradiance (G_t) using transposition models is achieved by using Equation 2.1.14 [86]. The global tilt irradiance (G_t) is a sum of the POA direct beam ($G_{b,t}$), POA ground reflected ($G_{g,t}$) and POA sky diffuse ($G_{d,t}$) irradiance

Table 6.2: Transposition models.

Model	Input variables
Isotropic [99]	DHI, θ_T
Sandia [10]	DHI, GHI, θ_Z
Klucher [100]	DHI, GHI, θ_T, θ_{Az}, θ_Z , α_s
Hay/Davies [101]	DHI, DNI, G_o , θ_T, θ_{Az}, θ_Z, α_s
Reindl [102]	DHI, DNI, GHI, θ_T, θ_{Az}, θ_Z, α_s
Perez [103]	DHI, DNI, G_o , θ_T, θ_{AOI}, AM

components. For the transposition models under investigation, the albedo (ρ_g) which is substituted into Equation 2.1.16 is a constant 0.2 except for the Sandia model which uses an albedo that is estimated from the sun zenith angle (θ_Z) as follows [86]:

$$\rho_g = 0.012 \cdot \theta_Z - 0.04. \tag{6.4.1}$$

The POA direct beam and ground reflected irradiance components are obtained according to Equation (2.1.15) and Equation (2.1.16) respectively. The transposition models treats the POA direct beam and the POA ground reflected components similarly but differs in the way they treat the POA sky diffuse irradiance on the plane of array. Diffuse radiation is typically separated into the isotropic component, the circumsolar diffuse component and the horizon brightening component [10]. The uniform irradiance from the sky dome is represented by the isotropic component whereas the forward scattering of radiation concentrated in the area immediately surrounding the sun is represented by the circumsolar diffuse or anisotropic component and the schematic representation is as shown in Figure 6.3 [104]. Various transposition models use different semi-empirical methods for determining these components, both isotropic and anisotropic models are widely used. Some of the commonly used diffuse irradiance models are discussed in the sections to follow.

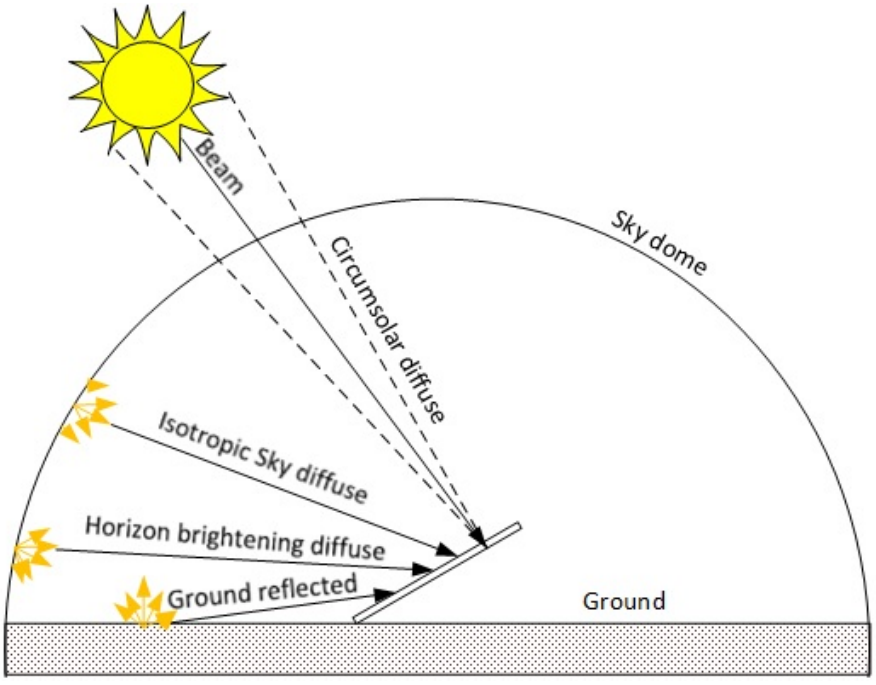

Figure 6.3: Schematic diagram showing the radiation incident on a tilted surface.

6.4.1 Isotropic

The Isotropic sky model described by Liu and Jordan forms the foundation from which transposition models are built [99]. It is the simplest model that assumes all diffuse radiation to be uniformly distributed across the sky dome, thus the sky diffuse irradiance on a tilted plane can be found from the tilt angle of the surface and the direct horizontal irradiance [105]. The Plane-Of-Array (POA) sky diffuse irradiance ($G_{d,t}$) is expressed as a fraction of the Diffuse Horizontal Irradiance G_d as follows:

$$G_{d,t} = G_d \cdot \left(\frac{1 + cos(\theta_T)}{2} \right), \tag{6.4.2}$$

where θ_T is the array tilt angle.

6.4.2 Sandia

The Sandia model developed by David King at the Sandia National Laboratories builds on the Isotropic model and adds an empirical correction term to account for the circumsolar and horizon brightening effects [10]. The model calculates the diffuse irradiance on an incline $G_{d,t}$ using the Diffuse Horizontal Irradiance (G_d), Global Horizontal Irradiance (G), surface tilt angle (θ_T) and sun zenith angle (θ_Z) as follows:

$$G_{d,t} = G_d \cdot \left(\frac{1 + cos(\theta_T)}{2} \right) + G \cdot \left(\frac{(0.12\theta_Z - 0.04)(1 - cos(\theta_T))}{2} \right). \tag{6.4.3}$$

6.4.3 Klucher

The Klucher model also incorporates the effect of circumsolar radiation and horizon brightening [100]. It is based on a study of clear sky conditions by Temps and Coulson and was modified to incorporate the conditions of cloudy skies [100]. Klucher found that the isotropic model underestimates the irradiance under clear and partly overcast conditions when there is increased intensity in the circumsolar region of the sky and near the horizon whilst it gives good results for overcast conditions [105]. Klucher's sky diffuse solar radiation incident on an inclined surface is formulated as follows [84]:

$$G_{d,t} = G_d \cdot \left[\left(\frac{1 + cos(\theta_T)}{2} \right) (1 + Fsin^3(\theta_T/2))(1 + Fcos^2\theta_Z sin^3\theta_Z) \right], \tag{6.4.4}$$

where, F is a modulating function which is equal to zero when the skies are completely overcast and the Klucher model reverts to the isotropic model. F is generally expressed as follows:

$$F = 1 - \left(\frac{G_d}{G} \right)^2. \tag{6.4.5}$$

6.4.4 Hay/Davies

The Hay/Davies model does not include the horizon brightening component but divides the diffuse irradiance from the sky into isotropic and circumsolar components with an anisotropic index based on the amount of Direct Normal Irradiance (G_n) relative to extra-terrestrial irradiance (G_o) [101]. The sky diffuse radiation using the Hay and Davies model is determined as follows:

$$G_{d,t} = G_d \cdot \left[A_i cos(\theta_{AOI}) + (1 - A_i) \frac{1 + cos(\theta_T)}{2} \right], \tag{6.4.6}$$

where θ_{AOI} is the angle of incidence and A_i is the anisotropy index that represents the transmittance through atmosphere for beam radiation and it is expressed as:

$$A_i = \frac{G_n}{G_o} \tag{6.4.7}$$

6.4.5 Reindl

The Reindl model extends the Hay and Davies model by taking into account the horizon brightening [102]. Thus it represents all three components of POA diffuse radiation, i.e. the isotropic diffuse, circumsolar and horizon brightening. The sky diffuse radiation formulation for the Rendl model is as follows:

$$G_{d,t} = G_d \cdot \left[A_i cos(\theta_{AOI}) + (1 - A_i) \frac{1 + cos(\theta_T)}{2} \right] \left(1 + \sqrt{\frac{G_n \cdot cos(\theta_Z)}{G}} sin^3(\frac{\theta_T}{2}) \right), \tag{6.4.8}$$

where the A_i is as defined in the Hay and Davies model, G_d is the Diffuse Horizontal Irradiance, θ_T is the array tilt angle , θ_{AOI} is the angle of incidence, G is the Global Horizontal Irradiance, G_n is the Direct Normal Irradiance and θ_Z is the sun's zenith angle.

6.4.6 Perez

The Perez model depends on a set of more complex empirical coefficients and the air mass (AM) instead of explicitly separating the sky diffuse into isotropic, circumsolar and horizon components [103]. The Perez model's basic formulation of the sky diffuse irradiance is as follows:

$$G_{d,t} = G_d \cdot \left[(1 - F_1) \left(\frac{1 + cos(\theta_T)}{2} \right) + F_1 \left(\frac{a}{b} \right) + F_2 sin(\theta_T) \right], \tag{6.4.9}$$

where F_1 and F_2 are empirically fitted complex functions that represent the circumsolar effect and horizon brightness respectively, G_d is the Diffuse Horizontal Irradiance, θ_Z is the solar zenith angle, θ_{AOI} is the angle of incidence and θ_T is the array tilt angle relative to the horizontal

surface. The constants a and b take into account the solar incidence angle on the considered slope. The terms F_1, F_2, a,and b are calculated using the following equations [84]:

$$a = max(0, cos(\theta_{AOI})), \tag{6.4.10}$$

$$b = max(cos(85°), cos(\theta_Z)), \tag{6.4.11}$$

$$F_1 = max\left[0, \left(f_{11} + f_{12}\Delta + \frac{\pi\theta_Z}{180°}f_{13}\right)\right], \tag{6.4.12}$$

$$F_2 = f_{21} + f_{22}\Delta + \frac{\pi\theta_Z}{180°}f_{23}. \tag{6.4.13}$$

The f coefficients are given in Table Q.1, defined for specific bins of clearness (ε) shown in Table Q.2 and given in Appendix Q, and expressed as [10]:

$$\varepsilon = \frac{\frac{G_d + G_n}{G_d} + \kappa\theta_Z^3}{1 + \kappa\theta_Z^3}, \tag{6.4.14}$$

where G_n is the Direct Normal Irradiance, κ is a constant equal to 5.535×10^{-6} for angles in degrees and 1.041 for angles in radians. Δ is calculated as follows:

$$\Delta = \frac{G_d \cdot AM_a}{G_o}, \tag{6.4.15}$$

where G_o is the extraterrestrial irradiance and AM_a is the absolute air mass.

6.5 Results and analysis

In this section the results obtained from the evaluation of decomposition and transposition models using measured data are presented in the form of RMSE and MBE values, and analysed. Using measured GHI, DHI and DNI values for Bloemfontein and Sutherland, the decomposition models listed in Table 6.1 were separately evaluated. In addition, combinations of decomposition and transposition models were evaluated using measured GHI as input, and compared with measured GPI values.

Observations showed that all the decomposition models under investigation including the Erbs model used in PVsyst simulation tool tend to overestimate the DNI and inherently underestimate the DHI during partly cloudy conditions, as shown in Figure 6.4. Conversely, the decomposition models overestimate the DHI during clear periods, whilst underestimating the DNI, and these results agree with the results of a study done by William Hayes in the USA [86]. Figure 6.5 shows the monthly percentage difference between measured and modelled DNI for Sutherland, and Figure 6.6 shows the comparison of the measured and modelled DHI for Bloemfontein. Table 6.3 and Table 6.4 show the performance of decomposition models in

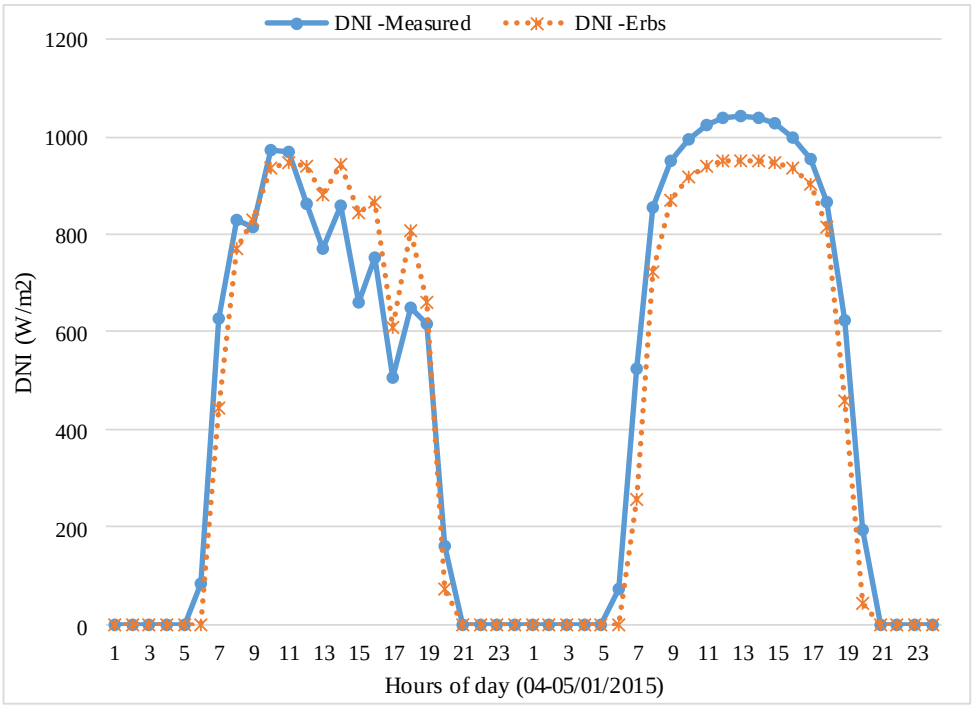

Figure 6.4: Estimation of DNI using Erbs decomposition model on a cloudy and on a clear day.

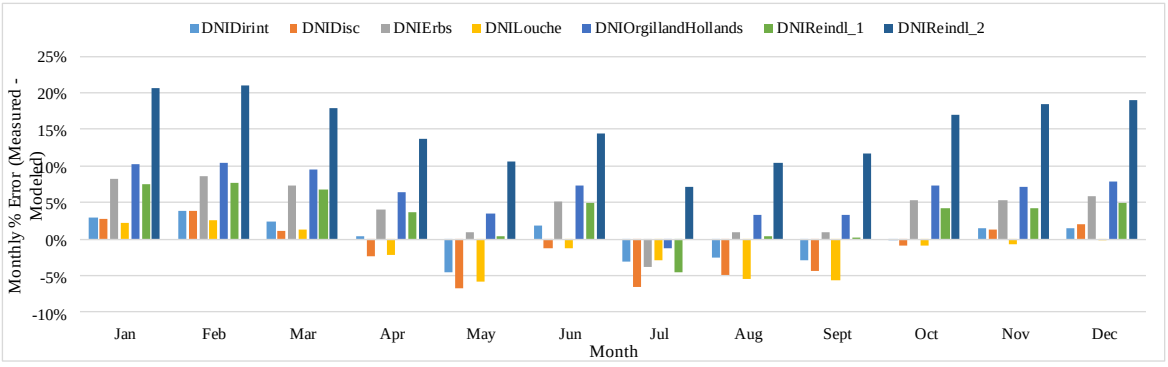

Figure 6.5: Monthly mean bias error between measured and modeled DNI for Sutherland.

estimating the DNI and DHI for Bloemfontein and Sutherland respectively, quantified using the RMSE and MBE metrics.

From the analysis of decomposition models, it can be seen that all the models show the same trend of overestimating the DHI and thus underestimating the DNI for both Bloemfontein and Sutherland in most months. It can be seen in Figure 6.5 and Figure 6.6 that the Disc, Dirint and Louche decomposition models give the best DNI and DHI estimates for South African climatic conditions. However Table 6.3 and Table 6.4 show that the Dirint model has the lowest absolute

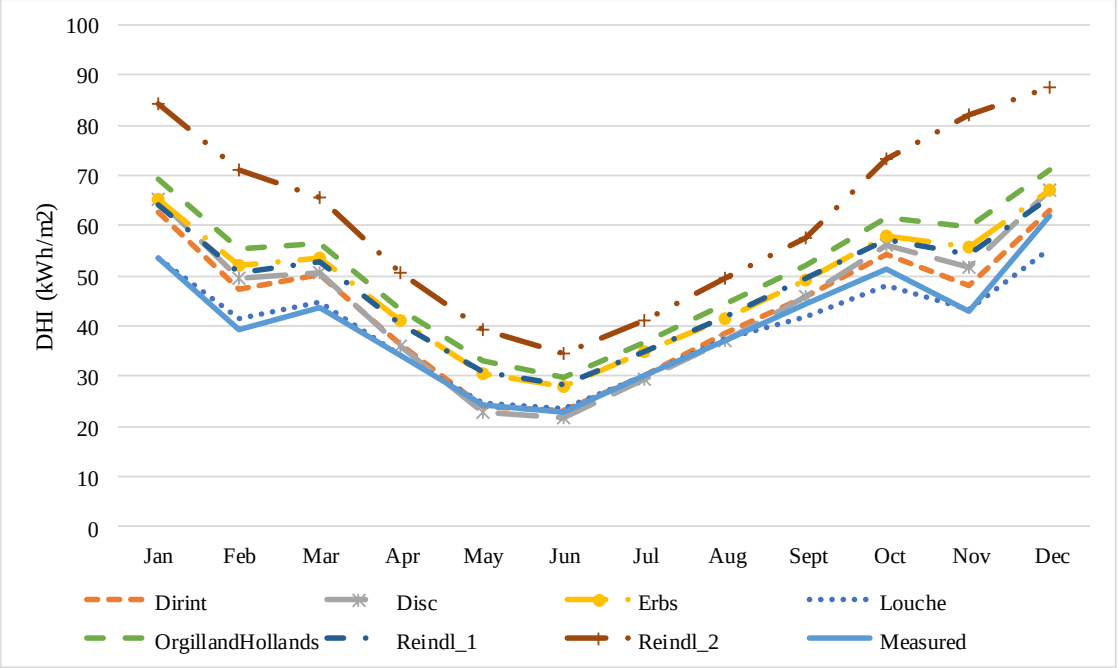

Figure 6.6: Estimation of DHI for Bloemfontein using irradiance decomposition models.

monthly RMSE values, thus there is less scatter in the model. The Dirint model estimates the DNI for Sutherland with mean absolute deviations within 3% for the majority of the months, as shown in Figure 6.5.

When decomposition models overestimate DHI they inevitably underestimate the DNI because of the relationship given in Equation 2.1.13. Thus a smaller GPI is the result of a smaller DNI since the plane of array is chosen to maximise the direct irradiance [86]. Figure 6.7, Figure 6.8 and Figure 6.9 show the percentage differences between the measured GPI from a currently operating 75 MW_P solar PV plant in South Africa and the GPI values generated from the six transposition models (namely Isotropic, Sandia, Klucher, Hay/Davies, Reindl and Perez), in combination with the Dirint, Erbs and Louche decomposition models, respectively. From the simulations done using measured GHI data, it was observed that all the transposition models show comparable performances when combined with the best performing decomposition models i.e. Dirint and Louche.

Further, the combination of Erbs decomposition model with the transposition models was also evaluated since it is the default decomposition model in the commonly used PVsyst simulation tool. The Hay/Davies and Reindl transposition models best approximate the GPI for the site in summer months, i.e. from January to February and then October to December, whereas the Perez transposition model best estimates the GPI for the 75 MW_P solar PV plant site in

Table 6.3: Decomposition model error - Sutherland.

DNI (G_n)			
Model	Monthly RMSE	Monthly MBE	Yearly MBE
Dirint	6.42	0.13%	0.66%
Disc	7.83	-1.31%	-0.47%
Erbs	15.72	4.05%	4.83%
Louche	6.70	-1.58%	-0.98%
Orgill and Hollands	20.45	6.26%	6.98%
Reindl_1	13.91	3.35%	4.09%
Reindl_2	44.74	15.19%	16.27%
DHI (G_d)			
Model	Monthly RMSE	Monthly MBE	Yearly MBE
Dirint	7.66	-17.59%	-16.64%
Disc	9.08	-18.45%	-17.31%
Erbs	13.11	-32.33%	-31.17%
Louche	4.59	-6.06%	-5.30%
Orgill and Hollands	15.92	-40.82%	-39.59%
Reindl_1	11.32	-27.83%	-26.81%
Reindl_2	33.29	-84.61%	-82.00%

winter months, i.e. March to September. Due to the inconsistency in the standard combination of decomposition and transposition models, measured GPI would reduce errors in forecasting the energy yield of a solar PV system. The GHI and GPI measurements used in this analysis were averaged from 4 weather stations on site in an attempt to reduce the errors due to sensor measurement bias. GPI measurements were taken using EKO MS-802 pyranometers mounted in the same orientation of the PV array, with a measuring uncertainty of 2%.

From Figure 6.7 to Figure 6.9 it can be seen that the combined bias in transposing GHI to GPI is within 2% monthly for the Perez transposition model and within 1% in summer months for the Hay/Davies transposition model. Klucher, Reindl, Hay and Perez transposition models showed an average monthly bias that is within 3% in combination whereas the worst performing models i.e. Isotropic and Sandia showed monthly bias as high as 5% in combination with the Dirint and Louche decomposition models. However, all the transposition models tend to underestimate the winter Global Plane Irradiance for the site, as shown in Figure 6.7, Figure 6.8 and Figure 6.9. The simulations done using Meteonorm satellite derived GHI as input

Table 6.4: Decomposition model error - Bloemfontein.

DNI (G_n)			
Model	Monthly RMSE	Monthly MBE	Yearly MBE
Dirint	4.98	0.36%	0.49%
Disc	6.09	-0.69%	-0.38%
Erbs	13.78	5.90%	5.89%
Louche	13.38	-0.27%	-0.27%
Orgill and Hollands	18.95	8.30%	8.26%
Reindl_1	13.22	5.71%	5.66%
Reindl_2	35.78	15.35%	15.50%
DHI (G_d)			
Model	Monthly RMSE	Monthly MBE	Yearly MBE
Dirint	4.44	-7.33%	-7.99%
Disc	5.93	-8.10%	-9.79%
Erbs	8.18	-19.48%	-18.69%
Louche	2.43	0.75%	1.53%
Orgill and Hollands	11.19	-27.12%	-26.18%
Reindl_1	7.52	-18.47%	-17.42%
Reindl_2	22.79	-52.22%	-51.88%

performed significantly worse mainly because the satellite data overestimated the measured GHI by 4.64% over the test period.

Table 6.5 shows the relative transposition model errors when evaluated against measured GPI. For this dataset, the Dirint plus Perez model combinations typically had the smallest hourly RMSE of 10.4 W/m^2, although the Louche plus Perez model combinations had only a slightly larger hourly RMSE of 11 W/m^2 as shown in Table 6.5. Model errors increased over short periods, from annual to monthly and increased further on daily time scales although not shown here, but as reported in literature [106]. The Sandia, Klucher, Hay, Reindl and Perez transposition models have overall annual and monthly mean bias errors that are below 2%, less than the uncertainty of the GPI pyranometer measurements[106]. Monthly and annual errors in modelled GPI matched with the errors in the simulated energy yield reported in [85], thus for this dataset the main contributor to the grid energy yield error was the modelled GPI. PVsyst software allows for the direct input of fixed tilt measured GPI and it is expected that the capability of using GPI for tracking systems will be added in future PVsyst releases [106].

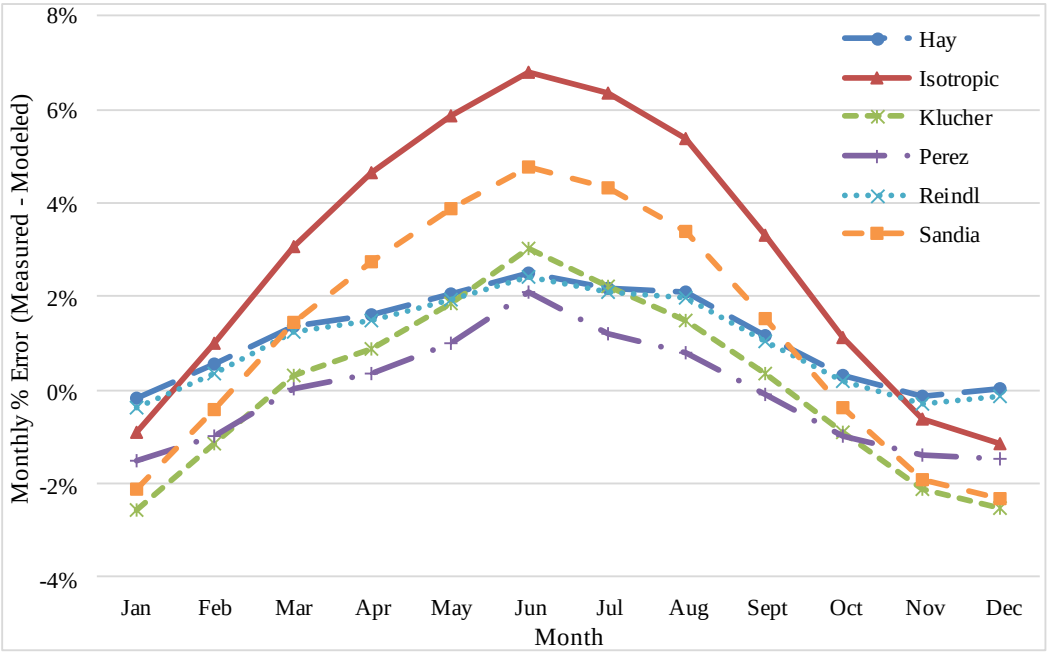

Figure 6.7: Monthly mean bias error (% difference) between measured and modelled GPI using the Dirint decomposition model.

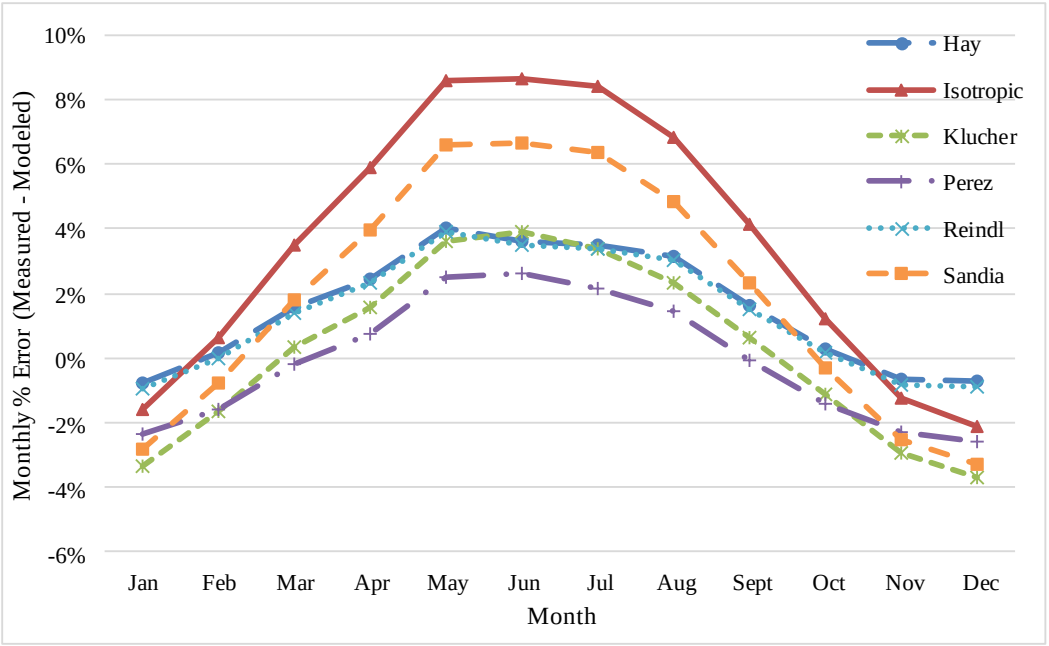

Figure 6.8: Monthly mean bias error (% difference) between measured and modelled GPI using the Erbs decomposition model.

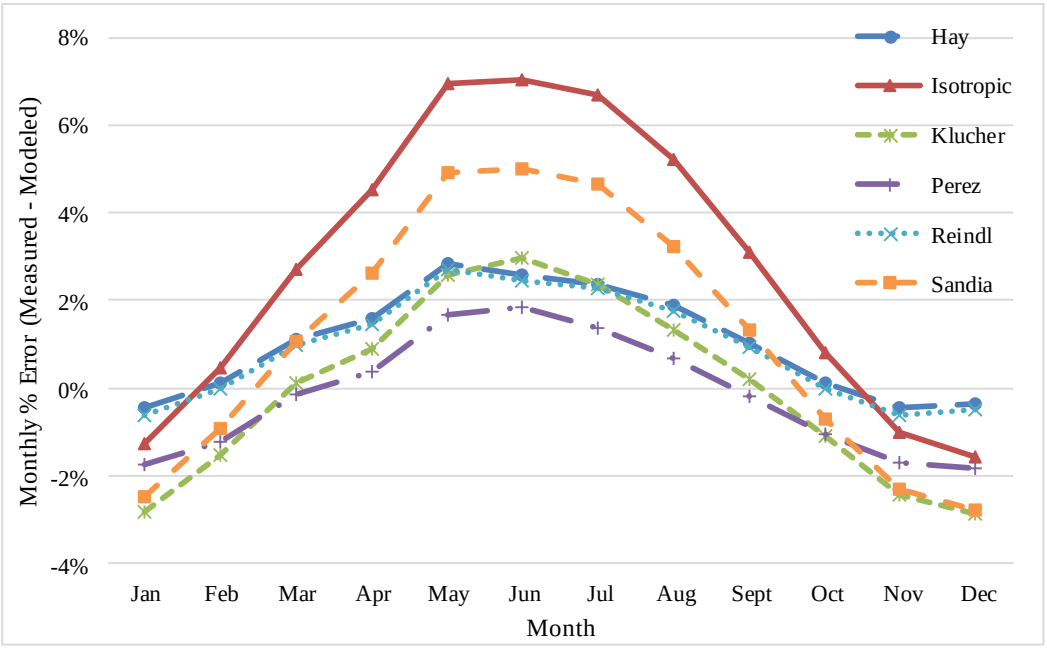

Figure 6.9: Monthly mean bias error (% difference) between measured and modelled GPI using the Louche decomposition model.

According to the MBE and RMSE analysis, the Perez transposition model performed best overall and its estimated GPI correlates closely with the measured GPI while having the lowest RMSE in combination with any of the decomposition models under investigation. The Reindl and Hay/Davies transposition models also produced good GPI estimates with RMSE values slightly larger than those of the Perez model, followed by the Klucher model. The results are in agreement with previous studies in [84, 86, 88, 95, 105]. The tilted surface irradiance models showed less sensitivity to the method for determining the Diffuse Horizontal Irradiance. Making use of measured Plane-Of-Array irradiance reduces reduces the errors between software simulated and measured energy yield, as can be observed in Figure 5.14 of Chapter 5.

6.6 Conclusion

Irradiance models that estimate GPI from GHI were evaluated for a South African region. Decomposition models showed similar trends of overestimating the DHI and inevitably underestimating the DNI for the sites under investigation. From the analysis, it was observed that all the decomposition models tend to overestimate the DNI during cloudy days and conversely underestimate the DNI during clear days. Based on the root mean square values, the best performing models were the Dirint, Louche and Disc decomposition models and the Perez, Reindl

Table 6.5: Average relative model error - GPI transposition using measured GHI as input.

Erbs decomposition model			
Model	Monthly MBE	Yearly MBE	Hourly RMSE (W/m^2)
Hay	1.52%	1.39%	13.7
Isotropic	3.57%	3.28%	23.7
Klucher	0.26%	0.07%	15.9
Louche	-0.08%	-0.22%	13.1
Reindl	1.37%	1.24%	13.5
Sandia	1.91%	1.64%	20.9
Louche decomposition model			
Model	Monthly MBE	Yearly MBE	Hourly RMSE (W/m^2)
Hay	1.03%	0.94%	11.4
Isotropic	2.80%	2.56%	19.3
Klucher	-0.03%	-0.17%	13.6
Louche	-0.17%	-0.26%	11.0
Reindl	0.90%	0.81%	11.3
Sandia	1.14%	0.93%	16.9
Dirint decomposition model			
Model	Monthly MBE	Yearly MBE	Hourly RMSE (W/m^2)
Hay	1.13%	1.06%	10.9
Isotropic	2.90%	2.69%	18.3
Klucher	0.07%	-0.06%	12.2
Louche	-0.09%	-0.17%	10.4
Reindl	1.00%	0.93%	10.8
Sandia	1.24%	1.06%	15.5

and Hay/Davies transposition models for the South African sites. However, all the transposition models showed little sensitivity to the irradiance decomposition model used. Model combinations that involved the Perez transposition model produced less bias, compared to the other transposition models and the results are in agreement with previous studies in [84, 88]. However, the Hay and Reindl transposition models appeared to outperform the Perez model in summer months. Overall, all the transposition models underestimated the winter irradiance for the 75 MW_P plant, with the Perez performing better with respect to winter months. The combined bias in transposing GHI to GPI using measured GHI as input and the Dirint

and Louche decomposition models is within 3% for the Perez, Reindl and Hay/Davies transposition models. The Dirint plus Perez model combinations typically had the smallest RMSE values, monthly bias within 2% and is the best performing combination for this dataset. Due to the inconsistency in the standard combination of decomposition and transposition models, measured GPI reduces errors in predicting the energy yield of a solar PV system. In conclusion, the choice of irradiance data and transposition model clearly contributes to the spread in the short and long term energy predictions.

CHAPTER 7

CONCLUSIONS AND RECOMMENDATIONS

In this chapter the main aspects of this research are presented, then conclusions and recommendations are given. The purpose of this research was to improve the PVsyst energy yield prediction model using measured data and to evaluate the irradiance decomposition and transposition models in order to find those that perform best under South African conditions. Different methodologies were applied to address different objectives in each chapter.

7.1 Introduction

Firstly, the history and background of solar PV was presented in Chapter 1, from the time the photovoltaic effect was introduced by Edmund Becquerel in 1839 to the current year, 2016. The historical change of PV module pricing from 1980 to 2015 was also presented and it was shown that the price of PV is now comparable to that of fossil fuels. A brief discussion of solar PV worldwide was done, followed by an overview of solar PV in South Africa. The prices implemented in the five successful bid windows in the first four years of the REIPPPP in South Africa were also given in this chapter. Of all the solar PV projects awarded in the first bidding window in South Africa, of interest was the first grid connected 75 MW_P Kalkbult solar PV system. The 75 MW_P solar PV system exhibited differences in the initial energy yield assessment and the actual plant performance in its first year of operation. The objectives taken to achieve the overall aim of this study as well as the thesis outline were also presented in Chapter 1.

7.2 Theoretical background

Theory behind solar PV systems was presented in Chapter 2. A brief introduction to the solar resource was made, with the solar geometry convention and irradiance presented. The data proved to be of great importance when evaluating the irradiance models that convert GHI into Plane-Of-Array irradiance. Consequently the physics behind solar PV systems, from the PV cell to the PV array was also presented. In addition, the various PV technologies and mounting

types were also presented. Finally, the PVsyst simulation software was described and a brief explanation of how it works was given. In order to produce reliable energy yield profiles using PVsyst, the right input data has to be given. The most substantial input data in energy yield simulation tools is the solar radiation, therefore it is essential to validate the data before implementing it.

7.3 Dataset integrity and reliability

Comparisons were done for various solar radiation data sources for Kalkbult site, namely: PVGIS-Helioclim, Climate-SAF PVGIS, SODA HelioClim-3, NASA-SSE, SolarGIS, Meteonorm6.1 and Meteonorm7.1. These different meteorological data sources give different values of solar radiation for the same site and this is due to the differences in the methods that were used to obtain the data, some use discrete grids that vary in size, other perform interpolations. The meteo-data sources also vary due to climate variability since the values are either measurements for given years or averaged periods and those vary from one source to another. The results of the analysis indicated that all the meteorological data sources under investigation agree within 5% of the reference measured solar radiation, therefore can be considered appropriate to be used for energy yield simulations. HelioClim-3 data gave a better representation of reality for the Kalkbult site. However it is best for each solar PV plant to have its own meteorological and solar radiation station on site to provide better energy forecasts. The choice of irradiance datasets may affect the output of a system by about 2-3%, so using high-accuracy irradiance sensors is the key to reducing the uncertainty between the measured and expected energy. After validating the solar radiation and ambient temperature data, the next step was to use it as input in PVsyst to do an initial energy yield assessment.

7.4 Solar PV system energy yield and performance analysis

After doing an initial energy yield assessment for the $75MW_P$ grid-connected, fixed tilt Kalkbult solar PV system, the yearly energy production of the installed system amounted to 149 868 MWh in the first year of operation, whereas the energy yield obtained from the initial simulation done in PVsyst6.39 underestimated the installed system's energy production by 6.4% and 5% using the Hay and Perez models respectively. It was observed that the differences between the measured energy yield and the PVsyst simulated energy were mostly due to the overestimation of system losses in the PVsyst software. Therefore it is necessary to improve the PVsyst energy prediction model by using calculated loss values instead of assumptions.

7.5 Improved loss factor model

Measured data was used to calculate the losses in the operational system and this resulted in an improved PVsyst model that, when simulated, gave a 4% higher yield when using the Hay irradiance model and just a yearly average difference of 0.78% between the measured and simulated energy yield when using the Perez model. Therefore the improved PVsyst energy prediction model is essential for accurately forecasting PV system generation capacity. It was also observed that the operational system significantly outperformed the software simulations especially in winter. The differences in the improved model and the grid yield observed in the winter season were mostly due to the solar radiation transposition models calculating relatively less Plane-Of-Array irradiance in winter months, and these models were then investigated further.

7.6 Irradiance models

Irradiance models that estimate the Plane-Of-Array (POA) Irradiance from Global Horizontal Irradiance were evaluated for the Northern Cape region of South Africa. Estimating the Plane-Of-Array irradiance involves two steps, the decomposition of Global Horizontal Irradiance into direct and diffuse horizontal components and then the transposition of these horizontal components into the Plane-Of-Array direct beam, ground reflected and diffuse components. The following irradiance decomposition models were evaluated: Erbs, Orgill and Hollands, Louche, Reindl_1, Reindl_2, DISC and Dirint.

Similar trends of decomposition models overestimating the Diffuse Horizontal Irradiance and inevitably underestimating the Direct Normal Irradiance for the sites in South Africa were observed. According to the analysis, all the decomposition models under investigation tend to underestimate the DNI during clear days and conversely overestimate the DNI during cloudy days. Then the following irradiance transposition models: Isotropic, Sandia, Klucher, Hay, Reindl and Perez were evaluated in combination with the best performing decomposition models. Based on the root mean square values, the Dirint, Louche and Disc decomposition models and the Perez, Reindl and Hay/Davies transposition models were the best performing irradiance models for the South African sites. However, all the transposition models showed little sensitivity to the irradiance decomposition model used and overall, all the transposition models underestimated the winter Plane-Of-Array irradiance for the 75 MW_P plant. The Dirint plus Perez model combinations typically had the smallest RMSE values, a monthly bias within 2% and is the best performing combination for this dataset. Due to the inconsistency in the

standard combination of decomposition and transposition models, measured Plane-Of-Array irradiance reduces errors in energy yield simulations of solar PV systems. On a monthly basis, simulations done using measured Plane-Of-Array irradiance were observed to be within 2% of the field recorded values. The choice of irradiance data, transposition and loss models clearly contributes to the spread in the short and long term energy predictions.

7.7 Recommendations

The goals of the research were achieved and from the work covered in this master's thesis, the following recommendations are made:

- Always evaluate satellite and measured meteorological data before implementing the data in simulation tools.
- Further investigation into soiling is required. For this study soiling losses were estimated based on 30-minute measured precipitation for the site. However, independent soiling measurements permit more accurate determination of soiling losses.
- Irradiance transposition and decomposition models that work best for South African conditions should be developed to improve energy yield simulation and forecasting accuracy.

Appendices

APPENDIX A

PVSYST INITIAL SIMULATION USING SATELLITE DERIVED DATA AS INPUT

The PVsyst report used by the utility provider , Scatec solar, to do the initial energy yield simulation for Kalkbult solar PV power plant is presented in this appendix. The PVsyst report is referred to in Chapter 1 and Chapter 4.

A.1 PVsyst file

Grid-Connected System: Simulation parameters

Project : **South_Arfrica**

Geographical Site	**Kalkbult**		**Country**	**South Africa**
Situation	Latitude	30.2°S	Longitude	24.1°E
Time defined as	Legal Time	Time zone UT+2	Altitude	1214 m
	Albedo	0.20		

Meteo data : Kalkbult, Synthetic Hourly data

Simulation variant : **Kalkbult_75MWp_Meteonorm_BYD**

Simulation date 09/05/12 10h05

Simulation parameters

Collector Plane Orientation	Tilt	30°	Azimuth	0°
50Sheds	Pitch	7.00 m	Collector width	3.34 m
Inactive band	Top	0.00 m	Bottom	0.00 m
Shading limit angle	Gamma	22.13 °	Occupation Ratio	47.7 %
Shadings electrical effect	Cell size	12.5cm	Strings in width	2

Models used	Transposition	Hay	Diffuse	Measured
Horizon	Free Horizon			
Near Shadings	No Shadings			

PV Array Characteristics

PV module	Si-poly	Model	**BYD 240 P6-30**	
		Manufacturer	BYD	
Number of PV modules		In series	24 modules	In parallel 13021 strings
Total number of PV modules		Nb. modules	312504	Unit Nom. Power 240 Wp
Array global power		Nominal (STC)	**75001 kWp**	At operating cond. 67154 kWp (50°C)
Array operating characteristics (50°C)		U mpp	649 V	I mpp 103411 A
Total area		Module area	**508407 m²**	Cell area 456381 m²

Inverter		Model	**Sunny Central 800CP**	
		Manufacturer	SMA	
Characteristics		Operating Voltage	570-820 V	Unit Nom. Power 800 kW AC
Inverter pack		Number of Inverter	84 units	Total Power 67200 kW AC

PV Array loss factors

Thermal Loss factor		Uc (const)	29.0 W/m²K	Uv (wind) 0.0 W/m²K / m/s
=> Nominal Oper. Coll. Temp. (G=800 W/m², Tamb=20°C, Wind=1 m/s.)				NOCT 45 °C
Wiring Ohmic Loss		Global array res.	0.11 mOhm	Loss Fraction 1.5 % at STC
Array Soiling Losses				Loss Fraction 3.0 %
Module Quality Loss				Loss Fraction 0.0 %
Module Mismatch Losses				Loss Fraction 2.0 % at MPP
Incidence effect, ASHRAE parametrization		IAM =	1 - bo (1/cos i - 1)	bo Parameter 0.05

System loss factors

AC wire loss inverter to transfo		Inverter voltage	360 Vac tri	
		Wires	12 m 3x30000 mm²	Loss Fraction 0.5 % at STC
External transformer		Iron loss (24H connection)	73923 W	Loss Fraction 0.1 % at STC
		Resistive/Inductive losses	0.0 mOhm	Loss Fraction 1.0 % at STC

Grid-Connected System: Simulation parameters (continued)

User's needs : Unlimited load (grid)

Grid-Connected System: Main results

Project : **South_Arfrica**

Simulation variant : **Kalkbult_75MWp_Meteonorm_BYD**

Main system parameters				
System type		**Grid-Connected**		
PV Field Orientation	Sheds disposition, tilt	30°	azimuth	0°
PV modules	Model	BYD 240 P6-30	Pnom	240 Wp
PV Array	Nb. of modules	312504	Pnom total	**75001 kWp**
Inverter	Model	Sunny Central 800CP	Pnom	800 kW ac
Inverter pack	Nb. of units	84.0	Pnom total	**67200 kW ac**
User's needs	Unlimited load (grid)			

Main simulation results

System Production — **Produced Energy** **143616 MWh/year** Specific prod. 1915 kWh/kWp/year

Performance Ratio PR 77.9 %

Normalized productions (per installed kWp): Nominal power 75001 kWp

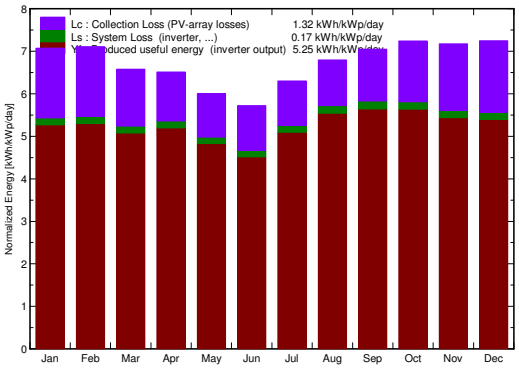

Performance Ratio PR

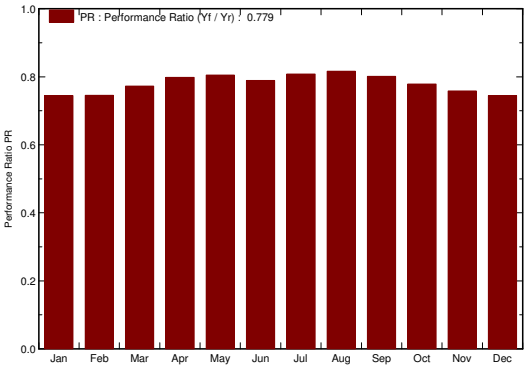

Kalkbult_75MWp_Meteonorm_BYD

Balances and main results

	GlobHor kWh/m²	T Amb °C	GlobInc kWh/m²	GlobEff kWh/m²	EArray MWh	E_Grid MWh	EffArrR %	EffSysR %
January	244.8	24.00	219.4	206.7	12629	12252	11.32	10.99
February	204.1	24.20	199.1	188.6	11481	11131	11.34	11.00
March	185.1	21.60	203.9	193.6	12178	11810	11.75	11.39
April	150.2	17.00	195.3	186.1	12060	11693	12.15	11.78
May	124.8	13.10	185.9	174.8	11583	11224	12.25	11.88
June	105.4	10.00	171.6	155.8	10495	10162	12.03	11.65
July	123.4	9.40	195.4	181.3	12228	11843	12.31	11.92
August	150.7	11.80	210.6	199.9	13302	12892	12.42	12.04
September	178.2	15.20	211.4	202.0	13116	12706	12.20	11.82
October	219.1	19.40	224.5	212.8	13519	13110	11.84	11.49
November	234.2	20.80	215.3	203.1	12626	12245	11.54	11.19
December	259.5	23.40	224.8	211.5	12939	12548	11.32	10.98
Year	2179.5	17.46	2457.1	2316.2	148155	143616	11.86	11.50

Legends:

GlobHor	Horizontal global irradiation	EArray	Effective energy at the output of the array
T Amb	Ambient Temperature	E_Grid	Energy injected into grid
GlobInc	Global incident in coll. plane	EffArrR	Effic. Eout array / rough area
GlobEff	Effective Global, corr. for IAM and shadings	EffSysR	Effic. Eout system / rough area

Grid-Connected System: Loss diagram

Project : **South_Arfrica**

Simulation variant : **Kalkbult_75MWp_Meteonorm_BYD**

Main system parameters	System type	**Grid-Connected**		
PV Field Orientation	Sheds disposition, tilt	30°	azimuth	0°
PV modules	Model	BYD 240 P6-30	Pnom	240 Wp
PV Array	Nb. of modules	312504	Pnom total	**75001 kWp**
Inverter	Model	Sunny Central 800CP	Pnom	800 kW ac
Inverter pack	Nb. of units	84.0	Pnom total	**67200 kW ac**
User's needs	Unlimited load (grid)			

Loss diagram over the whole year

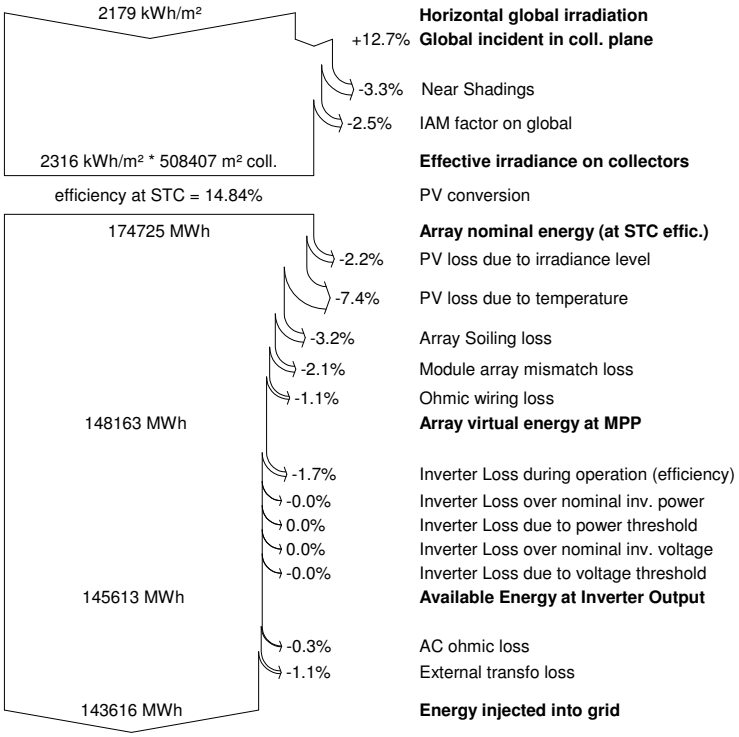

APPENDIX B

DIFFERENCES BETWEEN PVSYST VERSION 6 AND VERSION 5

In principle the models in version 6 of PVsyst have not been changed, however the several default values modifications may explain the noticeable variations in the final energy yield results. The information provided in this section is referred to in Chapter 2.

B.1 Transposition model

The Hay transposition model was judged more "robust" than the Perez model so it was proposed as default in the previous versions of PVsyst up to version 5. In Pierre Ineichen's recent studies it was found that the Perez model give slightly better results in terms of RMSE of hourly values. Therefore in PVsyst version 6 the Perez model is proposed as default. However the Perez model gives yearly values that are in the range of 0% to 2% higher than the Hay model, depending on the plane tilt and climate type.

B.2 PV module R_{serie} parameter

Up to version 5 of PVsyst, the R_{serie} was chosen in order to obtain a diode ideality factor (gamma value) of 1.35 for poly-crystalline models and 1.30 for mono-crystalline models. Research showed that this leads to the underestimation of low light performances. In version 6 the default Gamma value was fixed to 1.1 and according to recent studies this reduces the irradiance losses significantly, (by 2-3%) depending on climate. The adjustment only affect the modules for which the Rserie value was not specified by the manufacturer in the database.

B.3 Module quality and Mismatch losses

The default module quality loss was chosen as the average value between zero and the lower tolerance in the previous versions of PVsyst. In version 6 it is defined as the quarter between the lower and higher tolerance.

In previous versions the default mismatch loss parameter was proposed as 2%, nowadays the diminished mismatch default is 1%, corresponding to the narrower tolerance limits of the PV modules' Isc dispersion.

APPENDIX C

QUICK GUIDE FOR IMPORTING METEO-DATA INTO PVSYST

There are basically two ways of importing meteo-data for a year into PVsyst, namely: Importing sub-hourly meteo data in any ASCII format or using the PVsyst standard format. The latter is more suitable for reliable data since it doesn't include securities and error recoveries like the ASCII format way of importing meteo-data. The advantage of using the PVsyst standard format for hourly meteo-data is that it has a simplified import process as the information about the Geographical site is written in the file. The two ways are briefly described in the sections that follows. This appendix is referred to in Chapter 2 and Chapter 5.

C.1 PVsyst standard format for hourly meteo-data

Data is managed in an Excel spreadsheet, as shown in Table C.1. As shown in the table, the header lines begin by # and the first line acts as a file format identifier, with files not beginning with these tags not considered as PVsyst Standard files [19]. The necessary fields are in bold and additional fields (non-bold) may have to be defined, and one column for each date element is required. The decimal character should be a dot, with the data being horizon free, and the file has to be saved as a CSV(MS-DOS) file. The tool in PVsyst ,"Import meteo Data" is used for this option. Night data is mandatory and PVsyst requires the user to add all the 8760 lines of data set for a year and 8784 for a leap year. The year 1990 or 2059 is used to mark data that are not really measured (synthetic generation or averaged months). Missing data is defined as -99 and then it will be replaced by an average of the corresponding hour of the next and previous day [19]. The required data is as follows:

- GHI = Global Horizontal Irradiation [W/m^2]
- Tamb = Ambient temperature [°C]

The additional data is as follows:

- DHI = Global Horizontal Irradiance [W/m^2]
- DNI = Direct Normal Irradiance [W/m^2]

Table C.1: MS-DOS CSV sample file

# Meteo hourly data					
# Site	Kalkbult				
# Country	South Africa				
# Data Source	Measured				
# Time step	Hour				
# Year	2014				
# Latitude	-30.2				
# Longitude	24.1				
# Altitude	1214				
# Time Zone	2				
# Hour shift	0				
# Albedo	0.2				
# Plane tilt	30				
# Plane azimuth	0				
Year	**Month**	**Day**	**Hour**	**GHI**	**Tamp**
				W/m^2	°C
2014	1	1	0	0	25.152
2014	1	1	1	0	24.426
2014	1	1	2	0	23.324
2014	1	1	3	0	22.94
2014	1	1	4	0	22.798
2014	1	1	5	8.25875	22.494
2014	1	1	6	130.2725	25.954
2014	1	1	7	375.07	27.288
2014	1	1	8	601.0325	29.254
2014	1	1	9	811.0175	32.612
2014	1	1	10	973.435	35.177
2014	1	1	11	1075.245	36.616
2014	1	1	12	1135.38375	36.711
2014	1	1	13	1045.0075	37.176

- GPI = Plane of Array Irradiance
- WindVel = Wind velocity at $10m$ altitude $[m/sec]$

C.2 ASCII format for importing sub-hourly meteo-data into PVsyst

Unlike the PVsyst standard of importing meteo-data, this option has securities and error recoveries present. The data is prepared as a ".CSV",".DAT", or ".TXT" file and imported in PVsyst under "Databases", then "Import ASCII meteo file". The graphical user interface provided for this option is clear enough for one to import data with ease and information regarding this is found in the PVsyst help file [19].

APPENDIX D

PV MODULE DATA-SHEET

BYD P6-30 Series-3BB module datasheet, is referred to in Chapter 4 and Chapter 5.

BYD P6-30 Series-3BB

230W 235W 240W 245W 250W 255W

17.4 Efficiency
Average cell efficiency up to17.4%
Excellent optical performance

0~5w Tolerance
Positive tolerance 0~5W
Reliability for output performance

10 Years Warranty
10 years for product
25 year linear Warranty
25 years on 80.7% for performance

Grid
Residential roof top systems
On/Off-grid commercial systems
On/Off-grid utility systems

3rd Party test
TUV Salt corrosion resistance test
TUV Ammonia corrosion resistance test
5400Pa for Snow Load Test
2400Pa for Wind Load Test

Certification
IEC 61215, IEC 61730, UL1703,
ISO9001:2008, ISO14001:2004

Production Process

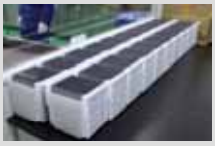
Wafer Production


Cell Production


Module Production


Module

About BYD

BYD (HK:1211), one of the world's largest PV manufacture, produces from wafer to module, committing to high quality sustainable products and continuous improvement. Integrating with Electrical Vehicles and Battery Energy Storage technology make BYD the world-leading solution provider from energy Generating to Consumption and Storage.

New Technology

NES
NES is a high technology and is widely used in BYD photovoltaic products, increasing the average cell efficiency up to 17.4%.

BYD(Shanghai) Industrail Co., Ltd.
No.999 Xiangjing Road,Songjiang,Shanghai,201611,P.R.China
Tel: +86-755-8988 8888 ext.53959
Website: www.bydenergy.com
Email: bydenergy@byd.com

BYD P6–30 Series-3BB

Edition No. EN-BYD- Oct-2011

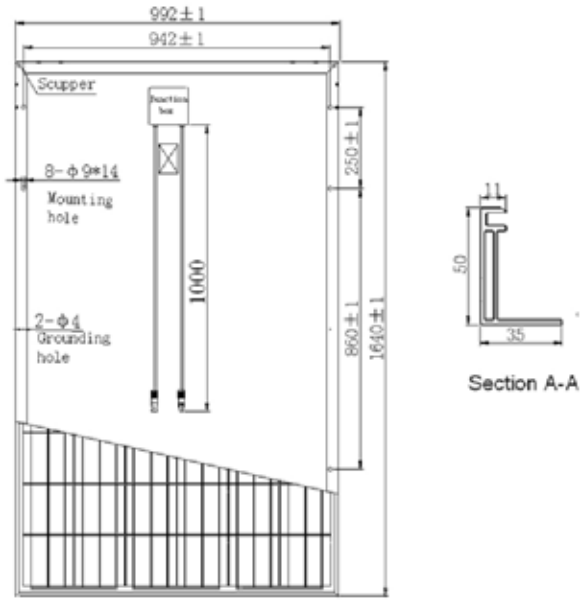

Mechanical Specifications	
Cell	Polycrystalline Silicon solar cells 156mm * 156 mm / 6 inch
No. of Cells	60 (6 *10) pcs
Dimension of Module	1640 mm * 992 mm * 50 mm / 64.6 inch * 39.1 inch *2.0 inch
Weight	19.6 kg / 43.21 lbs
Front Glass	3.2 mm tempered glass
Frame	Anodized aluminum alloy
Junction Box	IP65
Plug Connector	IP67
Bypass-Diodes	6 pcs. (IEC) / 3 pcs. (UL)
Max. Fuse Current Rating	15 A
Type of Connector	MC4,MC4 compatible, 0-1394462-4/6-1394461-2
Cable Section Area	4 mm² / 0.0062 Sq in
Cable Length	2 * 1000 mm / 2 * 39.4 inch

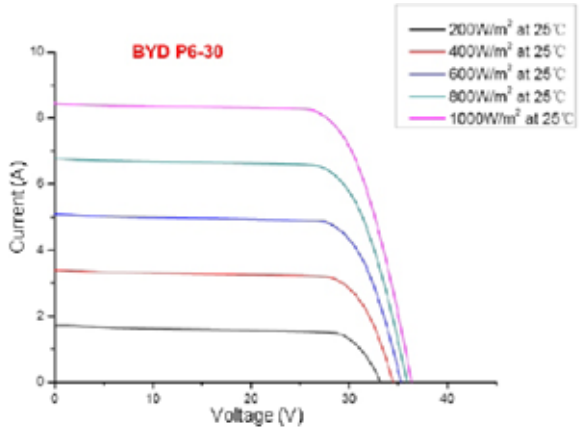

Temperature Coefficients	
Nominal Operating Cell Temperature (NOCT)	45℃ ± 2℃
Short-Circuit Current Temperature Coefficient	0.045%/℃
Open-Circuit Voltage Temperature Coefficient	-0.34%/℃
Peak Power Temperature Coefficient	-0.47%/℃

Package Information	
Package	40' HQ
Pcs / Pallet	20
Pallet / Container	28
Pcs / Container	560

BYD P6-30 Series Electrical Specification

Module / Item	BYD 230P6-30	BYD 235P6-30	BYD 240P6-30	BYD 245P6-30	BYD 250P6-30
Open Circuit Voltage (Voc)	36.75 V	37.07 V	37.54 V	37.80 V	38.00 V
Maximum Operating Voltage (Vmp)	28.67 V	29.06 V	29.55 V	30.06 V	30.40 V
Short Circuit Current (Isc)	8.50 A	8.69 A	8.90 A	8.94 A	8.98 A
Maximum Operating Current (Imp)	8.02 A	8.09 A	8.12 A	8.15 A	8.22 A
Maximum Power in STC (Pmax)	230 Wp	235 Wp	240 Wp	245 Wp	250 Wp
Module Efficiency	14.14%	14.44%	14.75%	15.06%	15.37%
Operating Temperature	-40℃~85℃				
Maximum System Voltage	1000 VDC(IEC) / 600 VDC (UL)				
STC: IRRADIANCE 1000W/m², Module Temperature 25℃, AM=1.5					

Note: Photovoltaic Simulator Test Tolerance ±3%

APPENDIX E

INVERTER DATA-SHEET

SUNNY CENTRAL Inverter datasheet, is referred to in Chapter 4 and Chapter 5.

SUNNY CENTRAL
500CP / 630CP / 720CP / 760CP / 800CP

SC 500CP-10 / SC 630CP-10 / SC 720CP-10 / SC 760CP-10 / SC 800CP-10

Economical
- Optiprotect ensures maximum plant availability
- Outdoor-rated enclosure allows for direct field deployment

Efficient
- Full nominal power at ambient temperatures up to 50° C
- 110% rated power at ambient temperatures up to 25° C

Flexible
- Configurable DC voltage range
- Optional: Extended input voltage range up to 1,100 V

Reliable
- Safe and easy installation due to separate connection area
- Powerful grid management functions (including LVRT)

SUNNY CENTRAL
500CP / 630CP / 720CP / 760CP / 800CP

Unmatched performance for utility-scale PV

The Sunny Central CP series maximizes project investment returns through innovative technology and time-saving features. Optiprotect integrates string failure detection into the inverter and centrally monitors up to 1,600 module strings without requiring conventional communication wiring in the field. The self-learning monitoring system significantly simplifies commissioning. Up to 32 motor-driven, adjustable DC inputs ensure maximum plant availability. And, thanks to its compact and weatherproof enclosure, the inverters can be loaded and transported with ease and set up almost anywhere.

Technical data	Sunny Central 500CP	Sunny Central 630CP
Input Data (DC)		
Max. DC power (@ cos φ=1)	560 kW	713 kW
Max. input voltage [1]	1000 V / 1100 V optional	1000 V / 1100 V optional
MPP voltage range (@ 25 °C / @ 50° C at 50 Hz)	449 V – 820 V / 430 V – 820 V [2]	529 V – 820 V / 500 V – 820 V [2]
MPP voltage range (@ 25° C / @ 50° C at 60 Hz)	449 V – 820 V / 436 V – 820 V [2]	529 V – 820 V / 505 V – 820 V [2]
Rated input voltage	480 V	550 V
Max. input current	1250 A	1350 A
Minimum input voltage / V_{MPP_min} at $I_{MPP} < I_{DCmax}$	429 V / 430 V	498 V / 500 V
Number of independent MPP inputs	1	1
Number of DC inputs	9 / 32 (Optiprotect)	9 / 32 (Optiprotect)
Output (AC)		
Rated power (@ 25 °C) / nominal AC power (@ 50 °C)	550 kVA / 500 kVA	700 kVA / 630 kVA
Nominal AC voltage / range	270 V / 243 V – 297 V	315 V / 284 V – 347 V
AC frequency / range	50 Hz, 60 Hz / 47 Hz ... 63 Hz	50 Hz, 60 Hz / 47 Hz ... 63 Hz
Rated frequency / rated voltage	50 Hz / 270 V	50 Hz / 315 V
Max. output current	1176 A	1283 A
Max. THD	< 3 %	< 3 %
Power factor at rated power / adjustable shift factor	1 / 0.9 leading ... 0.9 lagging	
Feed-in phases / connection phases	3 / 3	3 / 3
Efficiency [7]		
Max. efficiency / European efficiency / CEC efficiency	98.6 % / 98.4 % / 98.5 %	98.7 % / 98.5 % / 98.5 %
Protection		
Input side disconnection device	Motor-driven switch-disconnector / circuit breaker (Optiprotect)	
Output side disconnection device	AC circuit breaker	
DC overvoltage protection / AC overvoltage protection	Surge arrester type I / surge arrester type I	
Grid monitoring	●	●
Ground fault monitoring / Remote ground fault monitoring	o / o	o / o
Insulation monitoring	o	o
Surge arrester for auxiliary supply	●	●
Protection class (as per IEC 62103) / overvoltage category (as per IEC 60664-1)	I / III	I / III
General Data		
Dimensions (W / H / D)	2562 / 2279 / 956 mm (101 / 90 / 38 inch)	
Weight	1800 kg	1800 kg
Operating temperature range	-20 °C ... +50 °C	-20 °C ... +50 °C
Noise emission [5]	60 db(A)	60 db(A)
Max. self-consumption (in operation) / self-consumption (at night)	1700 W [4] / < 100 W	1700 W [4] / < 100 W
External auxiliary supply voltage	230 / 400 V (3 / N / PE)	230 / 400 V (3 / N / PE)
Cooling concept	OptiCool	OptiCool
Degree of protection: electronics / connection area (as per IEC 60529)	IP54 / IP23	IP54 / IP23
Application	Unprotected outdoors	Unprotected outdoors
Maximum permissible value for relative humidity (non-condensing)	15 % ... 95 %	15 % ... 95 %
Maximum operating altitude above MSL	2000 m	2000 m
Fresh air consumption	3000 m³/h	3000 m³/h
Features		
DC terminal	Ring terminal lug / cage terminal (Optiprotect)	Ring terminal lug / cage terminal (Optiprotect)
AC terminal	Ring terminal lug	Ring terminal lug
Display	o	o
Communication protocols	Ethernet (optical fiber optional), modbus	Ethernet (optical fiber optional), modbus
Sunny String-Monitor	RS485 / is not required (Optiprotect)	RS485 / is not required (Optiprotect)
Color of enclosure, door, base, roof	RAL 9016 / 9016 / 7005 / 7004	
Certificates and approvals (more upon request)	EN 61000-6-2, EN 61000-6-4, EEG conformity, Arrêté du 4/23/08, R.D. 1663 / 2000, R.D. 661 / 2007, BDEW-MSRL / FGW / TR8 [6]	
Classification of the ambient conditions (according to IEC 60721-3-4)	4S2, 4C2	
● Standard features o Optional features – Not available		
Type designation	SC 500CP-10	SC 630CP-10

Sunny Central 720CP	Sunny Central 760CP	Sunny Central 800CP	
808 kW	853 kW	898 kW	
1000 V / 1100 V optional	1000 V / 1100 V optional	1000 V / 1100 V optional	
577 V – 820 V / 525 V – 820 V [2) 3)]	609 V – 820 V / 554 V – 820 V [2) 3)]	641 V – 820 V / 583 V – 820 V [2) 3)]	
577 V – 820 V / 525 V – 820 V [2) 3)]	609 V – 820 V / 554 V – 820 V [2) 3)]	641 V – 820 V / 583 V – 820 V [2) 3)]	
565 V	595 V	620 V	
1400 A	1400 A	1400 A	
515 V / 515 V	545 V / 545 V	568 V / 570 V	
1	1	1	
9 / 32 (Optiprotect)	9 / 32 (Optiprotect)	9 / 32 (Optiprotect)	
792 kVA / 720 kVA	836 kVA / 760 kVA	880 kVA / 800 kVA	
324 V / 292 V – 356 V	342 V / 308 V – 376 V	360 V / 324 V – 396 V	
50 Hz, 60 Hz / 47 Hz ... 63 Hz	50 Hz, 60 Hz / 47 Hz ... 63 Hz	50 Hz, 60 Hz / 47 Hz ... 63 Hz	
50 Hz / 324 V	50 Hz / 342 V	50 Hz / 360 V	
1411 A	1411 A	1411 A	
< 3 %	< 3 %	< 3 %	
1 / 0.9 leading ... 0.9 lagging			
3 / 3	3 / 3	3 / 3	
98.6 % / 98.4 % / 98.5 %	98.6 % / 98.4 % / 98.5 %	98.6 % / 98.4 % / 98.5 %	
Motor-driven switch-disconnector / circuit breaker (Optiprotect)			
AC circuit breaker			
Surge arrester type I / surge arrester type I			
●	●	●	
o / o	o / o	o / o	
o	o	o	
●	●	●	
I / III	I / III	I / III	
2562 / 2279 / 956 mm (101 / 90 / 38 inch)			
1800 kg	1800 kg	1800 kg	
-20 °C ... +50 °C	-20 °C ... +50 °C	-20 °C ... +50 °C	
60 db(A)	60 db(A)	61 db(A)	
1700 W [4)] / < 100 W	1700 W [4)] / < 100 W	1700 W [4)] / < 100 W	
230 / 400 V (3 / N / PE)	230 / 400 V (3 / N / PE)	230 / 400 V (3 / N / PE)	
OptiCool	OptiCool	OptiCool	
IP54 / IP23	IP54 / IP23	IP54 / IP23	
Unprotected outdoors	Unprotected outdoors	Unprotected outdoors	
15 % ... 95 %	15 % ... 95 %	15 % ... 95 %	
2000 m	2000 m	2000 m	
3000 m³/h	3000 m³/h	3000 m³/h	
Ring terminal lug / cage terminal (Optiprotect)	Ring terminal lug / cage terminal (Optiprotect)	Ring terminal lug / cage terminal (Optiprotect)	
Ring terminal lug	Ring terminal lug	Ring terminal lug	
o	o	o	
Ethernet (optical fiber optional), modbus	Ethernet (optical fiber optional), modbus	Ethernet (optical fiber optional), modbus	
RS485 / is not required (Optiprotect)	RS485 / is not required (Optiprotect)	RS485 / is not required (Optiprotect)	
RAL 9016 / 9016 / 7005 / 7004			
EN 61000-6-2, EN 61000-6-4, EMC conformity, CE conformity, Arrêté du 4/23/08, R.D. 1663 / 2000, R.D. 661 / 2007, BDEW-MSRL / FGW / TR8[6)]			
4S2, 4C2			
SC 720CP-10	SC 760CP-10	SC 800CP-10	

1) Startup at DC voltage < 1000 V
2) At 1.05 $V_{AC, nom}$ and cos φ = 1
3) Further AC voltages, DC voltages and power classes can be configured (for more detailed information, see technical information "Innovations_CP" at www.SMA.de)
4) Self-consumption during nominal operation
5) Sound pressure level at a distance of 10 m
6) With complete dynamic grid support
7) Efficiency measured without internal power supply

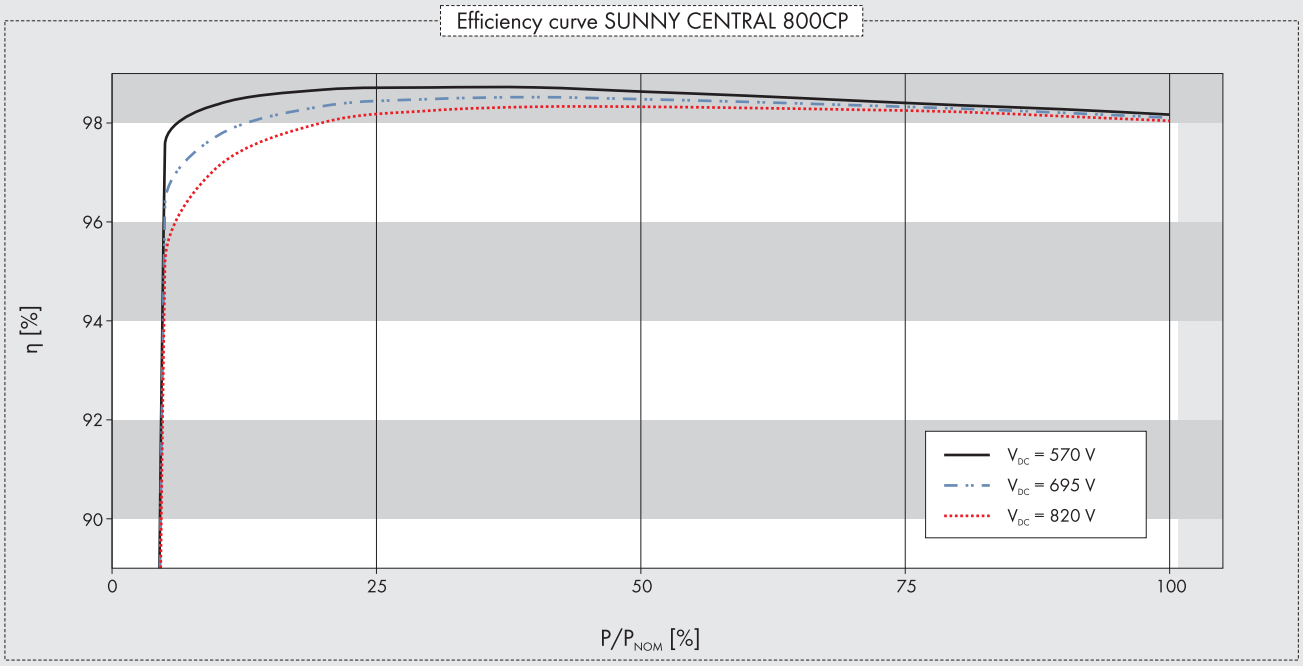

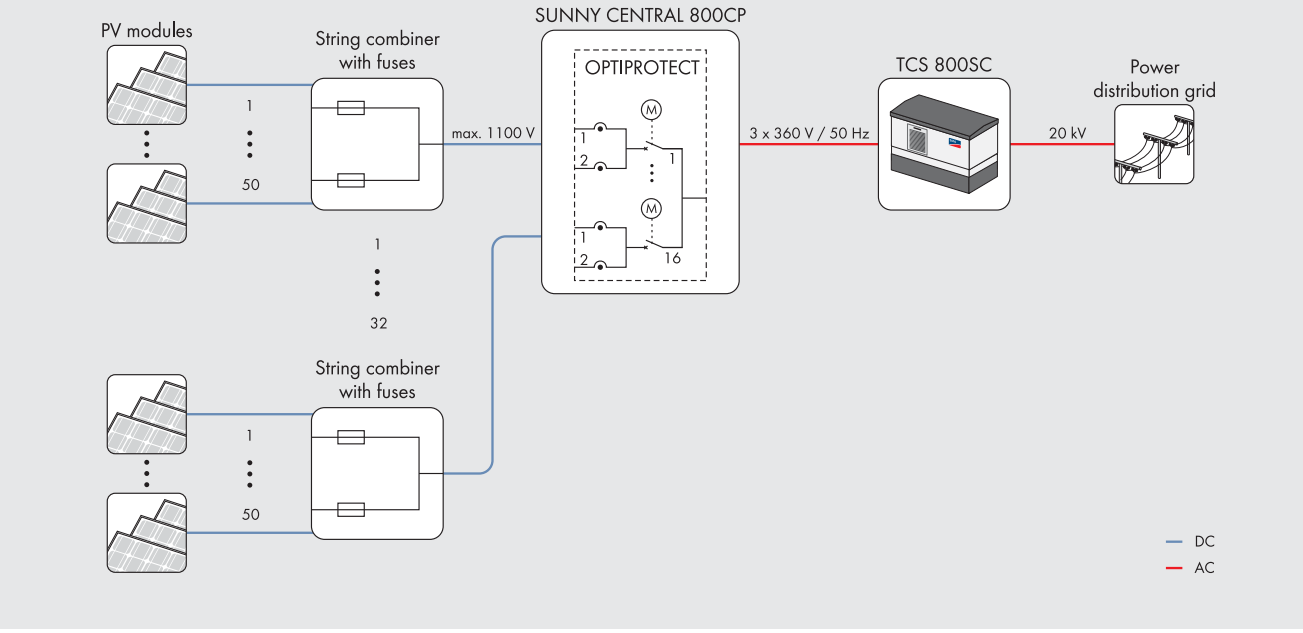

Toll Free +1 888 4 SMA USA
www.SMA-America.com

SMA America, LLC

APPENDIX F

INVERTER EFFICIENCY

F.1 Efficiencies of inverters

The efficiencies of the 84 inverters at Kalkbult solar PV plant in its first year of operation are presented in this appendix. The provided inverter efficiency data is referred to in Chapter 5.

Table F.1: Inverter efficiency during operational year 2014

Inverter	**Efficiency** %	**Inverter**	**Efficiency** %	**Inverter**	**Efficiency** %
1	96.75	29	97.13	57	96.80
2	97.45	30	97.43	58	98.47
3	96.73	31	95.59	59	98.04
4	96.60	32	96.62	60	97.11
5	97.74	33	98.11	61	98.39
6	97.91	34	98.39	62	96.95
7	97.28	35	98.26	63	98.39
8	96.59	36	97.03	64	96.79
9	96.95	37	97.15	65	97.32
10	96.98	38	98.60	66	95.51
11	96.22	39	96.39	67	97.34
12	95.63	40	95.92	68	98.00
13	97.86	41	96.64	69	97.55
14	97.73	42	96.20	70	96.96
15	98.09	43	97.56	71	97.97
16	97.70	44	97.20	72	97.70
17	98.27	45	97.58	73	98.35
18	96.81	46	97.44	74	94.94
19	98.28	47	96.45	75	97.90
20	97.72	48	97.59	76	98.06
21	98.18	49	97.24	77	97.71
22	98.56	50	98.05	78	97.40
23	97.74	51	98.07	79	98.27
24	98.12	52	97.84	80	97.96
25	97.74	53	97.34	81	96.88
26	96.88	54	97.50	82	97.62
27	98.14	55	96.67	83	97.99
28	96.95	56	97.45	84	98.21

APPENDIX G

PVSYST FILE USING GHI AS INPUT-HAY MODEL AND FIXED AXIS

The PVsyst file obtained when simulating the 75 MW_P solar PV plant as a fixed axis system with a tilt angle of thirty degrees using the Hay model and 30-minute averaged GHI data as input, is presented in this appendix. The PVsyst file is referred to in Chapter 5.

Grid-Connected System: Simulation parameters

Project : **Masters**

Geographical Site	**Kalkbult_site**		Country	**South Africa**
Situation	Latitude	30.2°S	Longitude	24.1°E
Time defined as	Legal Time	Time zone UT+2	Altitude	1214 m
	Albedo	0.20		
Meteo data:	**Kalkbult_site**	Imported - ASCII file		

Simulation variant : **New simulation variant**

Simulation date 01/08/16 15h11

Simulation parameters

Collector Plane Orientation	Tilt	30°	Azimuth	0°
50 Sheds	Pitch	7 m	Collector width	3.34 m
Inactive band	Top	0 m	Bottom	0 m
Shading limit angle	Gamma	22.13 °	Occupation Ratio	47.7 %

Models used	Transposition	Hay	Diffuse	Erbs, Meteonorm
Horizon	Free Horizon			
Near Shadings	Mutual shadings of sheds			

PV Array Characteristics

PV module	Si-poly	Model	**BYD 240 P6-30**	
Original PVsyst database		Manufacturer	BYD	
Number of PV modules		In series	24 modules	In parallel 13021 strings
Total number of PV modules		Nb. modules	312504	Unit Nom. Power 240 Wp
Array global power		Nominal (STC)	**75001 kWp**	At operating cond. 67007 kWp (50°C)
Array operating characteristics (50°C)		U mpp	639 V	I mpp 104927 A
Total area		Module area	**508407 m²**	Cell area 456306 m²

Inverter		Model	**Sunny Central 800CP**	
		Manufacturer	SMA	
Characteristics		Operating Voltage	583-820 V	Unit Nom. Power 800 kWac
Inverter pack		Nb. of inverters	84 units	Total Power 67200 kWac

PV Array loss factors

Array Soiling Losses

Jan.	Feb.	Mar.	Apr.	May	June	July	Aug.	Sep.	Oct.	Nov.	Dec.
1.8%	1.8%	1.8%	1.8%	1.8%	1.8%	1.8%	1.8%	1.8%	1.8%	1.8%	1.8%

Thermal Loss factor	Uc (const)	38.0 W/m²K	Uv (wind)	0.0 W/m²K / m/s
Wiring Ohmic Loss	Global array res.	0 mOhm	Loss Fraction	0.0 % at STC
Module Quality Loss			Loss Fraction	0.0 %
Module Mismatch Losses			Loss Fraction	1.3 % at MPP
Incidence effect, ASHRAE parametrization	IAM =	1 - bo (1/cos i - 1)	bo Param.	0.05

System loss factors

AC wire loss inverter to transfo	Inverter voltage	360 Vac tri		
	Wires: 3x30000.0 mm²	12 m	Loss Fraction	0.4 % at STC
External transformer	Iron loss (24H connexion)	73610 W	Loss Fraction	0.1 % at STC
	Resistive/Inductive losses	0.0 mOhm	Loss Fraction	2.0 % at STC

Grid-Connected System: Simulation parameters (continued)

User's needs : Unlimited load (grid)

Grid-Connected System: Main results

Project : **Masters**

Simulation variant : **New simulation variant**

Main system parameters				
System type	**Grid-Connected**			
PV Field Orientation	Sheds disposition, tilt	30°	azimuth	0°
PV modules	Model	BYD 240 P6-30	Pnom	240 Wp
PV Array	Nb. of modules	312504	Pnom total	**75001 kWp**
Inverter	Model	Sunny Central 800CP	Pnom	800 kW a
Inverter pack	Nb. of units	84.0	Pnom total	**67200 ac**
User's needs	Unlimited load (grid)			

Main simulation results

System Production — **Produced Energy** **146413 MWh/year** Spec. prod. 19 2 kWh/kWp/ye

Performance Ratio PR 7 %

Normalized productions (per installed kWp): Nominal power 75001 kWp

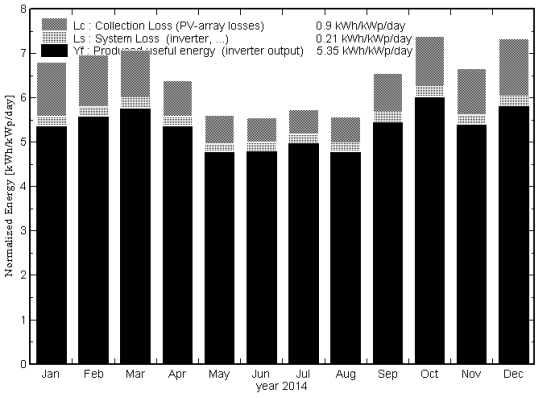

Performance Ratio PR

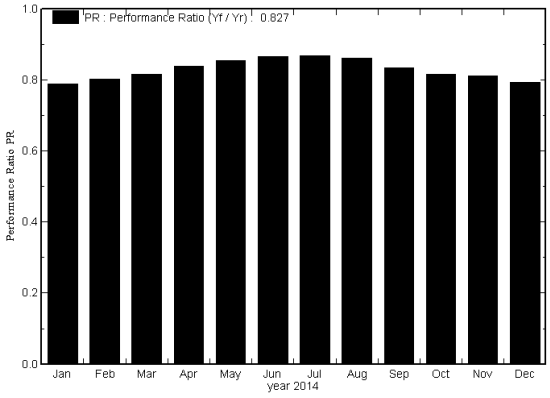

New simulation variant

Balances and main results

	GlobHor kWh/m²	T Amb °C	GlobInc kWh/m²	GlobEff kWh/m²	EArray MWh	E_Grid MWh	EffArrR %	EffSysR %
Jan. 14	234.8	26.52	210.9	194.6	12979	12492	12.10	11.65
Feb. 14	198.0	24.44	195.0	181.5	12204	11742	12.31	11.85
Mar. 14	196.6	21.04	219.4	205.4	13955	13421	12.51	12.03
Apr. 14	149.2	16.59	191.7	180.0	12557	12082	12.89	12.40
May 14	118.7	13.09	173.6	162.6	11564	11126	13.11	12.61
June 14	104.6	7.83	166.4	154.4	11249	10818	13.30	12.79
July 14	115.9	8.24	177.9	165.7	12056	11601	13.33	12.83
Aug. 14	129.5	11.59	172.4	161.6	11578	11131	13.21	12.70
Sep. 14	166.8	15.93	196.4	184.0	12770	12281	12.79	12.30
Oct. 14	222.3	20.56	228.9	213.8	14571	14005	12.52	12.04
Nov. 14	218.9	20.74	200.0	185.2	12667	12182	12.45	11.98
Dec. 14	261.7	26.10	227.1	210.4	14056	13532	12.17	11.72
Year	2117.0	17.69	2359.6	2199.2	152206	146413	12.69	12.20

Legends:

GlobHor	Horizontal global irradiation	EArray	Effective energy at the output of the array
T Amb	Ambient Temperature	E_Grid	Energy injected into grid
GlobInc	Global incident in coll. plane	EffArrR	Effic. Eout array / rough area
GlobEff	Effective Global, corr. for IAM and shadings	EffSysR	Effic. Eout system / rough area

Grid-Connected System: Loss diagram

Project : **Masters**

Simulation variant : **New simulation variant**

Main system parameters				
System type	**Grid-Connected**			
PV Field Orientation	Sheds disposition, tilt	30°	azimuth	0°
PV modules	Model	BYD 240 P6-30	Pnom	240 Wp
PV Array	Nb. of modules	312504	Pnom total	**75001 kWp**
Inverter	Model	Sunny Central 800CP	Pnom	800 kW a
Inverter pack	Nb. of units	84.0	Pnom total	**67200 ac**
User's needs	Unlimited load (grid)			

Loss diagram over the whole year

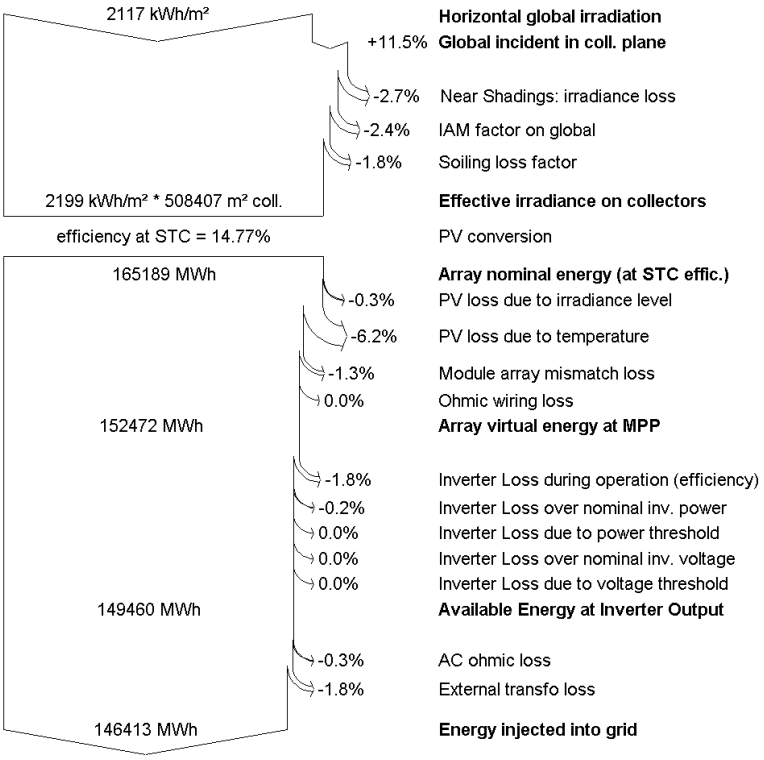

APPENDIX H

PVSYST FILE USING GHI AS INPUT-PEREZ MODEL AND FIXED AXIS

The PVsyst file presented in this appendix is referred to in Chapter 5. The PVsyst file gives a summary of results obtained when simulating the 75 MW_P solar PV plant using the Perez model and 30-minute averaged GHI data as input in PVsyst software package.

Grid-Connected System: Simulation parameters

Project : **Masters**

Geographical Site	**Kalkbult_site**		Country	**South Africa**
Situation	Latitude	30.2°S	Longitude	24.1°E
Time defined as	Legal Time	Time zone UT+2	Altitude	1214 m
	Albedo	0.20		
Meteo data:	**Kalkbult_site**	Imported - ASCII file		

Simulation variant : **New simulation variant**

Simulation date 01/08/16 14h59

Simulation parameters

Collector Plane Orientation	Tilt	30°	Azimuth	0°
50 Sheds	Pitch	7 m	Collector width	3.34 m
Inactive band	Top	0 m	Bottom	0 m
Shading limit angle	Gamma	22.13 °	Occupation Ratio	47.7 %

Models used	Transposition	Perez	Diffuse	Erbs, Meteonorm
Horizon	Free Horizon			
Near Shadings	Mutual shadings of sheds			

PV Array Characteristics

PV module	Si-poly	Model	**BYD 240 P6-30**	
Original PVsyst database		Manufacturer	BYD	
Number of PV modules		In series	24 modules	In parallel 13021 strings
Total number of PV modules		Nb. modules	312504	Unit Nom. Power 240 Wp
Array global power		Nominal (STC)	**75001 kWp**	At operating cond. 67007 kWp (50°C)
Array operating characteristics (50°C)		U mpp	639 V	I mpp 104927 A
Total area		Module area	**508407 m²**	Cell area 456306 m²

Inverter		Model	**Sunny Central 800CP**	
		Manufacturer	SMA	
Characteristics		Operating Voltage	583-820 V	Unit Nom. Power 800 kWac
Inverter pack		Nb. of inverters	84 units	Total Power 67200 kWac

PV Array loss factors

Array Soiling Losses

Jan.	Feb.	Mar.	Apr.	May	June	July	Aug.	Sep.	Oct.	Nov.	Dec.
1.8%	1.8%	1.8%	1.8%	1.8%	1.8%	1.8%	1.8%	1.8%	1.8%	1.8%	1.8%

Thermal Loss factor	Uc (const)	38.0 W/m²K	Uv (wind)	0.0 W/m²K / m/s
Wiring Ohmic Loss	Global array res.	0 mOhm	Loss Fraction	0.0 % at STC
Module Quality Loss			Loss Fraction	0.0 %
Module Mismatch Losses			Loss Fraction	1.3 % at MPP
Incidence effect, ASHRAE parametrization	IAM =	1 - bo (1/cos i - 1)	bo Param.	0.05

System loss factors

AC wire loss inverter to transfo	Inverter voltage	360 Vac tri		
	Wires: 3x30000.0 mm²	12 m	Loss Fraction	0.4 % at STC
External transformer	Iron loss (24H connexion)	73610 W	Loss Fraction	0.1 % at STC
	Resistive/Inductive losses	0.0 mOhm	Loss Fraction	2.0 % at STC

Grid-Connected System: Simulation parameters (continued)

User's needs : Unlimited load (grid)

Grid-Connected System: Main results

Project : **Masters**

Simulation variant : **New simulation variant**

Main system parameters				
System type		**Grid-Connected**		
PV Field Orientation	Sheds disposition, tilt	30°	azimuth	0°
PV modules	Model	BYD 240 P6-30	Pnom	240 Wp
PV Array	Nb. of modules	312504	Pnom total	**75001 kWp**
Inverter	Model	Sunny Central 800CP	Pnom	800 kW a
Inverter pack	Nb. of units	84.0	Pnom total	**67200 ac**
User's needs	Unlimited load (grid)			

Main simulation results

System Production — **Produced Energy** **148697 MWh/year** Spec. prod. 198.3 kWh/kWp/ye

Performance Ratio PR 82.6 %

Normalized productions (per installed kWp): Nominal power 75001 kWp

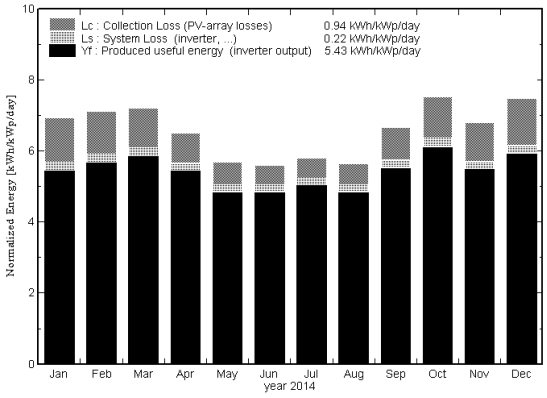

Performance Ratio PR

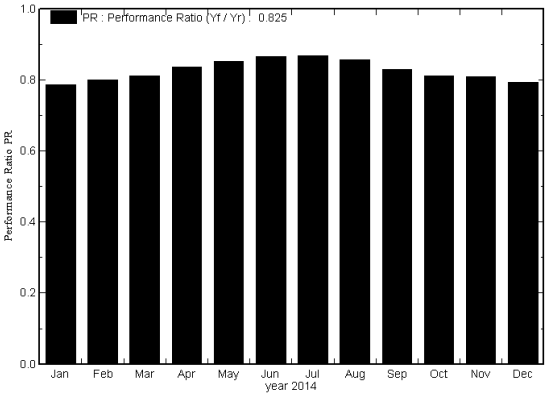

New simulation variant

Balances and main results

	GlobHor kWh/m²	T Amb °C	GlobInc kWh/m²	GlobEff kWh/m²	EArray MWh	E_Grid MWh	EffArrR %	EffSysR %
Jan. 14	234.8	26.52	215.3	198.5	13221	12724	12.08	11.63
Feb. 14	198.0	24.44	199.1	185.2	12431	11958	12.28	11.81
Mar. 14	196.6	21.04	223.9	209.4	14187	13641	12.46	11.99
Apr. 14	149.2	16.59	195.2	183.1	12755	12269	12.85	12.36
May 14	118.7	13.09	176.2	165.0	11727	11282	13.09	12.59
June 14	104.6	7.83	168.0	155.8	11347	10912	13.28	12.77
July 14	115.9	8.24	180.2	167.8	12200	11740	13.32	12.82
Aug. 14	129.5	11.59	175.3	164.3	11744	11287	13.18	12.66
Sep. 14	166.8	15.93	200.1	187.4	12971	12471	12.75	12.26
Oct. 14	222.3	20.56	233.4	217.8	14800	14222	12.47	11.99
Nov. 14	218.9	20.74	204.0	188.8	12877	12382	12.42	11.94
Dec. 14	261.7	26.10	232.2	215.0	14343	13807	12.15	11.70
Year	2117.0	17.69	2402.9	2238.1	154604	148697	12.66	12.17

Legends:

GlobHor	Horizontal global irradiation	EArray	Effective energy at the output of the array
T Amb	Ambient Temperature	E_Grid	Energy injected into grid
GlobInc	Global incident in coll. plane	EffArrR	Effic. Eout array / rough area
GlobEff	Effective Global, corr. for IAM and shadings	EffSysR	Effic. Eout system / rough area

Grid-Connected System: Loss diagram

Project : **Masters**

Simulation variant : **New simulation variant**

Main system parameters				
System type	**Grid-Connected**			
PV Field Orientation	Sheds disposition, tilt	30°	azimuth	0°
PV modules	Model	BYD 240 P6-30	Pnom	240 Wp
PV Array	Nb. of modules	312504	Pnom total	**75001 kWp**
Inverter	Model	Sunny Central 800CP	Pnom	800 kW a
Inverter pack	Nb. of units	84.0	Pnom total	**67200 ac**
User's needs	Unlimited load (grid)			

Loss diagram over the whole year

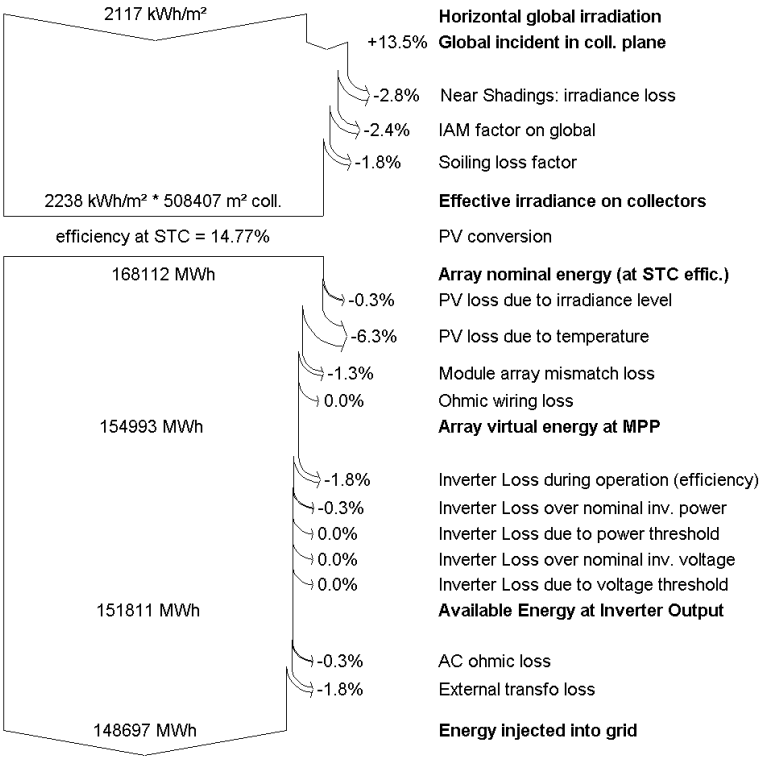

APPENDIX I

PVSYST FILE USING POA IRRADIANCE AS INPUT- HAY MODEL AND FIXED AXIS

A summary of the simulation done in PVsyst using measured 30-minute averaged POA irradiance data as input and the Hay model is presented in this appendix in form of a PVsyst file. The PVsyst file is referred to in Chapter 5.

Grid-Connected System: Simulation parameters

Project : **Masters**

Geographical Site	**Kalkbult_POA**		Country	**South Africa**
Situation	Latitude	30.2°S	Longitude	24.1°E
Time defined as	Legal Time	Time zone UT+2	Altitude	1214 m
	Albedo	0.20		
Meteo data:	**Kalkbult_POA**	Imported - ASCII file		

Simulation variant : **New simulation variant**

Simulation date 04/08/16 14h47

Simulation parameters

Collector Plane Orientation	Tilt	30°	Azimuth	0°
50 Sheds	Pitch	7 m	Collector width	3.34 m
Inactive band	Top	0 m	Bottom	0 m
Shading limit angle	Gamma	22.13 °	Occupation Ratio	47.7 %
Models used	Transposition	Hay	Diffuse	Erbs, Meteonorm
Horizon	Free Horizon			
Near Shadings	Mutual shadings of sheds			

PV Array Characteristics

PV module	Si-poly	Model	**BYD 240 P6-30**
Original PVsyst database		Manufacturer	BYD

Number of PV modules	In series	24 modules	In parallel	13021 strings
Total number of PV modules	Nb. modules	312504	Unit Nom. Power	240 Wp
Array global power	Nominal (STC)	**75001 kWp**	At operating cond.	67007 kWp (50°C)
Array operating characteristics (50°C)	U mpp	639 V	I mpp	104927 A
Total area	Module area	**508407 m²**	Cell area	456306 m²

Inverter	Model	**Sunny Central 800CP**		
	Manufacturer	SMA		
Characteristics	Operating Voltage	583-820 V	Unit Nom. Power	800 kWac
Inverter pack	Nb. of inverters	84 units	Total Power	67200 kWac

PV Array loss factors

Array Soiling Losses

Jan.	Feb.	Mar.	Apr.	May	June	July	Aug.	Sep.	Oct.	Nov.	Dec.
1.8%	1.8%	1.8%	1.8%	1.8%	1.8%	1.8%	1.8%	1.8%	1.8%	1.8%	1.8%

Thermal Loss factor	Uc (const)	38.0 W/m²K	Uv (wind)	0.0 W/m²K / m/s
Wiring Ohmic Loss	Global array res.	0 mOhm	Loss Fraction	0.0 % at STC
Module Quality Loss			Loss Fraction	0.0 %
Module Mismatch Losses			Loss Fraction	1.3 % at MPP
Incidence effect, ASHRAE parametrization	IAM =	1 - bo (1/cos i - 1)	bo Param.	0.05

System loss factors

AC wire loss inverter to transfo	Inverter voltage	360 Vac tri		
	Wires: 3x30000.0 mm²	12 m	Loss Fraction	0.4 % at STC
External transformer	Iron loss (24H connexion)	73610 W	Loss Fraction	0.1 % at STC
	Resistive/Inductive losses	0.0 mOhm	Loss Fraction	2.0 % at STC

Grid-Connected System: Simulation parameters (continued)

User's needs : Unlimited load (grid)

Grid-Connected System: Main results

Project : **Masters**

Simulation variant : **New simulation variant**

Main system parameters				
System type		**Grid-Connected**		
PV Field Orientation	Sheds disposition, tilt	30°	azimuth	0°
PV modules	Model	BYD 240 P6-30	Pnom	240 Wp
PV Array	Nb. of modules	312504	Pnom total	**75001 kWp**
Inverter	Model	Sunny Central 800CP	Pnom	800 kW a
Inverter pack	Nb. of units	84.0	Pnom total	**67200 ac**
User's needs	Unlimited load (grid)			

Main simulation results

System Production **Produced Energy** **148058338434 W/yea** Spec. Prod. 19 kWh/kWp/ye

Performance Ratio PR 8 %

Normalized productions (per installed kWp): Nominal power 75001 kWp

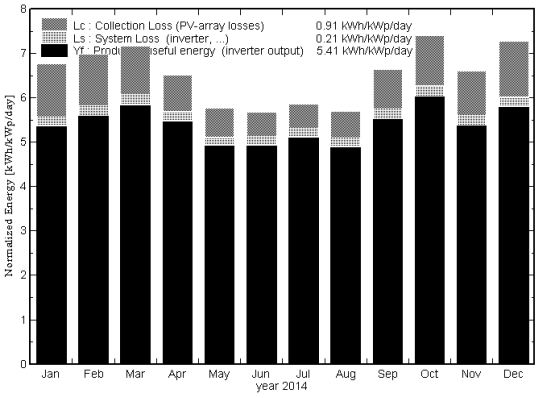

Performance Ratio PR

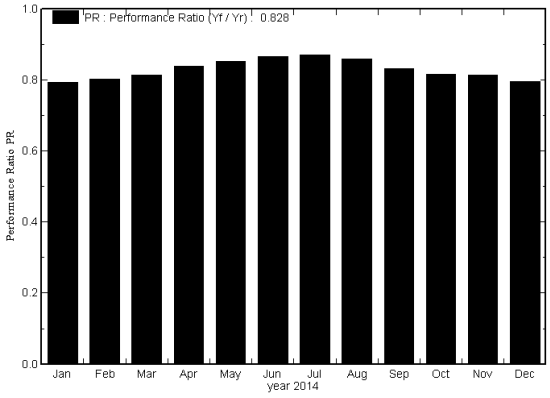

New simulation variant

Balances and main results

	GlobHor kWh/m²	T Amb °C	GlobInc kWh/m²	GlobEff kWh/m²	EArray kWh	E_Grid kWh	EffArrR %	EffSysR %
Jan. 14	230.5	26.55	209.7	194.2	12965912	12487112	12.16	11.71
Feb. 14	197.8	24.44	195.4	182.0	12236300	11772725	12.32	11.85
Mar. 14	199.1	21.04	222.4	208.3	14136146	13592092	12.50	12.02
Apr. 14	151.8	16.59	195.7	183.7	12804986	12319609	12.87	12.38
May 14	121.3	13.09	178.9	167.5	11907768	11456822	13.09	12.60
June 14	106.6	7.83	170.5	158.7	11536398	11093105	13.31	12.80
July 14	118.0	8.24	181.9	169.9	12343676	11876551	13.35	12.84
Aug. 14	132.0	11.59	176.8	165.8	11845785	11387998	13.18	12.67
Sep. 14	168.8	15.93	199.2	186.7	12934458	12436668	12.77	12.28
Oct. 14	222.2	20.56	229.3	214.3	14596305	14031100	12.52	12.04
Nov. 14	214.9	20.74	198.4	184.0	12595540	12112190	12.49	12.01
Dec. 14	254.6	26.10	225.8	209.4	14010771	13492366	12.20	11.75
Year	2117.4	17.70	2384.0	2224.5	153914044	148058338	12.70	12.22

Legends:

GlobHor	Horizontal global irradiation	EArray	Effective energy at the output of the array
T Amb	Ambient Temperature	E_Grid	Energy injected into grid
GlobInc	Global incident in coll. plane	EffArrR	Effic. Eout array / rough area
GlobEff	Effective Global, corr. for IAM and shadings	EffSysR	Effic. Eout system / rough area

Grid-Connected System: Loss diagram

Project : **Masters**

Simulation variant : **New simulation variant**

Main system parameters				
	System type	**Grid-Connected**		
PV Field Orientation	Sheds disposition, tilt	30°	azimuth	0°
PV modules	Model	BYD 240 P6-30	Pnom	240 Wp
PV Array	Nb. of modules	312504	Pnom total	**75001 kWp**
Inverter	Model	Sunny Central 800CP	Pnom	800 kW a
Inverter pack	Nb. of units	84.0	Pnom total	**67200 ac**
User's needs	Unlimited load (grid)			

Loss diagram over the whole year

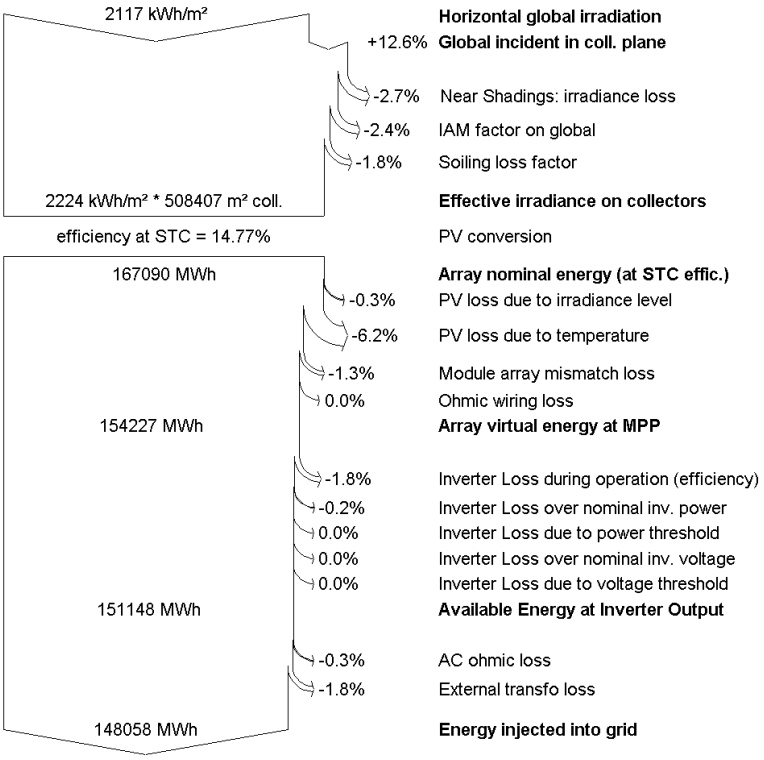

APPENDIX J

PVSYST LOSS MODEL VALIDATION USING 2015 MEASURED DATA

In this appendix the improved PVsyst loss model created from measured data obtained in 2014 is validated using data measured in 2015 at the 75 MW_P, Kalkbult solar PV plant. The validation of the PVsyst loss model is referred to in Chapter 5.

J.1 Improved PVsyst model validation

There are several ways of importing meteo-data into PVsyst and the methods relevant to this study are importing data using the PVsyst standard format and importing using the ASCII method. The former allows for the importing of hourly values whereas the latter allows for the importing of sub-hourly values. However, in this study meteo-data was imported into PVsyst using the ASCII method due to its advantages over the PVsyst standard format, as mentioned in Appendix C. Earlier on, the improved PVsyst loss model was validated using 2014 30-minute averaged data as input. In this section, the improved PVsyst model is validated using 30-minute interval meteo-data for 2015 imported into PVsyst using the ASCII method with time shift correction applied. Time shift correction will be explained in the section that follows.

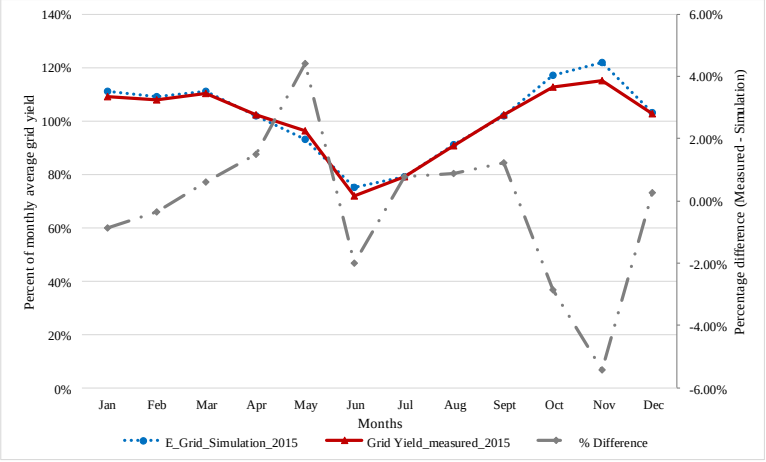

Figure J.1: Improved PVsyst model validation using data for 2015

Figure J.1 shows the measured versus simulated energy yield on the left vertical axis and the percentage differences between the two on the right vertical axis. The percentage differences between the measured and simulated energy yield for 2015 are within 2% for the majority of the months, less than the uncertainty of the PVsyst simulation tool, except for October, November and May. These differences in energy yield are in accordance with the respective differences in the measured and simulated global plane irradiance, caused by the irradiance models within the simulation tool not transposing GHI into GPI correctly. The deep in December is explained by the missing measured values of energy yield and irradiance from the 9th to the 12th of December as was observed in the measured data provided by Scatec Solar.

From the comparison of the results obtained from hourly input meteo-data and those from 30-minute interval data it was observed that the data with small time resolution gives better results. The monthly energy yield simulated from the 30-minute averaged values for 2015 is closer to the measured energy yield compared to that for 2014 obtained from hourly values. It was also observed that the solar radiation patterns for 2014 and 2015 are different. In the next section, the time shift correction applied when importing meteo-data into PVsyst is explained.

J.1.1 Time shift correction

In measured data values each record usually has a time label and depending on the data acquisition systems, the time labels may be referenced to the interval beginning, interval middle, interval end point or at any shifted time within the hour [19]. For example the recorded data time labelled 10:00 to 11:00 may actually be measurements accumulations from 10:10 to 11:10.

The time label refers to the beginning of the record and concerns the accumulation up to the next record in the PVsyst convention. PVsyst keeps its full-hour label, and calculations related to the solar geometry are done for the middle of the interval (10:30), when it should actually correspond to the middle of the irradiance measurement period.

For this reason, PVsyst defines a time shift correction expressed in minutes which may be associated with the meteo-data file. This applies to meteo data files imported into PVsyst and the time shift affects the shading, diffuse and transposition model computations, particularly in the mornings or evenings. The correction is applied to the middle value of the hour for the solar geometry calculations (in the recently given example, the computation of the solar geometry will be at 10:40 and the time shift correction will be -10 minutes) [19].

PVsyst offers tools for the evaluation of the time shift correction, either using the Hourly clearness index k_t morning/evening graph or comparison to the clear sky model. If the time shift is more than $\pm$30 min, it is advised to modify the begin or end interval choice or the time

zone of the reference site. The main cause of the discrepancy often observed between the POA original values and the transposed values is the fact that when importing meteo-data, PVsyst limits the values to reasonable values according to the clear sky model [19].

APPENDIX K

PVSYST FILE USING THE PEREZ MODEL AND SINGLE AXIS TRACKER AT ZERO DEGREES TILT ANGLE

PVsyst file showing the results when the $75_M W_P$ solar PV plant is simulated as a single axis tracker at a tilt angle of zero degrees using the Hay model. The PVsyst file is referred to in Chapter 5.

Grid-Connected System: Simulation parameters

Project : **Masters**

Geographical Site	**Kalkbult_site**		Country	**South Africa**
Situation	Latitude	30.2°S	Longitude	24.1°E
Time defined as	Legal Time	Time zone UT+2	Altitude	1214 m
	Albedo	0.20		
Meteo data:	**Kalkbult_site**	Imported - ASCII file		

Simulation variant : **New simulation variant**

Simulation date 02/08/16 14h34

Simulation parameters

Tracking plane, tilted Axis	Axis Tilt	0°	Axis Azimuth	0°
Rotation Limitations	Minimum Phi	-55°	Maximum Phi	55°
Backtracking strategy	Tracker Spacing	7 m	Collector width	3.34 m
Inactive band	Left	0 m	Right	0 m
Models used	Transposition	Perez	Diffuse	Erbs, Meteonorm
Horizon	Free Horizon			
Near Shadings	No Shadings			

PV Array Characteristics

PV module	Si-poly	Model	**BYD 240 P6-30**	
Original PVsyst database		Manufacturer	BYD	
Number of PV modules		In series	24 modules	In parallel 13021 strings
Total number of PV modules		Nb. modules	312504	Unit Nom. Power 240 Wp
Array global power		Nominal (STC)	**75001 kWp**	At operating cond. 67007 kWp (50°C)
Array operating characteristics (50°C)		U mpp	639 V	I mpp 104927 A
Total area		Module area	**508407 m²**	Cell area 456306 m²

Inverter		Model	**Sunny Central 800CP**	
		Manufacturer	SMA	
Characteristics		Operating Voltage	583-820 V	Unit Nom. Power 800 kWac
Inverter pack		Nb. of inverters	84 units	Total Power 67200 kWac

PV Array loss factors

Array Soiling Losses

Jan.	Feb.	Mar.	Apr.	May	June	July	Aug.	Sep.	Oct.	Nov.	Dec.
1.8%	1.8%	1.8%	1.8%	1.8%	1.8%	1.8%	1.8%	1.8%	1.8%	1.8%	1.8%

Thermal Loss factor	Uc (const)	38.0 W/m²K	Uv (wind)	0.0 W/m²K / m/s
Wiring Ohmic Loss	Global array res.	0 mOhm	Loss Fraction	0.0 % at STC
Module Quality Loss			Loss Fraction	0.0 %
Module Mismatch Losses			Loss Fraction	1.3 % at MPP
Incidence effect, ASHRAE parametrization	IAM =	1 - bo (1/cos i - 1)	bo Param.	0.05

System loss factors

AC wire loss inverter to transfo	Inverter voltage	360 Vac tri		
	Wires: 3x30000.0 mm²	12 m	Loss Fraction	0.4 % at STC
External transformer	Iron loss (24H connexion)	73610 W	Loss Fraction	0.1 % at STC
	Resistive/Inductive losses	0.0 mOhm	Loss Fraction	2.0 % at STC

Grid-Connected System: Simulation parameters (continued)

User's needs : Unlimited load (grid)

Grid-Connected System: Main results

Project : **Masters**

Simulation variant : **New simulation variant**

Main system parameters					
	System type	**Grid-Connected**			
PV Field Orientation	tracking, tilted axis, Axis Tilt	0°	Axis Azimuth	0°	
PV modules	Model	BYD 240 P6-30	Pnom	240 Wp	
PV Array	Nb. of modules	312504	Pnom total	**75001 kWp**	
Inverter	Model	Sunny Central 800CP	Pnom	800 kW a	
Inverter pack	Nb. of units	84.0	Pnom total	**67200 ac**	
User's needs	Unlimited load (grid)				

Main simulation results

System Production — **Produced Energy** **172358 MWh/year** Spec. prod. 22 kWh/kWp/ye

Performance Ratio PR 0 %

Normalized productions (per installed kWp): Nominal power 75001 kWp

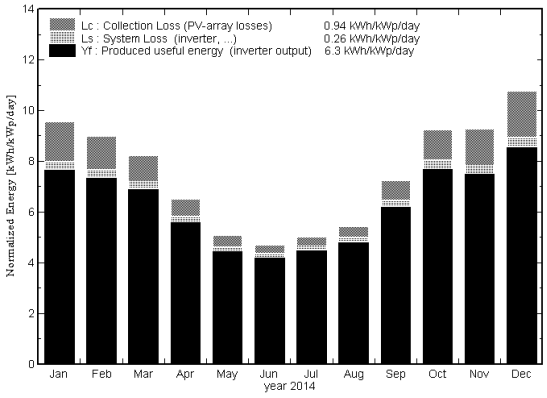

Performance Ratio PR

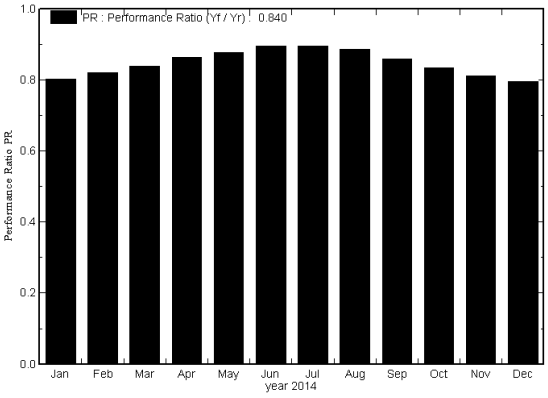

New simulation variant

Balances and main results

	GlobHor kWh/m²	T Amb °C	GlobInc kWh/m²	GlobEff kWh/m²	EArray MWh	E_Grid MWh	EffArrR %	EffSysR %
Jan. 14	234.8	26.52	296.0	286.1	18589	17830	12.35	11.85
Feb. 14	198.0	24.44	251.7	243.1	16146	15494	12.62	12.11
Mar. 14	196.6	21.04	254.9	245.7	16716	16056	12.90	12.39
Apr. 14	149.2	16.59	195.0	186.9	13124	12639	13.24	12.75
May 14	118.7	13.09	157.6	149.9	10771	10386	13.44	12.96
June 14	104.6	7.83	141.1	133.5	9832	9480	13.70	13.21
July 14	115.9	8.24	155.4	147.4	10829	10445	13.71	13.22
Aug. 14	129.5	11.59	168.2	160.8	11619	11188	13.58	13.08
Sep. 14	166.8	15.93	217.2	208.8	14564	13998	13.19	12.68
Oct. 14	222.3	20.56	286.9	277.2	18726	17960	12.84	12.31
Nov. 14	218.9	20.74	278.4	269.3	17674	16945	12.49	11.97
Dec. 14	261.7	26.10	333.7	323.0	20793	19936	12.26	11.75
Year	2117.0	17.69	2736.2	2631.6	179384	172358	12.90	12.39

Legends:

GlobHor	Horizontal global irradiation	EArray	Effective energy at the output of the array
T Amb	Ambient Temperature	E_Grid	Energy injected into grid
GlobInc	Global incident in coll. plane	EffArrR	Effic. Eout array / rough area
GlobEff	Effective Global, corr. for IAM and shadings	EffSysR	Effic. Eout system / rough area

Grid-Connected System: Loss diagram

Project : **Masters**

Simulation variant : **New simulation variant**

Main system parameters					
	System type	**Grid-Connected**			
PV Field Orientation	tracking, tilted axis, Axis Tilt	0°	Axis Azimuth	0°	
PV modules	Model	BYD 240 P6-30	Pnom	240 Wp	
PV Array	Nb. of modules	312504	Pnom total	**75001 kWp**	
Inverter	Model	Sunny Central 800CP	Pnom	800 kW a	
Inverter pack	Nb. of units	84.0	Pnom total	**67200 ac**	
User's needs	Unlimited load (grid)				

Loss diagram over the whole year

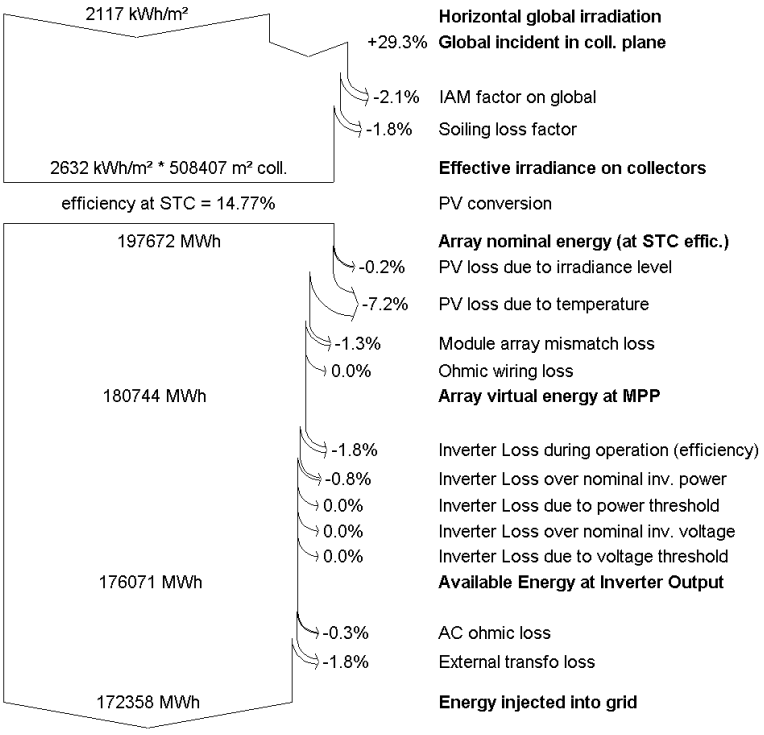

APPENDIX L

PVSYST FILE USING THE HAY MODEL AND SINGLE AXIS TRACKER AT ZERO DEGREES TILT ANGLE

PVsyst file showing the results when the $75_M W_P$ solar PV plant is simulated as a single axis tracker at a tilt angle of zero degrees using the Hay model. The PVsyst file is referred to in Chapter 5.

Grid-Connected System: Simulation parameters

Project : **Masters**

Geographical Site	**Kalkbult_site**		Country	**South Africa**
Situation	Latitude	30.2°S	Longitude	24.1°E
Time defined as	Legal Time	Time zone UT+2	Altitude	1214 m
	Albedo	0.20		
Meteo data:	**Kalkbult_site**	Imported - ASCII file		

Simulation variant : **New simulation variant**

Simulation date 02/08/16 14h15

Simulation parameters

Tracking plane, tilted Axis	Axis Tilt	0°	Axis Azimuth	0°
Rotation Limitations	Minimum Phi	-55°	Maximum Phi	55°
Backtracking strategy	Tracker Spacing	7 m	Collector width	3.34 m
Inactive band	Left	0 m	Right	0 m
Models used	Transposition	Hay	Diffuse	Erbs, Meteonorm
Horizon	Free Horizon			
Near Shadings	No Shadings			

PV Array Characteristics

PV module	Si-poly	Model	**BYD 240 P6-30**		
Original PVsyst database		Manufacturer	BYD		
Number of PV modules		In series	24 modules	In parallel	13021 strings
Total number of PV modules		Nb. modules	312504	Unit Nom. Power	240 Wp
Array global power		Nominal (STC)	**75001 kWp**	At operating cond.	67007 kWp (50°C)
Array operating characteristics (50°C)		U mpp	639 V	I mpp	104927 A
Total area		Module area	**508407 m²**	Cell area	456306 m²

Inverter		Model	**Sunny Central 800CP**		
		Manufacturer	SMA		
Characteristics		Operating Voltage	583-820 V	Unit Nom. Power	800 kWac
Inverter pack		Nb. of inverters	84 units	Total Power	67200 kWac

PV Array loss factors

Array Soiling Losses

Jan.	Feb.	Mar.	Apr.	May	June	July	Aug.	Sep.	Oct.	Nov.	Dec.
1.8%	1.8%	1.8%	1.8%	1.8%	1.8%	1.8%	1.8%	1.8%	1.8%	1.8%	1.8%

Thermal Loss factor	Uc (const)	38.0 W/m²K	Uv (wind)	0.0 W/m²K / m/s
Wiring Ohmic Loss	Global array res.	0 mOhm	Loss Fraction	0.0 % at STC
Module Quality Loss			Loss Fraction	0.0 %
Module Mismatch Losses			Loss Fraction	1.3 % at MPP
Incidence effect, ASHRAE parametrization	IAM =	1 - bo (1/cos i - 1)	bo Param.	0.05

System loss factors

AC wire loss inverter to transfo	Inverter voltage	360 Vac tri		
	Wires: 3x30000.0 mm²	12 m	Loss Fraction	0.4 % at STC
External transformer	Iron loss (24H connexion)	73610 W	Loss Fraction	0.1 % at STC
	Resistive/Inductive losses	0.0 mOhm	Loss Fraction	2.0 % at STC

Grid-Connected System: Simulation parameters (continued)

User's needs : Unlimited load (grid)

Grid-Connected System: Main results

Project : **Masters**

Simulation variant : **New simulation variant**

Main system parameters					
	System type	**Grid-Connected**			
PV Field Orientation	tracking, tilted axis, Axis Tilt	0°	Axis Azimuth	0°	
PV modules	Model	BYD 240 P6-30	Pnom	240 Wp	
PV Array	Nb. of modules	312504	Pnom total	**75001 kWp**	
Inverter	Model	Sunny Central 800CP	Pnom	800 kW a	
Inverter pack	Nb. of units	84.0	Pnom total	**67200 ac**	
User's needs	Unlimited load (grid)				

Main simulation results

System Production — **Produced Energy** **170345 MWh/year** Spec. prod. 22 kWh/kWp/ye

Performance Ratio PR 8 %

Normalized productions (per installed kWp): Nominal power 75001 kWp

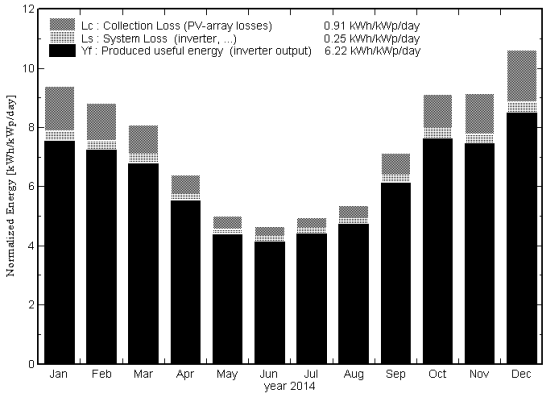

Performance Ratio PR

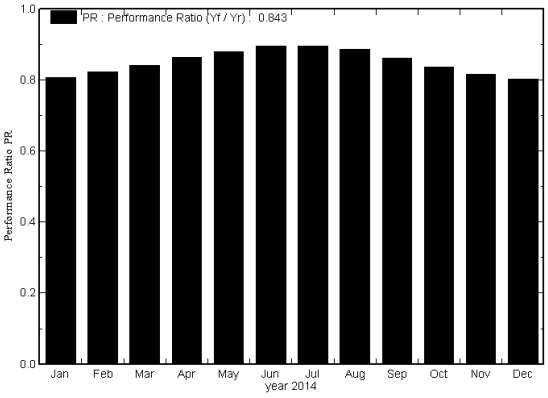

New simulation variant

Balances and main results

	GlobHor kWh/m²	T Amb °C	GlobInc kWh/m²	GlobEff kWh/m²	EArray MWh	E_Grid MWh	EffArrR %	EffSysR %
Jan. 14	234.8	26.52	290.9	281.3	18361	17616	12.42	11.91
Feb. 14	198.0	24.44	247.2	238.9	15907	15270	12.66	12.15
Mar. 14	196.6	21.04	250.9	241.9	16483	15837	12.92	12.42
Apr. 14	149.2	16.59	192.0	184.1	12937	12462	13.25	12.77
May 14	118.7	13.09	155.2	147.7	10615	10237	13.46	12.98
June 14	104.6	7.83	139.4	131.9	9722	9375	13.71	13.22
July 14	115.9	8.24	153.3	145.4	10691	10313	13.72	13.23
Aug. 14	129.5	11.59	165.9	158.5	11467	11044	13.60	13.10
Sep. 14	166.8	15.93	214.2	206.0	14390	13835	13.22	12.71
Oct. 14	222.3	20.56	282.5	273.2	18514	17761	12.89	12.36
Nov. 14	218.9	20.74	274.4	265.5	17536	16816	12.57	12.05
Dec. 14	261.7	26.10	328.8	318.4	20633	19780	12.34	11.83
Year	2117.0	17.69	2694.6	2592.7	177257	170345	12.94	12.43

Legends:

GlobHor	Horizontal global irradiation	EArray	Effective energy at the output of the array
T Amb	Ambient Temperature	E_Grid	Energy injected into grid
GlobInc	Global incident in coll. plane	EffArrR	Effic. Eout array / rough area
GlobEff	Effective Global, corr. for IAM and shadings	EffSysR	Effic. Eout system / rough area

Grid-Connected System: Loss diagram

Project : **Masters**

Simulation variant : **New simulation variant**

Main system parameters					
	System type	**Grid-Connected**			
PV Field Orientation	tracking, tilted axis, Axis Tilt	0°	Axis Azimuth	0°	
PV modules	Model	BYD 240 P6-30	Pnom	240 Wp	
PV Array	Nb. of modules	312504	Pnom total	**75001 kWp**	
Inverter	Model	Sunny Central 800CP	Pnom	800 kW a	
Inverter pack	Nb. of units	84.0	Pnom total	**67200 ac**	
User's needs	Unlimited load (grid)				

Loss diagram over the whole year

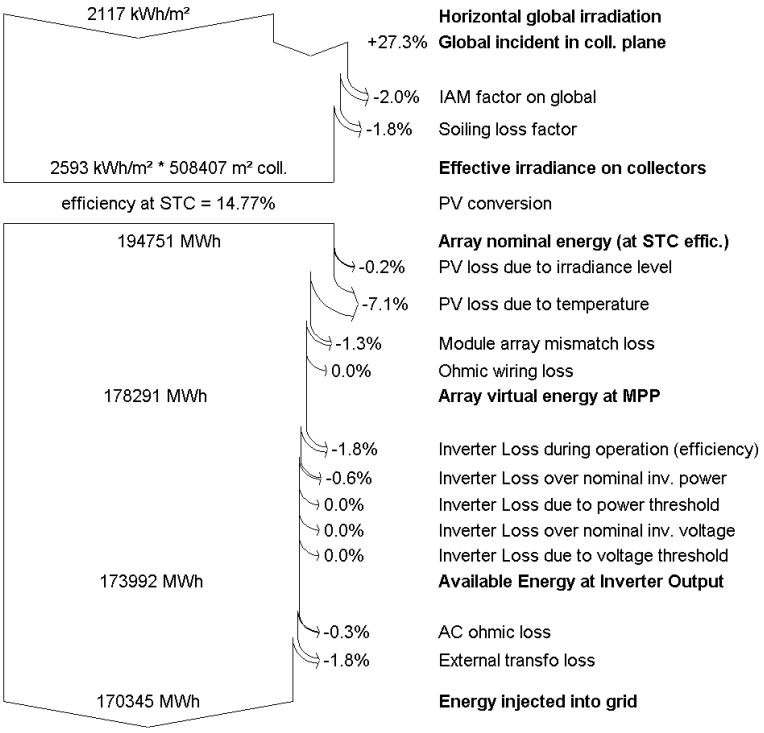

APPENDIX M

PVSYST FILE USING THE PEREZ MODEL AND SINGLE AXIS TRACKER AT THIRTY DEGREES TILT ANGLE

PVsyst file showing the results when the $75_M W_P$ solar PV plant is simulated as a single axis tracker at a tilt angle of thirty degrees using the Perez model. The PVsyst file is referred to in Chapter 5.

Grid-Connected System: Simulation parameters

Project : **Masters**

Geographical Site	**Kalkbult_site**		Country	**South Africa**
Situation	Latitude	30.2°S	Longitude	24.1°E
Time defined as	Legal Time	Time zone UT+2	Altitude	1214 m
	Albedo	0.20		
Meteo data:	**Kalkbult_site**	Imported - ASCII file		

Simulation variant : **New simulation variant**

Simulation date 02/08/16 14h36

Simulation parameters

Tracking plane, tilted Axis	Axis Tilt	30°	Axis Azimuth	0°
Rotation Limitations	Minimum Phi	-55°	Maximum Phi	55°
Backtracking strategy	Tracker Spacing	7 m	Collector width	3.34 m
Inactive band	Left	0 m	Right	0 m
Models used	Transposition	Perez	Diffuse	Erbs, Meteonorm
Horizon	Free Horizon			
Near Shadings	No Shadings			

PV Array Characteristics

PV module	Si-poly	Model	**BYD 240 P6-30**	
Original PVsyst database		Manufacturer	BYD	
Number of PV modules		In series	24 modules	In parallel 13021 strings
Total number of PV modules		Nb. modules	312504	Unit Nom. Power 240 Wp
Array global power		Nominal (STC)	**75001 kWp**	At operating cond. 67007 kWp (50°C)
Array operating characteristics (50°C)		U mpp	639 V	I mpp 104927 A
Total area		Module area	**508407 m²**	Cell area 456306 m²

Inverter		Model	**Sunny Central 800CP**	
		Manufacturer	SMA	
Characteristics		Operating Voltage	583-820 V	Unit Nom. Power 800 kWac
Inverter pack		Nb. of inverters	84 units	Total Power 67200 kWac

PV Array loss factors

Array Soiling Losses

Jan.	Feb.	Mar.	Apr.	May	June	July	Aug.	Sep.	Oct.	Nov.	Dec.
1.8%	1.8%	1.8%	1.8%	1.8%	1.8%	1.8%	1.8%	1.8%	1.8%	1.8%	1.8%

Thermal Loss factor	Uc (const)	38.0 W/m²K	Uv (wind)	0.0 W/m²K / m/s
Wiring Ohmic Loss	Global array res.	0 mOhm	Loss Fraction	0.0 % at STC
Module Quality Loss			Loss Fraction	0.0 %
Module Mismatch Losses			Loss Fraction	1.3 % at MPP
Incidence effect, ASHRAE parametrization	IAM =	1 - bo (1/cos i - 1)	bo Param.	0.05

System loss factors

AC wire loss inverter to transfo	Inverter voltage	360 Vac tri		
	Wires: 3x30000.0 mm²	12 m	Loss Fraction	0.4 % at STC
External transformer	Iron loss (24H connexion)	73610 W	Loss Fraction	0.1 % at STC
	Resistive/Inductive losses	0.0 mOhm	Loss Fraction	2.0 % at STC

Grid-Connected System: Simulation parameters (continued)

User's needs : Unlimited load (grid)

Grid-Connected System: Main results

Project : **Masters**

Simulation variant : **New simulation variant**

Main system parameters					
	System type	**Grid-Connected**			
PV Field Orientation	tracking, tilted axis, Axis Tilt	30°	Axis Azimuth	0°	
PV modules	Model	BYD 240 P6-30	Pnom	240 Wp	
PV Array	Nb. of modules	312504	Pnom total	**75001 kWp**	
Inverter	Model	Sunny Central 800CP	Pnom	800 kW a	
Inverter pack	Nb. of units	84.0	Pnom total	**67200 ac**	
User's needs	Unlimited load (grid)				

Main simulation results

System Production — **Produced Energy** **187602 MWh/year** Spec. prod. 25 kWh/kWp/ye

Performance Ratio PR %

Normalized productions (per installed kWp): Nominal power 75001 kWp

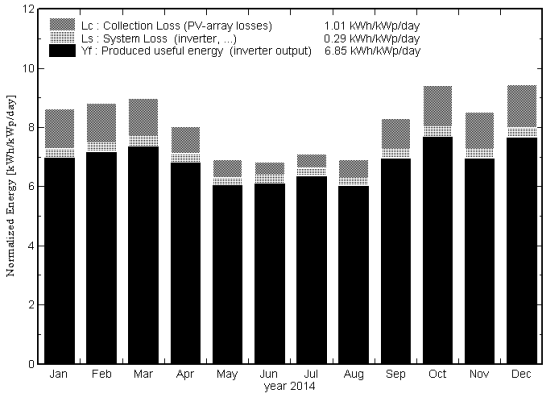

Performance Ratio PR

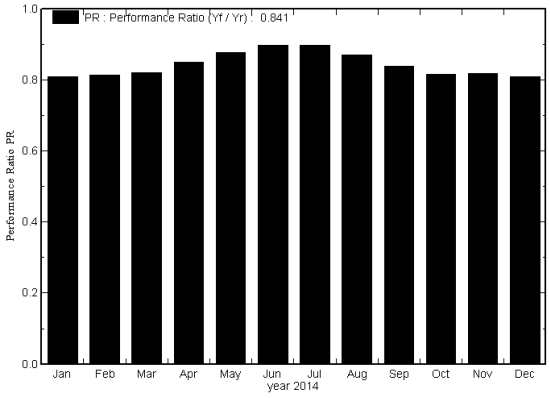

New simulation variant

Balances and main results

	GlobHor kWh/m²	T Amb °C	GlobInc kWh/m²	GlobEff kWh/m²	EArray MWh	E_Grid MWh	EffArrR %	EffSysR %
Jan. 14	234.8	26.52	267.5	257.7	16928	16240	12.45	11.94
Feb. 14	198.0	24.44	246.5	238.3	15709	15065	12.53	12.02
Mar. 14	196.6	21.04	278.7	269.9	17890	17152	12.63	12.11
Apr. 14	149.2	16.59	241.0	233.7	16036	15388	13.09	12.56
May 14	118.7	13.09	214.0	207.5	14679	14101	13.49	12.96
June 14	104.6	7.83	204.6	198.3	14356	13789	13.80	13.26
July 14	115.9	8.24	220.0	213.3	15428	14822	13.79	13.25
Aug. 14	129.5	11.59	214.4	207.8	14616	14022	13.41	12.87
Sep. 14	166.8	15.93	248.8	241.1	16332	15660	12.91	12.38
Oct. 14	222.3	20.56	291.8	282.4	18660	17878	12.58	12.05
Nov. 14	218.9	20.74	255.2	246.1	16354	15672	12.60	12.08
Dec. 14	261.7	26.10	293.2	282.6	18572	17812	12.46	11.95
Year	2117.0	17.69	2975.5	2878.5	195560	187602	12.93	12.40

Legends:

GlobHor	Horizontal global irradiation	EArray	Effective energy at the output of the array
T Amb	Ambient Temperature	E_Grid	Energy injected into grid
GlobInc	Global incident in coll. plane	EffArrR	Effic. Eout array / rough area
GlobEff	Effective Global, corr. for IAM and shadings	EffSysR	Effic. Eout system / rough area

Grid-Connected System: Loss diagram

Project : **Masters**

Simulation variant : **New simulation variant**

Main system parameters					
	System type	**Grid-Connected**			
PV Field Orientation	tracking, tilted axis, Axis Tilt	30°	Axis Azimuth	0°	
PV modules	Model	BYD 240 P6-30	Pnom	240 Wp	
PV Array	Nb. of modules	312504	Pnom total	**75001 kWp**	
Inverter	Model	Sunny Central 800CP	Pnom	800 kW a	
Inverter pack	Nb. of units	84.0	Pnom total	**67200 ac**	
User's needs	Unlimited load (grid)				

Loss diagram over the whole year

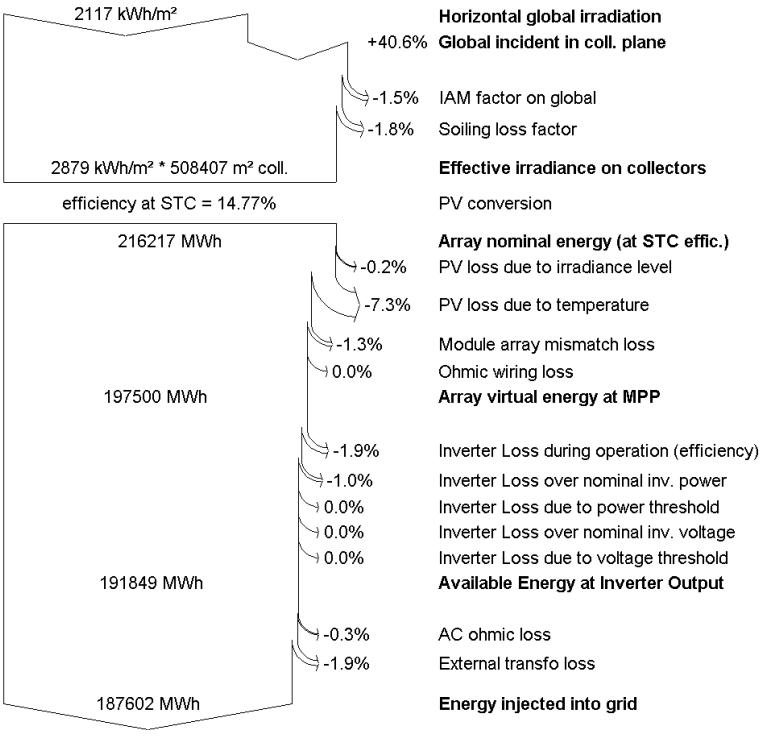

APPENDIX N

PVSYST FILE USING THE HAY MODEL AND SINGLE AXIS TRACKER AT THIRTY DEGREES TILT ANGLE

PVsyst file showing the results when the $75_M W_P$ solar PV plant is simulated as a single axis tracker at a tilt angle of thirty degrees using the Hay model. The PVsyst file is referred to in Chapter 5.

Grid-Connected System: Simulation parameters

Project : **Masters**

Geographical Site	**Kalkbult_site**		Country	**South Africa**
Situation	Latitude	30.2°S	Longitude	24.1°E
Time defined as	Legal Time	Time zone UT+2	Altitude	1214 m
	Albedo	0.20		
Meteo data:	**Kalkbult_site**	Imported - ASCII file		

Simulation variant : **New simulation variant**

Simulation date 02/08/16 14h21

Simulation parameters

Tracking plane, tilted Axis	Axis Tilt	30°	Axis Azimuth	0°
Rotation Limitations	Minimum Phi	-55°	Maximum Phi	55°
Backtracking strategy	Tracker Spacing	7 m	Collector width	3.34 m
Inactive band	Left	0 m	Right	0 m
Models used	Transposition	Hay	Diffuse	Erbs, Meteonorm
Horizon	Free Horizon			
Near Shadings	No Shadings			

PV Array Characteristics

PV module	Si-poly	Model	**BYD 240 P6-30**	
Original PVsyst database		Manufacturer	BYD	
Number of PV modules		In series	24 modules	In parallel 13021 strings
Total number of PV modules		Nb. modules	312504	Unit Nom. Power 240 Wp
Array global power		Nominal (STC)	**75001 kWp**	At operating cond. 67007 kWp (50°C)
Array operating characteristics (50°C)		U mpp	639 V	I mpp 104927 A
Total area		Module area	**508407 m²**	Cell area 456306 m²

Inverter		Model	**Sunny Central 800CP**	
		Manufacturer	SMA	
Characteristics		Operating Voltage	583-820 V	Unit Nom. Power 800 kWac
Inverter pack		Nb. of inverters	84 units	Total Power 67200 kWac

PV Array loss factors

Array Soiling Losses

Jan.	Feb.	Mar.	Apr.	May	June	July	Aug.	Sep.	Oct.	Nov.	Dec.
1.8%	1.8%	1.8%	1.8%	1.8%	1.8%	1.8%	1.8%	1.8%	1.8%	1.8%	1.8%

Thermal Loss factor	Uc (const)	38.0 W/m²K	Uv (wind)	0.0 W/m²K / m/s
Wiring Ohmic Loss	Global array res.	0 mOhm	Loss Fraction	0.0 % at STC
Module Quality Loss			Loss Fraction	0.0 %
Module Mismatch Losses			Loss Fraction	1.3 % at MPP
Incidence effect, ASHRAE parametrization	IAM =	1 - bo (1/cos i - 1)	bo Param.	0.05

System loss factors

AC wire loss inverter to transfo	Inverter voltage	360 Vac tri		
	Wires: 3x30000.0 mm²	12 m	Loss Fraction	0.4 % at STC
External transformer	Iron loss (24H connexion)	73610 W	Loss Fraction	0.1 % at STC
	Resistive/Inductive losses	0.0 mOhm	Loss Fraction	2.0 % at STC

Grid-Connected System: Simulation parameters (continued)

User's needs : Unlimited load (grid)

Grid-Connected System: Main results

Project : **Masters**

Simulation variant : **New simulation variant**

Main system parameters					
	System type	**Grid-Connected**			
PV Field Orientation	tracking, tilted axis, Axis Tilt	30°	Axis Azimuth	0°	
PV modules	Model	BYD 240 P6-30	Pnom	240 Wp	
PV Array	Nb. of modules	312504	Pnom total	**75001 kWp**	
Inverter	Model	Sunny Central 800CP	Pnom	800 kW a	
Inverter pack	Nb. of units	84.0	Pnom total	**67200 ac**	
User's needs	Unlimited load (grid)				

Main simulation results

System Production — **Produced Energy** **184793 MWh/year** Spec. prod. 24[illegible] kWh/kWp/ye[illegible]

Performance Ratio PR [illegible] %

Normalized productions (per installed kWp): Nominal power 75001 kWp

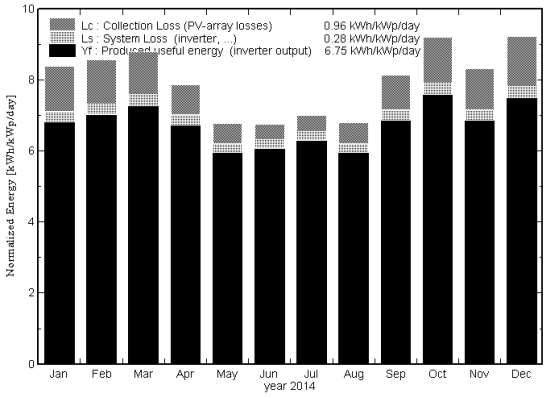

Performance Ratio PR

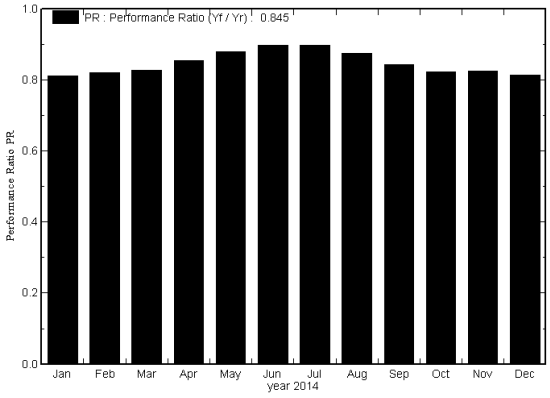

New simulation variant

Balances and main results

	GlobHor kWh/m²	T Amb °C	GlobInc kWh/m²	GlobEff kWh/m²	EArray MWh	E_Grid MWh	EffArrR %	EffSysR %
Jan. 14	234.8	26.52	260.5	251.1	16554	15888	12.50	12.00
Feb. 14	198.0	24.44	240.3	232.4	15405	14779	12.61	12.10
Mar. 14	196.6	21.04	272.6	264.3	17643	16915	12.73	12.20
Apr. 14	149.2	16.59	236.3	229.4	15795	15162	13.15	12.62
May 14	118.7	13.09	210.5	204.2	14457	13889	13.51	12.98
June 14	104.6	7.83	203.0	196.8	14230	13667	13.79	13.24
July 14	115.9	8.24	217.3	210.7	15237	14639	13.79	13.25
Aug. 14	129.5	11.59	210.7	204.3	14425	13841	13.47	12.92
Sep. 14	166.8	15.93	244.0	236.6	16120	15459	12.99	12.46
Oct. 14	222.3	20.56	285.7	276.6	18418	17653	12.68	12.16
Nov. 14	218.9	20.74	249.5	240.7	16111	15449	12.70	12.18
Dec. 14	261.7	26.10	286.0	275.8	18184	17451	12.50	12.00
Year	2117.0	17.69	2916.5	2822.8	192579	184793	12.99	12.46

Legends:

GlobHor	Horizontal global irradiation	EArray	Effective energy at the output of the array
T Amb	Ambient Temperature	E_Grid	Energy injected into grid
GlobInc	Global incident in coll. plane	EffArrR	Effic. Eout array / rough area
GlobEff	Effective Global, corr. for IAM and shadings	EffSysR	Effic. Eout system / rough area

Grid-Connected System: Loss diagram

Project : **Masters**

Simulation variant : **New simulation variant**

Main system parameters					
	System type	**Grid-Connected**			
PV Field Orientation	tracking, tilted axis, Axis Tilt	30°	Axis Azimuth	0°	
PV modules	Model	BYD 240 P6-30	Pnom	240 Wp	
PV Array	Nb. of modules	312504	Pnom total	**75001 kWp**	
Inverter	Model	Sunny Central 800CP	Pnom	800 kW a	
Inverter pack	Nb. of units	84.0	Pnom total	**67200 ac**	
User's needs	Unlimited load (grid)				

Loss diagram over the whole year

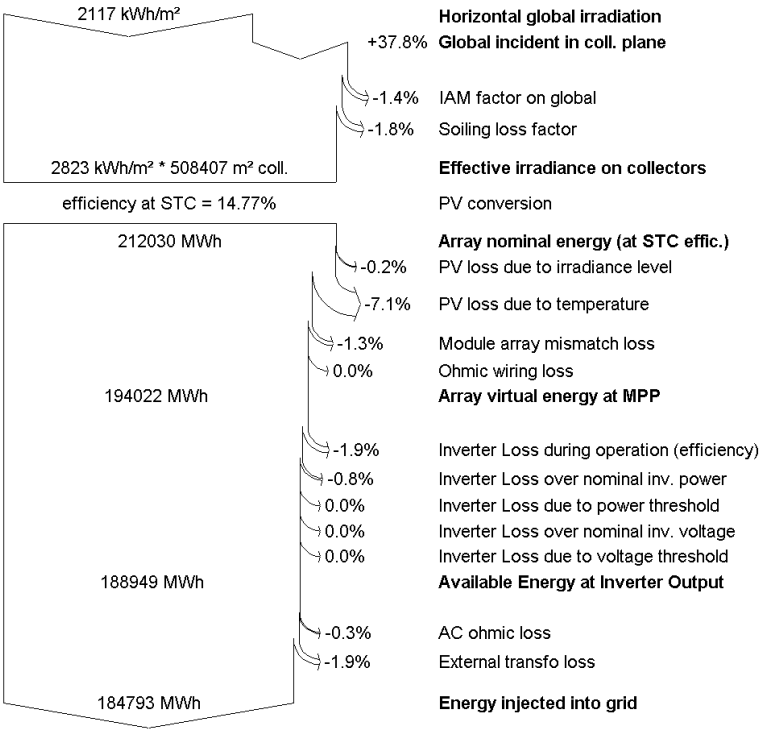

APPENDIX O

PVSYST FILE USING THE PEREZ MODEL AND DUAL AXIS TRACKER

PVsyst file showing the results when the $75_M W_P$ solar PV plant is simulated as a dual N-S axis tracker using the Perez model. The PVsyst file is referred to in Chapter 5.

Grid-Connected System: Simulation parameters

Project : **Masters**

Geographical Site	**Kalkbult_site**		Country	**South Africa**
Situation	Latitude	30.2°S	Longitude	24.1°E
Time defined as	Legal Time	Time zone UT+2	Altitude	1214 m
	Albedo	0.20		
Meteo data:	**Kalkbult_site**	Imported - ASCII file		

Simulation variant : **New simulation variant**

Simulation date 02/08/16 15h15

Simulation parameters

Backtracking strategy	Tracker Spacing	7 m	Collector width	3.34 m
Inactive band	Top	0 m	Bottom	0 m
Models used	Transposition	Perez	Diffuse	Erbs, Meteonorm
Horizon	Free Horizon			
Near Shadings	No Shadings			

PV Array Characteristics

PV module	Si-poly	Model	**BYD 240 P6-30**	
Original PVsyst database		Manufacturer	BYD	
Number of PV modules		In series	24 modules	In parallel 13021 strings
Total number of PV modules		Nb. modules	312504	Unit Nom. Power 240 Wp
Array global power		Nominal (STC)	**75001 kWp**	At operating cond. 67007 kWp (50°C)
Array operating characteristics (50°C)		U mpp	639 V	I mpp 104927 A
Total area		Module area	**508407 m²**	Cell area 456306 m²

Inverter		Model	**Sunny Central 800CP**	
		Manufacturer	SMA	
Characteristics		Operating Voltage	583-820 V	Unit Nom. Power 800 kWac
Inverter pack		Nb. of inverters	84 units	Total Power 67200 kWac

PV Array loss factors

Array Soiling Losses

Jan.	Feb.	Mar.	Apr.	May	June	July	Aug.	Sep.	Oct.	Nov.	Dec.
1.8%	1.8%	1.8%	1.8%	1.8%	1.8%	1.8%	1.8%	1.8%	1.8%	1.8%	1.8%

Thermal Loss factor	Uc (const)	38.0 W/m²K	Uv (wind)	0.0 W/m²K / m/s
Wiring Ohmic Loss	Global array res.	0 mOhm	Loss Fraction	0.0 % at STC
Module Quality Loss			Loss Fraction	0.0 %
Module Mismatch Losses			Loss Fraction	1.3 % at MPP
Incidence effect, ASHRAE parametrization	IAM =	1 - bo (1/cos i - 1)	bo Param.	0.05

System loss factors

AC wire loss inverter to transfo	Inverter voltage	360 Vac tri		
	Wires: 3x30000.0 mm²	12 m	Loss Fraction	0.4 % at STC
External transformer	Iron loss (24H connexion)	73610 W	Loss Fraction	0.1 % at STC
	Resistive/Inductive losses	0.0 mOhm	Loss Fraction	2.0 % at STC

Grid-Connected System: Simulation parameters (continued)

User's needs : Unlimited load (grid)

Grid-Connected System: Main results

Project : **Masters**

Simulation variant : **New simulation variant**

Main system parameters				
System type		**Grid-Connected**		
PV Field Orientation	tilt			
PV modules	Model	BYD 240 P6-30	Pnom	240 Wp
PV Array	Nb. of modules	312504	Pnom total	**75001 kWp**
Inverter	Model	Sunny Central 800CP	Pnom	800 kW a
Inverter pack	Nb. of units	84.0	Pnom total	**67200 ac**
User's needs	Unlimited load (grid)			

Main simulation results

System Production — **Produced Energy** **204819 MWh/year** Spec. prod. 273 kWh/kWp/ye

Performance Ratio PR 88 %

Normalized productions (per installed kWp): Nominal power 75001 kWp

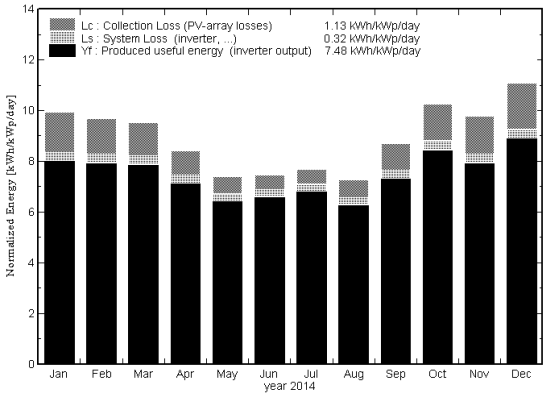

Performance Ratio PR

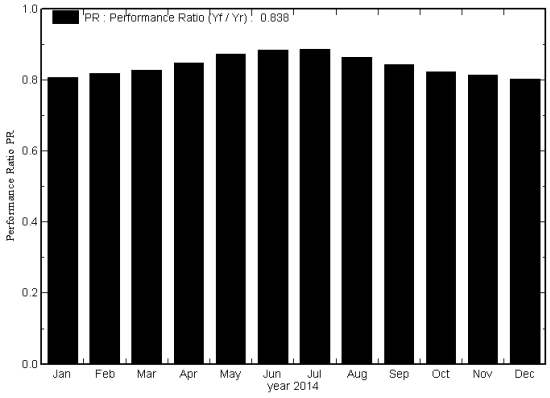

New simulation variant

Balances and main results

	GlobHor kWh/m²	T Amb °C	GlobInc kWh/m²	GlobEff kWh/m²	EArray MWh	E_Grid MWh	EffArrR %	EffSysR %
Jan. 14	234.8	26.52	308.2	299.0	19435	18657	12.40	11.91
Feb. 14	198.0	24.44	271.6	263.9	17383	16680	12.59	12.08
Mar. 14	196.6	21.04	295.4	287.2	19103	18324	12.72	12.20
Apr. 14	149.2	16.59	252.5	245.6	16764	16087	13.06	12.53
May 14	118.7	13.09	228.8	222.6	15602	14972	13.41	12.87
June 14	104.6	7.83	223.9	218.0	15499	14860	13.62	13.06
July 14	115.9	8.24	238.5	232.1	16525	15857	13.63	13.08
Aug. 14	129.5	11.59	225.7	219.5	15259	14639	13.30	12.76
Sep. 14	166.8	15.93	260.7	253.5	17206	16503	12.98	12.45
Oct. 14	222.3	20.56	317.8	309.1	20492	19648	12.68	12.16
Nov. 14	218.9	20.74	293.0	284.6	18637	17880	12.51	12.01
Dec. 14	261.7	26.10	343.7	333.8	21587	20713	12.35	11.85
Year	2117.0	17.69	3259.7	3168.8	213493	204819	12.88	12.36

Legends:

GlobHor	Horizontal global irradiation	EArray	Effective energy at the output of the array
T Amb	Ambient Temperature	E_Grid	Energy injected into grid
GlobInc	Global incident in coll. plane	EffArrR	Effic. Eout array / rough area
GlobEff	Effective Global, corr. for IAM and shadings	EffSysR	Effic. Eout system / rough area

Grid-Connected System: Loss diagram

Project : **Masters**

Simulation variant : **New simulation variant**

Main system parameters	System type	**Grid-Connected**		
PV Field Orientation	tilt			
PV modules	Model	BYD 240 P6-30	Pnom	240 Wp
PV Array	Nb. of modules	312504	Pnom total	**75001 kWp**
Inverter	Model	Sunny Central 800CP	Pnom	800 kW a
Inverter pack	Nb. of units	84.0	Pnom total	**67200 ac**
User's needs	Unlimited load (grid)			

Loss diagram over the whole year

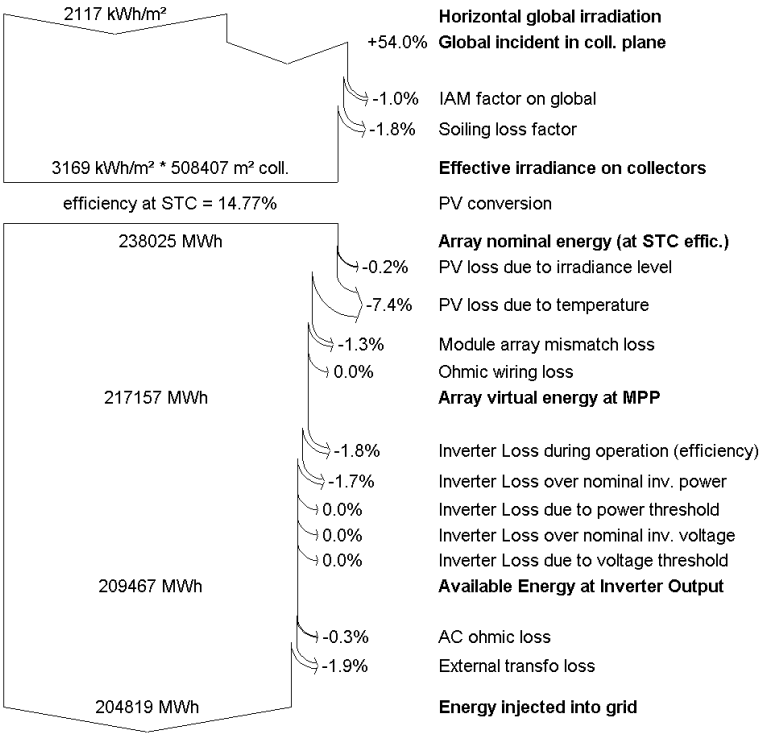

APPENDIX P

PVSYST FILE USING THE HAY MODEL AND DUAL AXIS TRACKER

PVsyst file showing the results when the $75_M W_P$ solar PV plant is simulated as a dual N-S axis tracker using the Hay model. The PVsyst file is referred to in Chapter 5.

Grid-Connected System: Simulation parameters

Project : **Masters**

Geographical Site	**Kalkbult_site**		Country	**South Africa**
Situation	Latitude	30.2°S	Longitude	24.1°E
Time defined as	Legal Time	Time zone UT+2	Altitude	1214 m
	Albedo	0.20		
Meteo data:	**Kalkbult_site**	Imported - ASCII file		

Simulation variant : **New simulation variant**

Simulation date 02/08/16 15h20

Simulation parameters

Backtracking strategy	Tracker Spacing	7 m	Collector width	3.34 m
Inactive band	Top	0 m	Bottom	0 m
Models used	Transposition	Hay	Diffuse	Erbs, Meteonorm
Horizon	Free Horizon			
Near Shadings	No Shadings			

PV Array Characteristics

PV module	Si-poly	Model	**BYD 240 P6-30**	
Original PVsyst database		Manufacturer	BYD	
Number of PV modules		In series	24 modules	In parallel 13021 strings
Total number of PV modules		Nb. modules	312504	Unit Nom. Power 240 Wp
Array global power		Nominal (STC)	**75001 kWp**	At operating cond. 67007 kWp (50°C)
Array operating characteristics (50°C)		U mpp	639 V	I mpp 104927 A
Total area		Module area	**508407 m²**	Cell area 456306 m²

Inverter		Model	**Sunny Central 800CP**	
		Manufacturer	SMA	
Characteristics		Operating Voltage	583-820 V	Unit Nom. Power 800 kWac
Inverter pack		Nb. of inverters	84 units	Total Power 67200 kWac

PV Array loss factors

Array Soiling Losses

Jan.	Feb.	Mar.	Apr.	May	June	July	Aug.	Sep.	Oct.	Nov.	Dec.
1.8%	1.8%	1.8%	1.8%	1.8%	1.8%	1.8%	1.8%	1.8%	1.8%	1.8%	1.8%

Thermal Loss factor	Uc (const)	38.0 W/m²K	Uv (wind)	0.0 W/m²K / m/s
Wiring Ohmic Loss	Global array res.	0 mOhm	Loss Fraction	0.0 % at STC
Module Quality Loss			Loss Fraction	0.0 %
Module Mismatch Losses			Loss Fraction	1.3 % at MPP
Incidence effect, ASHRAE parametrization	IAM =	1 - bo (1/cos i - 1)	bo Param.	0.05

System loss factors

AC wire loss inverter to transfo	Inverter voltage	360 Vac tri		
	Wires: 3x30000.0 mm²	12 m	Loss Fraction	0.4 % at STC
External transformer	Iron loss (24H connexion)	73610 W	Loss Fraction	0.1 % at STC
	Resistive/Inductive losses	0.0 mOhm	Loss Fraction	2.0 % at STC

Grid-Connected System: Simulation parameters (continued)

User's needs : Unlimited load (grid)

Grid-Connected System: Main results

Project : **Masters**

Simulation variant : **New simulation variant**

Main system parameters				
System type		**Grid-Connected**		
PV Field Orientation	tilt			
PV modules	Model	BYD 240 P6-30	Pnom	240 Wp
PV Array	Nb. of modules	312504	Pnom total	**75001 kWp**
Inverter	Model	Sunny Central 800CP	Pnom	800 kW a
Inverter pack	Nb. of units	84.0	Pnom total	**67200 ac**
User's needs	Unlimited load (grid)			

Main simulation results

System Production — **Produced Energy** **202059 MWh/year** Spec. prod. 26[illegible] kWh/kWp/ye[illegible]

Performance Ratio PR [illegible] %

Normalized productions (per installed kWp): Nominal power 75001 kWp

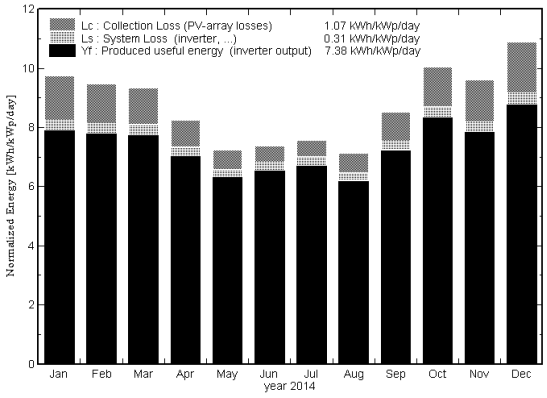

Performance Ratio PR

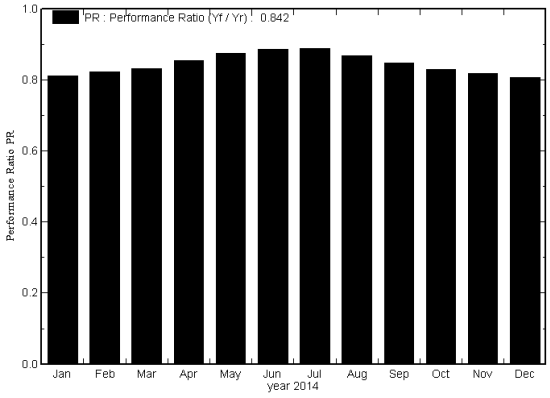

New simulation variant

Balances and main results

	GlobHor kWh/m²	T Amb °C	GlobInc kWh/m²	GlobEff kWh/m²	EArray MWh	E_Grid MWh	EffArrR %	EffSysR %
Jan. 14	234.8	26.52	302.0	293.3	19153	18386	12.47	11.97
Feb. 14	198.0	24.44	265.4	258.1	17086	16397	12.66	12.15
Mar. 14	196.6	21.04	289.1	281.3	18831	18061	12.81	12.29
Apr. 14	149.2	16.59	247.1	240.5	16506	15841	13.14	12.61
May 14	118.7	13.09	224.1	218.2	15337	14717	13.46	12.91
June 14	104.6	7.83	221.5	215.8	15358	14723	13.64	13.07
July 14	115.9	8.24	234.6	228.5	16299	15639	13.66	13.11
Aug. 14	129.5	11.59	221.2	215.2	15036	14425	13.37	12.83
Sep. 14	166.8	15.93	255.7	248.8	16989	16293	13.07	12.53
Oct. 14	222.3	20.56	311.7	303.3	20240	19411	12.77	12.25
Nov. 14	218.9	20.74	287.9	279.7	18444	17695	12.60	12.09
Dec. 14	261.7	26.10	337.6	327.9	21334	20470	12.43	11.93
Year	2117.0	17.69	3198.0	3110.6	210611	202059	12.95	12.43

Legends:

GlobHor	Horizontal global irradiation	EArray	Effective energy at the output of the array
T Amb	Ambient Temperature	E_Grid	Energy injected into grid
GlobInc	Global incident in coll. plane	EffArrR	Effic. Eout array / rough area
GlobEff	Effective Global, corr. for IAM and shadings	EffSysR	Effic. Eout system / rough area

Grid-Connected System: Loss diagram

Project : **Masters**

Simulation variant : **New simulation variant**

Main system parameters				
PV Field Orientation	System type	**Grid-Connected**		
	tilt			
PV modules	Model	BYD 240 P6-30	Pnom	240 Wp
PV Array	Nb. of modules	312504	Pnom total	**75001 kWp**
Inverter	Model	Sunny Central 800CP	Pnom	800 kW a
Inverter pack	Nb. of units	84.0	Pnom total	**67200 ac**
User's needs	Unlimited load (grid)			

Loss diagram over the whole year

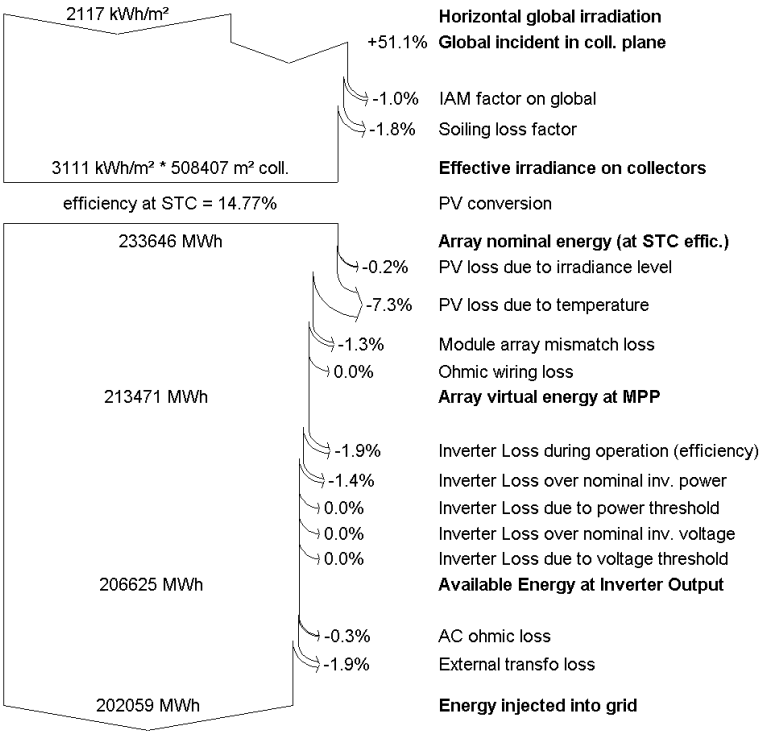

APPENDIX Q

PEREZ MODEL COEFFICIENTS FOR IRRADIANCE

The f coefficients given in Table Q.1, defined for specific bins of clearness (ε) shown in Table Q.2 are referred to in Chapter 6.

Table Q.1: Perez model coefficients for irradiance (from Table 6 in[103]).

ε bin	f_{11}	f_{12}	f_{13}	f_{21}	f_{22}	f_{23}
1	-0.008	0.588	-0.062	-0.06	0.072	-0.022
2	0.13	0.683	-0.151	-0.019	0.066	-0.029
3	0.33	0.487	-0.221	0.055	-0.064	-0.026
4	0.568	0.187	-0.295	0.109	-0.152	-0.014
5	0.873	-0.392	-0.362	0.226	-0.462	0.001
6	1.132	-1.237	-0.412	0.288	-0.823	0.056
7	1.06	-1.6	-0.359	0.264	-1.127	0.131
8	0.678	-0.327	-0.25	0.156	-1.377	0.251

Table Q.2: Sky clearness bins (from Table 1 in [103]).

ε bin	**Lower Bound**	**Upper Bound**
1 Overcast	1	1.065
2	1.065	1.230
3	1.230	1.500
4	1.500	1.9500
5	1.950	2.800
6	2.800	4.500
7	4.500	6.200
8 Clear	6.200	-

LIST OF REFERENCES

[1] G. M. Masters, *Renewable and Efficient Electric Power Systems*, 2nd ed. New Jersey: Wiley-IEEE Press., 2004.

[2] Y. Aldali, D. Henderson, and T. Muneer, "A 50 MW very large-scale photovoltaic power plant for Al-Kufra , Libya : energetic , economic and environmental impact analysis," no. July, pp. 277–293, 2011.

[3] S. Phillips and W. Warmuth, "Photovoltaics report," Fraunhofer Institute for Solar Energy Systems, ISE, Tech. Rep., 2016.

[4] H. Shimada, S. Miyazaki, K. Morikawa, Y. Hasegawa, K. Owada, M. Sato, and M. Nagasaka, "Performance Analysis and Modeling Results for a Large-Scale Grid-Connected Photovoltaic Plant," *28th European Photovoltaic Solar Energy Conference and Exhibition*, pp. 4134–4138, 2013.

[5] A. A. Babatunde and S. Abbasoglu, "Evaluation of field data and simulation results of a photovoltaic system in countries with high solar radiation," *Turkish Journal of Electrical Engineering & Computer Sciences*, vol. 23, pp. 1608–1618, 2015.

[6] GeoModelSolar, "Solargis Database." [Online]. Available: http://solargis.info/.[Accessed: 21-May-2016].

[7] M.Chidi, M.Nthontho, S.Chowdhury, and SP.Chowdhury, "Viability of Grid-Connected Domestic Solar Photovoltaic Systems in South Africa," University of Cape town, Cape Town, Tech. Rep., 2012.

[8] Department of Energy, "Independent Power Producers Procurement Programme (IPPPP)," Tech. Rep. March, 2016.

[9] L. S. Basha, "Analysis and evaluation tools development of photovoltaic modules and system performance," Master Thesis, Cairo University, 2012.

[10] Sandia National Laboratories, "PV Performance modeling collaborative," 2014. [Online]. Available: https://pvpmc.sandia.gov/modeling-steps/.[Accessed:20-March-2016].

[11] H. ZHENG, "Solar photovoltaic energy generation and conversion from devices to grid integration," Doctor of Philosophy, University of Alabama, 2013.

[12] C. Deline, "Characterising shading losses on partially shaded PV systems," NREL, Albuquerque, NM, Tech. Rep., 2010.

[13] A. Miller and B. Lumby, "Utility-Scale Solar Photovoltaic Power Plants A project Developer's Guide," International Finance Corporation 2015, Washington, D.C. 20433, Tech. Rep., 2015.

[14] NSE, "New Southern Energy," p. 1, 2016. [Online]. Available: http://www.newsouthernenergy.com/pv-solar-thin-film-vs-polycrystalline/.[Accessed:20-July-2016].

[15] N. Rome, A. Bosio, and A. Romeo, "An innovative process suitable to produce high efficiency CdTe/CdS thin film modules," *Solar Energy Materials and Sola Cells*, vol. 94, no. 1, pp. 2–7, 2010.

[16] E. C. Lechuga, "Analysis of the implementation of a photovoltaic plant in Catalonia," Ph.D. dissertation, Politechnika Łódzka, 2011.

[17] S. Deepthi, A. Ponni, R. Ranjitha, and R. Dhanabal, "Comparison of Efficiencies of Single-Axis Tracking System and Dual-Axis Tracking System with Fixed Mount," *International Journal of Engineering Science and Innovative Technology (IJESIT)*, vol. 2, no. 2, pp. 425–430, 2013.

[18] Renewable Energy Corporation ASA, "Real world performance exceeds expectations," Sandvika, Norway, Tech. Rep., 2012.

[19] A. Mermoud, "PVsyst." [Online]. Available: http://files.pvsyst.com/help/.[Accessed: 15-April-2016].

[20] PHOTON, "Photon Database of solar modules and inverters," 2016. [Online]. Available: http://www.photon.info/en/photon-databases.[Accessed:06-July-2016].

[21] Arup, "First Solar Energy Yield Simulations Module Performance Comparison for Four Solar PV Module Technologies," Consulting Engineers South Africa, Johannesburg, Tech. Rep. 1, 2015.

[22] P. Ineichen, "Long term satellite global, beam and diffuse irradiance validation," *Energy Procedia*, vol. 48, pp. 1586–1596, 2014.

[23] T. Nordmann, C. Luzi, and G. Mike, "Analysis of Long - Term Performance of PV Systems. Different Data Resolution for Different Purposes," International Energy Agency Photovoltaic Power Systems programme analysis, Tech. Rep., 2014.

[24] A. Woyte, M. Richter, D. Moser, S. Mau, N. H. Reich, and U. Jahn, "Monitoring of Photovoltaic Systems: Good Practices and Systematic Analyes," *28th European PV Solar Energy Conference and Exhibition*, 2013.

[25] B. Marion, J. Rodri, and J. Pruett, "Instrumentation for Evaluating PV System Performance Losses from Snow Preprint," in *National Solar Conference (SOLAR 2009)*, New York, 2009, pp. 1–6.

[26] A. Guerin de Montgareuil, "A new accurate method for outdoor calibration of field pyranometers," in *19th European Photovoltaic Solar Energy Conference and Exhibition*, Paris, France, 2004.

[27] Kipp & Zonen, "Pyranometers For the Accurate Measurement of Solar Irradiance," Tech. Rep., 1990.

[28] A. Spena, C. Cornaro, G. Intreccialagli, and D. Chianese, "Data Validation and Uncertainty Evaluation of the ESTER Outdoor Facility for Testing of Photovoltaic Modules," in *24th European Photovoltaic Solar Energy Conference*, 2009, pp. 3586 – 3589.

[29] A. Larsen and A. Larsen, "Forecasting mismatch losses : An empirical study investigating module level inverter- and string inverter systems," Bachelor of Science Thesis, KTH School of Industrial Engineering and Management Energy Technology, 2014.

[30] B. Espinar, P. Blanc, L. Wald, B. Gschwind, L. Ménard, E. Wey, C. Thomas, and L. Saboret, "HelioClim-3: a near-real time and long-term surface solar irradiance database," *COST WIRE workshop on "Remote Sensing Measurements for Renewable Energy"*, p. 4 pp., 2012.

[31] J. Remund, S. Kunz, C. Schilter, and S. Müller, "MeteoNorm handbook part 1:software," Switzerland, Tech. Rep., 2010.

[32] PVGIS, "PVGIS." [Online]. Available: http://re.jrc.ec.europa.eu/pvgis/apps4/pvest.php?map=africa.[Accessed:20-May-2016].

[33] NASA, "NASA-SSE database." [Online]. Available: https://eosweb.larc.nasa.gov/sse/.[Accessed:22-June-2016].

[34] C. Budig, J. Orozaliev, and K. Vajen, "Comparison of Different Sources of Meteorological Data for Central Asia and Russia," in *EuroSun 2010*, 34109 Kassel, Germany, 2010, p. 8.

[35] M. Šúri, J. Remund, T. Cebecauer, D. Dumortier, L. Wald, T. Huld, and P. Blanc, "First Steps in the Cross-Comparison of Solar Resource Spatial Products in Europe," *Eurosun 2008*, no. October, pp. 7–10, 2008.

[36] H. G. Beyer, C. Costanzo, and D. Heinemann, "Modifications of the heliosat procedure for irradiance estimates from satellite images," *Solar Energy*, vol. 56, no. 3, pp. 207–212, 1996.

[37] P. J. Axaopoulos, E. D. Fylladitakis, and K. Gkarakis, "Accuracy analysis of software for the estimation and planning of photovoltaic installations," *International Journal of Energy and Environmental Engineering*, vol. 5, no. 1, pp. 1–7, 2014.

[38] R. Meyer, "Site Assessment of Solar Resource Upington Solar Park," Stellenbosch University, Tech. Rep. 58, 2011.

[39] ScatecSolar, "Kalkbult South Africa 75 MW." [Online]. Available: http://www.scatecsolar.com/Portfolio/South-Africa/Kalkbult-South-Africa-75-MW.[Accessed:20-Oct-2015].

[40] M. Diez-Mediavilla, C. Alonso-Tristan, M. C. Rodriguez-Amigo, T. Garcia-Calderon, and M. I. Dieste-Velasco, "Performance analysis of PV plants: Optimization for improving profitability," *Energy Conversion and Management*, vol. 54, no. 1, pp. 17–23, 2012.

[41] BYD, "BYD P6 - 30 Series-3BB," pp. 1–2, 2011. [Online]. Available: http://www.italwarmi.it/fabbriche/images/byd-p6-36-3bb.pdf.[Accessed:20-May-2016].

[42] N. Strevel, L. Trippel, and M. Gloeckler, "Performance characterization and superior energy yield of First Solar PV power plants in high-temperature conditions," *PV International*, vol. 17, no. August, pp. 1–8, 2012.

[43] S. Giglmayr, A. C. Brent, P. Gauché, and H. Fechner, "Utility-scale PV power and energy supply outlook for South Africa in 2015," *Renewable Energy*, vol. 83, pp. 779–785, 2015.

[44] S. Dubey, J. N. Sarvaiya, and B. Seshadri, "Temperature dependent photovoltaic (PV) efficiency and its effect on PV production in the world - A review," *Energy Procedia*, vol. 33, pp. 311–321, 2013.

[45] SEIAPI, "Grid-connected PV systems (No Battery Storage)," no. 1, pp. 1–19, 2012.

[46] C. Chioncel, L. Augustinov, N. Gilich, and G. Tirian, "Acta Technica Corviniensis Bulletin of Engineering, Scientific Supplement of Annals of Faculty Engineering," *Hunedoara International Journal of Engineering 2009*, vol. 7, pp. 55–58, 2009.

[47] R. Faranda, M. Gualdoni, S. Leva, M. Monaco, and A. Timidei, "Analysis of a PV system with single-axis tracking energy production and performances," *3rd International Conference on Clean Electrical Power: Renewable Energy Resources Impact, ICCEP 2011*, vol. 2, pp. 130–136, 2011.

[48] C. R. N.H. Reich, B. Müller, A. Armbruster, K. Kiefer, W.G.J.H.M. van Sark, "Performance Ratio Revisited: Are PR >90% Realistic?" in *26th European Photovoltaic Solar Energy Conference and Exhibition*, 2011, pp. 3922 – 3929.

[49] T. Ishii, T. Takashima, and K. Otani, "Long-term performance degradation of various kinds of photovoltaic modules under moderate climatic conditions," *Progress in Photovoltaics: Research and Applications*, vol. 19, no. 2, pp. 170–179, mar 2011.

[50] W. van Sark and B. M. N.H. Reich, "Review of Pv Performance Ratio Development," Fraunhofer Institute for Solar Energy Systems ISE, Freiburg, Germany, Tech. Rep., 2012.

[51] T. Ishii, K. Otani, and T. Takashima, "Effects of solar spectrum and module temperature on outdoor performance of photovoltaic modules in round-robin measurements in Japan," *Progress in Photovoltaics: Research and Applications*, vol. 19, no. 2, pp. 141–148, mar 2011.

[52] S. Chokmaviroj, R. Wattanapong, and Y. Suchart, "Performance of a 500 kW P grid connected photovoltaic system at Mae Hong," *Renewable Energy*, vol. 31, no. 1, pp. 19–28, 2006.

[53] R. Bohra, "Performance Analysis of 1MW SPV Plant; Temperature Corrected PR," Malpani Group, India, Tech. Rep. September, 2014.

[54] T. Dierauf, A. Growitz, S. Kurtz, and C. Hansen, "Weather-Corrected Performance Ratio," *NREL Technical Report NREL/TP-5200-57991*, pp. 1–16, 2013.

[55] K. Chumpolrat, V. Sangsuwan, N. Udomdachanut, S. Kittisontirak, S. Songtrai, P. Chinnavornrungsee, A. Limmanee, J. Sritharathikhun, and K. Sriprapha, "Effect of ambient temperature on performance of grid-connected inverter installed in Thailand," *International Journal of Photoenergy*, pp. 1–6, 2014.

[56] M. Fthenakis, V. M.Frischknecht, R.Raugei, M.Kim, H. C.Alsema, E.Held, M.de Wild Scholten, "Methodology Guidelines on Life Cycle Assessment of Photovoltaic Electricity," Tech. Rep. 03, 2011.

[57] SMA Solar Technology AG, "Performance ratio," pp. 1–9, 2015.

[58] T. Huld, R. Gottschalg, H. G. Beyer, and M. Topič, "Mapping the performance of PV modules, effects of module type and data averaging," *Solar Energy*, vol. 84, no. 2, pp. 324–338, feb 2010.

[59] V. Sharma, A. Kumar, O. Sastry, and S. Chandel, "Performance assessment of different solar photovoltaic technologies under similar outdoor conditions," *Energy*, vol. 58, pp. 511–518, sep 2013.

[60] First Solar, "First Solar FS Series 3 Black PV Module," pp. 4–5, 2014. [Online]. Available: www.firstsolar.com/{~}/media/documents/data-sheets/products/moduledatasheet/pd-5-401-03{_}series3black-4.ashx.[Accessed:21-May-2015].

[61] A. B.-H. Ebenezer Nyarko Kumi, "Design and Analysis of a 1MW Grid- Connected Solar PV System in Ghana," *African Technology Policy Studies Network Working Paper Series*, no. 78, pp. 1–24, 2013.

[62] R. Gottschalg, T. R. Betts, D. G. Infield, and M. J. Kearney, "The effect of spectral variations on the performance parameters of single and double junction amorphous silicon solar cells," *Solar Energy Materials and Solar Cells*, vol. 85, no. 3, pp. 415–428, 2005.

[63] S. Kurtz, J. Newmiller, T. Dierauf, A. Kimber, J. Mckee, and R. Flottemesch, "Analysis of Photovoltaic System Energy Performance Evaluation Method," NREL, USA, Tech. Rep., 2013.

[64] J. Y. C. J. H. So, B. G. Yu, H. M. Hwang, G. J. Yu and I. Cho, "Performance Monitoring and Analysis of Middle Scale Grid-Connected PV System," *The 7th International Conference on Power Electronics*, pp. 451–454, 2008.

[65] J. S. Y. J. H. So, H. M. Hwang, B. G. Yu and G. J. Yu, "Loss analysis of grid-connected PV system using yield model," *Institute of Energy Research*, no. 3, pp. 4269–4271, 2011.

[66] G. Blaesser and D. Munro, "Guidelines for the Assessment of Photovoltaic Plants," *Institute for System Engineering and Informatics*, 1995.

[67] R. Yuan, H. Ding, J. Qian, Y. Chen, X. XI, and X. Yang, "Loss Analysis of a 100kW PV Inverter," in *International Power, Electronics and Materials Engineering Conference (IPEMEC 2015) Loss*, Beijing, China, 2015, pp. 746–753.

[68] M. T. K. Brecl, J. Kurnik, "Evaluation of Losses on Energy Yield Due to Self Shading of Free Standing PV Systems," in *24th European Photovoltaic Solar Energy Conference*, Hamburg, Germany, 2009, pp. 4038 – 4041.

[69] S. Elies, T. Reis, B. Müller, U. Kräling, and K. Kiefer, "Measuremtnt influence of row-shading on the performance of PV systems simulation and measurement," in *25th European Photovoltaic Solar Energy Conference and Exhibition*, Valencia, Spain, 2010, pp. 4640–4646.

[70] S. Vijayalekshmy, S. RamaIyer, and B. Beevi, "Evaluation of Power Losses in a Short String of Series-Connected and Parallel-Connected Photovoltaic Modules for Low Power Application," *International Conference on Control Communication and Computing (ICCC)*, pp. 125–130, 2013.

[71] M. Bui, C. Voelker, B. Li, and D. M. J. Doble, "Oblique angle of incidence measurement of PV modules on a solar simulator," in *26th European Photovoltaic Solar Energy Conference and Exhibition*, Hamburg, Germany, 2010, pp. 2165–2169.

[72] M. Gostein, J. R. Caron, and B. Littmann, "Measuring soiling losses at utility-scale PV power plants," *IEEE 40th Photovoltaic Specialist Conference, PVSC*, pp. 885–890, 2014.

[73] J. Zorrilla-Casanova, M. Piliougine, J. Carretero, P. Bernaola-Galván, P. Carpena, and Llanos Mora-López and Mariano Sidrach-de-Cardona, "Losses produced by soiling in the incoming radiation to photovoltaic modules," *Progress in photovoltaics: Research and applications*, vol. 21, no. February, pp. 790–796, 2012.

[74] J. R. Caron and B. Littmann, "Direct monitoring of energy lost due to soiling on first solar modules in California," *IEEE Journal of Photovoltaics*, vol. 3, no. 1, pp. 336–340, 2013.

[75] S. Shaari, K. Sopian, N. Amin, and M. N. Kassim, "The temperature dependence coefficients of amorphous silicon and crystalline photovoltaic modules using Malaysian field test investigation," *American Journal of Applied Sciences*, vol. 6, no. 4, pp. 586–593, 2009.

[76] J. J. Wysocki and P. Rappaport, "Effect of temperature on photovoltaic solar energy conversion," *Journal of applied physics*, vol. 31, no. 3, pp. 571–578, 2004.

[77] J. M. Kuitche, R. Pan, and G. Tamizhmani, "Statistical analysis of back surface vs. cell temperatures of c-Si modules using measurement error models," *Conference Record of the IEEE Photovoltaic Specialists Conference*, no. 3, pp. 2953–2956, 2012.

[78] C. Baltus, J. Eikelboom, and R. van Zolingen, "Analytical monitoring of losses in PV systems." *14th European Photovoltaic Solar Energy Conference*, no. July, pp. 1547–1550, 1997.

[79] Y. Ueda, K. Kurokawa, K. Kitamura, M. Yokota, K. Akanuma, and H. Sugihara, "Performance analysis of various system configurations on grid-connected residential PV systems," *Solar Energy Materials and Solar Cells*, vol. 93, no. 6-7, pp. 945–949, 2009.

[80] A.Chouder and S.Silvestre, "Analysis of power losses in PV systems," *Journal of Chemical Information and Modeling*, vol. 53, no. 9, pp. 1689–1699, 2013.

[81] F. Vignola, F. Mavromatakis, and J. Krumsick, "Performance of PV Inverters," *American Solar Energy Society - SOLAR 2008: Catch the Clean Energy Wave*, pp. 628 – 650, 2008.

[82] SMA Solar Technology AG, "Sunny Central datasheet," USA, pp. 1–4, 2001.

[83] A. Mermoud, "Modeling Systems Losses in PVsyst," University of Geneva, Geneva, Tech. Rep., 2013.

[84] S. A. Khalil and A. M. Shaffie, "A comparative study of total, direct and diffuse solar irradiance by using different models on horizontal and inclined surfaces for Cairo, Egypt," *Renewable and Sustainable Energy Reviews*, vol. 27, pp. 853–863, 2013.

[85] T. Mahachi and A. Rix, "PVsyst model improvement using field data from a 75 MWp solar PV power plant," in *Southern African Universities Power Engineering Conference*, 10.13140/RG.2.1.2518.6168 ,Vereeniging, South Africa, 2016, pp. 147–152.

[86] M. Lave, W. Hayes, A. Pohl, and C. W. Hansen, "Evaluation of global horizontal irradiance to plane-of-array irradiance models at locations across the United States," *IEEE Journal of Photovoltaics*, vol. 5, no. 2, pp. 597–606, 2015.

[87] M. Mesri and A. Choucha, "Evaluation of Global Solar Radiation Models for Inclined Surfaces," in *International Conference of Electrical, Automation and Mechanical Engineering (EAME 2015)*, no. Eame, Algeria, 2015, pp. 478–483.

[88] S. A. Khalil and A. M. Shaffie, "Performance of Statistical Comparison Models of Solar Energy on Horizontal and Inclined Surface," *Journal of Energy and Power (IJEP)*, vol. 2, no. 1, pp. 8–25, 2013.

[89] M. J. Brooks, S. du Clou, J. L. van Niekerk, P. Gauche, C. Leonard, M. J. Mouzouris, A. J. Meyer, N. van der Westhuizen, E. van Dyk, and F. J. Vorster, "SAURAN: A new resource for solar radiometric data in Southern Africa," *Journal of Energy in Southern Africa*, vol. 26, no. 1, pp. 2–10, 2015.

[90] J. Freeman, J. Whitmore, N. Blair, and A. P. Dobos, "Validation of multiple tools for flat plate photovoltaic modeling against measured data," *2014 IEEE 40th Photovoltaic Specialist Conference, PVSC 2014*, no. August, pp. 1932–1937, 2014.

[91] S. M. Robaa, "Evaluation of sunshine duration from cloud data in Egypt," *Energy*, vol. 33, no. 5, pp. 785–795, 2008.

[92] J. F. Orgill and K. G. T. Hollands, "Correlation equation for hourly diffuse radiation on a horizontal surface," *Solar Energy*, vol. 19, no. 4, pp. 357–359, 1977.

[93] D. G. Erbs, S. A. Klein, and J. A. Duffie, "Estimation of the diffuse radiation fraction for hourly, daily and monthly-average global radiation," *Solar Energy*, vol. 28, no. 4, pp. 293–302, 1982.

[94] A. Louche, G. Notton, P. Poggi, and G. Simonnot, "Correlations for direct normal and global horizontal irradiation on a French Mediterranean site," *Solar Energy*, vol. 46, no. 4, pp. 261–266, 1991.

[95] D. T. Reindl, W. A. Beckman, and J. A. Duffie, "Diffuse fraction correlations," *Solar Energy*, vol. 47, no. 4, pp. 311–312, 1991.

[96] E. L. Maxwell, "A Quasi-Physical Model for converting hourly GHI to DNI," Solar Energy Research Institute (SERI), Colorado, USA, Tech. Rep., 1987.

[97] R. Perez, P. Ineichen, E. Maxwell, R. Seals, and A. Zelenka, "Dynamic global-to-direct irradiance conversion models," *ASHRAE*, vol. 98, no. 1, pp. 354–369, 1992.

[98] D. R. Myers, *Solar radiation Practical: Modeling for Renewable Energy Applications*, A. Ghassemi, Ed. New York: CRC Press, 2013.

[99] B. Y. Liu and R. C. Jordan, "The interrelationship and characteristic distribution of direct, diffuse and total solar radiation," *Solar Energy*, vol. 4, no. 3, pp. 1–19, 1960.

[100] T. M. Klucher, "Evaluation of models to predict insolation on tilted surfaces," *Solar Energy*, vol. 23, no. 2, pp. 111–114, 1979.

[101] J. E. Hay, "Calculating solar radiation for inclined surfaces: Practical approaches," *Renewable Energy*, vol. 3, no. 4-5, pp. 373–380, 1993.

[102] D. T. Reindl, W. A. Beckman, and J. A. Duffie, "Evaluation of hourly tilted surface radiation models," *Solar Energy*, vol. 45, no. 1, pp. 9–17, 1990.

[103] R. Perez, P. Ineichen, R. Seals, J. Michalsky, and R. Stewart, "Modeling daylight availability and irradiance components from direct and global irradiance," *Solar Energy*, vol. 44, no. 5, pp. 271–289, 1990.

[104] S. Freitas, C. M. Catita, and P. Redweik, "Modelling solar potential in the urban environment : State-of-the-art review," no. August 2016, 2015.

[105] P. G. Loutzenhiser, H. Manz, C. Felsmann, P. A. Strachan, T. Frank, and G. M. Maxwell, "Empirical validation of models to compute solar irradiance on inclined surfaces for building energy simulation," *Solar Energy*, vol. 81, no. 2, pp. 254–267, 2007.

[106] O. W. Westbrook and F. D. Collins, "Energy model validation for large-scale photovoltaic systems," *Photovoltaic Specialists Conference (PVSC), 2013 IEEE 39th*, pp. 830–835, 2013.